博士論文

# Multi-Fidelity Uncertainty Quantification and Surrogate-Based Memetic Algorithm for Design Under Uncertainty

**（不確実性下での設計に対するMulti-Fidelity不確定性定量化とSurrogate-Based Memeticアルゴリズム）**

パラル　プラムヂタ　サトリア
Palar Pramudita Satria

A dissertation submitted to the Department of Aeronautics and Astronautics
in partial fulfillment of the requirements for the degree of
Doctor of Philosophy
in
Engineering
at
The University of Tokyo

August 2015

**Dissertation Defense Committee**

Professor Takeshi Tsuchiya, chair
Department of Aeronautics and Astronautics
The University of Tokyo

Professor Shinji Suzuki
Department of Aeronautics and Astronautics
The University of Tokyo

Professor Kenichi Rinoie
Department of Aeronautics and Astronautics
The University of Tokyo

Associate Professor Akira Oyama
Institute of Space and Astronautical Science
Japan Aerospace Exploration Agency

Associate Professor Koji Shimoyama
Department of Aeronautics and Astronautics
Tohoku University

*"Science may set limits to knowledge, but should not set limits to imagination"*

Bertrand Russell, British philosopher

# *Abstract*

This dissertation deals with the development and improvement of metaheuristic optimizer and uncertainty quantification (UQ) algorithm to tackle expensive engineering robust optimization problem. Due to the limited availability of computational budget, this tight budget has to be optimized to put it on the best use. This could be done via two ways: increasing the efficiency of the optimizer and improving the effectiveness of the UQ algorithms. An improvement of local surrogate-assisted multi-objective memetic algorithm (SS-MOMA) was investigated and studied in this work to improve the optimization algorithm's effectiveness to locates and exploits the Pareto front. The improvement on the optimizer side was mainly done by investigating the capability of various local search method to find the optimum of the subproblem. On the UQ side, a flexible and robust UQ method based on multi-fidelity non-intrusive polynomial chaos with regression was developed in this thesis. The method takes the advantage of flexible sampling and polynomial basis to estimate the polynomial coefficients as an alternative to the previously existing method that uses spectral projection. The improved optimizer shows that the local search based on achievement scalarizing and Chebyshev function were able to find higher quality solutions than the previous SS-MOMA that uses weighted-sum method for the local search. A dynamic normalization method based on the value of the offspring population was also introduced where the results on test problems clearly shows the improved diversity of the solutions. Moreover, on the UQ side, the new multi-fidelity algorithm successfully improved the approximation quality of the stochastic response surface with the requirement that the low-fidelity function should has high correlation and relatively low RMSE to the high-fidelity function. It was tested on several aerodynamic problems and shows evident improvement when the partially converged simulation was used as the low-fidelity samples. Both the optimizer and UQ were then applied to transonic airfoil robust optimization problem with the performance and robustness of lift-to-drag ratio as the objectives. Results on airfoil robust optimization revealed that the performance and robustness of lift-to-drag ratio are two conflicting objectives. However, closer examination revealed that only the airfoil with maximum mean is optimal in the true sense; although it is accompanied with high standard deviation. This is because the performance of the maximum mean airfoil is better than the other extremum airfoil over the response surface.

# List of publications during PhD thesis

**Conference publications**

- Palar, Pramudita Satria, Takeshi Tsuchiya, and Geoff Parks. "Decomposition-based Evolutionary Aerodynamic Robust Optimization with Multi-fidelity Point Collocation Non-intrusive Polynomial Chaos," in "Proceedings of the 17th AIAA Non-Deterministic Approaches Conference," AIAA, Kissimmee, Florida, 2015.
- Palar, Pramudita Satria, Takeshi Tsuchiya, and Geoff Parks. "Comparison of Scalarization Functions within a Local Surrogate Assisted Multi-objective Memetic Algorithm Framework for Expensive Problems," in "Proceedings of the 2015 IEEE Congress on Evolutionary Computation (CEC 2015)," IEEE, Sendai, Japan, 2015.

**Papers submitted to journal**

- Palar, Pramudita Satria, Takeshi Tsuchiya, and Geoff Parks. "Multi-fidelity Non-Intrusive Polynomial Chaos based on Regression," *Submitted*, Computer Methods in Applied Mechanics and Engineering, 2015
- Palar, Pramudita Satria, Takeshi Tsuchiya, and Geoff Parks. "Comparative Study of Local Search within a Surrogate-assisted Multi-objective Memetic Algorithm Framework for Expensive Problems," *Submitted*, Applied Soft Computing, 2015

# *Acknowledgements*

Everybody has different purpose for living. Some live for money and some live for fame. For me, the thirst and pursue of knowledge are the intangible things that motivated me for living; the knowledge for the advancement of the humankind and to understand our place in this vast universe. Completing a Ph.D is a small step forward for me to pursue this goal.

My greatest thanks goes to Professor Takeshi Tsuchiya for accepting me as a student in the University of Tokyo and for his constant guidance and advice for my research so I could finally complete my doctoral study.

I also want to say my sincere thanks to Professor Shinji Suzuki, Professor Kenichi Rinoie, Professor Akiya Oyama, and Associate Profesor Koji Shimoyama as the committees for my defense and for their very helpful feedback and suggestion to my research.

I wish to express my sincere thanks to the members of Suzuki-Tsuchiya laboratory: Dr. Chris Raabe, Dr. Jorg Entzinger, Dr. Yoshinori Matsuno, Mr. Takahiro Fujikawa, Mr. Kimura, Mr. Uemura, other laboratory members, and also our laboratory past members: Dr. Takuma Hino, and Dr. Adriana Andreeva Mori for the quality time and discussion about the research.

I would also like to thank Professor Geoffrey Thomas Parks for his guidance during my research stay as a visiting scholar in the University of Cambridge. His experience in the field of optimization and feedback about my research are very valuable to me. Special thanks also goes to Mr. Pranay Seshadri, Mr. Carlo Quaglia, and Mr. Valerio Lattarulo for the discussion and their time during my stay.

I also want to say my greatest thanks to the Japan International Cooperation Agency(JICA) for providing me with the scholarship to complete my doctoral study in the University of Tokyo. I am really thankful for helpful guidance and advice from Mr. Shigeya Goto and Ms. Kiuchi Marie during my time in Tokyo.

It is also important for me to express my gratitude to Associate Professor Lavi Zuhal in Bandung Institute of Technology who encouraged me to continue for PhD and for introducing and teaching me a proper way to do research. I also want to thanks Mr. Yohanes Bimo Dwianto for the fruitful discussion about memetic algorithm. I never thought before that discussion about research via Facebook chat could be so productive.

Finally, my special thanks goes to my wife, Anggraini, and my family for their constant support and encouragement that without them I would find it difficult to finish my PhD.

Lastly, I want to express my gratitude to the Japan country itself. I am really glad to be able to have a chance to study in Japan, a country that teaches me a lot about life philosophy, humanity, and worldly knowledge.

# Contents

# List of Figures

# List of Tables

*Dedicated to my parents, who give their son a freedom to choose his own path for living*

# Chapter 1

# Introduction

## 1.1 Engineering Robust Optimization - Motivation and Challenges

Competition in aerospace related business and race for more efficient designs have fostered the research and development of optimization method for aerospace design. Not just aerospace design, many engineering branches now also widely use optimization method to improve the performance of engineering products, to gain new insight and knowledge of the underlying physics, or to discover new phenomenons. Engineering optimization is now a rapidly advancing research field and topic in aerospace design. Many of the works are now focusing on the development of optimization algorithm, implementation aspect of the optimization method into the design process, and development of techniques to maximize the use of the available budget for optimization.

Aerospace design is characterized by a strong trade-off between the objectives to be optimized. Single-objective optimization of an engineering design very often produces a single solution which is superior in one aspect but has poor performance in other aspects. For example, a most aerodynamically effective wing shape typically has too smooth geometry, very difficult to be manufactured, and provides small space for structural components. Simply said, single objective optimization is an oversimplified approach where multi-objective optimization methodology that considers more than one objectives for an optimization process is required. Furthermore, to tackle the problem with interacting disciplines, the concept of multi-disciplinary optimization[1] methodology has been developed.

One of the main subjects in aerospace design and optimization is the field of aerodynamic optimization. This field is interesting due to the abundant challenge to be tackled. Aerodynamic design itself is one of the crucial parts for aerospace vehicle design. Aerodynamic design and optimization typically involve systematic alteration of the geometry to fulfill a specific requirement (for example, to find an airfoil with low drag) and computational tools to evaluate the performance of the aerodynamic bodies. The goal of optimization could be varied where investigating the trade-off between lift and drag coefficient

is only one of many example of the optimization objectives. In field of aerodynamics, the seminal paper that studied systematic procedure optimization of an aerodynamic shape is a paper by Hicks and Henne that pioneered the systematic procedure of the optimization of aerodynamic bodies[2]. Aerodynamic optimization is now an active research field with many researchers and practitioners around the world.

Methodology for aerodynamic optimization could be categorized into two streams: 1.) gradient based and 2.) non-gradient based optimization. Rapid development in gradient based method was triggered by research in adjoint method[3] that has its origin in the control theory. Adjoint method is an effective approach to calculate the derivatives for optimization purpose. The main limitation of gradient based method is that it only guarantees the discovery of the local optimum and its dependency to the initial solution. Even though the global optimum of the given problem could be found by using a multi-start gradient based method that starts from multiple solutions[4], gradient based method still found difficulties on more complex problems such as multi-objective or robust optimization problem. Moreover, adjoint method is also a discipline specific method in spite of its high effectiveness.

On the other hand, non-gradient based metaheuristics methods such as genetic algorithm[5] does not rely on the information of the gradients and can proceed to the optimum solution by relying only on the values of the objective function. Non-gradient based method is also suitable for multi-objective optimization purpose to discover the knowledge of the trade-off between the objectives. Aside from its simplicity, relatively easy implementation, and applicability to various problems (non-discipline specific method) that made the non-gradient based method becomes attractive, the main drawback of non-gradient based methods is that they typically need numerous function evaluations to reach the optimum solution/s. Method such as canonical genetic algorithm might needs about ten thousand to hundred thousand solutions to ensure that the high quality solutions are obtained. In aerospace engineering or any other engineering fields that require expensive partial differential equation (PDE) solver which could take minutes, hours, or even days, non-gradient based become practically not feasible. It still can be used to perform optimization process but the obtained optimized solution could still be far from the true global optimum for a given problem. To be able to release the full potential of genetic algorithm, improvement is needed to increase the performance of genetic algorithm to deal with expensive engineering problems. The challenge now is how to maximize the available computational budget where this could be done by the improvement of the existing optimization methodologies. One recently popular effort to deal with expensive engineering problem is by implementing the cheap replacement of the true function, which is popularly termed as the surrogate model. It is now very common to implement surrogate models to assist the process of expensive optimization in engineering problems.

Because the engineering products will be deployed to the real world that is full of uncertainty, optimization process that considers the effect of uncertainty is now on active and rapid development. This is motivated by the nature of traditional optimization that usually produces an over-optimized solution that performs excellent in on-design condition but deteriorates greatly on the off-design condition. The

presence of uncertainty that could significantly affects the nominal performance of an aerodynamic bodies is also motivating the development of robust optimization methodology. Such unsureness could exist due to the presence of uncertainty such as uncertain environmental condition and manufacturing error which are naturally not reducible; a so called aleatory uncertainty. Uncertainty could also arise from our lack of knowledge and understanding in the system under study which is termed the epistemic uncertainty. An example of the epistemic uncertainty is the choice of the non-physical parameters or assignment of $K - \epsilon$ value for turbulence modelling. Aleatoric uncertainty could be expressed in the probabilistic sense while the epistemic uncertainty could not. This is because assigning probability distribution to the epistemic uncertainty does not make sense due to the non-physical nature of the uncertainty itself. This different nature of the uncertainties results in different approach to understand and quantify the effect of the uncertainties to the system being investigated.

Optimization that does not consider uncertainty is simply termed as deterministic optimization where the counterpart of this is called robust optimization. The goal of robust optimization is to find the solution/s that is/are robust to the presence of uncertainty. If deterministic optimization is an expensive process, robust optimization is much more expensive since it involves the calculation of statistical moments that arise from the stochastic process. The main goal of robust optimization is typically to find solution/s that is/are optimal in the term of performance and robustness. This could be expressed in term of single objective mathematical equation which is simply the aggregate sum of the mean and robustness of solution. Another approach, since mean and robustness are typically two conflicting objectives, is the multi-objective approach that simultaneously optimize mean and robustness. An important part of robust optimization is the calculation of the robustness property which is usually expressed in the form of statistical moments. Because of its own complexity, a research field called uncertainty quantification (UQ) arose as a discipline and systematic way to calculate the effect of uncertainty into the system. The field of UQ ranging from theoretical discussion about the nature of uncertainties and development of the mathematical or statistical methods to calculate the effect of uncertainties. In a system where only the aleatory uncertainty is considered, the effect of the uncertainty could be mathematically expressed in the form of statistical moments such as mean and standard deviations.

Aerodynamic field provides vast research avenue for the study and application of optimization method to the aerodynamic design process. Optimization from aerodynamic point of view could be greatly beneficial to the overall aerospace product. In fact, the history of aerospace vehicle is about gaining speed and one of the keys lies in the aerodynamic technology. Beside of that, the system has to be safe, reliable, and environmentally friendly, which are very common requirements for the airliner.

In the scientific or industrial set-up, one does not always and rarely have the luxury of high performance massive supercomputers therefore limiting the available computational budget. Many researches in computational science dedicate the effort to speed up the computational PDE calculation, producing an accurate result with less computational time. On the other hand, the available computational

budget can also be optimized by having a better optimizer. Simply said, with the same amount of computational budget, good optimizer can find better solution compares to the worse optimizer. If robustness calculation is involved, effective UQ method can reaches better accuracy in the same amount of computational time with the other methods. Therefore, more relevant question to be tackled in the field of optimization is how to maximize the use of the available computational budget to achieve high quality solutions. In multi-objective problem, the goal is then to achieve high quality non-dominated solutions (the set of solutions with the optimum trade-off) with limited computational budget. This is the topic that this thesis revolves around, with contribution on the development of new algorithms.

## 1.2 Literature Review

Given the background and motivation, we review the existing literatures related to the field of optimization using metaheuristics, UQ, and robust optimization. The review of metaheuristics mainly refers to the past and recent development of the genetic algorithm method, that became the foundation of the development and improvement of the surrogate-based multi-objective optimization method in Chapter 3. On the other side, review of UQ fields heavily focus on the development of the methods based on polynomial chaos, as the foundation of Chapter 4.

### 1.2.1 Optimization using Metaheuristics and Surrogate Models

Heuristics optimization methods such as evolutionary algorithm travelled a long and windy road to find their way toward the acceptance in scientific community. The embryo of the evolutionary algorithms can be traced to the works of Schwefel and Rechenberg that performed experimental optimization for purposes such as reducing drag or increasing thrusts[6]. They found that traditional methods such as gradient based methods were not suitable for their purposes because of the presence of multiple local optimum and noisy measurement. To solve their problems, they developed evolution-strategy (ES) that optimizes solutions by a random but systematic manner. Motivated by its success in experimental optimization, they generalized and formalized the idea of the ES for application in general optimization problem that leads to the subsequent development of methods that are closely related to ES such as genetic algorithm. Genetic algorithm and ES are belong to the class of evolutionary algorithms, which is the optimization method that take concept from the Darwinian evolution.

A prominent metaheuristics method is the genetic algorithms (GA) method that was developed by by John Holland at the University of Michigan in the early 1970s[5]. GA directly mimics the process of Darwinian evolution and employs operators that are based on the biology jargon such as selection, crossover, and mutation, to solve the optimization problem. On the early times since its introduction, the method was not widely used and much of the works mainly deal with theoretical issues. Even until now there are very few theoretical basis for the metaheuristics based method which is in contrast to the

calculus based optimization method that heavily relies on the mathematical proof and strong theoretical basis. However, the ability of GA and the related methods to solve wide variety of problems accelerated its way toward the acceptance in the scientific community. The field of evolutionary algorithm was then advancing due to the rapid advancement of computational power and the necessity to solve difficult problems that are impossible or very difficult to be solved by gradient based approach. GA and other heuristic algorithms have now found their way in the scientific community and are now very popular methods in many research fields and practical applications.

Genetic algorithm has now became a popular algorithm in the field of global optimization. Thanks to its easy implementation and ability to deal with complex problems such as multi-modal and multi-objectives problem. GA can be used either for single or multi-objective problem with the difference is that on multi-objective problem the goal is typically to find the Pareto optimal set, or a set of solutions that are non-dominating to each others.

Beside of GA, many other metaheuristics to solve optimization algorithm have been developed and introduced. Among the popular algorithms are particle swarm optimization (PSO)[7], multi-objective evolutionary algorithm based on decomposition (MOEA/D)[8], $S$ metric selection evolutionary multi-objective algorithm (SMS-EMOA)[9], and ant colony optimization[10]. These algorithm are unique due to their principle and metaphors that are relevant to the problems they tried to solved. The last decade has witnessed the tsunami of new metaheuristics methods that borrow natural principle for the development of the algorithms. However, these algorithms suffers from critics due to the lack of novelty and minimum reference to the previous researches[11]. The critics suggest that the field of metaheuristics should move toward the promising direction instead of recycling the wheel.

One of the most popular genetic algorithm based method for multi-objective optimization is the non-dominated sorting genetic algorithm-II (NSGA-II)[12] due to its simplicity and excellent metaphor of optimization that is based on the principle of natural selection. NSGA-II algorithm relies on the non-dominated sorting operator that selects and keep the best solutions in term of the non-dominated front and diversity, ensuring that the solutions are steadily improved until it reach the true Pareto front. The NSGA-II has underwent subsequent development to the form of NSGA-III[13] to tackle many-dimensional problem. Several other algorithms use the concept of hypervolume to guide the search to find the Pareto front. Among popular hypervolume based method are HypE[14] and SMS-EMOA that were successfully tested on artificial and real test problems with few or many objectives. Aside from their advantages, NSGA-II and other type of evolutionary algorithms are mainly characterized by their slow convergence to the Pareto front[15] and this limits its full potential to be applied in real world problem. If the computational budget is limited, it is very possible that the terminated solutions is still far from the true Pareto front. Since EA needs numerous exact function call, the most adequate question is : how to optimize the available computational budget to find a set of solutions as good as possible? Many improvement of the algorithm were proposed, ranging from the modification of the evolutionary operator (intensive list could be seen in the book by Deb[16], hybrid with other optimizer such as

bacterial foraging [17], PSO[18, 19], Tabu Search[20], and implementation of local search algorithm (or memetic algorithm)[21, 22, 23, 24, 25, 26] to increase the efficiency of the optimizer. Memetic algorithm itself is an evolutionary algorithm equipped with local search module to perform local improvement of the solutions (individual)[27]. The name of the framework comes from the term of "meme" coined by Richard Dawkins in his book "The Selfish Gene"[28]. Use of a scalarizing function is one popular means of guiding the local search, although several other local search approaches such as the multi-objective Rosenbrock algorithm [21] and the hill climber with sidestep (HCS)[29] also exist. Memetic algorithm framework is an attractive approach that combines evolutionary operator with local search and could improve the performance of the base algorithm by exploiting the location near the solution to be improved to overcome the slow convergence problem of the EA. However, it hardly could solves the true expensive engineering problems which have limited computational budget because the local search procedure might still calls numerous function evaluations. Gradient information could assist the local search but not all problems readily provide this information. To cope with this problem, a methodology using multi-objective memetic algorithms with local surrogates has been developed [25].

The surrogate model methodology is an approximation the true function which act as a cheap replacement of the original exact function. By generating and evaluating the limited samples, a surrogate model is then built to predict the function value in the new unevaluated samples. Due to the requirement of numerous function evaluations needed by NSGA-II (or other multi-objective evolutionary algorithms) to reach the global optimum, combination of the multi-objective optimizer with surrogate modelling methodology is now a popular approach.

Methodology of surrogate models has been applied in cases such as airfoil optimization[30, 31, 32], compressor blade optimization[33], turbine blade[34]supersonic transport[35], wing optimization[36, 37, 38], and other applications. Kriging[39] is arguably the most widely used surrogate types due to its capability to predict the errors of the approximation and tunable hyperparameters that could affects the quality of approximation. To take the advantage of the availability of simulation with multiple level of fidelity, Co-kriging[40] method has been developed and successfully applied in multi-point optimization of airfoil[41] and turbine blade optimization[42], among others. Morever, excepted improvement (EI)[43] method that performs systematic and careful optimization by predicting the location of where the maximum improvement could be made is now a popular method to be used if the computational budget is very limited.

A combination of evolutionary algorithm with surrogate model could improves the search performance of the surrogate model especially if expensive function evaluation is involved and moderate number of function evaluations is available. The combination of the two methodologies is mainly done through the global surrogate modelling framework. The most traditional approach of using surrogate modelling is the global surrogate model approach [15] where all the available samples are used to build the surrogate model. The Pareto front of the approximation is then found using the optimizer and the exact function then evaluates the approximated Pareto front afterwards. This framework is used to good effect in

many engineering applications, some examples being studies by Keane [34] and multi-EGO by Jeong and Obayashi [30]. Various surrogate model exist, among the surrogate model that is common in the literature are radial basis function (RBF)[44], Kriging[45], polynomial regression[38], artificial neural network[46], and support vector regression[47]. Radial basis function and Kriging are the two prominent surrogate models commonly used in engineering and aerospace problems, especially Kriging that has the ability to predict errors over the decision space. Update of the approximated Pareto front could be done via several techniques such as random updates, secondary NSGA-II layer[15], or expected improvement (EI)[43]. However, implementation of the global surrogate modelling approach poses another difficulty in the form of the curse of dimensionality when the problem dimension increases [44]. Moreover, the training time of the hyperparameters (for Kriging) increases exponentially with increasing number of samples. One way to deal with longer training time is to use data-parallel learning and build localized surrogate model[48], but still the framework of surrogate model itself is a global one. To cope with these problems, a local surrogate model implemented inside the local search module of multi-objective memetic algorithm was developed[25].

Evolutionary algorithm optimization with local search based on a local surrogate was first introduced by Ong et al. [44] for a single-objective problem. Instead of using a global surrogate modelling framework that has a tendency to get trapped in local optima, their approach implements a trust region framework using radial basis functions (RBFs) inside the local search and local surrogate framework. Furthermore, an extension of this framework to multi-objective optimization, known as the single surrogate assisted multi-objective memetic algorithm (SS-MOMA), and a generalized surrogate version (GS-MOMA) have also been introduced [25]. The use of multiple surrogates [49] was also introduced to improve the approximation quality of the surrogate model. Several other algorithms that use the local surrogate concept have since appeared in the literature, with examples of such algorithms being the multi-objective memetic algorithm with aggregate surrogate model (ASM-MOMA) [50], which builds the surrogate model based on the distance to the currently non-dominated set, and the genetic diversity memetic algorithm (GDMA) [51]. A study of the effect of various local search methods (not scalarizing functions) on ASM-MOMA performance is given by Pilat et al. [52].

The main advantage of this local search-local surrogate framework is the combination of the power of an evolutionary operator and local search-local surrogate to, respectively, explore and exploit the search space. The use of a local surrogate also greatly reduces the number of function calls needed during the local search procedure. The algorithm perform local search on the offspring of the current generation and use weighted sum function to guide the local search implemented inside trust region framework.

The method is still open to the improvement since there are still some challenges to be tackled before it could be used practically in real world application. From algorithmic aspect, the weighted sum function has difficulty to deal with non-convex Pareto front. This difficulty might appears especially if the computational budget is low, thus an alternative is needed for the local search method. A fundamental aspect of the local surrogate assisted evolutionary algorithm (or local search in general) is the type

of scalarizing function employed within the local search module. The choice of scalarizing function could have a profound effect on the performance of an evolutionary algorithm with a local surrogate framework. However, despite its importance, there are few studies comparing different scalarizing functions within an evolutionary algorithm framework. One such study is the recent paper by Derbel et al. [53] that uses a (1+$\lambda$)-EA optimizer and tested this on bi-objective NK-landscapes. Furthermore, proper constraint handling method is required to deal with real problem. Simplicity of the constraint handling method implemented inside the surrogate objective memetic algorithm is also desired to reduce the complexity of the optimization code. In this thesis we improve the existing methodologies with practical application in mind. The improvement is done by equipping the SS-MOMA with achievement scalarizing function and various type of local search, simple adaptive constraint handling method, and normalization of the objective function. We also studied the effect of randomized weights and various normalization to the search capability of the optimizer.

### 1.2.2 Robust Optimization and Uncertainty Quantification

The presence of uncertainty is inevitable in an engineering or physical system. An example in aerospace engineering field is the uncertainty in the flight condition such as the uncertainties of Mach number and angle of attack where these uncertainties could affect the performance of the aerodynamic bodies. To understand and predict the effect of the uncertainties to the model under study, a systematic methodology of UQ was developed. An expensive partial differential equation solver is frequently employed to predict the physics of the system under study but it only made the prediction on a single condition without considering the uncertainty.

Deterministic aerodynamic optimization is a well studied research area and its literature is wide. The stream of adjoint-based optimization, triggered by the work of Jameson[3], is a well-established method and widely applied to aerodynamic design cases. Some of the application of adjoint-based method are application to airfoil design[54], wing[55, 56], high-lift configuration[57], complex aircraft configuration[58], supersonic bi-plane airfoils[59], helicopter rotor design[60], and flapping wing[61]. On the non-gradient side, early researches on the application of evolutionary algorithm to aerodynamic design can be traced in the work of Yamamoto and Inoue[62], Obayashi and Oyama[63], Oyama, Obayashi, Nakahashi, and Nakamura [64], Quagliarella and Della Cioppa[65]. Application of genetic algorithms and related metaheuristics method to aerodynamic design optimization are very popular. Some recent researches and applications are the application to vertical-axis wind turbine optimization[66], high-lift systems[67], Mars exploration aircraft[68], and over-the-wing-nacelle-mount configuration[69]. A comprehensive review on the application of multi-objective evolutionary algorithms in aeronautical design is the paper Aries-Montano, Coello Coello, and Mezura Montes[70]. An example of the innovation in this research is the use of surrogate model where the comprehensive review can be found in the paper of Forrester and Keane[71].

On the robust optimization part, early researches in robust optimization are the work of Lewis and Huyse and other researches which considers airfoil robust optimization under uncertain condition[72, 73]. Application of robust optimization methodology to airfoil problems is also well studied[74, 75, 76]. Keane compares three different optimization algorithms for robust optimization of turbine blades[34] by using Monte Carlo simulation (MCS) to calculate the statistical moments. Following this study, a multi-fidelity robust optimization was then introduced to minimize the computational cost[42] of turbine blades robust optimization. Previous studies that combine evolutionary algorithms and stochastic expansion can be found in the papers by Dodson and Parks[77], Ghizu et al.[78], Kato et al.[79], Cinnella and Herdus[80], Shimoyama[81], Song[82], and Walter[83]. A comprehensive survey of robust optimization can be found in the paper of Beyer and Sendhoff [84]. UQ is a fundamental part of the robust optimization and on the system where aleatoric uncertainty dominates, calculation of statistical moments plays a big part.

The simplest way to obtain the statistical moments in order to understand the effect of uncertainty to the system being investigated is by performing Monte Carlo simulation (MCS) and then averaging the results to obtain the mean performance and other statistical moments. By the law of large numbers, performing more simulation would result in more accurate statistical properties. However, to obtain an accurate value of the statistical moments MCS method typically needs ten to hundred thousand deterministic simulation where clearly this method is impractical if the deterministic simulation comes from an expensive computational fluid dynamics (CFD) or finite element method (FEM). Much of the research now is devoted on the development of the method that could compute accurate statistical properties with less and less computational budget. Some of these methods are Bayesian Monte Carlo[85], Taylor-based methods of moments[76], or univariate reduced quadrature method[86]. The main goal of these methods is the same : to reduce the number of deterministic evaluations while retaining the accuracy. One of the UQ method that is still in active and rapid development is the method based on the polynomial chaos expansion (PCE). PCE works by approximating the stochastic response surface between the random input and output of interest by using the orthogonal polynomials. The power of PCE is located on its mathematically rigorous concept[87], strong theoretical basis, and ability to converge to machine precision. On the early development of PCE methodology, PCE was a highly intrusive method[88, 89] where it is necessary to modify the existing codes to be able to perform UQ procedure, which is quite cumbersome. This means that we cannot perform UQ procedure using the intrusive method if we do not have the access to the PDE solver codes. An alternative is by using the non-intrusive PCE[90] by performing multiple simulations and use special techniques (regression/spectral projection) to estimate the coefficients needed to build the polynomial expansion. A non-intrusive alternative is more popular nowadays because there is no need to modify the codes and the relation between the random input and the outputs could be treated as the black-box function.

A combination of PDE solver and UQ methodology provides an excellent framework to predicts the impact of the uncertainties to the output of interest. Since the first time it was introduced, there have been many researches to improve the efficiency of NIPC. Much of these methods have the common

goal to reduce the number of deterministic simulation while still retaining the same or higher accuracy. The techniques to calculate coefficients in NIPC are mainly classified into two classes : 1) Spectral projection, where the responses are projected to the basis function using inner products and employ the orthogonal polynomial to obtain the coefficients, or 2) Point collocation, where the coefficients are obtained by performing least squares[91].

Tensor product is the traditional way to expand the polynomial expansion and the collocation points if the spectral projection approach is used but it greatly suffers from the curse-of-dimensionality. To reduce the curse-of-dimensionality problem, sparse tensor product spaces method that was first introduced by Smolyak[92] could be employed. Sparse grids method has underwent further investigation for applications to stochastic collocation method and UQ together with the adaptivity[93, 94, 95]. A proper and correct way to calculate the polynomial chaos coefficients using sparse grid was introduced with the name of sparse pseudospectral approximation method (SPAM)[96]. An adaptive version of the SPAM was developed to reduce the computational cost by focusing the growth of the sparse grids on important dimension[97].

An adaptive sampling method for point-collocation was introduced by using the aid of multi-variate interpolation (MIR)[98] to predict the location where the discrepancy between the current polynomial-expansion and local MIR surrogate is high[99]. Point-collocation method was also applied intensively in airfoil application for robust optimization purpose in the presence of aleatoric, epistemic, or mixed uncertainty[100, 101, 102]. Point-collocation method was already applied to hypersonic reentry flows[103, 103], synthetic jet actuator[104], and any other applications. It was also well suited for application to epistemic UQ that uses non-probabilistic theory such as evidence theory[105]. Furthermore, least angle regression (LAR) method[106] could be employed to choose the best polynomial basis to improve the accuracy of the method which had underwent subsequent development by incorporating principal component analysis[107].

Beside of the polynomial chaos based method, some other recent methods for UQ purpose are simplex stochastic collocation[108] that use piecewise polynomials to approximate the stochastic response surface, adaptive sampling Kriging-based monte carlo simulation[109], and univariate reduced quadrature technique[86]. PCE which is based on the global polynomial approximant encounter serious difficulty in problems with strong discontinuity. One way to tackle this problem is to use piecewise type approximation[108, 110, 111], rational function[112, 113], or multi-element probabilistic collocation method[114, 115]. Uncertainty quantification in shock-dominated flow might exhibits this kind of discontinuity so other methods are more approriate for this kind of cases compares to the standard PCE. Approximation of the multi-modal functions for either UQ or optimization purpose can be done using methods such as combination of polynomial chaos and Kriging[116] where the idea is to use polynomial chaos to capture global landscape with Kriging approximating local behaviour of the function.

Sensitivity analysis procedure can be readily performed using polynomial chaos expansion[117, 118, 119], thanks to the use of the orthogonal polynomials. Sensitivity analysis study has a purpose to investigate

the contribution of the variables to the quantities of interest (QoI) and also the interaction between variables. This is useful if the dimensionality is high and dimensional reduction is needed beforehand.

It is common to encounter the availability of multiple level of simulation fidelity in the PDE-based system. Generally, the high fidelity simulation takes longer computational time but has higher accuracy where the low fidelity simulation is faster but the accuracy is lower. The availability of multiple fidelity level is popular in assisting the process of optimization, prominently in aerodynamic optimization field. Examples of such works are the multi-fidelity optimization of the low boom supersonic business[120], transonic airfoils[121, 122], rotor blade[123], and flapping flight[124]. The design of experiment method (especially Kriging) also take advantage of this multi-fidelity with the development of Co-kriging method[40]. A multi-fidelity Kriging was also applied to airfoil optimization case[41]. Recently, an interest to employ simulations with multiple level of fidelity for UQ has fostered the development of multi-fidelity UQ. A recent multi fidelity UQ method is the multi-fidelity NIPC developed by Ng and Eldred[125] that employs multiple fidelity simulation to perform UQ incorporated to the different level of sparse grid. The method successfully reduce the computational work in several test problems as long as the low-fidelity stochastic response output trend could assist to sufficiently predict the high fidelity one[125]. Application to vertical axis wind turbine[126] is an example of the method's application. The drawback of the method is that because it relies on the spectral projection method to calculate the coefficients the number and location of collocation points could not be arbitrary. The limited choice sample size made the user/designer have less flexibility in performing UQ with limited computational time or sample locations. Furthermore, the method still suffers from the curse-of-dimensionality even though the sparse-grids could gives some remedy to reduces the effect. With this spirit, we develop a multi-fidelity extension of point collocation non-intrusive polynomial chaos (PCNIPC) that has the advantage of flexibility in choosing the number and location of collocation points. Such advantages are practically useful when flexibilities are needed. A slightly similar method is the multi-fidelity method that use corrected space mapping for robust optimization purpose[127]. However, the method developed in this thesis uses the correction term to estimate the coefficients and is specifically designed for UQ purpose.

## 1.3 About this Thesis

The main contribution on this thesis lies on two parts where the main goal is to develop an effective framework for engineering robust optimization. The first part is the improvement of the surrogate-based algorithm to perform multi-objective optimization while the second one is the introduction of a new multi-fidelity algorithm for UQ with polynomial chaos. Both optimizer and UQ algorithms were improved and developed to increase the efficiency of robust optimization that uses evolutionary algorithm as the main optimizer.

The optimization algorithm is wrapped inside the multi-objective memetic algorithm framework that uses local surrogate to assist the local search to improve the offsprings. Single surrogate assisted multi-objective memetic algorithm (SS-MOMA)[25] is used as the base algorithm for improvement. Various type of local search is studied in this thesis to see whether improvement could be made by introducing different type of scalarizing function or local search methodology. Study on the effect of randomized weights and normalization method were also performed. The improved algorithm is then tested on various artificial and real (aerodynamic) test problems and compared with the original SS-MOMA and NSGA-II algorithms. We also discuss the practical and implementation issue of the algorithm to the real world optimization problem.

Furthermore, we also developed the new multi-fidelity framework for regression based NIPC. The development itself is motivated by the need of flexibility and robustnesss to perform UQ. A multi-fidelity point-collocation non-intrusive polynomial chaos (PCNIPC) is developed in thesis to tackle UQ problem by incorporating regression based coefficient estimation, unstructured samples, and multi-fidelity framework. The algorithm itself is based on the projection based multi-fidelity NIPC algorithm developed by Ng and Eldred[125]. One of the drawbacks of the algorithm is that it relies on sparse grids to build the low and high fidelity samples. The method is very effective on low dimension but the number of collocation points could blow up in high dimension because the sparse grids methodology still suffers the curse-of-dimensionality problem. In contrast, the MF-PCNIPC developed in this thesis is very flexible in choosing the location of low- and high-fidelity samples and there are much flexibility in building the polynomial basis. The sampling methodology takes advantage of the nested sequence to effectively determine the samples because the high fidelity samples are automatically the subset of the low fidelity samples if nested sequence is used. To test and see the capabilities of multi-fidelity NIPC, the new UQ algorithm is tested on various test problems from low to high number of random variables including aerodynamics problems. Furthermore, practical concern and issues of the algorithms were also discussed.

Finally, both the improved optimizer and new UQ algorithm are applied to aerodynamic robust optimization case. The objectives are to minimize the mean and standard deviation of lift-to-drag ratio in the presence of aleatory uncertainty. The selected non-dominated solutions obtained from this procedure were then investigated to reveal some characteristics of the robust shape.

Even though most of the application in this thesis is on the field aerodynamic optimization, the developed and improved methods is generic in the sense that it could be applied to various field and not limited to aerodynamic field only.

## 1.4 Research Objectives

Based on the motivations and backgrounds, the objectives of this researches are as follows:

**1. To enhance and improve the existing multi-objective optimization algorithm with surrogate model to tackle expensive multi-objectives optimization problem.**
Application of surrogate model in aerodynamic optimization is not new but there are still many room for improvements. Application of surrogate model to multi-objective optimization problem wrapped inside memetic algorithm framework is still not widely explored so there are still some challenges that lie ahead. Here in this thesis the focus is on the study of the effectiveness of various local search methodology to be implemented inside the optimizer. The goal is to study the effect of different local search methodology and to what extend that it affects the search process. Moreover, several improvements and practical aspects are considered to maximize the potential of surrogate based memetic algorithm framework for real expensive engineering optimization problem.

**2. To improve an existing UQ methodology based on multi-fidelity point-collocation non-intrusive polynomial chaos.**

Currently existing UQ methodology based on PC-NIPC still left room for improvement in the flexibility to be applied for expensive UQ problem. In this thesis, a multi-fidelity extension of PC-NIPC is presented to increase the efficiency and flexibility of the PCE method when solver with two or more fidelity level are available. The multi-fidelity PCNIPC was then studied and tested in some artificial and artificial aerodynamic problems to study the advantages and drawbacks of this method.

**3. To develop an effective framework for robust optimization that combines evolutionary algorithm, polynomial chaos expansion, and surrogate model.**
Due to the complexity of the problem (high dimension, uncertainties, and expensive evaluation) of robust optimization problem, an effective framework to obtain the optimum solutions with minimum cost is desired. The framework introduced in this thesis is a combination of memetic algorithm with surrogate models and multi-fidelity point-collocation NIPC method as the optimizer and UQ algorithm, respectively. Improvements of both methodologies were studied in this thesis to increase the efficiency of the framework. Combining all of these concepts is crucial to be able to effectively perform real world robust optimization, hence combining all the concepts and algorithms into one framework is also the goal of this thesis.

## 1.5 Structures of this thesis

The structure of this thesis is as follows:

- **Chapter 1** presents an introduction of this thesis. The chapter includes the background and motivation of the thesis, literature review, about the thesis, thesis objectives, and structures of this thesis.

- **Chapter 2** contains basic theory of optimization, surrogate models, UQ using polynomial chaos, and robust optimization.

- **Chapter 3** deals with the improvement of an existing surrogate-assisted multi-objective memetic algorithm to solve an expensive multi-objective optimization problem. The SS-MOMA algorithm that acts as the basis and building block for improvement is explained first where an improved version of the SS-MOMA algorithm is then explained in detail. The chapter ends with the numerical experiment on artificial and aerodynamic problems to study and comparison of the capability of the improved optimizer to the original SS-MOMA and NSGA-II.

- **Chapter 4** deals with the development of new framework for multi fidelity UQ based on polynomial chaos that uses regression to estimate the polynomial coefficients. The chapter starts by brief explanation of the previously existing multi-fidelity PCE based on spectral projection. A thorough explanation of the regression-based (point-collocation) multi-fidelity polynomial chaos is then given together with results on artificial and aerodynamic test problems.

- **Chapter 5** deals with the application of both improved optimizer and new UQ algorithm to aerodynamic robust optimization problem.

- **Chapter 6** summarizes the results and findings from this thesis with the conclusion and possible future works.

# Chapter 2

# Fundamental Theories

This chapter explains the theoretical foundation of multi-objective optimization, genetic algorithm, surrogate model, robust optimization, and uncertainty quantification. At the end of the chapter the contribution of the thesis to the research community is briefly explained. The focus of this thesis is on the expensive optimization problems because it is a typical challenge that needs to be addressed by the engineering community. Expensive here means that the available budget to perform simulations needed for optimization is limited and this is especially true if robust optimization is involved. For example, a single evaluation that solves Navier-Stokes equation or finite element method that take about minutes or hours can be considered as an expensive simulation in the context of optimization using metaheuristics optimizer.

## 2.1 Multi-Objective Optimization

Optimization is a systematic process that has a goal to find a best solution or a set of solutions given some set of available alternatives. Mathematically speaking, the general goal of optimization is to find solution/s with a set of design variables that produces the optimum value of the objective function where the objective function itself is a function of the design variables. This best solution is called the optimal solution and no other solutions in the problem space are better than this solution. For the ease of clarity we will define an optimization process as the minimization of a function where maximization can be transformed into minimization by simply multiplying it with a minus term. The optimization problem can be expressed mathematically as:

$$\text{minimize: } f(x) \tag{2.1}$$

$$\text{s.t: } \boldsymbol{g(x)} \leq 0 \tag{2.2}$$

$$\boldsymbol{h(x)} = 0 \tag{2.3}$$

$$x \in \Omega \tag{2.4}$$

The aim is to find the solution $x$ that minimizes the single objective $f(x)$ and satisfies the inequality constraint $\boldsymbol{g(x)}$ and equality constraints $\boldsymbol{h(x)}$. $\boldsymbol{g(x)}$ and $\boldsymbol{h(x)}$ are the vector of $L$ inequality constraints $\boldsymbol{g(x)} = [(g_1(x), g_2(x), ..., g_L(x)]$ and $N$ equality constraints $\boldsymbol{h(x)} = [(h_1(x), h_2(x), ..., h_N(x)]$, respectively. $\Omega$ is the set of decision vectors that is bounded by its upper and lower values. In calculus language, the minimum solution has zero gradients of the objective function with respect to the design variables. This means that the optimum solution could be find by calculus based methods that rely on the gradient information of the solution.

A typical illustration of the single-objective optimization problem is depicted in Fig. 2.1 where the goal is to find the maximum (remember that maximization is simply a negative minimization) solution of $f(x)$ that has single design variable. The optimization problem could exhibits a single-peak (unimodal) or multiple peak (multimodal). In unimodal problem there is only a single peak which correspondents directly to the global optimum of the problem, which is the solution A in Fig. 2.1a. Multi-modal problem is more difficult because it exhibits multiple local optimum and there is a possibility that the optimizer will get trapped in the local optimum (solution B, C, D, or E) and unable to found the global optimum (solution A) as it is shown in Fig 2.1b. Usually there is a little or no interest with the local optimum and the task is only to find the global optimum of the optimization problems.

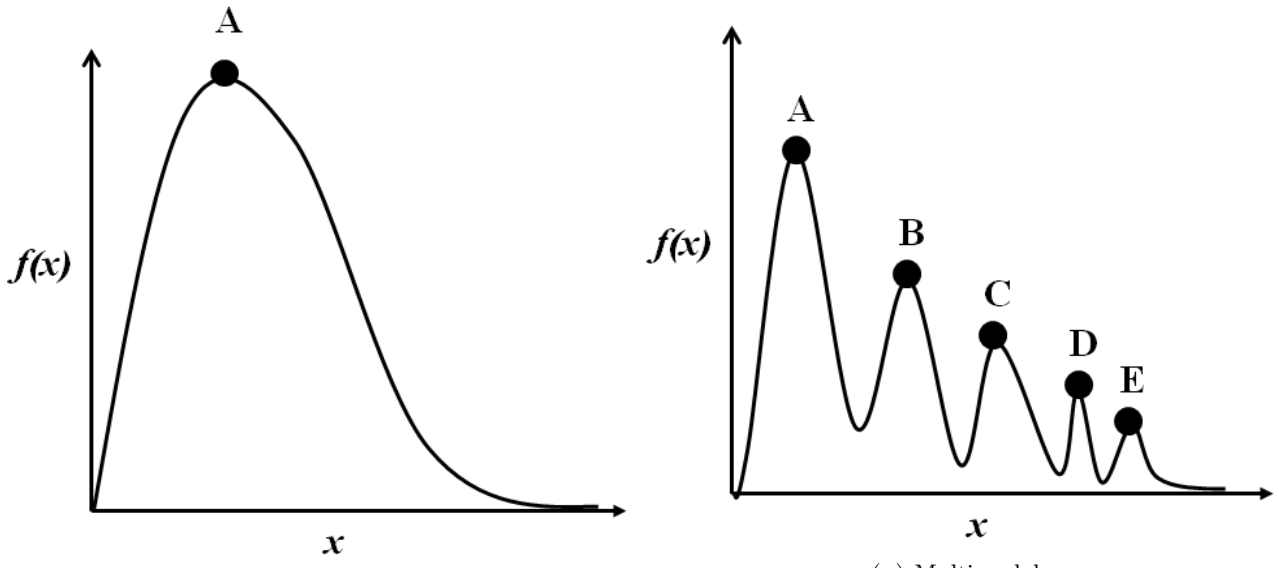


(A) Unimodal.

(B) Multimodal.

FIGURE 2.1: Illustration of single-objective optimization.

Real engineering design and optimization rarely involve one objective to be optimized. Most cases involve two or more objectives that have to be simultaneously optimized to obtain optimized practical designs where this type of optimization is called multi-objective optimization. Multi-objective

optimization problem can be mathematically expressed as:

$$\text{minimize: } [f_1(x), f_2(x), ..., f_M(x)] \tag{2.5}$$
$$\text{s.t: } \boldsymbol{g(x)} \leq 0 \tag{2.6}$$
$$\boldsymbol{h(x)} = 0 \tag{2.7}$$
$$x \in \Omega \tag{2.8}$$

Where the integer $M$ is the number of objectives. The optimal solution in multi-objective optimization is the collection of solutions that do not dominate each other and are not dominated by all other possible solutions in the objective space set. "Dominance" and "Pareto-optimality" could be mathematicaly defined as[16]:

- **Definition 1: Dominance** In the multi-objective problem where multiple objective functions $\boldsymbol{f(x)} = [(f_1(x), f_2(x), ..., f_M(x)]^T$ must be minimized, a solution $\boldsymbol{x}_i$ is said to dominate the other solution $\boldsymbol{x}_j$ if all the following inequalities are satisfied:

$$f_k(x_i) \leq f_k(x_j), ^{\forall} k = 1, 2, \ldots, M$$
$$f_k(x_i) < f_k(x_j), ^{\exists} k = 1, 2, \ldots, M$$

- **Definition 1: Pareto-optimality** A solution $\boldsymbol{x}_i \in \Omega$ is said to be Pareto-optimal if there is no other solution $\boldsymbol{x}_j \in \Omega$ which dominates $\boldsymbol{x}_i$

This optimal set is called Pareto front which is the goal of multi-objective optimization and is illustrated in Fig. 2.2. Single-objective optimization procedure will find one solution that lies in edge of the Pareto front (solution A and B in Fig. 2.2). Good multi-objective optimization algorithm will return the solutions that covers a wide section of the Pareto front.

Also shown in the figure are the ideal and nadir point which components are the lower and upper bound of each objective in the Pareto optimal set, respectively.

The simplest approach to solve multi-objective optimization problem is to transform the multi-objective problem into a single-objective problem which is the aggregate sum of the objective functions with defined weights:

$$\text{minimize: } \sum_{i=1}^{M} w_i f_i(x) \tag{2.9}$$

Where $w_i = (w_1, w_2, ...w_M)$ is a weight vector and $\sum_{i=1}^{M} w_i = 1$

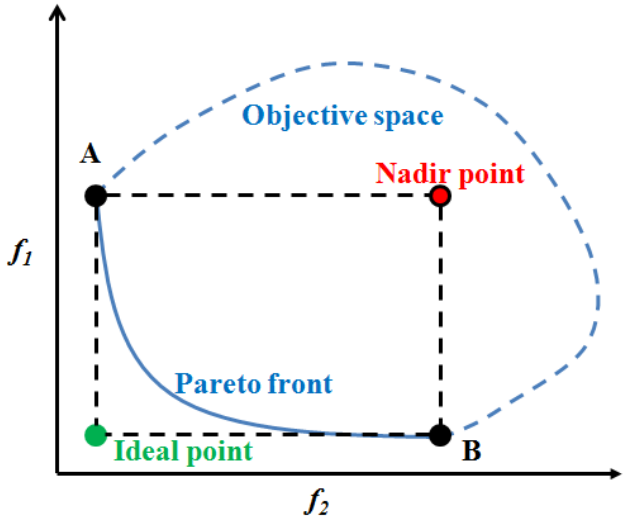


FIGURE 2.2: Illustration of multi-objective optimization.

The drawback of the aggregate-sum method is that it cannot adequately solves problems with non-convex and discontinuous Pareto front. Moreover, to cover the entire Pareto front (for convex Pareto front) the optimization problem has to be solved numerous times by varying the weights, which could be expensive.

A non-gradient based metaheuristic method is attractive due to its ability to simultaneously solve the multi-objective optimization problem to find the Pareto front. Genetic algorithm is one popular example of metaheuristics method that use Darwinian concept of natural evolution for the metaphor. The metaheuristic evolutionary approach is considered in this thesis as a method to discover the Pareto front. For more detail on classical method in multi-objective optimization reader is suggested to refer to more specific paper or books[128].

## 2.2 Multi-Objective Optimization with Genetic Algorithm

Genetic algorithm (GA), which is based on the principle natural evolution, does not need any gradient information to search and solve the optimization problems. Instead of starting with a single solution, GA starts with a set of population of solutions that evolved from generation to generation by mainly relying on the information of the objective function values and fitness function. If the objective function is the equation that needs to be optimized, fitness function is the quality indicator of the solution that defined its fitness to be selected as the parent for the next generation. GA improves the quality of solution by iteratively trying to improve the solution in each iteration until it reach the convergence criteria. The advantage of GA and other non-gradient based metaheuristics method is that the likelihood to discover the global optimum is higher than the gradient based method.

Multi objective optimization using GA relies on different quality assessment for solution compares to single objective optimization. If in single-objective optimization the objective function is equal to the fitness function, multi-objective optimization uses different concept for fitness function due to the existence of multiple optimum solutions that lies on the Pareto front. Multi-objective optimization method such as non-dominated sorting genetic algorithm (NSGA)[129] uses the principle of non-dominated sorting to measure the quality of solution.

The goal of the multi-objective optimization with GA is to find finite representative solutions of the Pareto front. This set of solutions has to be as close as possible to the true Pareto front (convergence) and should represents a wide range of the Pareto front (diversity). Some possible scenarios of the solutions returned by the GA are depicted in Fig. 2.3. The final solutions could have a high diversity property but lack in the quality of convergence to the Pareto front as it is shown in Fig. 2.3a. Other scenario is depicted in Fig. 2.3b where the convergence is very good but is lacking of the diversity, causing some important information to be missed on the undiscovered section. Fig. 2.3c shows the ideal final solutions generated by GA where the solutions are very close to the Pareto fronts and can cover a wide section of the Pareto front, thus give optimum (or near optimum) information of the Pareto front. However, if there are too few points available this could results in a lack of information, as it is depicted in Fig 2.3d where many sections of the Pareto front are not covered.

The application of genetic algorithm (and evolutionary algorithm in general) to the multi-objective optimization field is revolutionary due to its ability to find the whole Pareto front in a single run of optimization algorithm. This has driven an interest to the specific field of genetic/evolutionary algorithm called multi-objective optimization using genetic algorithm (MOGA). One of the successful MOGA is the NSGA-II developed by the research group in evolutionary algorithm at IIT Kanpur[12] and has been widely applied to many research field and real world application. Even though some new algorithms such as multi-objective particle swarm optimization (MOPSO)[130], multi-objective evolutionary agorithm based on decomposition (MOEA/D)[8], $S$-metric selection evolutionary multi-objective algorithm (SMS-EMOA)[9], and hypervolume based algorithm (HypE)[14] have been developed and studied, NSGA-II is still a popular algorithm due to its proven capability in many applications. The SMS-EMOA and HypE are algorithms that mainly rely on the principle of maximizing the hypervolume which is closely connected to obtaining a good quality Pareto front. This approach is useful in high dimension where the performance of dominance based algorithm deteriorates. Nonetheless, on low dimension problems such as two or three dimensions of objective function the non-domination principle is still particularly useful.

In this thesis, we refer only to the genetic algorithms where detail of other algorithms such as MOPSO and MOEA/D could be found on their original papers. GA's main operator are the crossover and mutation operation that alter the solutions and increase the quality of solutions from generation to generation. Selection operator has a purpose to control the quality of solutions and to select the better solutions as the parents for the next generation. Crossover operator combines and exchanges the genetic

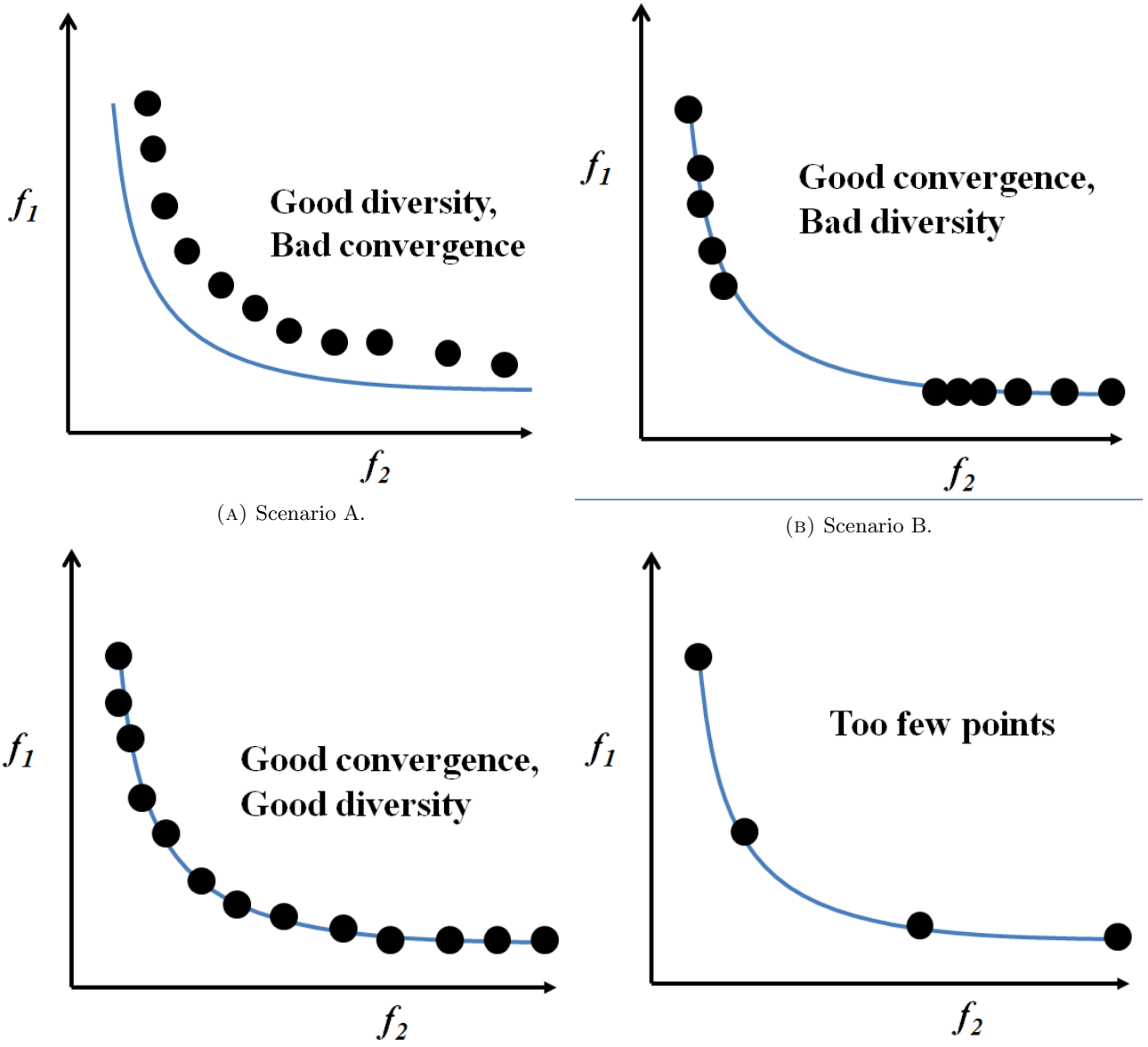


(A) Scenario A.

(B) Scenario B.

(C) Scenario C.

(D) Scenario D.

FIGURE 2.3: Possible result's scenarios of multi-objective optimization.

information of the parents to produce offspring that has a hopefully improved fitness value. Therefore, good crossover operator ensures that the quality of solutions improved from generation to generation. However, applying crossover operator only is not enough because it is able to evolves the solution but it is prone to the local optimality. If the optimizer got trapped at local optimum, the GA relies on the mutation operator to make the solution "jump" and escapes from the local optimum. The work in this thesis uses NSGA-II as the basic foundation for the single-surrogate assisted multi-objective memetic algorithm (SS-MOMA, explained in Chapter 3) so we explain the basic algorithm of NSGA-II in detail first. On explaining the NSGA-II, we mainly refer to its original paper[12] where the detail of its distinct operators could be seen in this paper. More details of the evolutionary operators can be found in the Appendix B.

Non-dominated sorting genetic algorithm II (NSGA-II) is one of the multi-objective genetic algorithm (MOGA) that can search multiple Pareto-optimal solutions in a single run. It is a modification of the previous method of NSGA[129] because of some criticisms such as[12]:

- High computational complexity of non-dominated sorting.
- Lack of elitism.
- Need for specifying a user-defined sharing parameter $\sigma_{share}$.

NSGA-II works with the additional two main systems in approaching the Pareto-optimal region and preserves the diversity among the Pareto-front solutions. To approach the Pareto-optimal region, NSGA-II uses a system called fast non-dominated sorting approach. The algorithm will divide the solutions of the population $P$ from the first to the last front of Pareto-optimal region. The first front is the candidate of the Pareto-optimal solutions.

To preserve the diversity of the solutions, NSGA-II uses a system called crowding distance calculation. This is a system to calculate the average distance of two points on either side of one solution in each front. This distance quantity serves as an estimation of the perimeter of the cuboid formed by using the nearest neighbors as the vertices. The overall crowding distance value is calculated as the sum of individual distance values corresponding to each objective. Each objective is normalized before calculating the crowding distance. From these two schemes, for two solutions, the solution preferred is the solution with lower (better) rank. If both solutions are in the same front, the solution with lesser crowded region is preferred.

The fast non-dominated sorting and crowding distance calculation are the fundamental tools in NSGA-II. The main loop of the process, however, is also quite different from other basic GAs. The main loop of NSGA-II (either binary or real NSGA-II) is as follows:

1. A random initial parent population $P_c$ of size $N$ is created.
2. Fitness values for each solution in the population corresponding to each objective are calculated. For binary NSGA-II, each solution is decoded first.
3. The solutions in the population are then sorted based on their non-domination rank and crowding distance.
4. The tournament selection, recombination, and mutation operators are used to create an offspring population $P_o$ of size $N$.
5. To ensure the elitism, a combined population $R_o = P_c \bigcup P_o$ is formed.
6. The solutions in population $R_o$ are then sorted to get the non-dominated fronts of the population $R_t$.

7. To create new population $P_{c+1}$ with size $N$, $N$ solutions with best rank (lowest front) and best crowding distance (largest distance) form population $R_t$.

8. Step 4 to Step 7 are repeated by using $P_{c+1}$ as the parent population to create offspring population $P_{o+1}$ and combined population $R_{o+1}$.

The term $o$ is the number of generation of the population.

As explained in the previous subchapter, constraints may hinder GA in converging to Pareto-optimal region and causing difficulty to maintain the diversity of the solutions in one front. For the purpose to overcome the hindrance of the constraints, the constraints need to be handled[131].

The constraint handling method uses the tournament selection, where two solutions are picked from the population and the better solution is chosen. In the presence of constraints, the solutions may be feasible or infeasible. Therefore, there may be three situations for each solution:

- Both solutions are feasible.
- One solution is feasible, while the other one is infeasible.
- Both solutions are infeasible.

Because of these three situations, the definition of non-dominated solution is modified into the following criteria:

*Definition*: A solution $x_i$ is said to constrained-dominate a solution $x_j$ if any of the following conditions is true.

- Solution $x_i$ is feasible and solution $x_j$ is not.
- Solution $x_i$ and $x_j$ are both infeasible, but solution $x_i$ has a smaller overall constraint violation.
- Solution $x_i$ and $x_j$ are both feasible and solution $x_i$ dominates solution $x_j$.

We adopt a simple adaptive constraint handling method to deal with multiple constraints with different magnitudes. Assuming that the maximum constraint violation is not already known (the minimum violation is zero, of course), the maximum violation value is updated on the fly. The adaptive constraint violation equation for $k$ number of constraint is:

$$c_{tot} = \sum_{i=1}^{k} |\frac{c_i}{c_{i_{max}}}| \tag{2.10}$$

where $c_{tot}$, $c_i$, and $c_{i_{max}}$ are the total constraint violation, the constraint violation for each constraint term, and the maximum constraint violation value found so far, respectively. The maximum possible value for $c_{tot}$ is thus the total number of the constraint terms.

The single-surrogate assisted multi-objective memetic algorithm (SS-MOMA) which will be explained in Chapter 3 uses the NSGA-II as the basis algorithm with the addition of local search and local surrogate model. Therefore, we briefly explained surrogate model with focus on the radial basis function and Kriging type surrogate model.

## 2.3 Surrogate Modelling

Surrogate model works by approximating the true function with the "surrogate" function and uses this surrogate to predict the function value at new location. Surrogate model is an active ongoing research trend in the optimization community due to its capability to greatly assist the optimization process. The use of surrogate model is highly useful if the underlying black box function is expensive and consumes a long computational time. Polynomial regression and artificial neural network (ANN) are two examples of early surrogate model methods. More early popular surrogate model to be applied for various application are the surrogates which are based on radial basis function (RBF) or Kriging, which we are focusing on in this thesis.

The approximation starts by choosing the samples $\mathbf{X} = \{x^{(1)}, x^{(2)}, ..., x^{(n)}\}^T$ and the responses $y = \{y^{(1)}, y^{(2)}, ..., y^{(n)}\}^T$ where $n$ is the number of samples. Using this information of samples location and response, a specific surrogate model method can then be used to build the approximation model of the black-box function. The concept of approximation using RBF and Kriging is explained in the following, where that explanation refers to the book written by Forrester et al. [132].

### 2.3.1 Radial Basis Function

A radial basis function (RBF) is a real-valued function which the value depends on the distance from the origin. The expression for RBF approximation $\hat{f}$ is:

$$\hat{f}(x) = \mathrm{w}^{\mathrm{T}}\boldsymbol{\psi} = \sum_{i=1}^{n_c} w_i \psi\big(||x - c^{(i)}||\big) \tag{2.11}$$

Where $x$ and $c^i$ are the prediction site and the centres of the basis function, respectively. The centre of the basis function $c^i$, which are the samples to be evaluated, can be chosen by using methods such as random sampling, latin hypercube sampling, low-discrepancy sequence, or any other methods. The behaviour of the real function is then modelled by the information obtained from this samples and the type of the RBF functions used. Several type or RBF type functions are listed in the following:

- linear $\Psi(r) = r$
- cubic $\Psi(r) = r^3$
- thin plate spline $\Psi(r) = r^3$
- Gaussian $\Psi(r) = e^{-r^2/(2\sigma^2)}$
- multiquadric $\Psi(r) = (r^2 + \sigma^2)^{1/2}$
- inverse multiquadric $\Psi(r) = (r^2 + \sigma^2)^{-1/2}$

Linear, cubic, and thin plate splines are parameter free RBF while Gaussian, multiquadric, and inverse multiquadric needs further estimation of the parameters (such as $\sigma$).

The following equation has to be solved to obtain $w$:

$$\Psi \mathrm{w} = \mathrm{y} \tag{2.12}$$

where $\Psi_{i,j} = \psi\big(||x^{(i)} - x^{(j)}||\big)$, $i$, $j$ = 1,...,$n$, and is called the *Gram matrix*. Here $n = n_c$ because the $\Psi$ matrix is a square form matrix.

A complex and nonlinear function can be expressed by the finite linear combination of the radial basis function, which is the strong point of the RBF type approximation.

If the noise corrupts function to be modelled, a regularization parameter $\lambda$ can be used that results in the regression type approximation instead of interpolation. The $w$ then should be estimated by:

$$w = (\Phi + \lambda \mathrm{I})^{-1} \mathrm{y} \tag{2.13}$$

### 2.3.2 Kriging

Kriging approximates the function to be modelled by the combination of the basis function of:

$$\psi^i = \exp\Bigg( -\sum_{j=1}^{k} \theta_j |x_j^{(i)} - x_j|^{p_j} \Bigg) \tag{2.14}$$

Kriging basis has a tunable vector $\boldsymbol{\theta} = \{\theta_1, \theta_2, ..., \theta_k\}^T$ which means that the width of the basis function can vary. The exponent of the Kriging basis $\mathbf{p}_j = \{p_1, p_2, ..., p_k\}^{\mathbf{T}}$ is also tunable and can be varied for each dimension. These parameters are called the hyperparameters which can be tuned to minimize the approximation error. This flexibility of the hyperparameters allows Kriging to approximate a very complex function with a finite number of samples.

The hyperparameters can be optimized by performing the maximization of the log-likelihood function:

$$\ln(L) \approx -\frac{n}{2}\ln(\hat{\sigma}^2) - \frac{1}{2}\ln|\mathbf{\Psi}| \tag{2.15}$$

Where $\mathbf{\Psi}$ is the correlation of the random variables:

$$\text{cor}[Y(x^{(i)}), Y(x^{(l)})] = \exp\left( -\sum_{j=1}^{k} \theta_j |x_j^{(i)} - x_j^{(l))}|^{p_j} \right) \tag{2.16}$$

A correlation matrix $\mathbf{\Psi}$ can then be calculated by:

$$\mathbf{\Psi} = \begin{pmatrix} \text{cor}[Y(x^{(1)}), Y(x^{(1)})] & \cdots & \text{cor}[Y(x^{(1)}), Y(x^{(n)})] \\ \vdots & \ddots & \vdots \\ \text{cor}[Y(x^{(n)}), Y(x^{(1)})] & \cdots & \text{cor}[Y(x^{(n)}), Y(x^{(n)})] \end{pmatrix} \tag{2.17}$$

Where the maximum likelihood estimates for $\mu$ and $\sigma^2$ are:

$$\hat{\mu} = \frac{\mathbf{1}^{\mathrm{T}}\mathbf{\Psi}^{-1}\mathbf{y}}{\mathbf{1}^{\mathrm{T}}\mathbf{\Psi}^{-1}\mathbf{1}} \tag{2.18}$$

$$\hat{\sigma}^2 = \frac{(\mathbf{y} - \mathbf{1}\mu)^{\mathbf{T}}\mathbf{\Psi}^{-1}(\mathbf{y} - \mathbf{1}\mu)}{n} \tag{2.19}$$

After the hyperparameters value are set, the Kriging predictor is:

$$\hat{y}(x) = \hat{\mu} + \psi^{\mathrm{T}}\Psi^{-1}(y - 1\hat{\mu}) \tag{2.20}$$

The log-likelihood function can be optimized using direct search methods such as genetic algorithm and followed with local search methodology. The study on the optimization of these hyperparameters can be found in Toal[133].

## 2.4 Uncertainty Quantification and Robust Optimization

An approach to consider uncertainty in the optimization is to perform robust optimization where the goal is to find a single or set of robust solutions. Instead of optimizing in a single design point only, robust optimization considers the possible solutions in the vicinity of on-design solution or due to the effect of uncertainty. The robust solution is then can be defined as a solution that is optimum in term of the original objective function and the stability of the solution to the disturbances. An example in aerospace engineering is the airfoil that is optimized on a single flight condition typically results in an

over-optimized airfoil that has poor off-design performance in different flight condition. Such solution is unstable and typically is not preferred. Therefore, an alternative that consider this uncertainty is needed. The goal of the robust optimization is then to optimize the statistical quality of the solution and not only its deterministic counterpart. Simultaneously optimizing the mean $\mu$ and standard deviation $\sigma$ or performing single aggregate function are two common approaches. The aggregate sum is simply defined as:

$$\text{minimize} : f(x) = \mu(x) + \sigma(x) \tag{2.21}$$

The multi-objective approach for robust optimization can be defined as:

$$\text{minimize} : \mu(x), \sigma(x) \tag{2.22}$$

An iillustration of the multi-objective robust optimization is shown in Fig. 2.4. The objective spaces consist of the mean and standard deviation of the solutions where the goal is to find the Pareto front or the best tradeoff between the performance and robustness. An illustration of the robust and non-robust solution is given in Fig. 2.5. Shown in this picture are two solutions of A and B which are located in the peak of local and global optimum of a single variable $x$, respectively, with maximization of the $y$ as the objective. A deterministic optimization surely will choose solution B as the optimum solution. However, even though the solution B is the global optimum, a small disturbance of the variable $x$ could results in a drastic degradation of the performance, which is undesirable. Solution A has lower performance than the solution B but it is more robust to the presence of the uncertainty in the variable $x$; a small disturbance only affects its performance slightly. Therefore, in the presence of the uncertainty, the solution A might be more preferable to the decision maker. Nonetheless, in the language of multi-objective decision making, solution A and B are non-dominating to each other. This is where multi-objective robust optimization play its parts to present both alternatives (and any other alternatives) to the decision maker and not just single solution only.

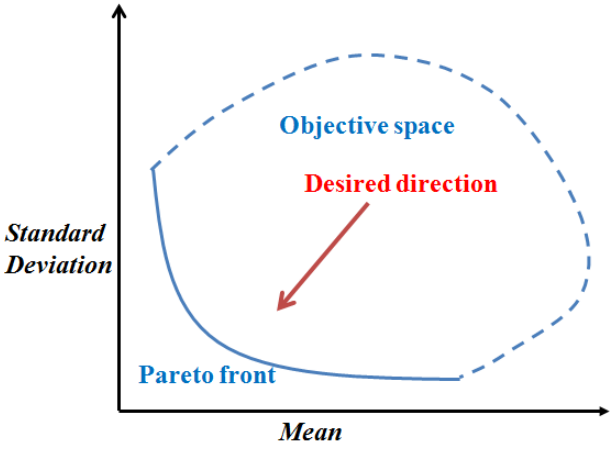


FIGURE 2.4: Illustration of multi-objective robust optimization.

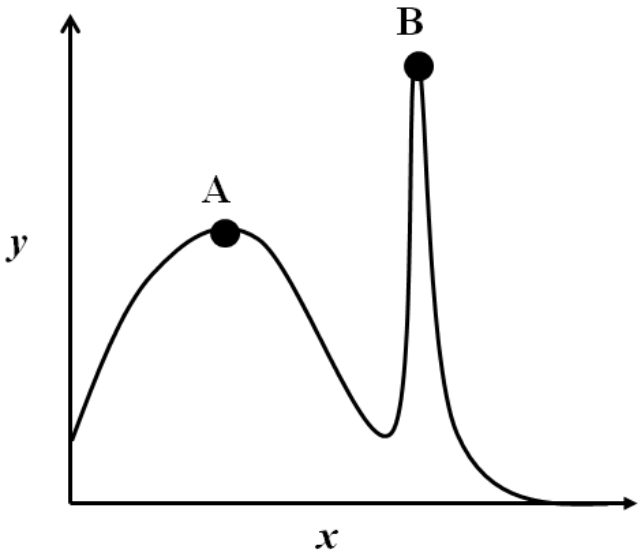


FIGURE 2.5: Illustration of robust optimization versus deterministic optimization.

Considering the nature of the uncertainty, uncertainty could be classified into two categories which are the aleatoric uncertainty and epistemic uncertainty. Aleatoric uncertainty is a natural randomness in the process and is not reducible where an example of this is the uncertainty in the physical parameters or the operating condition. On the other side, epistemic uncertainty is caused by our lack of knowledge and is reducible with any new knowledge or information. An example of the epistemic uncertainty is the non-physical parameters or parameters in the turbulence modelling. Aleatoric uncertainty could be well defined with the probability theory and assigned a probability distribution. On the other side, epistemic uncertainty can not be expressed in the probabilistic sense and needs other theories or treatment to describe it such as the evidence theory[134]. This leads to different treatment in the real application and might lead to different objectives in robust optimization. In this thesis, we mainly deal with the aleatoric uncertainty although the method itself can be applied to the epistemic uncertainty by assigning different theories.

To be able to investigate the effect of the uncertainty to the system, a tool to measure the statistical properties is needed and this is where uncertainty quantification (UQ) plays its part. The most direct and easiest way to quantify uncertainty is to employ Monte Carlo simulation (MCS). MCS works by generating a number of possible realizations from a given probability distribution and then aggregating the results which could be very expensive if expensive simulation is employed. Imagine an MCS with ten thousand simulations where each simulation consumes one day, surely it is not a way that will be preferred by anybody. Therefore, research is progressing toward quantifying the uncertainty with as few deterministic simulation as possible. Speed-up can be achieved by employing special techniques such as Bayesian Monte Carlo[85], Taylor expansion based method[76], univariate reduced quadrature method[86], or polynomial chaos. Bayesian Monte Carlo works by performing Monte Carlo simulation on the approximation function where Gaussian process/Kriging is one of the possible choices to

be employed as the surrogate model. The disadvantage of Bayesian Monte Carlo is that additional parameter tuning could be needed (especially if Kriging is employed) and its accuracy decreased for high dimensional random space (curse-of-dimensionality). Moment of method is limited only to small disturbance and the quality of approximation is greatly decreased for high disturbance[135]. Polynomial chaos expansion (PCE) is now a popular choice because of its effectiveness and mathematically rigorous technique[87]. It works by approximating the functional form of random variable and orthogonal polynomial and then use the coefficient of the polynomial term to determine the statistical properties[87]. In simple way, the PCE could be viewed as a surrogate model with a given weight function that could differs from one probability distribution to the others. PCE was first developed with intrusive property, but since the underlying equation has to be modified, this was proved to be difficult and results in the alternative of non-intrusive polynomial chaos (NIPC). The latter is a common approach now because it greatly reduces the complexity of applying polynomial chaos for uncertainty quantification. This thesis gives special attention to the NIPC which is used for uncertainty quantification for all of the cases in this work.

Polynomial chaos method is well suitable to deal with smooth function but found difficulties in approximating functions with multi-modality (even though the term of multi-modality is more suitable for optimization literature) or exhibits discontinuity (Fig. 2.6). Several way to deal with discontinuous function is by using multi-element probabilistic collocation method[114, 115], methods with rational function[112], or piecewise based method such as simplex element stochastic collocation[108]. Uncertainty quantification in shock-dominated flow might exhibits this kind of discontinuity so other method is more suitable for this kind of cases than the standard PCE. Nonetheless, if the uncertainty in the aerodynamic coefficients and not a specific location in the flow domain is to be considered, the function characteristic is still likely to be smooth; thus, PCE method can be used. If the function is smooth but corrupted by noise (Fig. 2.6d), this noise can be filtered by using PCE approximation with sufficiently low or moderate polynomial order.

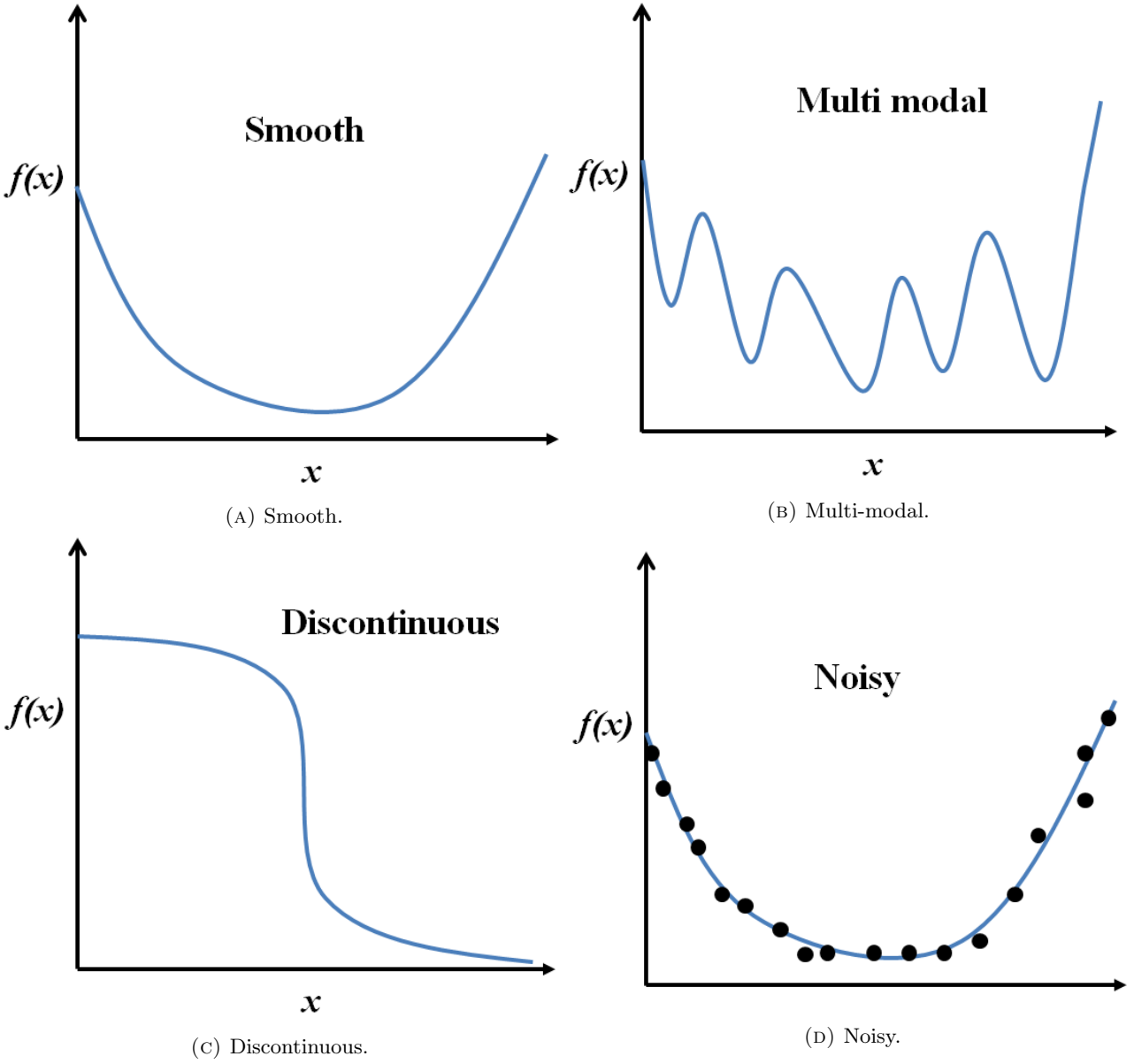


(A) Smooth.

(B) Multi-modal.

(C) Discontinuous.

(D) Noisy.

FIGURE 2.6: Possible behaviours of the underlying function for UQ purpose.

In this thesis, PCE was used to calculate the statistical value of a certain solution for robust optimization. The polynomial chaos is coupled with the developed evolutionary algorithm to create an effective methodology for multi-objective robust optimization where moderate number of deterministic simulation is available. We refer to the papers by Eldred, Webster, and Constantine[91], Eldred and Burkardt[87] for the explanation of the polynomial chaos methodology in this thesis.

## 2.5 Uncertainty Quantification using Polynomial Chaos Expansion

Polynomial chaos expansion (PCE), or "Wiener Chaos expansion", is a method for systematic quantification of uncertainty in a system that use orthogonal polynomials of random variables to approximate

| Distribution type | Polynomial chaos | Support range |
|---|---|---|
| Gaussian | Hermite chaos | $(-\infty, \infty)$ |
| Gamma | Laguerre chaos | $[0,\infty)$ |
| Beta | Jacobi chaos | $[a, b]$ |
| Uniform | Legendre chaos | $[a, b]$ |

TABLE 2.1: Standard forms of continuous PDF and their Askey Scheme polynomials.

the stochastic response surface. It is now a popular UQ method in the field of engineering due to its strong mathematical basis. PCE has now been widely applied in many application that consider the uncertainty in the system. In the heart of the PCE method are the orthogonal polynomials and spectral representation of the random process. Because of this, the understanding of orthogonal polynomial basis is explained first before moving to the polynomial chaos method itself.

### 2.5.1 Orthogonal Polynomials

Orthogonal polynomials is the important building block of the PCE method and the understanding of orthogonal polynomial is fundamental in polynomial chaos. The orthogonal polynomial sequence is a family of polynomials such that the collection of polynomials in the sequence are orthogonal to each other by inner product relation. For a given probability distribution, a specific polynomial sequence serves as an optimal basis for approximation where the polynomial itself comes from Askey scheme of hypergeometric orthogonal polynomials. As an example, Legendre polynomials serves as an optimal basis for a uniform distribution that has weight function of 1 and support range of $[a, b]$ where $a$ and $b$ are real values. Table 2.1 shows the Askey scheme of continuous hyper-geometric polynomials corresponding to their probability density function. For illustration of the orthogonal polynomials, a sequence of Hermite polynomials that is optimal given a normal probability distribution of the random variables until 4th-order are as follows:

$$\begin{aligned}
\psi_0(\xi) &= 1 \\
\psi_1(\xi) &= \xi \\
\psi_2(\xi) &= \xi^2 - 1 \\
\psi_3(\xi) &= \xi^3 - 3\xi \\
\psi_4(\xi) &= \xi^4 - 6\xi^2 + 3
\end{aligned}$$

If a probability distribution is not exists in Askey scheme, a closely-related distribution could be used so the polynomials from Askey Scheme can be applied but results in degradation of the convergence rates. Example of this is the application of Hermite polynomials to the random variables that are distributed with log-normal distribution. Another way is by using special techniques such as Stieltjes procedure[136] to numerically generate the orthogonal polynomials together with the Gauss points

and weights specifically for an arbitrary distribution. For detail and thorough explanation about the orthogonal polynomial reader can refer to the Gautschi's book[137].

### 2.5.2 Non-Intrusive Polynomial Chaos Expansion

The concept of uncertainty quantification using stochastic expansion method is to approximate the functional form between the stochastic response output and each of its random inputs with the following chaos expansion:

$$R = a_0 b_0 + \sum_{i_1=1}^{\infty} a_{i_1} B_1(\xi_{i_1}) + \sum_{i_1=1}^{\infty} \sum_{i_2=1}^{i_1} a_{i_1 i_2} B_2(\xi_{i_1}, \xi_{i_2}) + \sum_{i_1=1}^{\infty} \sum_{i_2=1}^{i_1} \sum_{i_3=1}^{i_2} a_{i_1 i_2 i_3} B_3(\xi_{i_1}, \xi_{i_2}, \xi_{i_3}) \; + \; ... \quad (2.23)$$

which is simply shortened as

$$R = \sum_{j=0}^{\infty} \alpha_j \Psi_j(\xi) \quad (2.24)$$

For practical purpose the expansion has to be truncated in some level so the expression become:

$$R = \sum_{j=0}^{P} \alpha_j \Psi_j(\xi) \quad (2.25)$$

Because of the orthogonality property of the polynomials in the polynomial chaos expansion, the statistical moment of the response can be readily evaluated using the information of the coefficients. The mean is simply the first PCE coefficients which is given by:

$$\mu_R = E[R] = \int_{\Omega} R(\vec{x}, \vec{\xi}) \rho(\vec{\xi}) d\vec{\xi} = \alpha_0 \quad (2.26)$$

The variance can be obtained with the following equations:

$$\sigma_R^2 = \mathrm{Var}[R] = \int_{\Omega} (R(\vec{x}, \vec{\xi}) - \mu_R)^2 \rho(\vec{\xi}) d\vec{\xi} = \sum_{j=1}^{P} \alpha_j^2 \langle \Psi_j^2(\xi) \rangle \quad (2.27)$$

The first way to calculate the coefficients is by using the Galerkin projection:

$$\alpha_j = \frac{\langle R, \Psi_j \rangle}{\langle \Psi_j^2 \rangle} \quad (2.28)$$

For Galerkin/spectral projection approach, a concept of quadrature is fundamental where one-dimensional quadrature formula is defined as follows:

$$\mathscr{U}^i(f)(\xi) = \sum_{j=1}^{m_i} u(\xi_j^i) w_j^i \quad (2.29)$$

Another approach to calculate the coefficients is to use linear regression approach:

$$\Psi\alpha = R \tag{2.30}$$

That could be expanded further as

$$\begin{pmatrix} \Psi_0(\xi_0) & \Psi_1(\xi_0) & \cdots & \Psi_P(\xi_0) \\ \Psi_0(\xi_1) & \Psi_1(\xi_1) & \cdots & \Psi_P(\xi_1) \\ \vdots & \vdots & \ddots & \vdots \\ \Psi_0(\xi_P) & \Psi_1(\xi_P) & \cdots & \Psi_P(\xi_P) \end{pmatrix} \begin{pmatrix} \alpha_0(x) \\ \alpha(x) \\ \vdots \\ \alpha_P(x) \end{pmatrix} = \begin{pmatrix} R(x,\xi_0) \\ R(x,\xi_1) \\ \vdots \\ R(x,\xi_P) \end{pmatrix}$$

The coefficients are obtained by solving the above linear system of equation which needs $N_t$ deterministic function evaluations. This approach is termed non-intrusive point collocation and this approach is useful if flexibility is needed. The point collocation approach allow the flexibility to choose the number of sampling points and the polynomial basis. However, the interpolation properties is not preserved for this approach but reasonable accuracy can be obtained with method such as least angle regression (LAR)[106]. The point-collocation approach usually combines sampling with total order expansion (explained later) as follows:

$$N_t = 1 + P = 1 + \sum_{s=1}^{p} \frac{1}{s!} \prod_{r=0}^{s+1} (n+r) = \frac{(n+p)!}{n!p!} \tag{2.31}$$

Where $p$ and $n$ are the polynomial order and random input dimension, respectively. An overdetermined system where the number of samples is more than the number of polynomial basis can be solved using least squares approach. Hosder recommended to use the over sampling ratio ($OSR$)[138], which is defined as the ratio between number of samples and the number of polynomial basis, of 2. This value of $OSR$ reduces the condition number and the possibility of overfitting. By introducing the $OSR$, the number of function evaluations needed will be $N_t = 2(n+p)!/(n!p!)$ if total-order rule is used to truncate the polynomial expansion. Zhang Yi proposed an adaptive method to reduce the OSR by carefully add the samples based on the convergence check of the difference of total response surface error until the error convergence criterion is reached[102].

To extend the orthogonal polynomial basis for multi-variable approximation, special methods have to be used. Some important methods are tensor product expansion, Smolyak sparse grids, and total order/hyperbolic expansion.

### Tensor product quadrature

Tensor product expansion includes all combination of the one-dimensional polynomial for higher dimension. Consider a multi-index $\mathbf{i} = (i_1, \ldots, i_N) \in \mathbb{N}_+^n$, the tensor product operator to expand the

expansion can be mathematically defined as:

$$\mathscr{Q}_{\mathbf{i}}^{n} u(y) = (\mathscr{U}^{i_1} \otimes \ldots \otimes \mathscr{U}^{i_n})(f)(\xi) = \sum_{j_i=1}^{m_{i_n}} \ldots \sum_{j_n=1}^{m_{i_n}} f(\xi_{j_1}^{i_1}, \ldots, \xi_{j_n}^{i_n})(w_{j_1}^{i_1} \otimes \ldots \otimes w_{j_n}^{i_n}) \tag{2.32}$$

For example, multidimensional basis polynomials with two-dimension, Hermite polynomials, and a second-order expansion are

$$\begin{aligned}
\Psi_0(\xi) &= \psi_0(\xi_1)\psi_0(\xi_2) = 1 \\
\Psi_1(\xi) &= \psi_1(\xi_1)\psi_0(\xi_2) = \xi_1 \\
\Psi_2(\xi) &= \psi_2(\xi_1)\psi_0(\xi_2) = \xi_1^2 - 1 \\
\Psi_3(\xi) &= \psi_0(\xi_1)\psi_1(\xi_2) = \xi_2 \\
\Psi_4(\xi) &= \psi_1(\xi_1)\psi_1(\xi_2) = \xi_1\xi_2 \\
\Psi_5(\xi) &= \psi_2(\xi_1)\psi_1(\xi_2) = (\xi_1^2 - 1)\xi_2 \\
\Psi_6(\xi) &= \psi_0(\xi_1)\psi_2(\xi_2) = (\xi_2^2) - 1 \\
\Psi_7(\xi) &= \psi_1(\xi_1)\psi_2(\xi_2) = \xi_1(\xi_2^2 - 1) \\
\Psi_8(\xi) &= \psi_2(\xi_1)\psi_2(\xi_2) = (\xi_1^2 - 1)(\xi_2^2) - 1
\end{aligned}$$

The total number of polynomial term $N_t$ for tensor-product expansion is:

$$N_t = \prod_{i=1}^{n} (p_i + 1) \tag{2.33}$$

Tensor product is routinely employed with the spectral projection method to estimate the polynomial coefficients. By using tensor product, the collocation points are also built using tensor product approach by using the roots of orthogonal polynomials.

The main drawback of tensor product is that the number of collocation points grow exponentially with the increase in the dimension of probability space. In high dimensions ($n > 4$), tensor products become inefficient due to the curse of dimensionality and sometimes impractical for real application. As for example, the number of polynomial basis for $n = 5$ and 4th order polynomial is 3125. This is practically infeasible if for each collocation points an expensive simulation has to be called.

### Smolyak sparse grids

Smolyak sparse grid[92, 96] offers remedy for the curse of dimensionality by giving less number of collocation point that is built using smaller tensor product. Smolyak sparse grid is a combination of smaller tensor product with small number of points in mind. Consider $\mathscr{U}^0 = 0$ for $i \geq 1$ and then:

$$\Delta^i = \mathscr{U}^i - \mathscr{U}^{i-1} \tag{2.34}$$

Where $|\mathbf{i}| = i_1 + ... + i_n$. The isotropic Smolyak quadrature formula is given by:

$$\mathscr{A}(w,n) = \sum_{|\mathrm{i}|\leq w,n} (\Delta^{i_i} \otimes \ldots \otimes \Delta^{i_n}) \tag{2.35}$$

Or in other form:

$$\mathscr{A}(w,n) = \sum_{w+1\leq|\mathrm{i}|\leq w+n} (-1)^{w+n-|\mathrm{i}|} \binom{n-1}{w+n-|\mathrm{i}|} .(\Delta^{i_i} \otimes \ldots \otimes \Delta^{i_n}) \tag{2.36}$$

To simplify the form:

$$\mathscr{A}(w,n) = \sum_{w+1\leq|\mathrm{i}|\leq w+n} c(\mathrm{i})(\Delta^{i_i} \otimes \ldots \otimes \Delta^{i_n}) \tag{2.37}$$

where

$$c(\mathrm{i}) = (-1)^{w+n-|\mathrm{i}|} \binom{n-1}{w+n-|\mathrm{i}|} \tag{2.38}$$

Similar to the tensor product, sparse grids method is usually used with the spectral projection method to ensure an optimum approximation by using the collocation points from the roots of orthogonal polynomials. However, sparse grids method is still not flexible in determining the number and location of collocation points because it have to follow some certain rules. Sparse grids method also suffers, in a mild scale, the curse of dimensionality in moderate to high dimension. It becomes much more difficult to control the growth of collocation points in relatively high dimension. Difficulties is also encountered if some collocation points failed to return any value. Even though this problem could be solved by imputing the failed collocation points[139], the sparse grids method still not offers the user high flexibility.

### Total order/hyperbolic expansion

Another important alternative is to use total-order expansion that preserves basis of polynomials up to a fixed total-order specification. Total order expansion is routinely used with the point collocation approach and the samples could be located in arbitrary location, providing high flexibility and robustness. Another advantage is that if, for example, one or some collocation points failed to returned a real value, regression could still be used to obtain the coefficients.

Consider an index defined by:

$$|\mathbf{i}| = ||\mathbf{i}||_1 = i_1 + ... + i_n \tag{2.39}$$

Total-order expansion retain the indices with the following scheme:

$$A^{n,p} \equiv \{\mathbf{i} \in \mathbb{N}^n : ||\mathbf{i}||_1 \leq p\} \tag{2.40}$$

An example for $n = 2$ and second-order expansion are:

$$\Psi_0(\xi) = \psi_0(\xi_1)\psi_0(\xi_2) = 1$$
$$\Psi_1(\xi) = \psi_1(\xi_1)\psi_0(\xi_2) = \xi_1$$
$$\Psi_2(\xi) = \psi_0(\xi_1)\psi_1(\xi_2) = \xi_2$$
$$\Psi_3(\xi) = \psi_2(\xi_1)\psi_0(\xi_2) = \xi_1^2 - 1$$
$$\Psi_4(\xi) = \psi_1(\xi_1)\psi_1(\xi_2) = \xi_1\xi_2$$
$$\Psi_5(\xi) = \psi_0(\xi_1)\psi_1(\xi_2) = \xi_2$$

The total number of polynomial term $N_t$ for total-order expansion is:

$$N_t = \frac{(n+p)!}{n!p!} \tag{2.41}$$

To further reduce the number of terms, the hyperbolic scheme[106] could be used:

$$A^{n,p} \equiv \{\mathbf{i} \in \mathbb{N}^n : ||\mathbf{i}||_q \leq p\} \tag{2.42}$$

where

$$||\mathbf{i}||_q \equiv (\sum_{j=1}^{n} i_j^q)^{\frac{1}{q}} \tag{2.43}$$

The use of the hyperbolic scheme, depending on the value of $q$, gives more stress to retain the main effects and low-order interactions. The smaller value of $q$, the lesser number of polynomial basis that would be retained. In fact, applyinq $q = 1$ will result in ordinary total order expansion. The hyperbolic scheme could be used with the ordinary strategy of applying OSR of 2 to ensure numerical stability. Reducing the value of $q$ results in the scheme that retains the low-order interaction and favour the main effects as it is illustrated in Fig. 2.7.

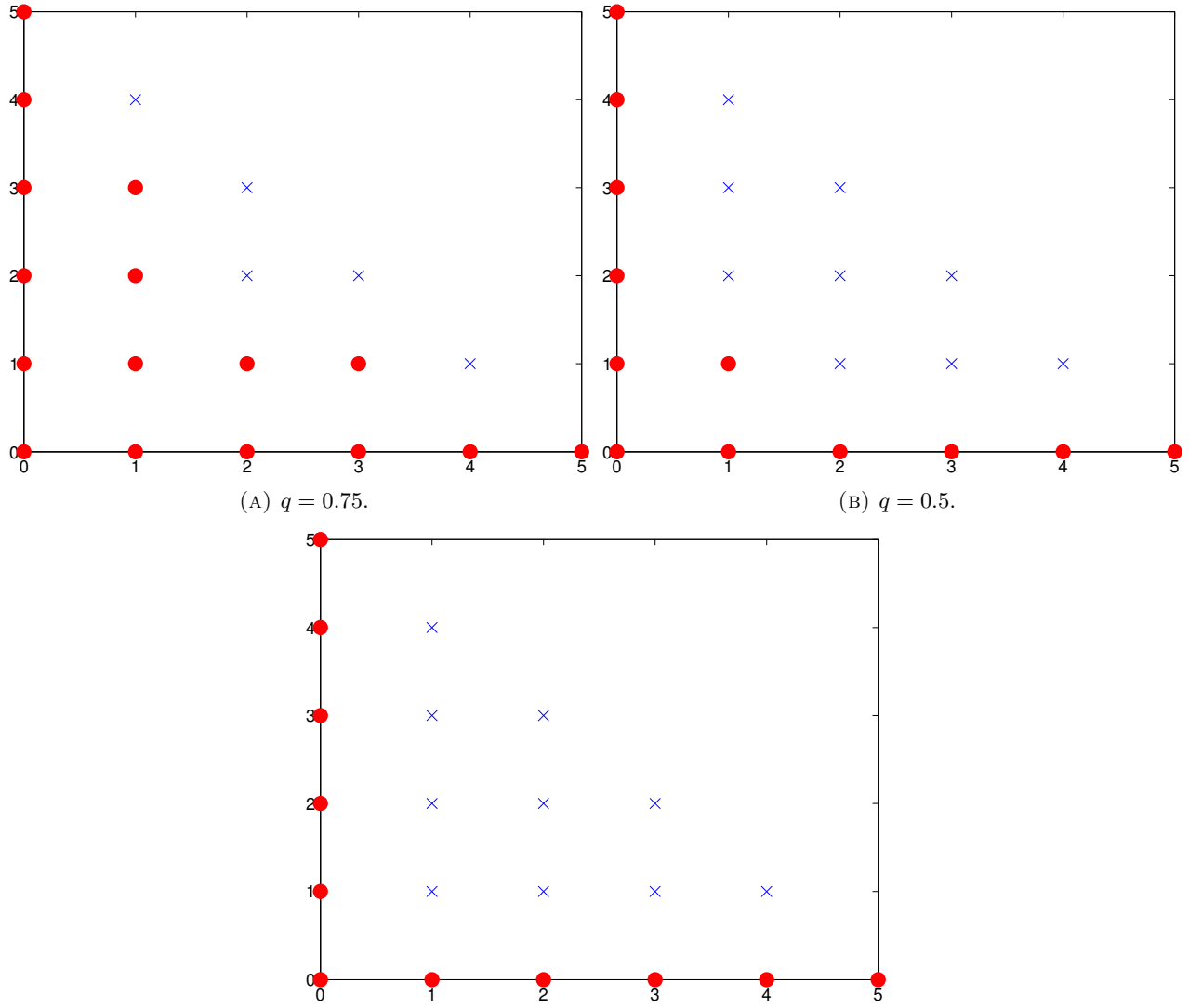


(A) $q = 0.75$.

(B) $q = 0.5$.

(C) $q = 0.25$.

FIGURE 2.7: Illustration of hyperbolic truncation scheme where blue crosses and red dots are polynomial basis generated with total-order and hyperbolic truncation with the specified $q$ value, respectively.

## 2.6 New Algorithms and Framework for Expensive Multi-Objective Optimization and Robust Optimization

This thesis introduces the improved and new approaches to deal with multi-objective robust optimization problem. The development of these new algorithms and framework is motivated by several limitation of the related methods for optimization and uncertainty quantification. Classical motivation of maximizing the use of the availability of computational budget for expensive optimization problem also drive this research.

For robust optimization, there are two possible efforts to optimize the efficiency of the available of computational budget: developing a better optimization algorithm or highly efficient uncertainty quantification algorithm. This is done by first investigating the limitation of the previously existing methods to deal with robust optimization problem. Several improvements were then proposed to improve the effectiveness and efficiency of the optimizer and UQ algorithm.

On the optimization part, we investigate the effect of various local search methodology to assist the surrogate-based memetic algorithm based on the SS-MOMA[25]. The original SS-MOMA algorithm uses weighted sum to search the local surrogate model. We investigate various local search methodologies to study whether improvement could be made by introducing different type of local search and performing numerical experiments on selected test functions. The strengths and weaknesses of each local search methodology also need to be studied to derive the guide for proper choice of local search for local-surrogate based multi-objective memetic algorithm.

A multi-fidelity uncertainty quantification based on non-intrusive polynomial chaos and regression to estimate the polynomial coefficients was introduced in this thesis. This is motivated by the needs of flexibility and robustness of the UQ algorithm for robust optimization purpose. By using regression for coefficients estimation, the user is now equipped with very high flexibility in determining the number, location of samples, and the polynomial basis. However, proper study is needed to derive the best practical and implementation issue for the new algorithm. Its strengths and weaknesses are discussed after the numerical experiments on artificial and real test problems.

Both algorithm were then applied to real world robust optimization case to study the applicability of the improved optimizer and UQ algorithm to the real problem. Even so, the improvement of the optimizer and UQ algorithm could be seen separately and does not need to be seen from viewpoint of robust optimization.

# Chapter 3

# Improved Local Surrogate Assisted Memetic Algorithm

An improvement of the local surrogate-assisted memetic algorithm is presented in this chapter. The explanation of the single surrogate-assisted multi-objective memetic algorithm (SS-MOMA) as the building block of the optimizer is explained first. Explanation of various local search methodologies such as achievement scalarizing function (ASF), Chebyshev, and random mutation hill climber (RMHC) was given next as an alternative to the original weighted sum of the SS-MOMA. Furthermore, we also studied the effect of normalization and random weights to the search performance of the optimizer. SS-MOMA with various local search were investigated and their capabilities on various test problem were studied and discussed. The improved algorithm was then tested on aerodynamic problem to see its capability on real problems.

## 3.1 Local Surrogate-Assisted Multi-Objective Memetic Algorithm

SS-MOMA is an algorithm developed by Lim, Jin, Ong, and Sendhoff [25] and falls in the class of multi-objective memetic algorithms [23]. SS-MOMA uses NSGA-II algorithm as the building block with the local search based on local surrogate methodology instead of using global surrogate model that has a tendency to got trapped in the local optimum. The search using global surrogate has a high probability to get stucked which is caused by the Kriging update that cannot obtain any new information, since the global surrogate based search only depends on the surrogate model itself[42]. This is in contrast with the approach that combines the ability of both evolutionary operator and surrogate model such as the SS-MOMA algorithm. The local search is applied to improve the efficiency of the optimizer with the search is performed on the local surrogate model. The local search works by first building a surrogate model by using the individual in action with its nearest neighbors and then search this surrogate model

using method such as sequential quadratic programming (SQP) guided by scalarizing function or other methods that rely on the principles such as non-domination.

SS-MOMA is an algorithm developed by Lim et al. [25] and falls in the class of multi-objective memetic algorithms[23]. SS-MOMA uses NSGA-II algorithm as the building block with the local search based on local surrogate methodology instead of using global surrogate model that has a tendency to got trapped in the local optimum. The local search is applied to improve the efficiency of the optimizer with the local surrogate model helping to provide an estimate of the direction in which improvement can be obtained. The local search works by first building a surrogate model using the individual in action and its nearest neighbors, and then searches this surrogate model using sequential quadratic programming (SQP) guided by a scalarizing function or other methods that relies on the principle such as domination principle.

The main loop of SS-MOMA is essentially the same as NSGA-II except in its local search module. The purpose of the local search module is to perform local improvement of solutions that pass this module. In contrast to single-objective optimization, the treatment of local search in the multi-objective case is not straightforward because the multi-objective problem has to be converted into a single-objective one. This conversion could take the form in scalarizing function which is a single-objective representation of the original multi-objective problem. The alternatives to a scalarizing function are methods that directly deal with the original multi-objective form and use operators that guide the search by the domination principle.

Since the focus of our study is to improve the methodologies by introducing various local search methods and considering real-world problems, SS-MOMA, rather than the generalized version (GS-MOMA) that uses multiple different types of surrogates, is employed for simplicity. Nonetheless, there is still much room for improvement of the SS-MOMA. This is one of the main aims of this thesis Furthermore, several modifications are necessary to deal with practical expensive applications. In this thesis we are not focusing on comparison of surrogate models but on the study and improvement of the local search and practical concerns of the SS-MOMA.

We studied the effects of different types of local search on the search-convergence trend. The original SS-MOMA used a WS scalarizing function; here we also use an achievement scalarizing function (ASF), Chebyshev function, and random mutation hill climber (RMHC) and compare it with WS. Practical concerns such as the normalization of the objective functions during local search and constraint handling were also considered.

### 3.1.1 General Framework and Pseudocode

The main backbone of the original NSGA-II is the non-dominated sorting operator. This operator sorts the solutions from parents and offspring based on the non-domination fronts and diversity of

the current solutions. This procedure ensures that only the best solutions from the viewpoints of domination and diversity are passed on to the next generation. In the memetic algorithm framework, the offspring will usually undergo a local search module before the selection procedure. SS-MOMA algorithm applies this memetic algorithm concept and perform a selection on the parents, offspring, and after-local-search solution. For each local search, a surrogate model is built and the surrogate is searched using either a scalarizing function or domination-based local search. The optimum local solution from this surrogate is then evaluated using the exact function and the result is returned to the optimizer for further non-dominated sorting. If the trust region framework is employed, the single-objective optimization continues and is refined until a criterion is reached.

The SS-MOMA described in the original paper employs several generations without a local surrogate phase first to gather the data to build the local surrogate later. In this study, we modify the database building phase by generating the initial sampling plans using Latin hypercube sampling (LHS)[140], a low discrepancy sequence, or any other design of experiment method. This initialization has the purpose of spreading the samples uniformly in the search space to create space-filling initial samples for the local surrogate building phase. These initial samples form the first SS-MOMA population but its size does not to be equal to that of subsequent populations. Non-dominated sorting is used to select the best individuals from the first population to continue to the second generation.

SS-MOMA employs evolutionary operators on the parents to generate the offspring solutions; these offspring are subjected to local search. The local search module creates the after-local-search solutions. Non-dominated sorting is performed on the parents, offspring, and after-local-search solutions to create the new parents for the next generation.

The pseudocode and main loop of SS-MOMA are shown in detail in Algorithm 1.

initialize parent population $P_c$;
evaluate initial population;
start the generation counter $o = 1$;
**while** *computational budget is not exhausted* **do**
  perform evolutionary operator and generate offspring population $P_o$;
  evaluate the solutions;
  **/****Local Search Phase****/**;
  **for** *each individual* $\boldsymbol{x}$ *in the* $P_o$ **do**
    Build the sampling plan by choosing $m$ nearest points to $\mathbf{x}$ in the database;
    Build $M$ surrogate model for each objective function (Chebychev, ASF, RMHC) or aggregate function (weighted sum) using this sampling plan;
    Search the surrogate model to find the optimum point of the defined scalarizing function $\mathbf{x_{opt}}$;
    Evaluate $\mathbf{x_{opt}}$ with the exact function;
    Enter $\mathbf{x_{opt}}$ into the after-local-search solutions $A_l$;
  **end**
  perform non-dominated sorting on $P_c$, $P_o$ and $A_l$ to create the new parent population $P_{c+1}$;
  increase the generation counter $o = o + 1$;
**end**

**Algorithm 1:** SS-MOMA main loop.

In the original SS-MOMA paper, the only scalarizing function used in the local search is the WS. The disadvantage of WS is that it favours convex sections of the Pareto front (in minimization cases) and encounter difficulties for non-convex parts. This effect might not be significant if the number of function evaluations is high as in the original SS-MOMA paper, but it may well affect performance if the available budget is low. Therefore, in this thesis combination of SS-MOMA with various local search methodology is studied.

### 3.1.2 Surrogate Model Building Phase

The surrogate model had to first be built before the local search could proceed. The upper and lower bounds used to build the response surface were exactly the maximum and minimum values of the sampling points decision variables, respectively. We always normalized decision variables of the surrogate model to [0,1] because disparately scaled decision variables could negatively affect the quality of the surrogate.

The approximation started by choosing samples $\mathbf{X}= \{x_{(1)}, x_{(2)}, ..., x_{(n)}\}^T$ and responses $y=\{y_{(1)}, y_{(2)}, ..., y_{(n)}\}^T$. Using this information concerning samples location and responses, a specific surrogate model method can then be used to build the approximation model of the black-box function. The concept of an approximation using RBF and Kriging is explained in the following subsection, where that explanation refers to a book written by Forrester et al. [132].

The approximation starts by choosing the samples:

$$X = \{x^{(1)}, x^{(2)}, ..., x^{(n)}\}^T \tag{3.1}$$

and the responses

$$y = \{y^{(1)}, y^{(2)}, ..., y^{(n)}\}^T \tag{3.2}$$

Any type of surrogate model can then be used to build the surrogate models. Here, we used a linear spline RBF and Kriging to approximate the response surface where the sampling points used were the individual to be improved and its neighbors. We chose linear spline RBF[44] because of its very fast training time relative to the Kriging that needs hyperparameters tuning. Beside of that, the choice of surrogate model affects the accuracy of the approximation but it does not affect the direction of the search, which is dictated by the type of the local search used. In real world application it is suggested to use more robust type of surrogate model such as Kriging or polynomial regression[141].

### 3.1.3 Local Search Method

The aim of local searching is to find the optimum of the surrogate model that is defined by the type of scalarizing function or local search methodologies. The local search is performed on the surrogate; hence, the computational cost is not an issue. The choice of local search method is important because it can affect the convergence of the optimization and behavior of the evolved solutions. This avenue of research has still not been explored much, especially in the context of expensive multi-objective optimization using a genetic algorithm. In this thesis, several local search methods are studied with test functions used are reflecting some possible characteristics of the Pareto front. We also limit our study by focusing on the implementation aspect and comparison of various local search methods and not stressing the development of a "silver bullet" and power algorithm to solve the expensive multi-objective optimization method (recall the no-free lunch theorem). The local search methods compared in this thesis are explained in the following:

#### 1. Weighted sum

The WS approach works by assigning a convex combination of different objectives. Let $w_i$ be a weight vector where $w_i > 0$ and the sum of the weight vector is equal to one, the expression for WS is:

$$\text{minimize: } \sum_{i=1}^{M} w_i f_i(x) \tag{3.3}$$

where $w_i = (w_1, w_2, ...w_M)$ is a randomly generated weight vector and $\sum_{i=1}^{M} w_i = 1$ with $M$ is the number of the objectives.

#### 2. Achievement scalarizing function

ASF uses a definite reference point $\bar{z}_i$ to improve the current solution. The expression for the ASF approach is:

$$\text{minimize: } \max_{i=1}^{M} w_i(f_i(x) - \bar{z}_i) \tag{3.4}$$

where $w_i = (w_1, w_2, ...w_M)$ is a randomly generated weight vector and $\sum_{i=1}^{M} w_i = 1$. ASF improves the individual solution by leading the initial solution which acts as the reference point $\bar{z}$ in a certain direction defined by the weights. Note that in the hybrid NSGA-II paper by Sindhya, Miettinen, and Deb[142] the weights were fixed and depended only on the estimated upper and lower bound of the objective spaces $(1/(Z_{max} - Z_{min}))$, whereas in this thesis the weights were varied to allow more exploration during the local search phase. The advantage of ASF is that an optimal solution of a given achievement function is a guaranteed Pareto optimum. Furthermore, achievement scalarizing function is also independent to the convexity of the problem[142, 143].

According to Wierzbicki[143], an ASF $s_R = \mathbf{R}^m \rightarrow \mathbf{R}$ is said to be:

1. **Increasing:** if for any $y^1, y^2 \in \mathbf{R}^m, y_i^1 \leq y_i^2$ for all $i \in N_m$, then $s_R(y^1) \leq s_R(y^2)$
2. **Strictly increasing:** if for any $y^1, y^2 \in \mathbf{R}^m, y_i^1 < y_i^2$ for all $i \in N_m$, then $s_R(y^1) < s_R(y^2)$
3. **Strongly increasing:** if for any $y^1, y^2 \in \mathbf{R}^m, y_i^1 \leq y_i^2$ for all $i \in N_m$, and $y^1 \neq y^2$ then $s_R(y^1) < s_R(y^2)$.

These properties ensure that the optimum solution of an ASF problem is Pareto optimum.

### 3. Chebyshev function

The expression for the Chebyshev-based local search is exactly the same as ASF. However, instead of using the individual to be improved as the reference point $\bar{z}$, Chebyshev based local search uses the upper bounds for normalization (of the offspring or of all evaluated solutions) as the reference point. With this, the individual to be improved will move as far as possible from the defined upper bounds to the desired optimum direction dictated by the weights. Because basically this function is also the ASF type function, all properties of the ASF hold for the Chebyshev local search. One reason of why the upper bounds are used as the reference point is to allow more diverse search since the search will move toward a same point if the lower bounds are used. The concept of Chebyshev-based local search in this study was inspired by the use of Chebyshev function in MOEA/D[8].

### 4. Random mutation hill climber

RMHC[144, 145] is based on non-domination principle and works by searching the neighborhood of a current solution by generating a mutant solution. The mutant solution is then compared with the current solution and accepted when it dominates over it. This means that mutant solutions are continuously generated until there is an improvement in the mutant. This improved mutant is then accepted as the next step and then mutation is performed again until the computational budget is exhausted. In this thesis, a polynomial mutation operator[12] is used to generate the mutants.

RMHC is a very simple algorithm and it does not need any normalization of the objective spaces. It might be expensive to apply RMHC as the surrogate model is not involved; however, here, the computational cost of optimizing the surrogate is not the issue since RMHC performs the search on the local surrogate model. The RMHC algorithm is formally defined in Algorithm 2.

This algorithm also applies to the constrained problems. To deal with constrained problems, the mutant is accepted wunder the following conditions:

generate initial solution $x_s$; in the in local search case, the initial solution is the solution to be improved;
evaluate initial solution;
**while** *computational budget is not exhausted* **do**
    generate the mutant solution $x_{mut}$ by perturbing $x_s$ with polynomial mutation;
    evaluate the mutant;
    **if** $x_{mut} \succ x_s$ **then**
        $x_s = x_{mut}$;
    **else**
        do nothing;
    **end**
**end**

**Algorithm 2:** RMHC loop.

- If $x_s$ violates the constraint, and $x_{mut}$ does not violate the constraint
- If both $x_s$ and $x_{mut}$ violate the constraint, but $x_{mut}$ has a lower constraint violation value (constraint dominate).
- If both $x_s$ and $x_{mut}$ do not violate the constraints, but $x_{mut}$ dominates $x_s$

Any more sophisticated non-domination based methods can be used as a replacement for RMHC but here RMHC is elaborate enough to search the surrogate since the surrogate model can be evaluated cheaply. Fig. 3.1 shows an example of the application of RMHC in ZDT1 problem without using any surrogate. Shown in this figure is the evolution of the solution that was accepted as the next step until it reached the final solution where the computational budget is exhausted. No surrogate model was used in this demonstration but it can gives adequate picture of how RMHC works.

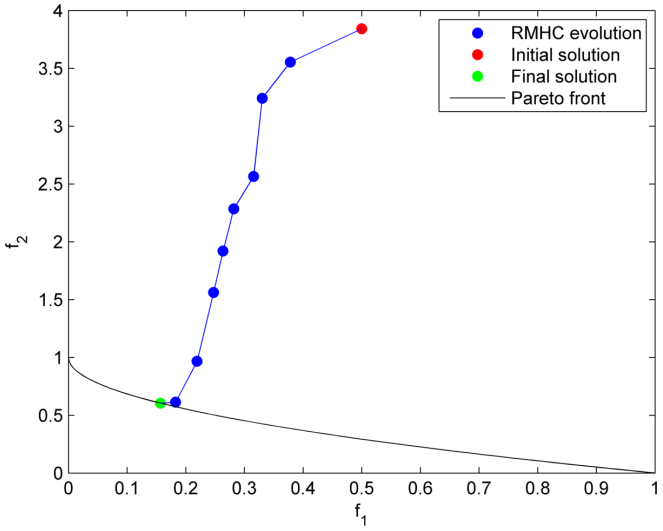


FIGURE 3.1: Demonstration of the evolution of solutions using RMHC on ZDT1 problem.

Here, for sake of clarity we refer to SS-MOMAs with ASFs, WSs, RMHCs, and Chebyshev as SS-MOMA-ASF, SS-MOMA-WS, SS-MOMA-RMHC, and SS-MOMA-CHEB, respectively. On the surrogate model phase, we build surrogate models for each objective function if ASF, Chebyshev, or RMHC methodologies are employed, and one surrogate model for weighted sum type local search. Our preliminary study shows that using the surrogate model build directly from ASF is not adequate due to the existence of flat landscape of the ASF.

### 3.1.4 Normalization

Objective functions of different magnitude are commonly encountered in real optimization problems. An example of this is to be found in the aerodynamic domain, where the lift and drag coefficients have disparately scaled values, with the former ideally being much greater than unity and the latter much less. If such a scaling difference is great, a simple WS scalarizing function favors the objective that changes in value most during optimization, resulting in a biased search direction. Thus, in this study SS-MOMA always normalizes the objective functions when local search is performed to negate this effect. Several normalization methods exist and different normalization methods can affect the search. Here, normalization is only used when scalarizing-function-based local searches such as ASF and WS are applied, where RMHC does not need normalization. We studied two different normalization methods for local search in this thesis. The first one was based on the upper and lower bounds of the generated offspring solutions, whereas the second one used the estimated upper and lower bounds of the objective space. We expected that, due to the effects of normalization, similar behavior would be observed for other types of scalarizing function. Therefore, we studied the normalization by using only ASF as the local search method. The two normalization methods studied in this thesis are given below:

#### Normalization with maximum and minimum of the offspring solutions

This normalization method is imposed using the estimated maximum and minimum objective function values of the intermediate population when the search on the local surrogate is performed by replacing the objective $f_i$ with [146]:

$$\bar{f}_i = \frac{f_i - f^*_{i_{min}}}{f^*_{i_{max}} - f^*_{i_{min}}} \tag{3.5}$$

where $f^*_{i_{max}}$ and $f^*_{i_{min}}$ are the maximum and minimum values of $f_i$ among the offspring, respectively.

#### Normalization with estimated maximum and minimum of the objective spaces

The mathematical expression of this type of normalization is similar to the the equation 3.5 except now the $f^*_{i_{max}}$ and $f^*_{i_{min}}$ are the upper and lower bounds of $f_i$ among all evaluated solutions, respectively.

The importance of normalization is illustrated in Fig. 3.2 where WS scalarizing function was used on the ZDT1 problem but with the second objective scaled to be ten times larger. The figure shows that if normalization is applied the quality of solutions found improves. This is because normalization ensure that the local search process is not biased towards the objective function with larger variation.

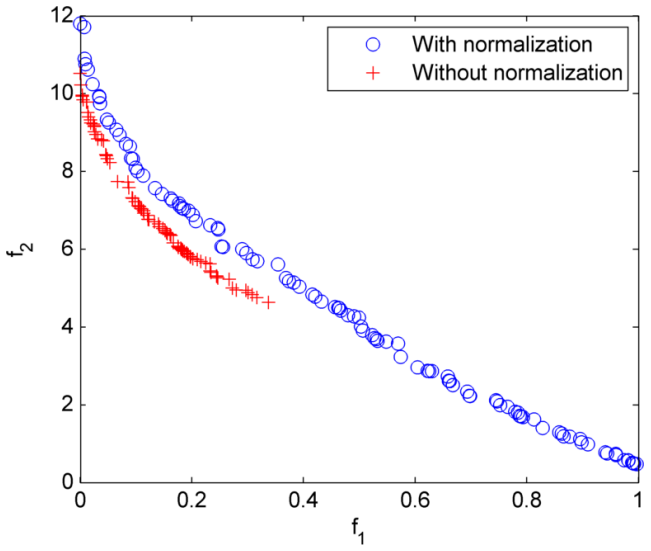


FIGURE 3.2: Examples of the final non-dominated solutions on the ZDT1 problem with and without normalization.

### 3.1.5 Constraint Handling

The constraint-handling method is necessary if constraints are present. Engineering problems typically involve constraints and we equipped the SS-MOMA with a constraint-handling method to deal with this kind of problem. A simple adaptive-constraint handling method that is just the sum of the violated constraint is adopted by SS-MOMA in this thesis. Careful consideration is needed because the values of the constraints can have different magnitudes and this is why normalization is needed. Assuming that the maximum constraint violation is not known first (the minimum is zero), the maximum violation value is updated on the fly. The following is the equation for the adaptive constraint violation technique for $m$ objectives:

$$c_{tot} = \sum_{i=1}^{m} \left| \frac{c_i}{c_{i_{max}}} \right| \tag{3.6}$$

where $c_{tot}$, $c_i$, and $c_{i_{max}}$ are total constraint violation, constraint violation for each constraint term, and maximum constraint violation value found so far, respectively. With this, the maximum value for $c_{tot}$ is the total number of constraint terms itself; for example, if the number of constraints is three, then the maximum value of $c_{tot}$ is three). This simple constraint-handling proved to be effective without any need for a complex constraint-handling mechanism and is applicable to high dimensional constraint spaces.

Constraint-handling in the local search module is done by building the surrogate model of the constraint function and using it to perform the constrained SQP algorithm (if the scalarizing function is used). The constraint-violation value cannot be directly used on the surrogate model because the zero values (solutions that do not violate the constraint) will cause the surrogate-building to become difficult. However, in some real cases the constraint function is analytical and can be directly used without any need to build the surrogate model. An example of this type of constraint is the thickness of an airfoil, which can be evaluated quickly.

## 3.2 Study on Artificial Problems

To study the capabilities of SS-MOMA with various local search methods, we applied the algorithm to several unconstrained artificial problems and compared the results with those of the original NSGA-II and SS-MOMA with WS. The characteristics of the test functions varied from convex/non-convex to continuous/discontinuous Pareto fronts. To simulate the real-world problems, the number of decision variables was set to a moderate value and the computational budget was assumed to be limited (less than 2000 function evaluations).

### 3.2.1 Unconstrained Problems

We compared SS-MOMA with various types of local search and the original NSGA-II in ZDT1, ZDT2, ZDT3[147], CONV1, and CONV2[148, 29] test problems. Each of the problems had the characteristics of concave (ZDT1, CONV1, CONV2), nonconcave (ZDT2), or discontinuous (ZDT3) Pareto fronts and served as good benchmarks for optimizer test. The number of decision variables for all ZDT test problems was set to 15 to simulate the typical number of decision variables in real engineering applications. CONV1 had a convex Pareto front but its scale was relatively smaller with respect to the entire objective spaces. Another characteristic of the CONV1 problem is that its Pareto front does not coincides with the bounds of objective spaces such as in the ZDT problems. The CONV2 problem, while exhibiting the same characteristics as the CONV1 problem, has three objectives to be optimized.

The ZDT1, ZDT2, and ZDT3 problems are of the form:

$$\text{Minimize} = \begin{cases} f_1(x) = x_1 \\ f_2(x) = g(x)h(f_1(x), g(x)) \end{cases} \tag{3.7}$$

where

$$g(x) = 1 + \frac{9}{n-1}\sum_{i=2}^{n_d} x_i \tag{3.8}$$

The formulation of $h(f_1(x), g(x))$ is different for each ZDT problem and is listed in Table 3.1:

TABLE 3.1: Details of ZDT1, ZDT2, and ZDT3 problems.

| Problem | $h(f_1(x), g(x))$ |
|---|---|
| ZDT1 | $1 - \sqrt{\frac{f_1(x)}{g(x)}}$ |
| ZDT2 | $1 - \left(\frac{f_1(x)}{g(x)}\right)^2$ |
| ZDT3 | $1 - \sqrt{\frac{f_1(x)}{g(x)}} \sin(19\pi f_1(x))$ |

The decision variables for ZDT1, ZDT2, and ZDT3 are:

$$0 \leq x_i \leq 1$$
$$1 \leq i \leq n_d$$

where $n_d$ is the number of decision variables. To simulate a real-world problems, the dimensionality of the decision variables for ZDT problems were set to 15.

The parameters for the optimizer is listed in Table 5.2:

TABLE 3.2: Parameter of SS-MOMA.

| | |
|---|---|
| Initial Population | 150 |
| Population size | 26 |
| Maximum generation | 26 |
| Crossover | Simulated binary crossover |
| Mutation | Polynomial mutation |
| $P_{cro}$ | 0.9 |
| $P_{mut}$ | $1/n_d$ |

The CONV1 problem was formulated as:

$$\text{Minimize} = \begin{cases} f_1(x) = (x_1 - 1)^4 + \sum_{j=2}^{n_d} (x_j - 1)^2 \\ f_2(x) = \sum_{j=1}^{n_d} (x_j + 1)^2 \end{cases} \tag{3.9}$$

The CONV2 problem was formulated as:

$$\begin{aligned} &\text{Minimize} = f_i(x) = \sum_{\substack{j=1 \\ j \neq i}}^{n_d} (x_j - a_j)^2 + (x_i - a_i)^4, i = 1, 2, 3 \\ &a_1 = (1, ..., 1) \in \mathbb{R} \\ &a_2 = (-1, ..., -1) \in \mathbb{R} \\ &a_3 = (1, -1, 1, -1, ...) \in \mathbb{R} \end{aligned} \tag{3.10}$$

The decision variables for both CONV1 and CONV2 problems were:

$$-5 \leq x_i \leq 5$$

The dimensionality of decision variables for CONV1 and CONV were set to 16 and 18, respectively.

For all tests on artificial problems the results were averaged from 10 ten runs due to the stochastic nature of the optimizers. Before we moved into the result and comparison of various local searches to the test functions, we studied the effect of randomization of weight and normalization on the ASF-based searches. The purpose of this study was to seek the best practice of the implementation of ASF-based searches to guide the local surrogate-based optimizer. We only used an ASF type scalarizing function for the normalization study because the Chebyshev type was similar to the ASF differing only in the reference point used.

### 3.2.2 Performance Metrics

The performance metrics used were the generational distance (GD), diversity, and hypervolume metric (the latter was only used for the real-world problem):

#### 3.2.2.1 Generational Distance

The GD metric shows how close the current non-dominated solutions to the real Pareto fronts. The metric is calculated by computing the minimum Euclidean distance from each current non-dominated solution $P*$ to the nearest Pareto-optimal solution $P$. The Pareto-optimal solutions of the ZDT and CONV problems were already known, thus this metric can be used with this knowledge. The minimum possible value of the GD metric is zero, when the non-dominated solutions are equal to Pareto-optimal solutions themselves.

$$\text{GD}(P*, P) = \frac{\sum_{v \in P*} d(v, P)}{|P*|} \tag{3.11}$$

Here, $d(v, P)$ is the minimum Euclidean distance between $v$ and the points in the Pareto front $P$.

#### 3.2.2.2 Modified Diversity Metric

While the GD metric shows how close the solutions to the Pareto front, it does not indicate whether the obtained solutions are diverse. The diversity metric provides information about the diversity and spread of the solutions and together with the GD metric served as adequate indicators of the solutions quality. The diversity metric is calculated using the following equation:

$$\Delta = \frac{d_f + d_l + \sum_{i=1}^{N-1} (d_i - \bar{d})}{d_f + d_l + (N-1)\bar{d}} \tag{3.12}$$

where $d_i$ and $\bar{d}$ are the Euclidean distance between consecutive solutions in the set $N$ and the average of those distances, and $d_f$ and $d_l$ are the Euclidean distances between the extreme solutions and the boundary solutions of the computed non-dominated set. Note that we do not use the absolute term here in order to be able to monitor the convergence of the diversity metric; this is why we called the metric as a modified diversity metric.

#### 3.2.2.3 Hypervolume Metric

Hypervolume is a $M$-volume enclosed by the reference point and solutions in the objective function space. The following definition is taken from the paper of Bader and Zitzler[14] that explained the hypervolume definition and the HypE algorithm.

Let $A \in \Psi$ be a Pareto set approximation and $R \subset Z$ be a reference set of mutually nondominating objective vectors (note that dominated solutions are not included in the total hypervolume calculation), the hypervolume indicator $I_H$ can be defined as:

$$I_H(A, R) := \lambda(H(A, R)) \tag{3.13}$$

where

$$H(A, R) := \{z \in Z; \sqsupseteq a \in A \sqsupseteq r \in R : f(a) \leq z \leq r\} \tag{3.14}$$

and $\lambda$ is the Lebesque measure with $\lambda(H(A, R) = \int_{R^n} 1_{H(A,R)(z)dz}$ with $1_{H(A,R)}$ is the characteristic function of $H(A, R)$

Given the front $f(A)$ and the reference set $R$ (typically a single point is enough), the set $H(A, R)$ is the set of objective vectors enclosed by $f(A)$ and $R$.

$$H(S, A, R) := (\cup H(s, R))\backslash(\cup H(a, R) \tag{3.15}$$

### 3.2.3 Effect of Randomized Weights

The introduction of randomized weights, hypothetically, should have been able to improve the performance of the optimizer especially in terms of diversity. In the local search scheme of Sindhya, Miettinen, and Deb[142] the ASF was equipped with a fixed weight of one (only normalized), whereas in this thesis, we tried to compare the performance of the local search with fixed and randomized weight to see if the hypothesis was true. A normalization based on the upper and lower bounds of the offspring solutions was used since it performed the best as it was explained in the previous subsection. We used ZDT1, ZDT2, and ZDT3 problems to represent three types of Pareto fronts. The boxplot results are depicted in Fig. 3.3, where it can be seen that, on average, in the ZDT1, ZDT2, and ZDT3 problems, the SS-MOMA-ASF-R (randomized weights) surpassed the SS-MOMA-ASF-F (fixed weights). An exception is in the ZDT3 problem where the GD mean of SS-MOMA-ASF-F was lower than that of SS-MOMA-ASF-R. Even so, the diversity of the SS-MOMA-ASF-R was better than that of SS-MOMA-ASF-F which clearly showed that the randomized weights increased the diversity of the evolved solutions. In the ZDT2 problems, the SS-MOMA-ASF-F suffered the "diversity trap" due to the fixed weights scheme limiting the ability of the optimizer to perform more exploration of the problem's space. One method for solving this problem is the diversity-enhancement method detailed in Sindhya, Miettinen, and Deb[142]. The method adds complexity to the optimizer and here the randomized weight offered a simpler method to enhance the diversity. However, it is worth performing further experiments in which the randomized weights and diversity-enhancement methods are combined.

It is clear that the introduction of randomized weight in the ASF function can greatly enhance the diversity of the evolved solutions. It turned out that the randomized weights offered high variation in the search direction of the offspring solutions, thus allowing the exploration of a larger section of the Pareto front. Although the convergence of non-randomized weights seemed better than that of randomized weights in the ZDT3 problem, its mean diversity value was worse than that of the scheme with random weights.

### 3.2.4 Effect of Normalization

We studied the effect of normalization on the optimization process and compared various normalization schemes on the local search. Here, we compared two various types of normalization explained in Subsection 3.1.4):

- Normalization using the upper and lower bounds of the offspring solutions (SS-MOMA-ASF-off).

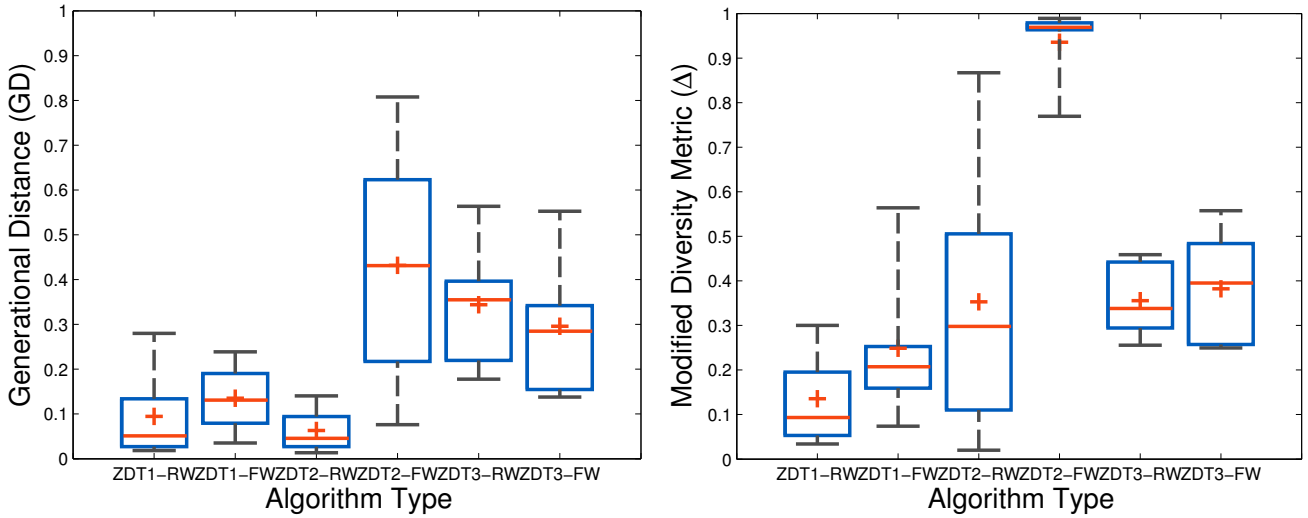


(A) Generational distance.

(B) Modified Diversity metric.

FIGURE 3.3: Convergence of performance indicators of SS-MOMA-ASF with randomized and fixed weights on ZDT1, ZDT2, and ZDT3 problems.

- Normalization using the estimated upper and lower bounds of the objective spaces (SS-MOMA-ASF-obj).

To limit our study, we compared different types of normalization only in the ZDT1, ZDT2, and ZDT3 problems to see how they affected the search; the result is shown in Fig. 3.4. Random weight generation was used since it was the original scheme of SS-MOMA algorithm.

For the ZDT1 problem, there was no great difference observed between SS-MOMA-ASF-off and SS-MOMA-ASF-obj from the GD convergence point of view; even though it can be seen that SS-MOMA-ASF-off slightly outperformed SS-MOMA-ASF-obj in the mean sense in the ZDT1 and ZDT3 problems. The boxplot results of the GD at the end of the optimization process showed that SS-MOMA-ASF-off had a higher standard deviation of the GD, which was reasonable because the changing value for normalization introduced another aspect of randomness into the search process. The difference between two normalization methods is more notable for the convergence of the diversity metric, where SS-MOMA-ASF-off surpassed the SS-MOMA-ASF-obj and produced a more diverse set of solutions in general.

SS-MOMA-ASF-off had a superior diversity performance in the ZDT2 problem than SS-MOMA-ASF-obj where the difference itself was quite notable. Although the mean of the GD was lower (and thus, better) for SS-MOMA-ASF-obj, the difference itself was very slight. SS-MOMA-ASF-obj had a higher probability to fall into the "diversity trap" of the ZDT2 problem than SS-MOMA-ASF-off, as indicated in the boxplot depicted in Fig. 3.4b. Morever, the standard deviation of the diversity metric was very large for SS-MOMA-ASF-obj with respect to SS-MOMA-ASF-off in the ZDT2 problem. It is safe to

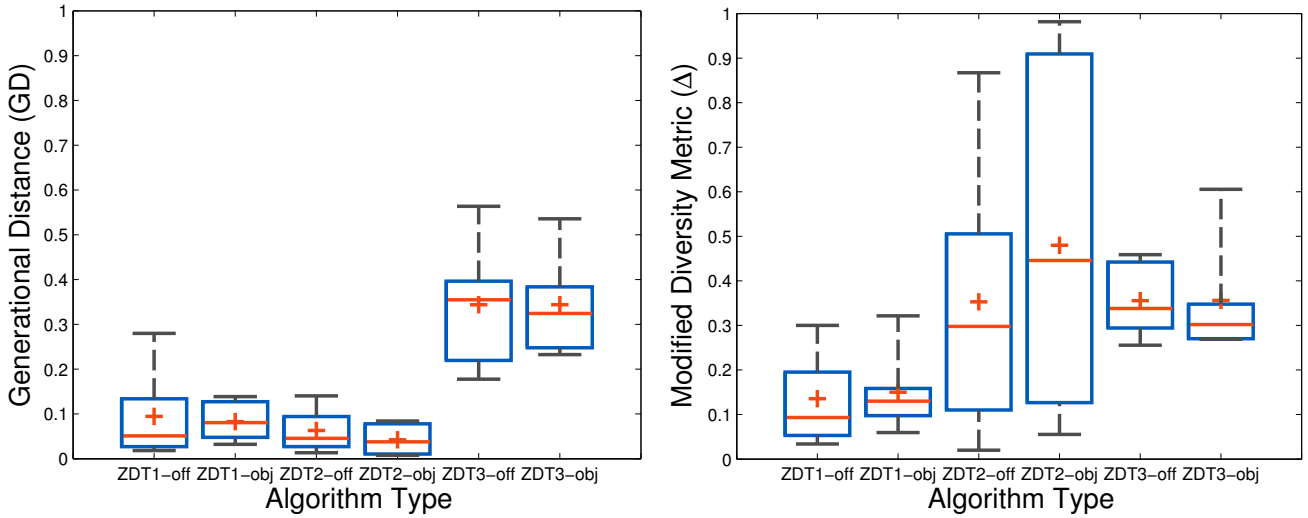


(A) Generational distance.

(B) Modified Diversity metric.

FIGURE 3.4: Performance indicators convergence of SS-MOMA-ASF with different type of normalization on ZDT1, ZDT2, and ZDT3 problems.

conclude here that normalization using the objective values of the offspring offered a higher performance than the estimated bounds of the entire objective spaces of the ZDT2 problem.

On ZDT3 problem, it is not clear which normalization method was the best. From a GD point of view, SS-MOMA-ASF-off could reach the lowest GD value but its overall standard deviation was higher than that of SS-MOMA-ASF-obj. The diversity result showed a similar mean value for both methods, but the standard deviation was higher for SS-MOMA-ASF-off. On the other hand, on average, SS-MOMA-ASF-obj had a better diversity performance but one run shows a much worse value.

Based on this small observation, we chose the upper and lower bounds of the offsprings as the normalization method due to its higher performance on average compared with the other option. Normalization of this type ensured more consistent diversity and a greater exploration of the optimization process. Moreover, we expect that the inconsistency of the SS-MOMA-ASF-obj scheme would be more observable if the objective range of Pareto front is much smaller than the range of the entire objective space; a good reason to choose the SS-MOMA-ASF-off scheme.

### 3.2.5 Result on Artificial Problems

This subsection shows and explains the results obtained by applying SS-MOMA with various local searches and NSGA-II to the selected test problems. Based on the study of normalization and randomized weights, we used randomized weights and normalization using upper and lower bounds among the offpsring solutions for all local search based on scalarizing function for all test problems.

### ZDT1

The result for the ZDT1 problem showed that SS-MOMA-CHEB greatly outperforms the others in the aspect of GD and diversity metric convergence to the Pareto front as indicated by its superiority in the convergence of all indicators shown in Figs. 3.5 and 3.6 and Table 3.3. Its very low standard deviation meant that SS-MOMA-CHEB was very consistent at discovering the Pareto front in the ZDT1 problem. SS-MOMA-ASF had a higher standard deviation of the performance than SS-MOMA-CHEB but it could find higher quality non-dominated solutions than SS-MOMA-WS and SS-MOMA-RMHC. The higher standard deviation was probably due to the highly randomized nature of the SS-MOMA-ASF caused by random weight generation and changing reference points (solutions to be improved) for the local search.

In this particular problem, SS-MOMA-RMHC also performed well and had good GD convergence properties although it was still inferior to SS-MOMA-CHEB. Moreover, the depiction of the convergence of the $\Delta$ metric in Fig. 3.5b showed that SS-MOMA-RMHC was slow during early and middle generation but was able to surpasses SS-MOMA-WS at the end of the search process. This trend was probably caused by the search direction of SS-MOMA-RMHC that focused on nearly similar direction. This was in contrast with the scalarizing function type that had high exploratory characteristics due to the random weight generation. SS-MOMA-RMHC needed some extra time to be able to explore and cover wider sections of the Pareto front. This was also caused by the characteristics of ZDT type problems with objective space that coincides with the Pareto front on $f_1 = 0$. We expect that SS-MOMA-RMHC would perform for real-world problems that do not exhibits this characteristic. The original NSGA-II, as it was expected, was inferior to the SS-MOMA with all types of local search.

The non-dominated solutions from independent run with best and worst GD of each algorithm are depicted in Fig. 3.7. Qualitatively speaking, it can be seen that the best solutions obtained by SS-MOMA-ASF and SS-MOMA-CHEB were surpassing those of the other local searches in quality.

In general, in ZDT1 problem all types of local search could converge to the Pareto front with sufficient accuracy without any problem in the diversity of the solutions, but it is clear that ASF and Chebyshev-type local search was superior to SS-MOMA-RMHC, SS-MOMA-WS (which was the original local search for SS-MOMA), and the original NSGA-II.

TABLE 3.3: Mean and standard deviation of GD and $\Delta$ of the final solutions of ZDT1 problem.

| Algorithm | $\mu$(GD) | $\sigma$(GD) | $\mu(\Delta)$ | $\sigma(\Delta)$ |
|---|---|---|---|---|
| SS-MOMA-ASF | 0.095 | 0.108 | 0.135 | 0.100 |
| SS-MOMA-WS | 0.179 | 0.055 | 0.215 | 0.055 |
| SS-MOMA-RMHC | 0.072 | 0.019 | 0.174 | 0.087 |
| SS-MOMA-CHEB | 0.026 | 0.013 | 0.045 | 0.022 |
| NSGA-II | 0.931 | 0.059 | 0.552 | 0.0344 |

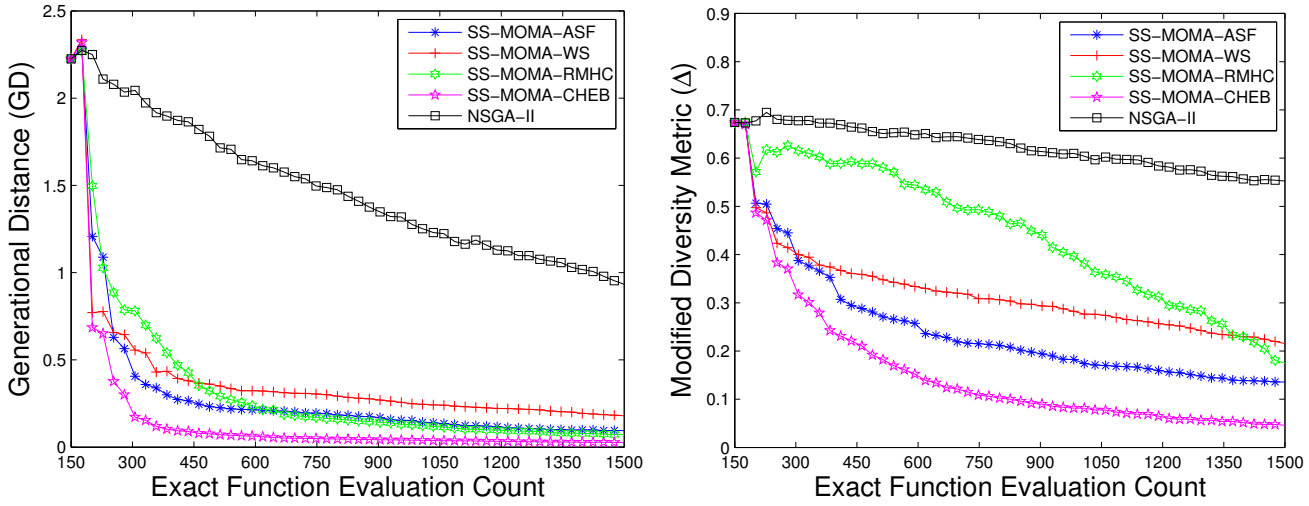


(A) Generational distance. (B) Modified Diversity metric.

FIGURE 3.5: Performance indicators convergence of various algorithms on ZDT1 problem.

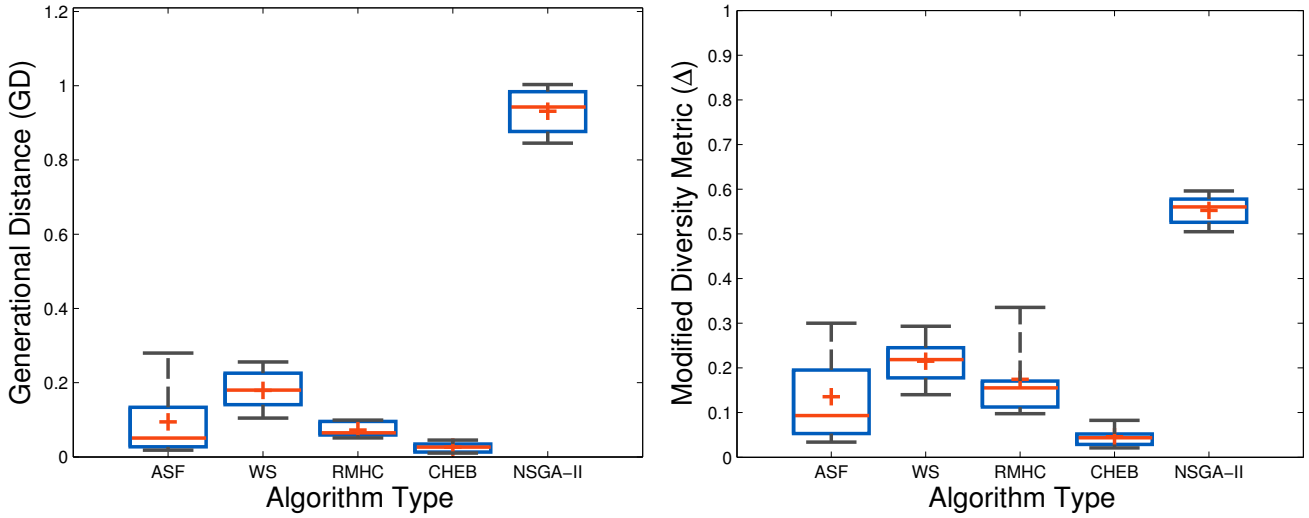


(A) Generational distance. (B) Modified Diversity metric.

FIGURE 3.6: Final results boxfplot of various algorithms on ZDT1 problem.

### ZDT2

The results obtained from experiment for the ZDT2 problem are shown in Figs. 3.8, 3.9, and Table 3.4. For the ZDT2 problem, SS-MOMA-ASF clearly outperformed the other types of local search and NSGA-II. Both SS-MOMA-WS and SS-MOMA-RMHC suffered greatly from the "diversity trap" of the ZDT2 problem where the solution only found a very small portion of the Pareto front; the solutions were concentrated in one part only as depicted in Fig. 3.10. SS-MOMA-RMHC suffered this problem worse than SS-MOMA-WS; the mean value of the diversity metric showed that the diversity of the non-dominated solutions was extremely low. The failure of RMHC in the ZDT2 problem was due to the landscape of the ZDT2 problem that directed the search into a small portion of the Pareto front. To

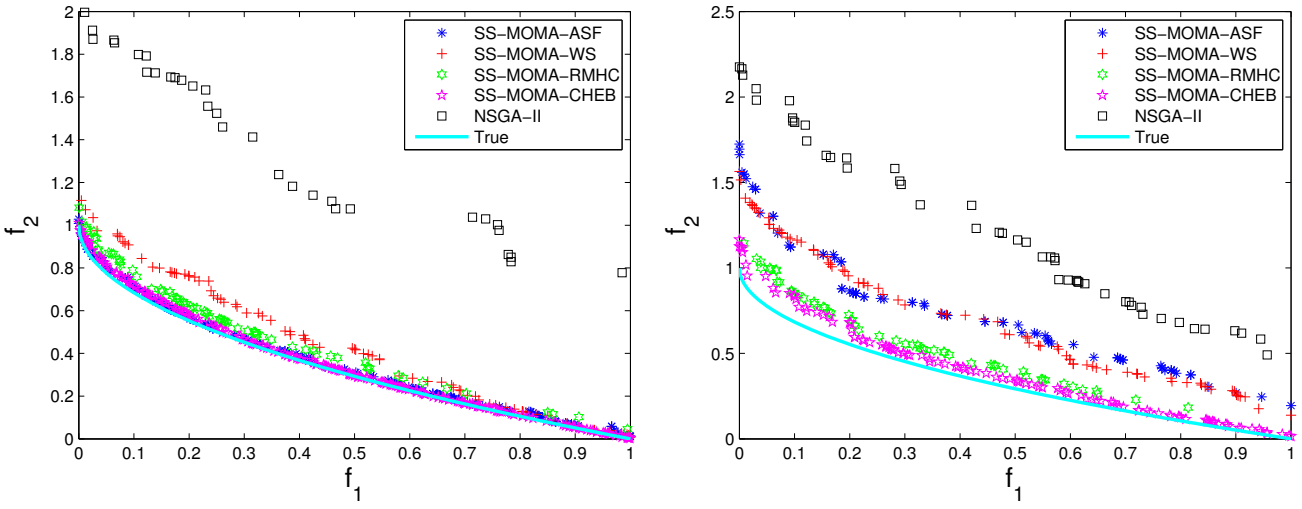


(A) Best solutions. (B) Worst solutions.

FIGURE 3.7: Solutions with best and worst GD from various algorithms on ZDT1 problem.

say that RMHC was independent or dependent on the convexity of the problems is not correct because RMHC only depended on whether the next step dominated the current solution or not. Therefore, for each improvement of an individual solution, there was nothing like an optimal solution of a given subproblem. This was in contrast to the local search that used scalarizing functions that offered an optimal solution depending on the type of scalarizing function and weights for a given subproblem.

To see if the original NSGA-II also suffered from the same problem, we tested it with the same numbers of population and generation at which the result clearly showed that original NSGA-II also failed to discover a large portion of the Pareto front. This means that pure evolutionary operator was also the source for the relatively low performance of all schemes, where the implementation of a local search with a WS and RMHC could not help in increasing the performance of the optimizer for this particular problem. In contrast, the introduction of ASF or Chebyshev-type local searches into the memetic algorithm scheme could remedy and enhance the diversity of the solutions. This higher performance of SS-MOMA-ASF and SS-MOMA-CHEB was due to the properties of achievement type scalarizing function that were independent to the convexity of the problem. In this problem, we showed that the memetic algorithm with WS had difficulty solving the non-convex problem. This was contrary to the result in the original SS-MOMA paper[25] where the scheme with a WS was able to find an entire of the Pareto front. The failure of SS-MOMA-WS in our case might have been caused by the inability of NSGA-II with a low population size and maximum generation number and a WS scalarizing function to perform well for the ZDT2 problem. In this particular problem, the independence to the convexity of the problem was important and this was the reason why SS-MOMA-ASF and SS-MOMA-CHEB clearly outperformed the others.

Comparing SS-MOMA-ASF and SS-MOMA-CHEB, the former was able to find more diverse solutions than the latter, although the standard deviation was still very high due to the "diversity trap" difficulty.

On some runs, SS-MOMA-CHEB was able to overcome the diversity trap but many of the runs suffered. The diversity quality of SS-MOMA-CHEB was much lower than that of SS-MOMA-ASF, even though it had the great convergence property of GD. The difficulties of SS-MOMA-CHEB were due to a less dynamic exploration nature than the SS-MOMA-ASF. Once the reference point was set on a point near the boundary of the objective spaces that caused the "diversity trap", it became difficult for the SS-MOMA-CHEB to escape. On the other hand, SS-MOMA-ASF had a higher possibility of escaping because of the dynamic nature of the reference point for local improvement.

Clearly, the superior method on ZDT2 problem was SS-MOMA-ASF. Fig. 3.10 showing solutions with best and worst GD confirms this.

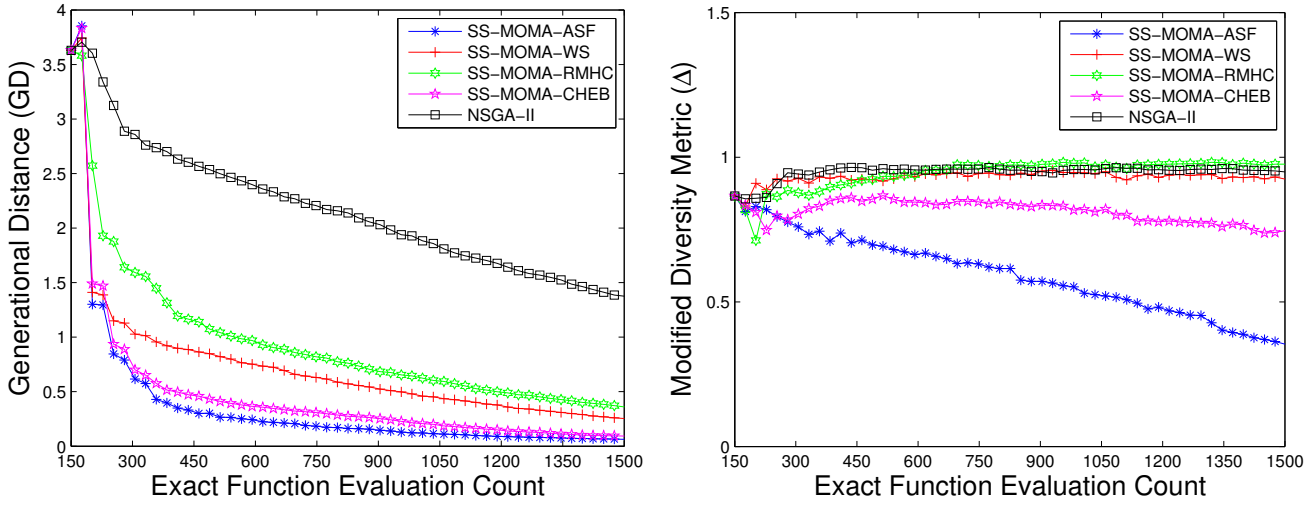


(A) Generational distance.

(B) Modified Diversity metric.

FIGURE 3.8: Performance indicators convergence of various algorithms on ZDT2 problem.

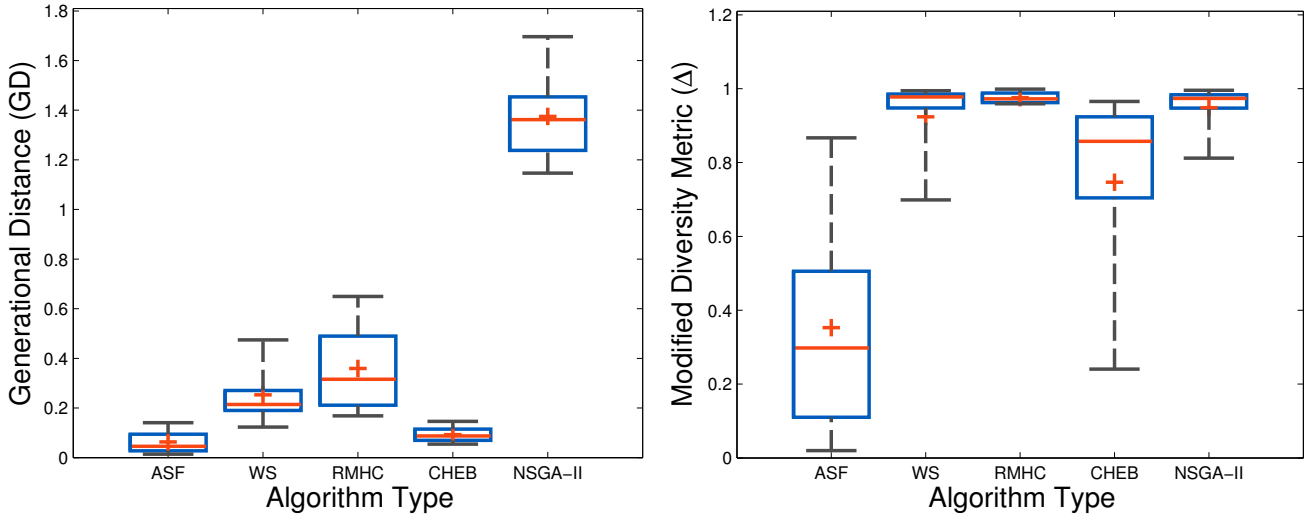


(A) Generational distance

(B) Modified Diversity metric

FIGURE 3.9: Final results boxfplot of various algorithms on ZDT2 problem.

TABLE 3.4: Mean and standard deviation of GD and $\Delta$ of the final solutions on ZDT2 problem.

| Algorithm | $\mu$(GD) | $\sigma$(GD) | $\mu(\Delta)$ | $\sigma(\Delta)$ |
|---|---|---|---|---|
| SS-MOMA-ASF | 0.63 | 0.047 | 0.353 | 0.315 |
| SS-MOMA-WS | 0.253 | 0.127 | 0.924 | 0.117 |
| SS-MOMA-RMHC | 0.359 | 0.183 | 0.976 | 0.015 |
| SS-MOMA-CHEB | 0.092 | 0.033 | 0.747 | 0.272 |
| NSGA-II | 1.375 | 0.200 | 0.949 | 0.081 |

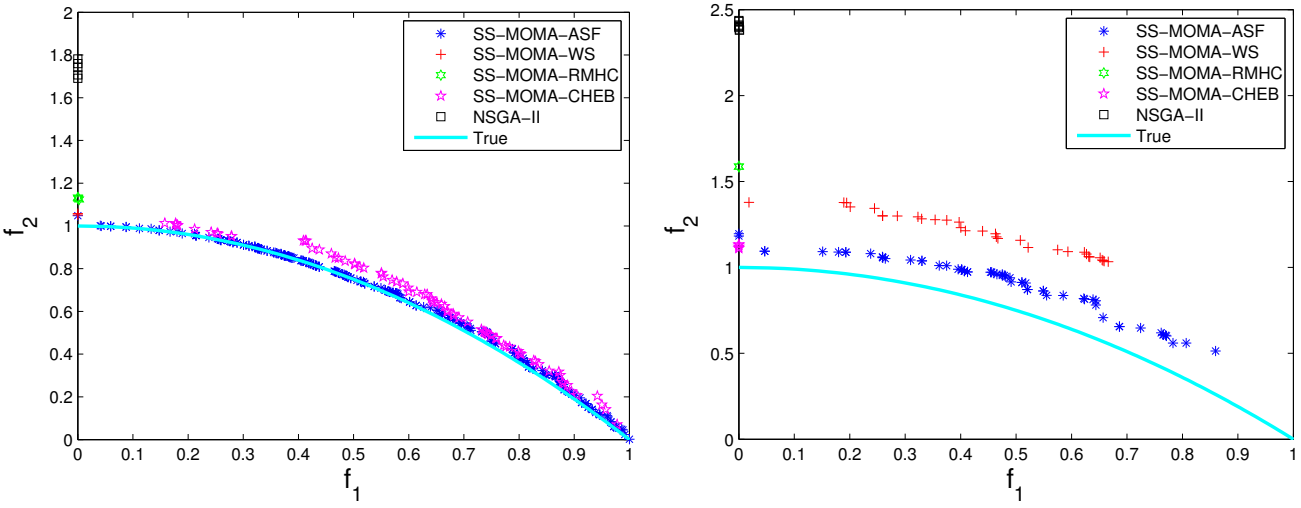


(A) Best solutions.

(B) Worst solutions.

FIGURE 3.10: Solutions with best and worst GD from various algorithms on ZDT2 problem.

### ZDT3

The results show that this problem was more difficult than either ZDT1 or ZDT2 from the viewpoint of approaching the Pareto front. In fact, neither local search method could get very close to the true Pareto front of ZDT3. Nevertheless, optimization with a local search was still far better than optimization without it, as indicated by the performance metrics presented in Table 3.5 and Figs. 3.11 and 3.12. On average, SS-MOMA-ASF and SS-MOMA-CHEB surpassed SS-MOMA-WS in term of convergence to the Pareto front and diversity of the solution, although SS-MOMA-ASF had a higher standard deviation on the diversity metric. SS-MOMA-RMHC had the best GD convergence property but its diversity metric was worse than those of other local searches. This again shows that the domination-based local search was inferior to the scalarizing function type local search on the complex Pareto front, as it was also shown by the result in ZDT2 problem.

One of the problems of SS-MOMA-ASF was the difficulty of exploring the entire Pareto front if the current solutions were already very near to the Pareto front but still not well distributed. This might be one of the explanation of why SS-MOMA-CHEB surpassed SS-MOMA-ASF from the diversity aspect

on ZDT3 problem. SS-MOMA-CHEB performed better than SS-MOMA-ASF and was able to better explore the Pareto front. This was because the SS-MOMA-CHEB used reference point which was defined by the upper and lower bounds of the offpsring solutions and not the individual to be improved. This means that given an appropriate weights and the reference point, the optimum point of the given Chebyshev function could located far from the individual solution to be improved.

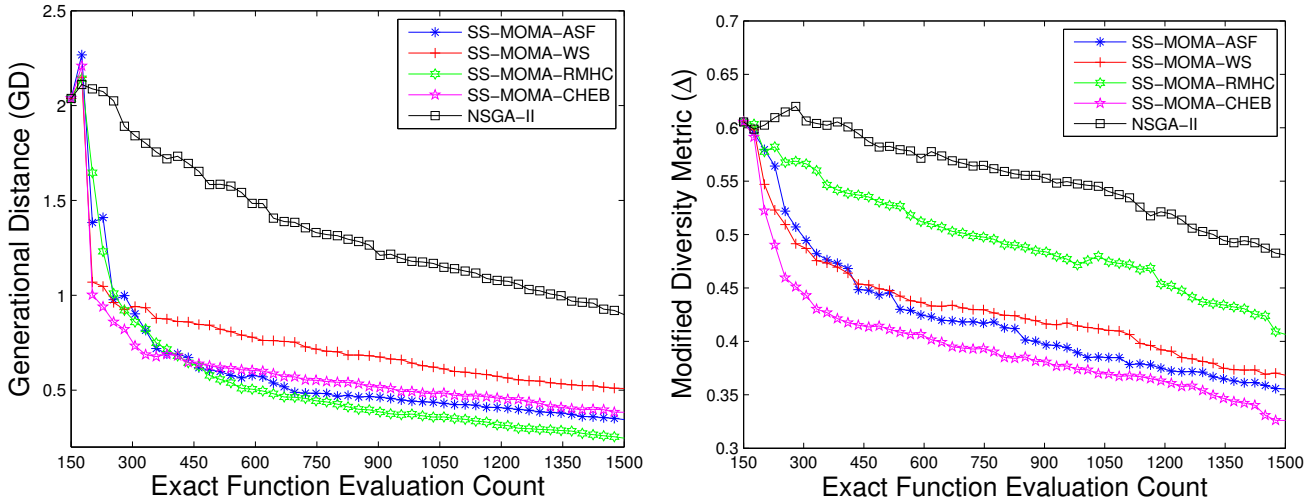


(A) Generational distance. (B) Modified Diversity metric.

FIGURE 3.11: Performance indicators convergence of various algorithms on ZDT3 problem.

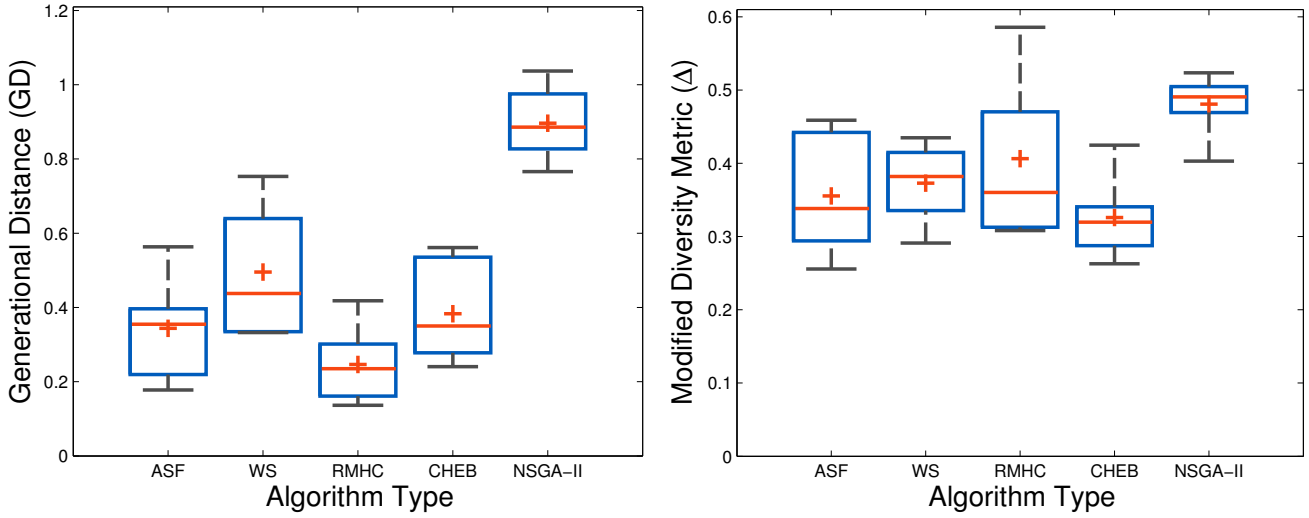


(A) Generational distance. (B) Modified Diversity metric.

FIGURE 3.12: Final results boxplot of various algorithms on ZDT3 problem.

### CONV1

The CONV1 function had more of the characteristics of a true optimization problem because the boundary of the Pareto fronts did not coincide with the boundary of the decision space. The dimensionality

TABLE 3.5: Mean and standard deviation of GD and $\Delta$ of the final solutions on ZDT3 problem.

| Local search | $\mu$(GD) | $\sigma$(GD) | $\mu(\Delta)$ | $\sigma(\Delta)$ |
|---|---|---|---|---|
| ASF | 0.344 | 0.141 | 0.356 | 0.081 |
| WS | 0.495 | 0.172 | 0.373 | 0.055 |
| RMHC | 0.246 | 0.104 | 0.406 | 0.111 |
| CHEB | 0.383 | 0.128 | 0.326 | 0.058 |
| NSGA-II | 0.896 | 0.101 | 0.481 | 0.046 |

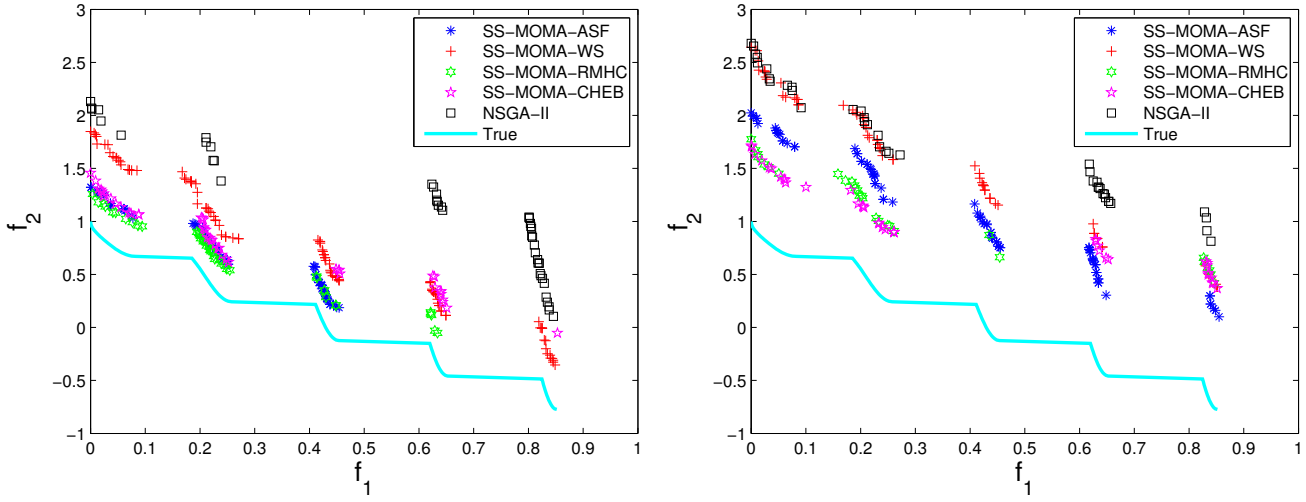


(A) Best solutions.

(B) Worst solutions.

FIGURE 3.13: Solutions with best and worst GD from various algorithms on ZDT3 problem.

of this problem was set to 16. This dimensionality was chosen after solving CONV1 using NSGA-II with high numbers of population and generation with various dimensions to see which one had good characteristics of the Pareto front. To be able to use the GD and diversity metric for performance comparison, the "true" Pareto front was found first by applying ordinary NSGA-II with a population size and generation of 100 and 400, respectively. This "true" Pareto front was then used as the reference point for calculating of the performance metric.

From the results shown in Figs. 3.14 and 3.15, and Table 3.6. SS-MOMA-ASF was the best performer for the CONV1 problem and was superior to other local search methods in terms of the diversity metric performance. The other local search methods had approximately the same performance from a generational distance point of view where all local search methods converged to the Pareto front in a relatively similar performance. The original NSGA-II was again the worst performer (it is not visible in the GD metric on Fig. 3.15 due to its very high value), suggesting that applying a local surrogate-based local search is always beneficial, regardless of the local search method being used. The experiment on this function showed that although the function was relatively easy to approximate because of the unimodality of each objective function, the choice of the scalarizing function could greatly impact the

evolved solutions, thus affecting their quality. In this case, SS-MOMA-ASF was able to explore a wide section of the Pareto front compared with the other local search method, thanks to the effect of randomized weight and suitable normalization methods. As shown in Fig. 3.16, even the worst solutions obtained with SS-MOMA-ASF feature a diverse set of solutions compared to the other local searches. The performance of SS-MOMA-CHEB was comparable to that of SS-MOMA-WS in this particular problem. Although the SS-MOMA-CHEB was slightly better in terms of diversity than SS-MOMA-WS. SS-MOMA-RMHC obtained a good convergence set of solutions but with an evidently lower diversity than the others.

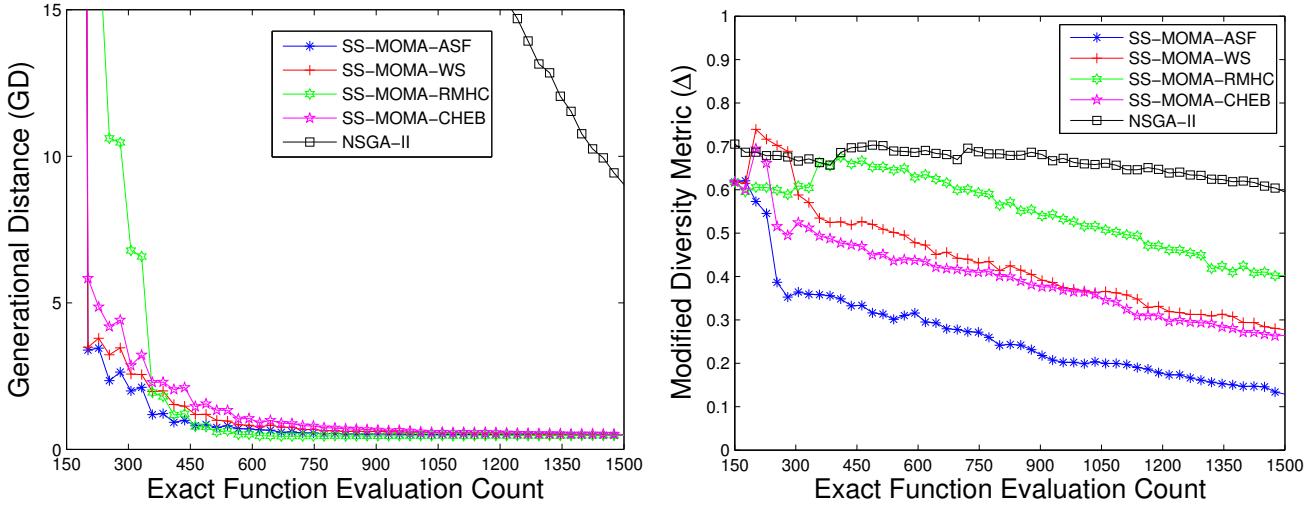


(A) Generational distance.

(B) Modified Diversity metric.

FIGURE 3.14: Performance indicators convergence of various algorithms on CONV1 problem.

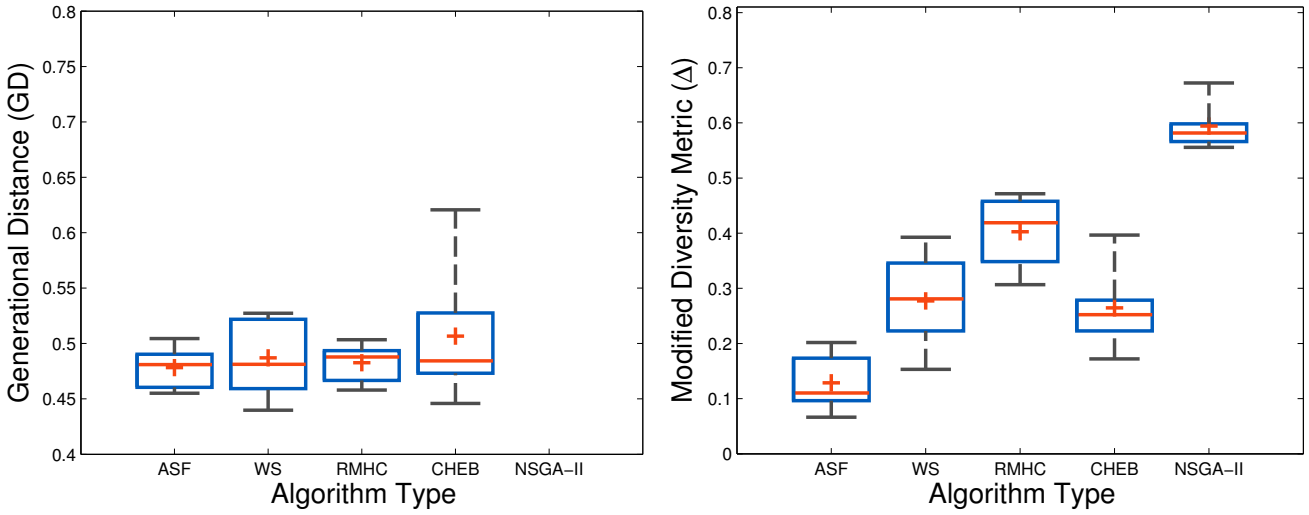


(A) Generational distance.

(B) Modified Diversity metric.

FIGURE 3.15: Final results boxplot of various algorithms on CONV1 problem.

TABLE 3.6: Mean and standard deviation of GD and $\Delta$ of the final solutions on CONV1 problem.

| Local search | $\mu$(GD) | $\sigma$(GD) | $\mu(\Delta)$ | $\sigma(\Delta)$ |
|---|---|---|---|---|
| ASF | 0.478 | 0.019 | 0.128 | 0.051 |
| WS | 0.487 | 0.035 | 0.277 | 0.088 |
| RMHC | 0.483 | 0.017 | 0.402 | 0.063 |
| CHEB | 0.507 | 0.066 | 0.264 | 0.078 |
| NSGA-II | 8.999 | 1.771 | 0.594 | 0.043 |

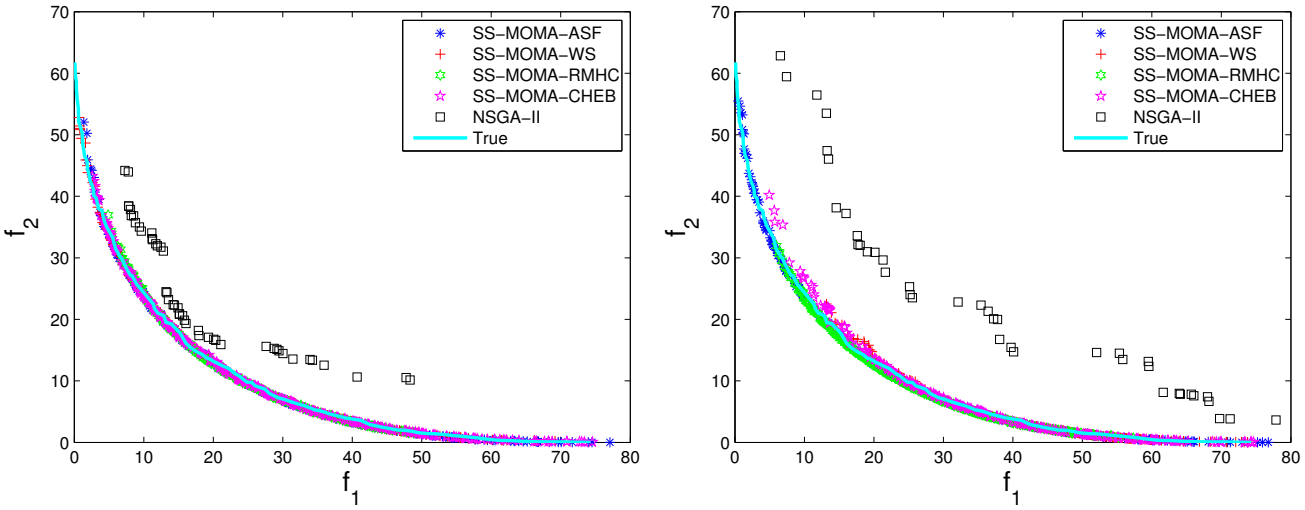


(A) Best solutions. (B) Worst solutions.

FIGURE 3.16: Solutions with best and worst GD from various algorithms on CONV1 problem.

### CONV2

The "true" Pareto front from the CONV2 problem was obtained in the same fashion as the CONV1 problem. The results of this problem are depicted in Fig. 3.17 and 3.18, and Table 3.7. The best and worst solutions from each algorithm are not depicted here due to the visualization difficulty of visualizing three-dimensional solutions. As it can be seen from the figures and table, all local search method had similar convergence results for the GD metric, but the difference was clearly visible for the performance of the diversity metric on the three-dimensional CONV2 problem. The result shows that SS-MOMA-CHEB could find a more diverse solution, as indicated by the lower mean and standard deviation of the $\Delta$ metric. In this CONV2 function, SS-MOMA-ASF had a worse diversity metric than SS-MOMA-CHEB or even SS-MOMA-RMHC. The lower diversity performance of SS-MOMA-ASF on CONV2 function might have been caused by its lower exploration capability if the solutions were already very close to the Pareto front. Solutions that were already in the vicinity of the Pareto front tended to be similar if the weights were varied.On the other hand, SS-MOMA-CHEB had a higher exploration capability in the vicinity of the Pareto front due to the higher sensitivity to the varied weights.

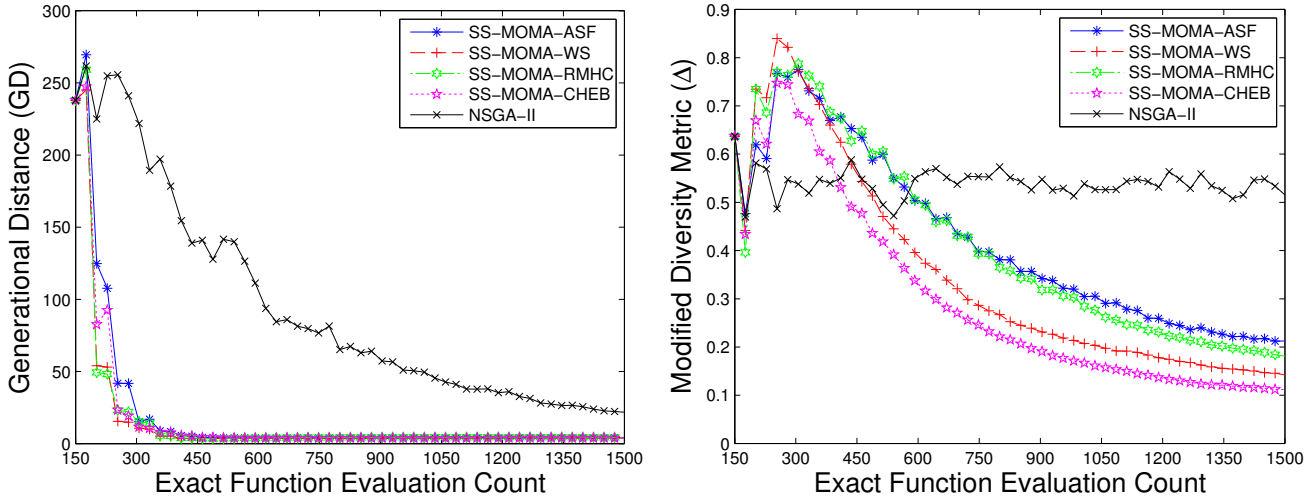


(A) Generational distance. (B) Modified Diversity metric.

FIGURE 3.17: Convergence of performance indicators of various algorithms of CONV2 problem.

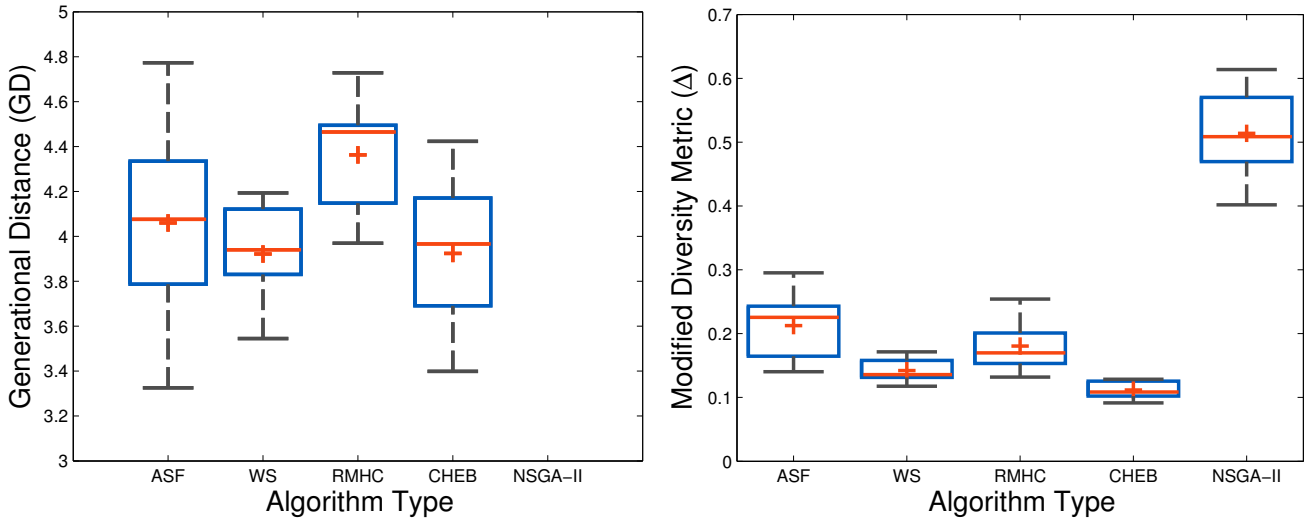


(A) Generational distance (B) Modified Diversity metric

FIGURE 3.18: Boxplot of final results of various algorithms of CONV2 problem.

### 3.2.6 Test on Constrained Problem

The purpose of this test was to see the applicability of constraint-handling method equipped to SS-MOMA. We did not perform a thorough test on constrained problem because unconstrained test was sufficient to observe the capability of the local search methods. Therefore, what we wanted to investigate here is either the constraint handling method was successfully applied to SS-MOMA or not. The CTP1 test problem[131] was used to test the constrained version of SS-MOMA where ASF was employed as the local search function. The expression for CTP1 is as follows:

TABLE 3.7: Mean and standard deviation of GD and $\Delta$ of the final solutions of CONV2 problem.

| Local search | $\mu$(GD) | $\sigma$(GD) | $\mu(\Delta)$ | $\sigma(\Delta)$ |
|---|---|---|---|---|
| ASF | 4.060 | 0.492 | 0.212 | 0.0560 |
| WS | 3.921 | 0.231 | 0.142 | 0.0197 |
| RMHC | 4.363 | 0.276 | 0.180 | 0.0437 |
| CHEB | 3.924 | 0.3736 | 0.116 | 0.0142 |
| NSGA-II | 21.693 | 9.488 | 0.513 | 0.0782 |

$$\begin{aligned} \text{Minimize} &= \begin{cases} f_1(x) = x_1 \\ f_2(x) = g(x)\exp(-f_1(x), g(x)) \end{cases} \\ \text{subject to} &= \begin{cases} C_1(x) = f_2(x) - 0.858\exp(-0.541/g_x) \\ C_2(x) = f_2(x) - 0.728\exp(-0.295/g_x) \end{cases} \end{aligned} \tag{3.16}$$

The dimension of the CTP1 problem was set to 15. The challenge for the optimizer in the CTP1 problem is that it has to be able to found the Pareto front that was located in the vicinity of the infeasible area[131]. We tested the constrained SS-MOMA on one function only for the purpose of demonstrating its efficacy on the constrained problem. The capability of improved SS-MOMA itself was already well demonstrated on the unconstrained problems. Fig. 3.19 depicts the illustration of constrained and unconstrained Pareto front of the CTP1 problem where 10000 samples were generated using Halton sequence. As it could be seen from the figure, the presence of the constraint changes the Pareto front of the unconstrained problem where the Pareto front was now located in the border of feasible and infeasible area.

The SS-MOMA-ASF was used to test the constraint handling method and only one run was performed because our goal here was to show the constraint handling method's applicability. Result on CTP1 problem, as it shown in Fig. 3.20 showed that the constrained SS-MOMA was able to deal with constrained problem and arrived into good quality non-dominated solutions that satisfied the constraints. Moreover, the local search was able to perform careful search to find optimized solutions that did not violate the constraint. This is indicated in the depiction of all solutions generated in one run where it could be seen that only very few solutions generated by constrained SS-MOMA violated the constraint. To conclude, the result shows that the SS-MOMA equipped with the proposed constraint handling method was able to deal with constrained problem and ready to be applied to real optimization problems. The adaptive constraint handling is also attractive because it could be applied in the sum of the constration violation context and results in only one constraint value for each solutions to avoid complex constraint handling method.

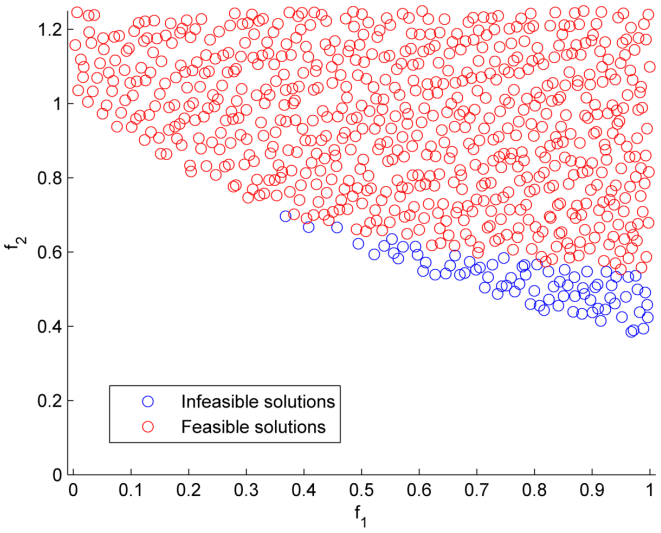


FIGURE 3.19: Depiction of CTP1 problem.

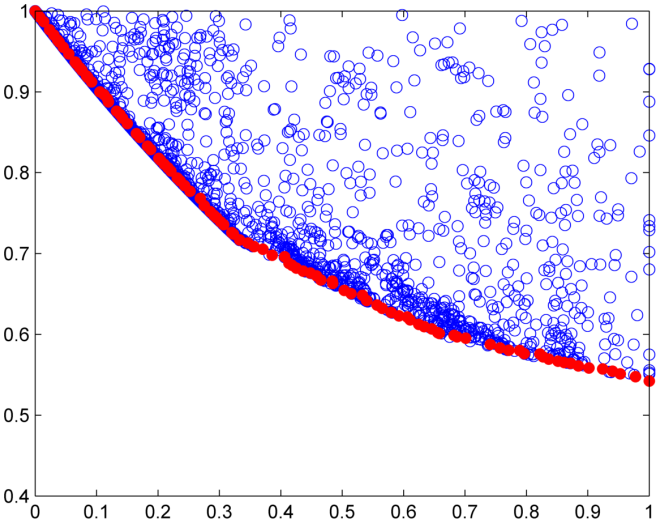

FIGURE 3.20: Result obtained by constrained SS-MOMA-ASF of CTP1 problem.

### 3.2.7 Summary of Artificial Test Problems

Results on artificial problems showed that, in general, the local search which were based on the ASF and Chebyshev function performed better than WS and RMHC. SS-MOMA-ASF was the best performer on the ZDT2 and CONV1 problems but SS-MOMA-CHEB can found solutions with higher quality than the others on ZDT1, ZDT3, and CONV2 problems. Based on this results, it can be said that the search based on ASF or Chebyshev type function were more robust than the original WS to be applied in SS-MOMA algorithm with limited number of function evaluations.

The success of ASF/Chebyshev based local search was mainly caused by the independency to the convexity of the problem and direct mapping to the Pareto optimum for a given reference point and weights. Local search methods based on the scalarizing function (ASF, Chebyshev, and WS) were also found to be better than the RMHC that does not need normalization and random weights generation.

Even though there were additional difficulties such as the determination of the weights and reference point for the scalarizing function, they were still more robust than the method based on non-domination operator. We still do not have enough evidence to say whether SS-MOMA-ASF is better than the SS-MOMA-CHEB or vice versa; more test problems are needed. However, for real application we have more confidence to use ASF/Chebyshev based search instead of the WS to guide the local search of SS-MOMA. It is important to test this hypothesis on real world optimization problem. Because of this, on the real test problem given on the following subsection we use SS-MOMA-ASF in conjunction with the Chebyshev function to be compared directly with SS-MOMA-WS.

## 3.3 Application to Airfoil Optimization

Due to the higher capability of achievement-type scalarizing function to guide the local search for SS-MOMA algorithm, the SS-MOMA with achievement-type scalarizing function was used for the airfoil optimization case to see its usefulness in real engineering-optimization problems. The test on a real engineering problem was also essential for determining the practicability of concepts such as normalization and constraint handling of in real world optimization problems. For real-world problem, the SS-MOMA-ASF was used as the base algorithm and switched to Chebyshev based local search if the ASF search got stucked. We chose SS-MOMA-ASF as the base algorithm because it was more robust to find non-convex section of the Pareto front than SS-MOMA-CHEB. Since the Pareto front shape of the problem is unknown beforehand, it is better to use optimizer with local search which is robust to any possible shape of the Pareto front. However, in our problem, there were some occasions when search using ASF cannot further improves the solution (the solution obtained by SQP was similar to the individual to be improved) so the local search method was automatically switched to Chebyshev based by simply changing the reference point if this occurred in a given subproblem.

The flow-solver used to solve the Euler equation was SU2[149]. Here we did not use the Navier-Stokes equation because the present purpose was to demonstrate the capabilities of SS-MOMA-ASF; hence, a relatively quick evaluation was needed. It is not that expensive to solve the Euler flow around the airfoil, especially if a high-performance computer is available. Nonetheless, it serves as a good benchmark problem for demonstration of the optimizer. The Euler mesh was generated in an unstructured way using distmesh algorithm[150] and used the airfoil coordinates to create the mesh. An example of the resulting mesh generated by the distmesh algorithm is shown in Figure 3.21.

One also has to be careful when determining the neighbors of the solution to be improved. This is because the decision variables could be disparately scaled, and if the ranges of the variables were not normalized the surrogate building scheme could detect the wrong neighbors. The normalization could be done simply by transforming the decision variables to the 0-1 range.

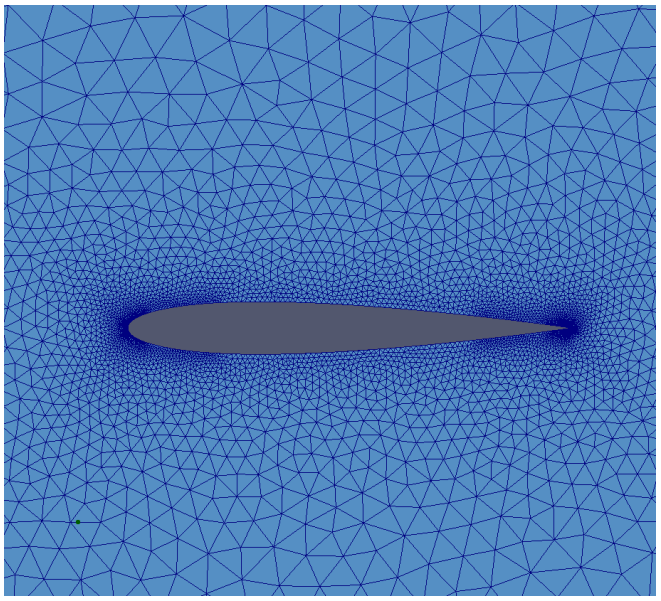

FIGURE 3.21: Mesh used in the airfoil optimization problem.

Not all generated airfoils returned aerodynamic coefficients because some had erroneous geometries or failed CFD-convergence. Even though we tried to minimize these possibilities, there was no way to guarantee that all generated solutions were error free. If cases like this occurred, then the solution was automatically given a very large value, thus eliminating its chance of survival. Moreover, these solutions were not included in the archive for building surrogate models. This was done to ensure that the surrogate-building process would not be affected by the presence of erroneous solutions.

The optimization case refers to the cases explained in Ray and Tsai[151] and Vicini and Quagliarella[152]. The former deals with airfoil optimization while the latter was a redesign of an ONERAM6 wing. The population number and maximum generation number were set to 26 and 11, respectively, where the first population was initialized with a Halton sequence[153] with 150 samples, resulting in a total number of exact function calls of $150 + (26 \times 2 \times 11) = 722$ resembling the optimization case with a limited budget. The crossover and the mutation probability were set to 0.9 and $1/n$ where $n$ was the number of decision variables. For all optimizers (SS-MOMA-ASF with Chebyshev, SS-MOMA-WS, NSGA-II) the number of the independent runs is three.

The decision variables were 16 dimensional class-shape-transformation (CST) parameters[154] (8 for each surface) with zero value on the trailing edge ordinate and a thickness set to 0.001. The datum airfoil was RAE2822, with CST parameters found by minimizing the error between the true RAE2822 and the CST-made airfoil shape. The CST parameters were then varied to $\pm 20\%$ as the upper and lower bounds of the decision variables. For this problem, the objective functions were:

$$\text{minimize: } \frac{C_d}{C_l^2}, C_m^2$$

$$\text{Subject to: } t_{\max} \geq 11.5\%$$

We wanted to observe the performances of the optimizers when applied to problems with high dimension, where it is very likely that the global surrogate model will fail. For the surrogate model, we used Kriging due to its robustness[141]. The training time for the Kriging hyperparameters could be considered to be negligible relative to the function evaluation cost.

### Optimization result

So as to use GD and $\Delta$ metric as performance indicators, the reference non-dominated solutions were obtained using solutions from all runs and optimizers. The upper bounds of these non-dominated solutions were then used as a reference point for hypervolume calculation. The statistical results obtained from NSGA-II, SS-MOMA-ASF, and SS-MOMA-WS are shown in Tables. 3.8, 3.9, and 3.10 and Fig. 3.22. The results indicated that the performance of SS-MOMA-ASF and SS-MOMA-WS obviously surpassed that of NSGA-II algorithm. The solutions obtained from NSGA-II, however, were not so poor in quality compared with those of the other algorithms, despite of the high-dimensionality of the problem. Nonetheless, the use of the local-surrogate and memetic algorithm framework clearly improved the quality of the obtained solutions. From the GD point of view, SS-MOMA-ASF was on par with SS-MOMA-WS (see Tables 3.8 and 3.9); the value did not differ much, even though SS-MOMA-ASF slightly outperformed SS-MOMA-WS. The superiority of SS-MOMA-ASF to the SS-MOMA-WS could be clearly observed from the lower mean of final diversity metric from the three runs. From hypervolume point of view, the hypervolume metric of the solutions found by SS-MOMA-ASF was also higher than either NSGA-II or SS-MOMA-WS. An examination of all evolved Pareto fronts from the three runs in Fig. 3.22 clearly shows that the results from SS-MOMA-ASF had a larger diversity than those from SS-MOMA-WS.

| | **1st run** | **2nd run** | **3rd run** | **Mean** |
|---|---|---|---|---|
| GD | 9.966E-05 | 8.709E-05 | 3.265E-05 | 7.313E-05 |
| $\Delta$ | 2.047E-01 | 2.412E-02 | 4.328E-01 | 2.205E-01 |
| H | 1.361E-04 | 1.375E-04 | 1.378E-04 | 1.371E-04 |

TABLE 3.8: Mean and standard deviation of GD and $\Delta$ of the final solutions from the aerodynamic test problem with SS-MOMA-ASF.

| | **1st run** | **2nd run** | **3rd run** | **Mean** |
|---|---|---|---|---|
| GD | 5.094E-05 | 8.141E-05 | 1.321E-04 | 8.813E-05 |
| $\Delta$ | 3.445E-01 | 5.609E-01 | 5.44E-01 | 4.79E-01 |
| H | 1.373E-04 | 1.365E-04 | 1.347E-04 | 1.361E-0.4 |

TABLE 3.9: Mean and standard deviation of GD and $\Delta$ of the final solutions from the aerodynamic test problem with SS-MOMA-WS.

Figure. 3.23 depicts the airfoil with the lowest first objective ($C_d/C_l^2 = 0.0045, C_m^2 = 0.0155$), lowest second objective ($C_d/C_l^2 = 0.0170, C_m^2 = 0.0037$) found by combining the results from all optimizers, and RAE 2822 airfoil. Table 3.11 and Fig. 3.24 show the aerodynamic coefficients value and the surface

| | 1st run | 2nd run | 3rd run | Mean |
|---|---|---|---|---|
| GD | 4.252E-04 | 7.418E-04 | 5.163E-04 | 5.611E-04 |
| Δ | 5.381E-01 | 2.814E-01 | 1.773E-01 | 3.323E-01 |
| H | 1.297E-04 | 1.251E-04 | 1.552E-04 | 1.367E-04 |

TABLE 3.10: Mean and standard deviation of GD and Δ of the final solutions from the aerodynamic test problem with NSGA-II.

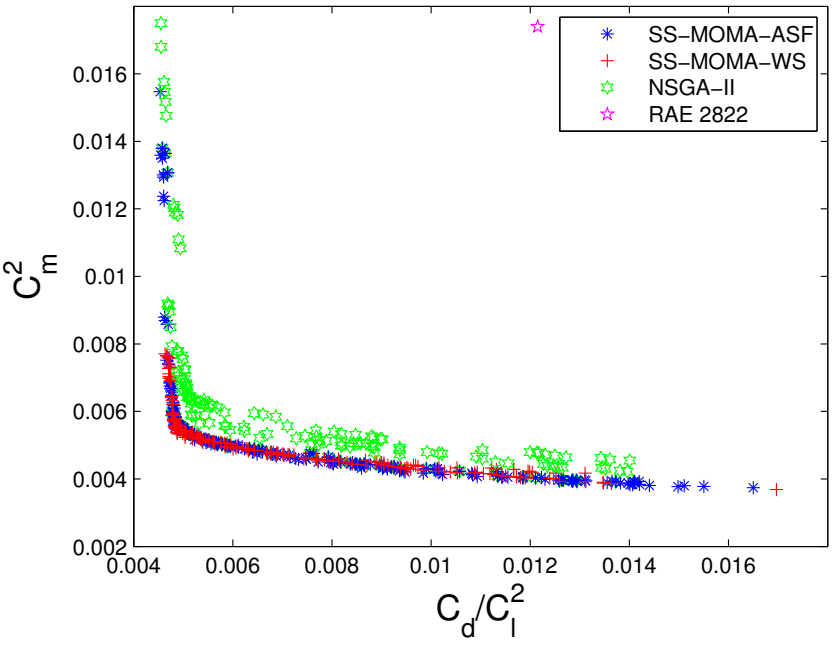


FIGURE 3.22: Non-dominated solutions obtained by SS-MOMA-ASF, SS-MOMA-WS and NSGA-II from the airfoil optimization case.

pressure coefficient ($C_p$) plot of the extremums and RAE 2822 airfoil. Depiction of the pressure field is given in Fig. 3.25 that clearly shows the presence of shock wave with different magnitude for each airfoil.

Based on the observation, the lower surface shape of the airfoil with lowest $C_d/C_l^2$ closely resembles the RAE 2822 with the difference mainly could be seen on the upper surface where it has smaller upper crest height compares to the RAE 2822. The lowest $C_d/C_l^2$ airfoil has smaller $C_d$ than the datum airfoil but almost similar value of $C_l$ and $C_m$. As it can be observed from the $C_p$ plot and pressure field depiction, lowest $C_d/C_l^2$ airfoil has nearly similar location of shock wave but reduced intensity of the shock wave that reduces the wave drag. This reduced $C_d$ corresponds directly to the increment of the aerodynamic efficiency $C_d/C_l^2$. On the other hand, we observed that the location of the shock wave of the lowest $C_m^2$ airfoil moves closer toward the leading edge thus reduces the magnitude of the pitching moment; which was consistent with the previous observation[151]. However, lowest $C_m^2$ airfoil has smaller $C_l$ and higher $C_d$ with respect to the RAE 2822 due to the presence of stronger shock wave (see Fig. 3.25b) that contributes to its low aerodynamic efficiency.

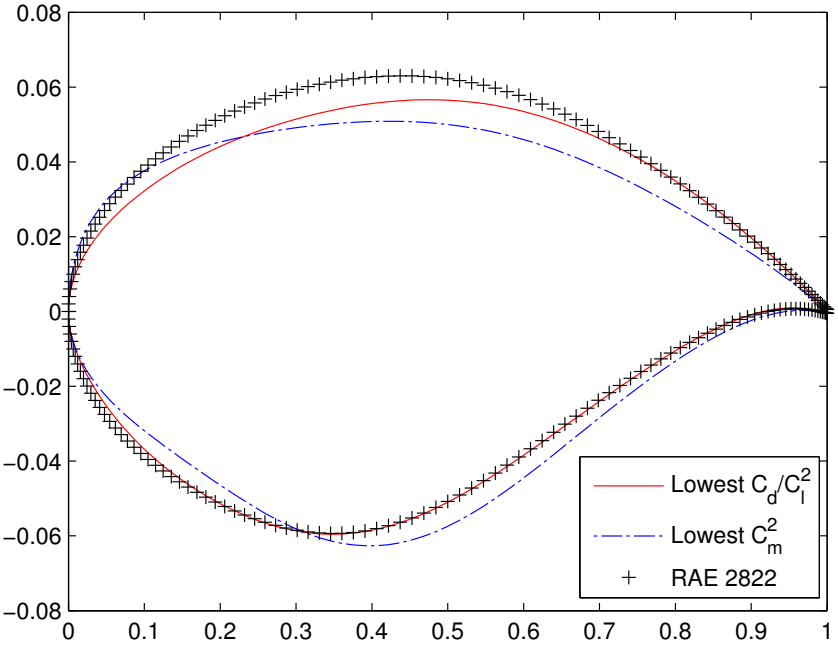


FIGURE 3.23: Geometry of the extremum airfoils and RAE 2822 found by the optimizers.

| | $C_l$ | $C_d$ | $C_m$ |
|---|---|---|---|
| **Airfoil A** | 0.824 | 0.00310 | -0.124 |
| **Airfoil B** | 0.650 | 0.00717 | -0.0608 |
| **RAE 2822** | 0.840 | 0.00859 | -0.1318 |

TABLE 3.11: Aerodynamic coefficients of the extremum and RAE 2822 airfoil.

## 3.4 Lesson Learned

This chapter explained the improvement of the methodology of the SS-MOMA for dealing with computationally expensive problems by introducing various local search methodologies beside of the standard WS method. The first local search alternative was the ASF-based local search method which worked by optimizing the achievement type function using the individual solution to be improved as the reference point. A slightly different version of the ASF-based search studied in this thesis was the Chebyshev-based search that uses the upper and lower bounds of the offspring solutions as a reference point. Beside of the ASF and Chebyshev local search, a non-scalarizing function local search which is random mutation hill climber (RMCH) was also studied and compared with the others. The improvements were also done by studying the effect of normalization, constraint handling, and enhanced diversity by introducing random weights generation. The study shows that the ASF and Chebyshev based search performed as the best over the others, they surpassed the local searches based on WS and RMHC on all test functions. SS-MOMA-CHEB surpassed the SS-MOMA-ASF on ZDT1, ZDT3, and CONV2 problems, while SS-MOMA-ASF found higher quality and more diverse solutions on ZDT2 and CONV1 problem. SS-MOMA-ASF that cannot performed well on CONV2 problem suggests that its performance was decreased in high dimensional objectives spaces; although more test are needed to confirm

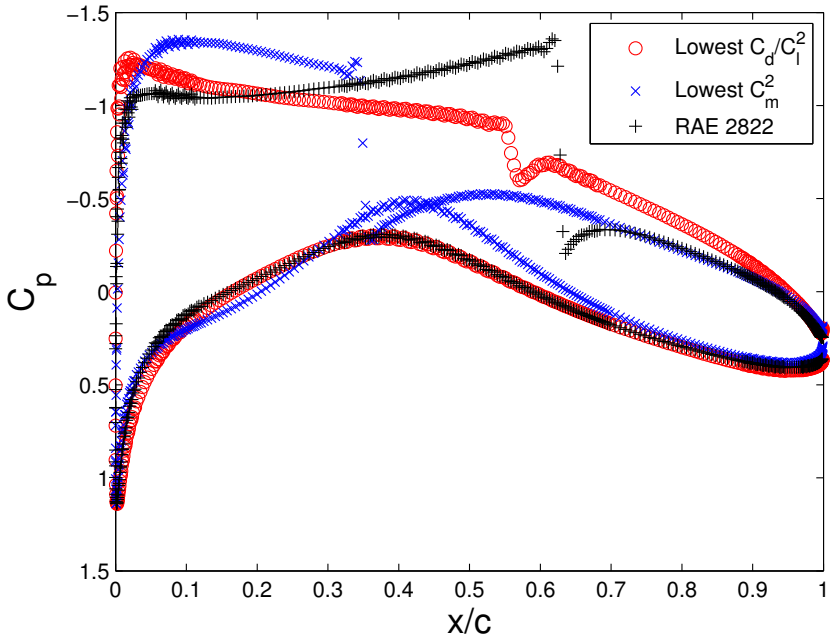


FIGURE 3.24: Plot of pressure coefficient ($C_p$) of the extremums and RAE 2822 airfoil.

this hypothesis.

A real-world aerodynamic optimization problem was tested with aerodynamic efficiency and moment coefficient as the objectives. The result showed that the SS-MOMA-ASF used in conjunction with Chebyshev based local search found better quality solutions compared to the NSGA-II and SS-MOMA-WS. This proved that the improved method gives higher possibility and confidence to find higher quality solutions within limited budget.

On the next chapter we will explain the development of a new and improved method of uncertainty quantification based on point-collocation non-intrusive polynomial chaos.

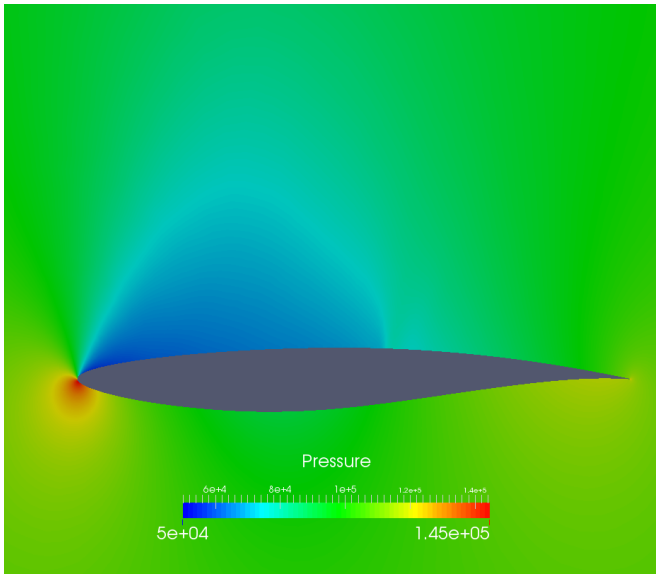


(A) Min $C_d/C_l^2$

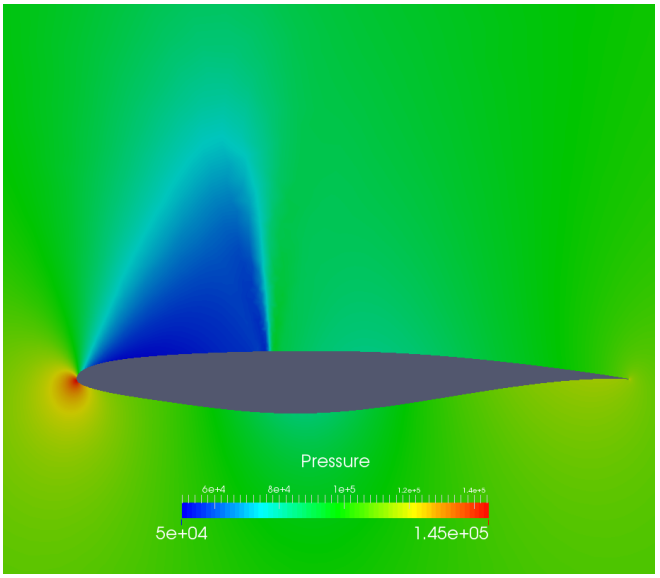


(B) Min $C_m^2$

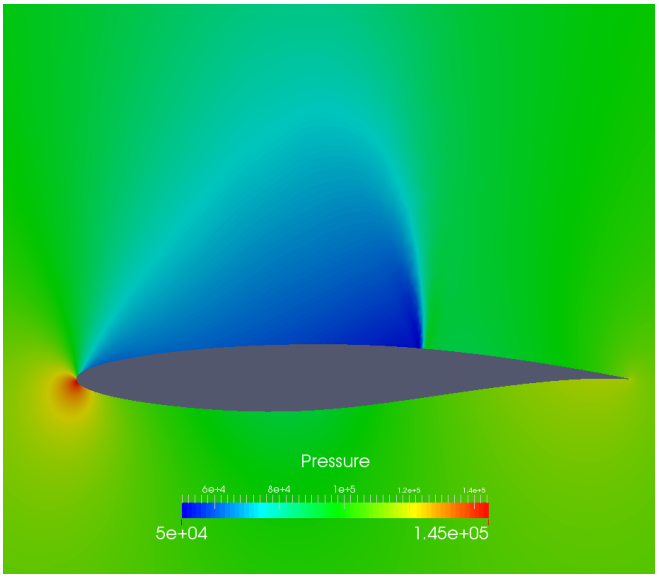


(C) RAE 2822

FIGURE 3.25: Pressure field depiction of the extremums and RAE 2822 airfoils.

# Chapter 4

# Multi-Fidelity Uncertainty Quantification

This chapter starts by the explanation of the concept of multi-fidelity uncertainty quantification using polynomial chaos. A multi-fidelity point collocation non-intrusive polynomial chaos (MF-PCNIPC) that uses regression to calculate the polynomial chaos coefficients, which is developed in this thesis, is explained next as an alternative to the previous method which uses spectral projection. The implementation issue is then explained together with the numerical results on artificial function and aerodynamic problems. Finally, the chapter ends with the conclusion of this part and the lesson learned.

## 4.1 Multi-fidelity Non-intrusive Polynomial Chaos based on Regression

In engineering simulations it is common to encounter various simulation methods with different levels of fidelity. An obvious example of this is any simulation where the mesh density used to discretize the domain can be varied. A simulation with a larger number of elements provides greater accuracy but consumes more computational resource compared to a simulation with fewer elements. If simulations with multiple levels of fidelity are available, these can be exploited to aid the UQ process using a polynomial chaos expansion. The extension of NIPC to multi-fidelity (MF) UQ was first proposed by Ng and Eldred [125]. When using simulations with different levels of fidelity, UQ accuracy can be improved as long as the LF expansion can capture the trend well. The method has been shown to work well on several test problems but also to give no significant improvement in a case where the trends of the HF and LF simulations differ. A disadvantage of this method is that the number of collocation points cannot be defined arbitrarily because these points have to follow set rules, such as using the roots of the orthogonal polynomials, and extend into higher dimensions with tensor products or sparse

grids. It is advantageous for the number of collocation points (or samples) to be flexible in order to be able to easily control the number of deterministic simulations needed for UQ purposes, especially when the random variable dimensionality is moderate to high. We have therefore developed a MF UQ scheme using PCNIPC (MF-PCNIPC) as the base algorithm.

Ng and Eldred's MF expansion is a combination of LF and correction expansions that can take additive or multiplicative form, or a combination of the two [125]. In this work, we only use the additive form; other details can be found in Ng and Eldred's original paper. The additive version of the combined expansion is:

$$C(\xi) = R_{\text{high}}(\xi) - R_{\text{low}}(\xi) \tag{4.1}$$

so

$$R_{\text{high}}(\xi) = R_{\text{low}}(\xi) + C(\xi) \tag{4.2}$$

where $C(\xi)$ is the correction term, defined as the error between the LF ($R_{\text{low}}$) and HF expansion ($R_{\text{high}}$). In the paper by Ng and Eldred [125], the expansion is built using a sparse grid rule but here it can be generalized to any polynomial term built by any rule (tensor product, sparse grid, or total order expansion). The most important rule is that the polynomial term in the correction expansion has to be a subset of the LF expansion. The polynomial expansion for the response surface approximation can then be expressed as:

$$\tilde{R}_{\text{high}} = \sum_{j \in \Gamma_{w-r,n}} (\alpha_{\text{low}_j} + \alpha_{C_j}) \Psi_j(\xi) + \sum_{j \in \Gamma_{w,n} \setminus \Gamma_{w-r,n}} (\alpha_{\text{low}_j}) \Psi_j(\xi) \tag{4.3}$$

where $\Gamma_{w,n}$ are the indices for the bases of the combined fidelity expansion with a number of polynomial bases $w$ and dimension $n$, whereas $\Gamma_{w-r,n} \subset \Gamma_{w,n}$ are the common bases of the LF and correction expansions and $r < w$ is the indices offset between the LF and correction expansions. In our application where a total order or hyperbolic truncation is used, $r$ is defined as the degree offset between the LF and correction expansion.

Using this single expansion, the moments can then be calculated using the following formulation:

$$\mu_R \approx \alpha_{\text{low}_0} + \alpha_{\text{C}_0} \tag{4.4}$$

$$\sigma_R^2 \approx \sum_{j \in \Gamma_{w-r,n} \setminus 0} (\alpha_{\text{low}_j} + \alpha_{C_j}) \langle \Psi_j^2(\xi) \rangle + \sum_{j \in \Gamma_{w-r,n}} (\alpha_{\text{low}_j}) \langle \Psi_j^2(\xi) \rangle \tag{4.5}$$

The key difference between MF-PCNIPC and MF-NIPC based on spectral projection is that, instead of using spectral projection, the coefficients are now calculated using regression. Such an approach offers flexibility in the choice of the number and location of samples, and the polynomial basis. What

also needs to be highlighted is the difference between the model fusion method used in MF-PCNIPC and the correction method used in MF-NIPC based on OSM. MF-NIPC based on OSM [155] works by correcting the output first and then building a single PCE. In contrast, the MF-PCNIPC model fusion method in this work uses two PCEs, the LF and correction expansions. The advantage of using model fusion compared to OSM is that the correction can be applied to the whole domain using the correction PCE, for which the polynomial degree can be tuned to increase accuracy.

Because multiple fidelity simulations are now involved, a strategy has to be derived and developed to identify the best practice for using MF-PCNIPC. We will explain the methodology by explaining in detail the components of MF-PCNIPC. The important components of MF-PCNIPC are the sampling method, the algorithm to generate the polynomial basis, and the way to combine the LF and correction expansions into a single expansion. These components are explained in the following subsections.

### 4.1.1 Sampling Method

To perform MF-PCNIPC, sampling is performed on the probability space according to the defined probability distribution. To be able to incorporate MF UQ, some of the HF simulation samples have to be a subset of the LF ones to allow some of the LF samples to be corrected by the HF simulation. The sampling method used in MF-PCNIPC can be structured (orthogonal polynomial roots, Newton-Cotes, with tensor product or sparse grid rules) or unstructured (random sampling, Latin hypercube sampling, low-discrepancy sequence). Unstructured sampling is typically used for uniform distributions but transformations to non-uniform probability distributions can readily be performed using the quantile information of the given distribution. If a structured grid is employed, the polynomial basis should be constructed in the same fashion with the type of the grid employed (tensor product or sparse grids) to allow optimal approximation of the stochastic response surface given the structured grid. This is not possible for an unstructured grid since the sampling points are not correlated with the polynomial basis, so the least squares method is the most convenient way to obtain the coefficients of the polynomial basis. However, structured sampling is a special domain of spectral-projection-based NIPC, so we do not use such sampling methods in our approach. The use of unstructured grids allows more flexibility in the number and location of samples and is much more robust to problem of failed simulations compared to structured grids. Here we suggest the use of a low-discrepancy sequence such as a Halton sequence [153] to build the sampling plan in an unstructured way. The advantage of using a low-discrepancy sequence as the sampling method is that every high fidelity (HF) sample $\mathbf{X}_{\text{high}} = \{x^{(1)}, ..., x^{(N_{s_h})}\}$ is a subset of low-fidelity (LF) samples in a higher number of samples $\mathbf{X}_{\text{low}} = \{x^{(1)}, ..., x^{(N_{s_l})}\}$, so $\mathbf{X}_{\text{high}} \subset \mathbf{X}_{\text{low}}$ where $N_{s_h} < N_{s_l}$.

Another similar methodology is nested Latin hypercube sampling (LHS) [106], which also allows the nesting of sampling points. We suggest the use of a low-discrepancy sequence due to its high space-filling and nested properties. An advantage of performing MF UQ with a low-discrepancy sequence is

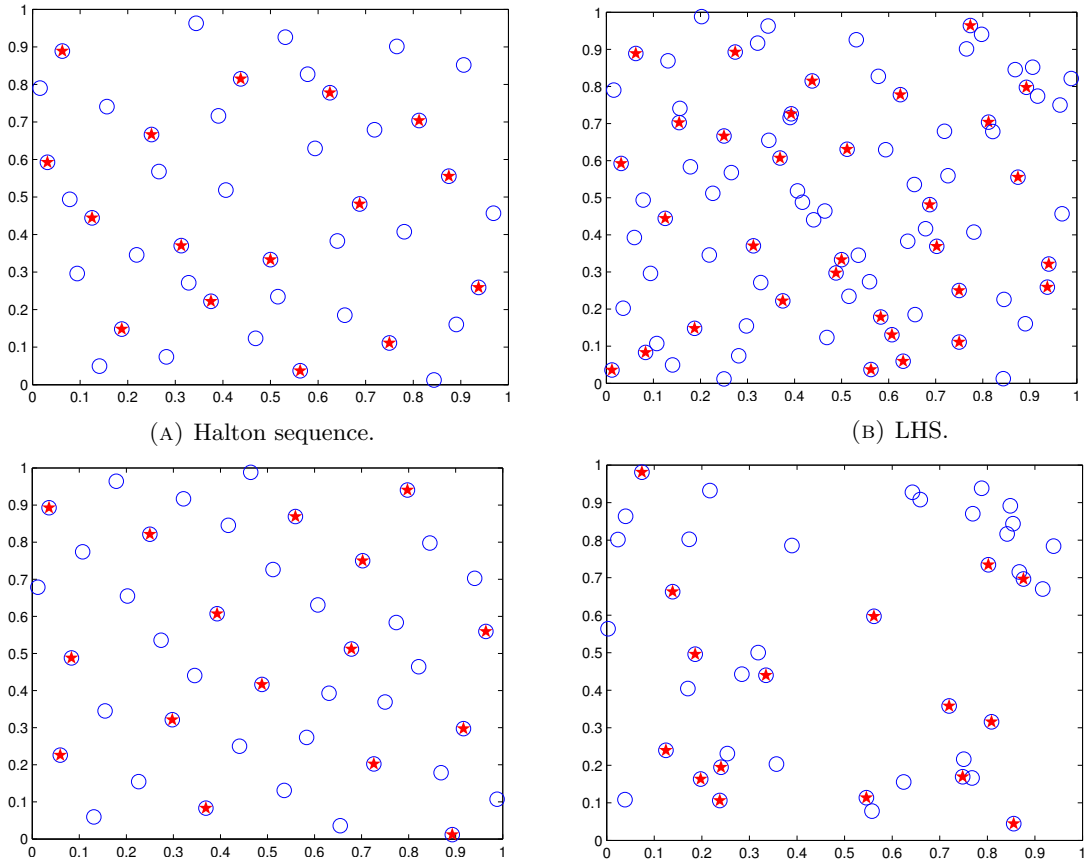

(A) Halton sequence. (B) LHS.

(C) Optimized LHS. (D) MCS.

FIGURE 4.1: Examples of LF and HF samples in MF-PCNIPC where the blue circles and red stars are LF and HF samples, respectively, generated using various methods.

the ease with which the location of the LF and HF samples can be adjusted. Another advantage of using a random sampling plan, LHS, or a low-discrepancy sequence is that the number of samples can be chosen arbitrarily. In application, an arbitrary number of sampling plans can be employed and the polynomial basis will adjust to the number of sampling plans. This option is convenient if the available computational budget is limited and the location of samples cannot be arranged in a structured way. In Ng and Eldred's approach, the LF and HF samples have to be built using sparse grids, so there is a restriction on the flexibility in determining the number of samples.

If the sampling plan is fixed and allows no additional samples, a good option is to use an optimized LHS plan [132]. An optimized LHS plan is built by maximizing the space-filling property given a definite number of LF samples. The HF samples are then chosen from the optimized LF samples using specific algorithms such as an exchange algorithm [132]. In the experiments in this thesis we use a Halton sequence because consistency is needed to study the performance of MF-NIPC on various test problems.

Fig. 4.1 shows examples of LF and HF samples generated using various methods.

### 4.1.2 Generating the Polynomial Basis

PCNIPC allows great flexibility in choosing the polynomial basis. If structured grids are used the polynomial basis has to be built using the same rules that were used to build the grids. We do not use structured grids since they are the preserve of the spectral-projection approach. The polynomial basis for unstructured grids should be built using a different method, and a common method used to truncate the polynomial basis in PCNIPC is the total order expansion truncation method. The curse of dimensionality (especially for high-dimension random variables) can be further reduced by using a hyperbolic truncation [106].

In practice, the polynomial basis can adapt to the number of collocation points because the number of samples can be arbitrary. For example, in a case where $n = 2$ with $N_s = 17$ and an OSR of 1, then the selected polynomial basis is generated using $p = 4$, giving a polynomial basis of 15. If UQ is performed by determining the polynomial basis first, the number of collocation points can be determined by multiplying the polynomial basis by the OSR value. Too high an OSR value might result in an overkill approximation, whereas an OSR of 1 gives a high probability of over-fitting due to the low condition number. The optimal OSR value according to Hosder is 2 [138], and we use that value in all our examples to ensure the numerical stability of the approximation. Nonetheless, if the MF scheme is employed, the polynomial order of the correction expansion should be lower than that of the LF expansion, irrespective of what methods are used to generate the basis and collocation points. The concept is to correct the lower-order elements of the LF expansion by the correction function, and then to capture the higher-order elements (not captured by correction expansion) to predict the higher-order behaviour of the true function.

### 4.1.3 Main Algorithm

The main algorithm is then as follows:

1. **Low-fidelity expansion**
   (a) Build the LF polynomial expansion with any rule. If total order/hyperbolic truncation is used, determine the value of LF expansion hyperbolic exponent $q_l$.
   (b) Determine the number of LF collocation points $N_{s_l}$.
   (c) Build the LF sampling plans $\mathbf{X}_{\text{low}}$.
   (d) Calculate the deterministic output value for each LF collocation point.
   (e) Solve the linear equations to obtain the LF polynomial coefficients $\alpha_{\text{low}}$.
2. **Multi-fidelity expansion**

(a) Build the correction polynomial expansion with any rule. If total order/hyperbolic truncation is used, determine the value of correction expansion hyperbolic exponent $q_c$ ($q_h$ for single HF-PCE).

(b) Determine the number of HF collocation points $N_{s_h}$, where $N_{s_h} < N_{s_l}$.

(c) Build the HF sampling plans $\mathbf{X}_{\text{high}}$.

(d) Calculate the deterministic output value for each HF collocation point.

(e) Calculate the difference between the HF and LF deterministic output values at $\mathbf{X}_{\text{high}}(C(\xi))$.

(f) Solve the linear equations to obtain the correction polynomial coefficients $\alpha_{\text{C}}$.

3. **Calculate the moments**

(a) Build a single expansion as a combination of the LF and correction polynomial expansions.

(b) Use the combined expansion to calculate analytic moments using Eqs. (4.4) and (4.5).

Strategies with different truncation orders for the LF and correction expansions are also possible. For example, the LF expansion can be used to capture high-order interactions while the correction expansion captures the main effects. Of course, it is assumed here that LF samples are very quick to evaluate compared to HF ones, so an abundant number of LF samples are readily available. This strategy is particularly useful if the aim is to reduce the number of HF samples while keeping an OSR of 2, the value recommended in many references [138]. To further reduce the OSR or improve the efficiency, an adaptive strategy [102] or adaptive sampling [99] could be employed. These options are not explored in this thesis.

The choice of polynomial order and hyperbolic truncation order for the correction and LF expansions will depend on user preference, which is constrained by the available computational budget and the ratio of the computational cost of HF and LF evaluations. Note that a higher degree and hyperbolic exponent typically give more accurate approximations since more of the polynomial basis is captured. However, care needs to be exercised, because if the order of the polynomial basis is too high, this could result in overfitting.

## 4.2 Global Sensitivity Analysis

For optimization purpose, identification of the impact of the variables to the quantity of interest (QoI) could gives additional benefit for purposes like dimensional reduction. In the UQ module, dimensionality reduction could reduce the complexity of uncertainty quantification process and increase the computational efficiency. Dimensionality reduction is also beneficial to the optimization by identifying design variables that gives significant impact to the objective functions where the variables that have

least impacts could be excluded from the design variables to reduce the complexity of the design variables. We also performed sensitivity analysis on some selected problem by applying the MF-PCNIPC. The advantage of applying method based on PCE is that the Sobol indices, which are the coefficients for variance based sensitivity analysis, can be readily evaluated using the PCE coefficients information[117]. If multi-fidelity scheme is employed, the coefficients are the combination of the coefficients obtained by low-fidelity and the correction expansion.

We fist define the index set $\boldsymbol{u}$ as $\boldsymbol{u} = \{i_1, ..., i_s\} \subset \{1, ..., p\}$, where $p$ is random input dimension. To obtain the sobol coefficient for the term $\boldsymbol{u}$, the following expression is used:

$$S_{\boldsymbol{u}} = \alpha_{\boldsymbol{u}}^2 \langle \Psi_{\boldsymbol{u}}^2(\xi) \rangle / \sigma_R^2 \tag{4.6}$$

The total PC-based sensitivity indices is then easily calculated by the following equation:

$$S_i^{tot} = \sum_{\mathscr{I}_i} S_{\boldsymbol{u}}, \quad \mathscr{I}_i = \{\boldsymbol{u} \supset i\} \tag{4.7}$$

This procedure is easy and can be performed soon after the coefficients is obtained.

If the low-fidelity function is highly predictive ($R^2 \geq$0.999), the Sobol coefficients from the low-fidelity function is sufficient enough to get the knowledge of the sensitivity of the variables to the QoI. However, to make sure that the Sobol indices could give the sensitivity analysis with greater accuracy, multi-fidelity PCE should be employed.

In the sections that follow, we will present the results of the application of our MF-PCNIPC methodology to a number of artificial and real-world computational test cases. We also studied the effect of the correlation and error between the LF and HF functions to the approximation accuracy of the MF-PCNIPC on some problems.

## 4.3 Computational Test Cases

We applied MF-PCNIPC to several artificial and real-world problems to examine the capabilities of the method. The test cases consist of three artificial problems and two engineering (aerodynamic) problems. On some artificial functions, the LF expression of the original function is constructed in such a way as to simulate various cases of correlation between the LF and HF functions. For the airfoil problem, we tested several types of LF simulation to investigate how this affects the accuracy and computational cost of MF-PCNIPC on the particular problems. Monte Carlo simulation with $10^7$ samples is used as a benchmark for all artificial test problems to monitor the convergence of the mean and standard deviation.

### 4.3.1 Four dimensional exponential function

The four dimensional exponential function[138] is characterized by the dominant main effect and low order interaction. The function is expressed as:

$$f_(x) = e^{(1.5(x_1+x_2+x_3+x_4))} \tag{4.8}$$

To simulate the low-fidelity simulations, the low fidelity exponential function is expressed as:

$$f_l(x) = 1.2e^{(1.3(x_1+x_2+x_3+x_4))} \tag{4.9}$$

Where $x_i = x_i(\xi i)(i, = 1, ..., 4)$ are uniform random variables with a mean value of 0.4 and a coefficient of variation of 40%[138]. Using hundred thousand samples, the $R^2$ and root mean square error (RMSE) of the low- to the high-fidelity function are 0.998 and 2.53, respectively, which indicates that the low- and high-fidelity functions are highly correlated with the low-fidelity function inaccurately predict the value of the high-fidelity function. Monte Carlo simulation using hundred thousand samples was employed to calculate the mean and standard deviation as a benchmark.

We varied the hyperbolic exponent $q$ by 0.4, 0.6, and 0.8 (for both low- and correction-expansion) and set the order of low-fidelity polynomial expansion to 12. The growth of the polynomial basis size could be seen in Fig 4.2 where the number of collocation points is just the cardinality times the $OSR$ value. The order of correction-expansion were then varied from 2 to 9 and the results obtained from multi- and high-fidelity approximation are compared. From the result shown in Fig. 4.3 and Fig. 4.4, it could be seen that with any $q$ value for both low- and correction-expansion, a more accurate approximation could be obtained by applying the multi-fidelity scheme compares to the single-fidelity scheme. This means that the low-fidelity functions is sufficiently predictive of the high-fidelity function so an increased of the accuracy with the same number of high-fidelity function call could be obtained.

In this particular problem, MF-PCNIPC with $q = 0.4$ could not sufficiently approximates the true function due to the strong interactions between variables in this particular function that are difficult to be captured with low $q$ value. The multi-fidelity scheme with $q = 0.4$ gives improvement by reducing the approximation error of exact mean and standard deviation over the high-fidelity PCE but is stil not able to capture the important polynomial basis. Increasing the $q$ value results in more accurate approximation since the important interaction basis is now captured, as it could be seen in the result where MF-PCNIPC with $q = 0.6$ and $q = 0.8$ has higher accuracy than $q = 0.4$. However, increasing $q$ value results in higher computational cost so one has to be wise in determining the $q$ value. In this four-dimensional function, an error of mean and standard deviation value below 0.1% (see Fig. 4.4)can be reached with 5th and 8th order MF-PCNIPC utilizing $q = 0.8$ and $q = 0.6$, respectively. The scheme with $q = 0.4$ could not reach tolerable error level even when it is already aided by the low-fidelity

polynomial expansion. Judging from the results, using $q = 0.6$ is then a balanced trade off between the accuracy and computational cost.

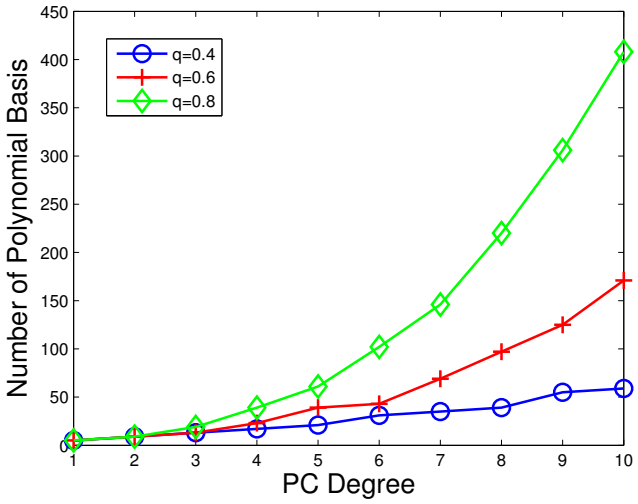


FIGURE 4.2: Number of polynomial basis for $n = 4$ with various $q$ value.

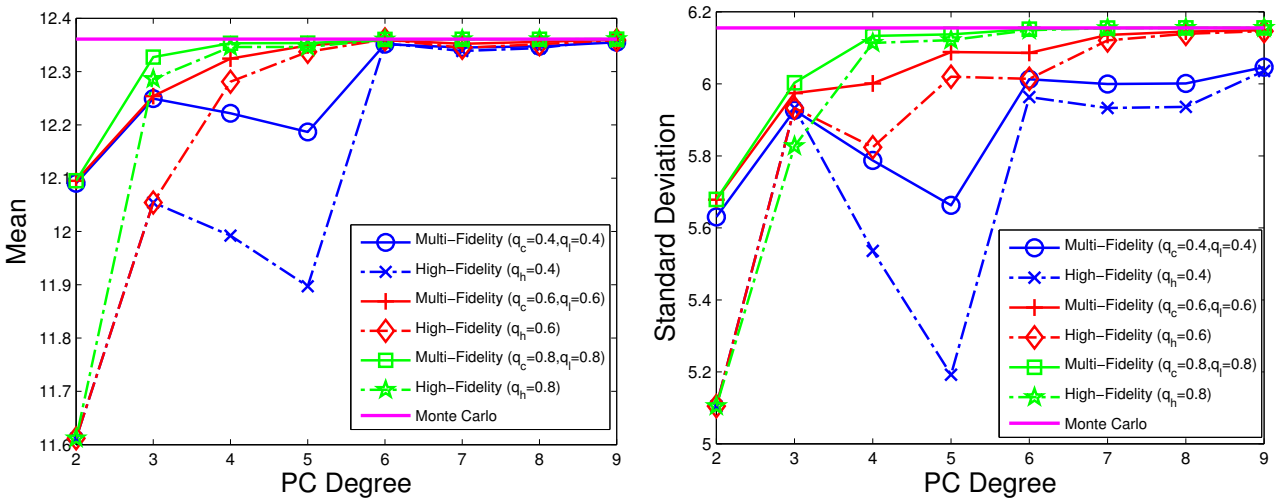


(A) Mean

(B) Standard Deviation

FIGURE 4.3: Convergence of the mean and standard deviation for the exponential problem obtained with PCNIPC and MF-PCNIPC with $12^{\text{th}}$-order low-fidelity PCE.

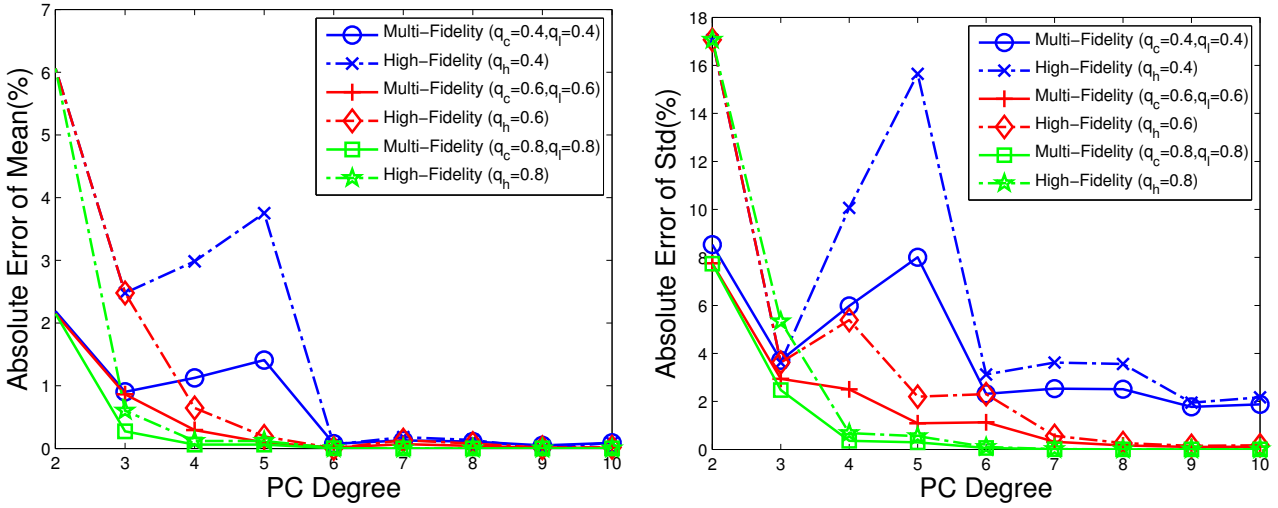


(A) Mean (B) Standard Deviation

FIGURE 4.4: Absolute error of the mean and standard deviation for the exponential problem obtained with PCNIPC and MF-PCNIPC with $12^{\text{th}}$-order low-fidelity PCE.

### 4.3.2 Eight dimensional borehole function

The borehole function is an eight-dimensional function that models water flow through a borehole [156]. Mathematically it is expressed as:

$$f_h(x) = \frac{2\pi T_u(H_u - H_l)}{\ln(r/r_w)\left(1 + \frac{2LT_u}{\ln(r/r_w)r_w^2 K_w} + \frac{T_u}{T_l}\right)} \tag{4.10}$$

where the various parameters are as defined in Table 4.1.

The LF function [156] is expressed as:

$$f_l(x) = \frac{5T_u(H_u - H_l)}{\ln(r/r_w)\left(1.5 + \frac{2LT_u}{\ln(r/r_w)r_w^2 K_w} + \frac{T_u}{T_l}\right)} \tag{4.11}$$

For UQ purposes, the random variables are distributed as shown in Table 4.1.

As can be anticipated given the similarities between Eqs. (4.10) and (4.11), the $R^2$ correlation and root-mean-square error (RMSE) analysis of the LF borehole function with respect to the HF one confirm that the functions are highly correlated with an $R^2$ value of 0.9999. The LF function, however, is inaccurate as indicated by the RMSE value of 18.4.

For this problem, a 12th-order polynomial is used to approximate the LF function and aid the MF expansion. Applying total order expansion results in a rapidly increasing polynomial basis size (number of terms in the PCE) due to the high-dimensionality of the borehole function, and, because of this, we

| Random variable | Definition | Probability distribution |
|---|---|---|
| $r_w$ | radius of borehole (m) | Uniform [0.05; 0.15] |
| $r_a$ | radius of influence (m) | Uniform [100; 50000] |
| $T_u$ | transmissivity of upper aquifer ($m^2$/yr) | Uniform [63700; 115600] |
| $H_u$ | potentiometric head of upper aquifer (m) | Uniform [990; 1100] |
| $T_l$ | transmissivity of lower aquifer ($m^2$/yr) | Uniform [63.1; 116] |
| $H_l$ | potentiometric head of lower aquifer (m) | Uniform [700; 820] |
| $L$ | length of borehole (m) | Uniform [1120; 1680] |
| $K_w$ | hydraulic conductivity of borehole (m/yr) | Uniform [9855; 12045] |

TABLE 4.1: Random variable distributions for the borehole test case.

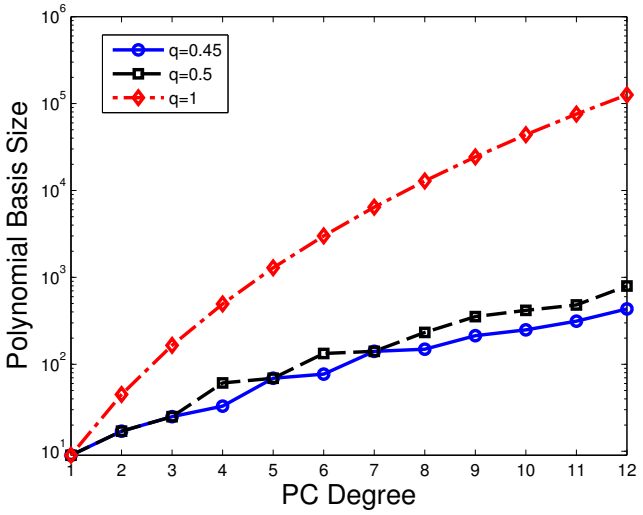


FIGURE 4.5: Polynomial basis size for the borehole problem ($n = 8$ with $q = 0.4, 0.45, 1$).

compare the MF and single-fidelity schemes using a low value of the hyperbolic truncation exponent. We applied two sets of hyperbolic exponents: $q_l, q_c = 0.45$ and $q_l, q_c = 0.5$. The growth in the polynomial basis size can be seen in Fig. 4.5. The number of the collocation points equals this number multiplied by the OSR value, which is 2 in our study. The convergence of the mean and standard deviation values and errors are shown in Fig. 4.6 and Fig. 4.7, respectively.

Thanks to the very high correlation between the LF and HF borehole functions, MF-PCNIPC can provide accurate approximations of the mean and standard deviation values at lower computational cost than HF-PCNIPC. It can be seen that the higher the value of the hyperbolic exponent $q$, the greater the proportion of the polynomial basis captured by the LF expansion, thus giving a more accurate prediction of the stochastic response surface. However, one has to be careful in determining the value of hyperbolic truncation exponent and order of the LF expansion by considering the available computational budget, especially if the dimensionality of the problem is high. An error level in the mean and standard deviation (compared to the result obtained by MCS) of about 0.2% can be achieved on this problem with MF-PCNIPC with a 4th-order polynomial and $q = 0.5$, while HF-PCNIPC cannot achieve the same level of accuracy even with an 8th-order polynomial.

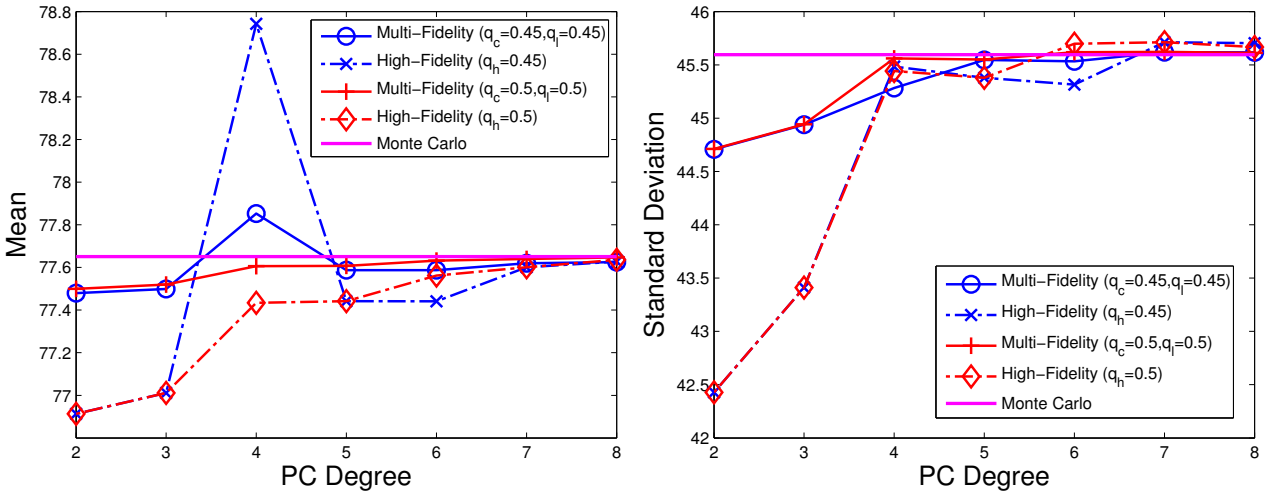


(A) Mean (B) Standard deviation

FIGURE 4.6: Mean and standard deviation convergence histories for the borehole problem obtained with PCNIPC and MF-PCNIPC with a 12th-order LF-PCE.

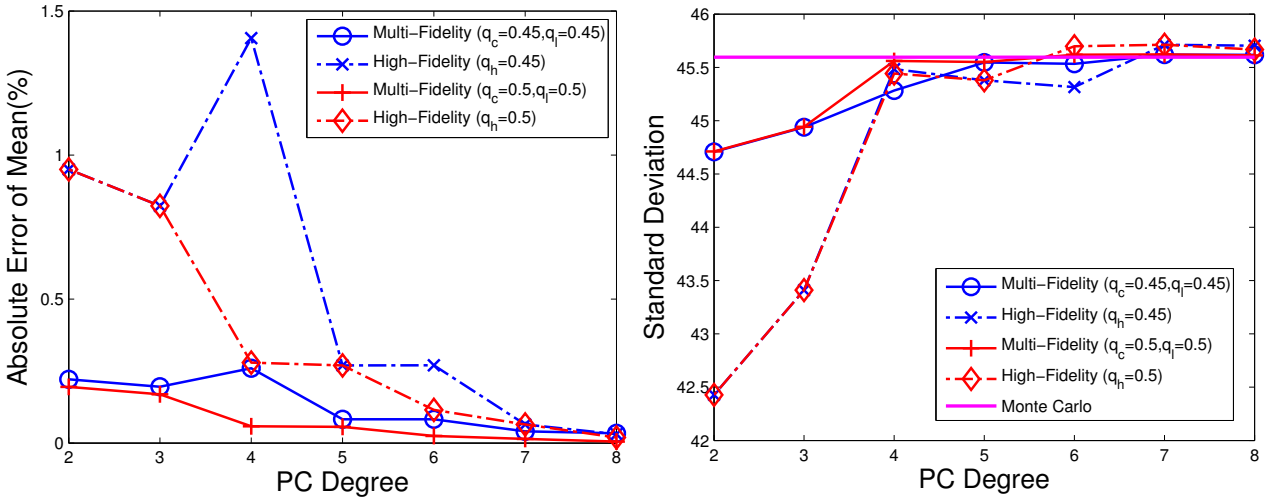


(A) Mean (B) Standard deviation

FIGURE 4.7: Mean and standard deviation error convergence histories for the borehole problem obtained with PCNIPC and MF-PCNIPC with a 12th-order LF-PCE.

### 4.3.3 Two dimensional branin function

The MF Branin function was first introduced in the context of testing the performance of co-kriging with different correlation levels of the LF function [157]. We use the same function now in the context of MF approximation with polynomial chaos and analyze the effect of various LF Branin functions on the approximation quality of MF-PCNIPC. Such an investigation is important because not all LF representations will necessarily increase the accuracy of the approximation with respect to the HF one. The LF Branin function is equipped with a tunable parameter $A$ that alters the correlation and RMSE

between the LF function and the HF one. Again, note that the LF and HF functions here are not computationally 'cheap' and 'expensive' in any real sense.

The HF Branin function is expressed as:

$$f_h = \left(x_2 - \frac{5.1}{4\pi^2}x_1^2 + \frac{5}{\pi}x_1 - 6\right)^2 + 10\left(1 - \frac{1}{8\pi}\right)\cos(x_1) + 10 \tag{4.12}$$

and the LF function as:

$$f_l = f_e - (A + 0.5)\left(x_2 - \frac{5.1}{4\pi^2}x_1^2 + \frac{5}{\pi}x_1 - 6\right)^2 \tag{4.13}$$

where $x_1, x_2 \in [0, 1]$ and $A$ is tunable in the range $[0, 1]$.

To simplify the analysis, $A$ takes only three values in this investigation: [0, 0.514, 1]. These parameter values correspond to three extreme levels of correlation and RMSE. The case with $A = 0$ generates a LF Branin function that has the highest level of correlation and lowest RMSE ($R^2 = 0.983$, RMSE=34.03) and theoretically is the best LF representation of the real function. In contrast, the case with $A = 0.514$ gives a LF Branin function that has the lowest correlation level and a moderate error ($R^2 = 0$, RMSE=69.01). The case with $A = 1$ correlates quite well with the true Branin function but has the highest RMSE ($R^2 = 0.83$, RMSE=102.09). For MF-PCNIPC, we use a 10th-order polynomial for the LF expansion and $q_c, q_l = 1$. The convergence of mean and standard deviation is shown in Fig. 4.8, while that of the errors is shown in Fig. 4.9.

The results show that with a very low degree (1 and 2) correction PCE, only the LF function with $A = 0$ could significantly improve the performance of the approximation compared to the single-fidelity one. In contrast, MF-PCNIPC with the LF Branin functions given by $A = 0.514$ and $A = 1$ combined with a very low degree correction PCE only results in a worse approximation for which the RMSE values between the MF approximation and the true Branin function become poor. This is evident with the lowest correction PCE degree of 1, but the same can also be seen for a PCE degree of 2, although the case with $A = 0.514$ approximates the single-fidelity approximation more accurately than when $A = 1$. The higher accuracy for $A = 0.514$ compared to $A = 1$ is surprising since the former appears to exhibit no correlation at all with the HF function. The case with $A = 1$ suggests that RMSE also affects the accuracy of the approximation even though the LF function has a high correlation with the real one; indeed, this confirms the previous observations of Ng and Eldred in the context of MF-NIPC [125]. Surprisingly, the MF scheme with all types of LF function offers greater accuracy than the single-(high)-fidelity approach from correction PCEs of degree 3 upwards.

To further investigate this result, we perform further analysis by checking the behaviour of the PC coefficients of the LF and HF Branin functions. This investigation is possible due to the two-dimensional (2D) nature of the Branin function. Analysis of Fig. 4.10 shows that the discrepancies between the LF

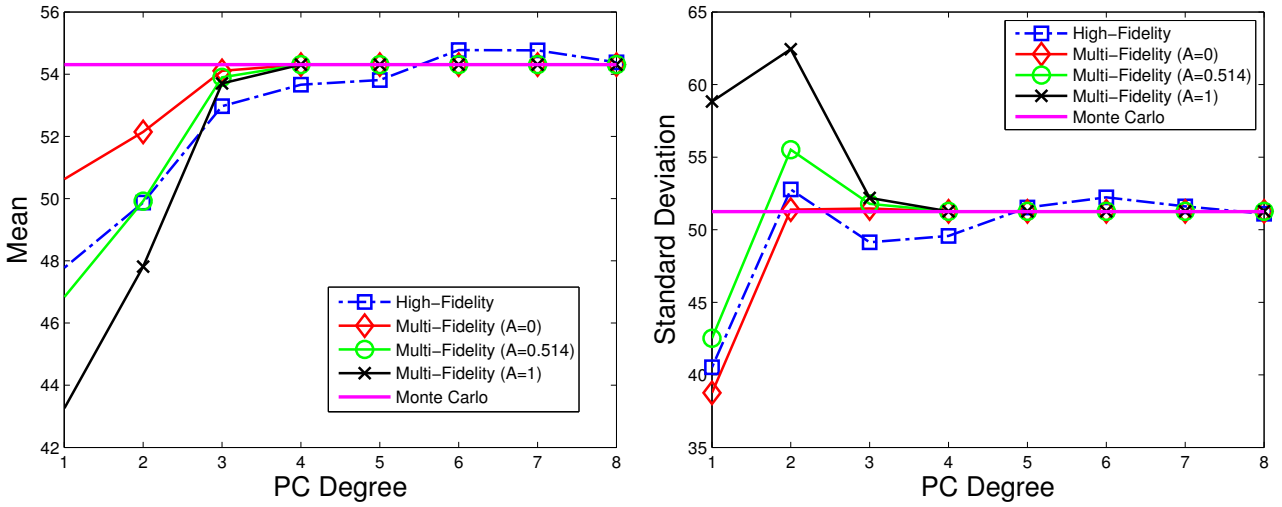


(A) Mean

(B) Standard deviation

FIGURE 4.8: Mean and standard deviation convergence histories for the Branin function obtained with PCNIPC and MF-PCNIPC with a 10th-order LF-PCE.

and HF functions are mainly associated with the lower-order polynomials. The errors in the higher-order polynomials are tolerably small and need only small corrections. The LF Branin functions have different degrees of correlation with the true Branin function. Even in the $A = 0.514$ case, where the correlation is small, the LF Branin function captures the behaviour of the higher-order main effects of the true Branin function. This is why with a sufficiently high degree correction polynomial all the LF functions give a very accurate approximation: the lower-order degree approximation is corrected by the MF scheme. The HF expansion without the aid of a LF-PCE does not obtain a very accurate approximation until the PCE degree is at least 8.

Results for the Branin function show that, as long as the LF function can capture the important features of the HF function, the MF scheme can yield a more accurate approximation. A questionable approximation will be obtained if there are aspects of the LF basis that are not corrected by the correction expansion and these aspects are not sufficiently representative of the HF function. In the $A = 0$ case, the higher-degree basis can mimic the features of the HF basis function very well so a more accurate approximation can be achieved.

However, it is important to note that even though the LF low-correlation Branin function can be used to improve accuracy with respect to the HF-PCE on moderate degree polynomials, using a function with a very low correlation in the MF-PCNIPC scheme on real applications is not suggested or recommended. This is because the user cannot be sure whether such similarities with the HF function exist or not.

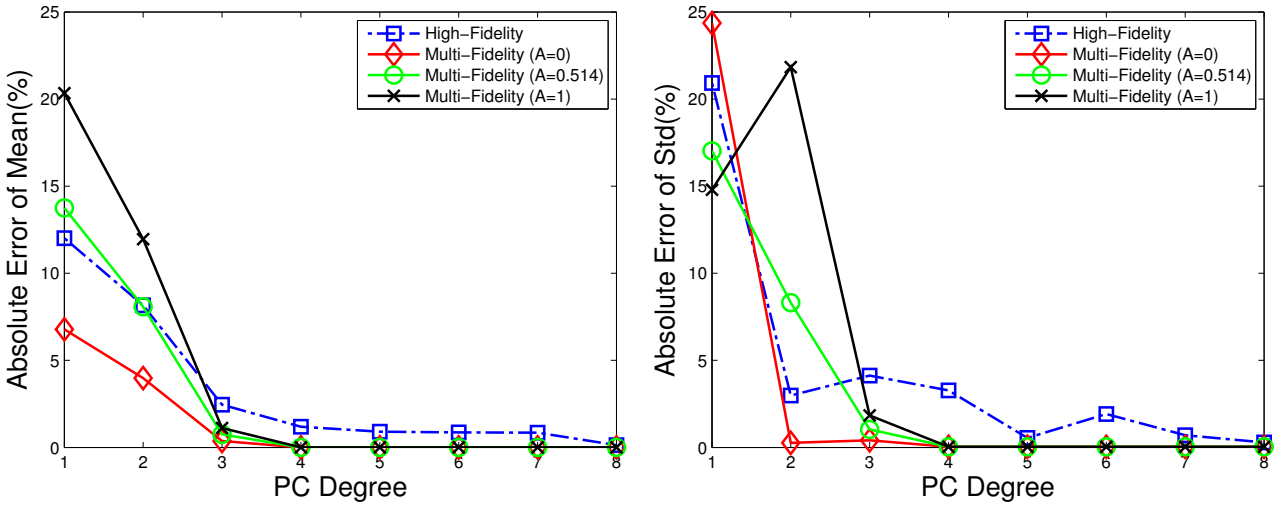


(A) Mean (B) Standard deviation

FIGURE 4.9: Mean and standard deviation error convergence histories for the Branin function obtained with PCNIPC and MF-PCNIPC with a 10th-order LF-PCE.

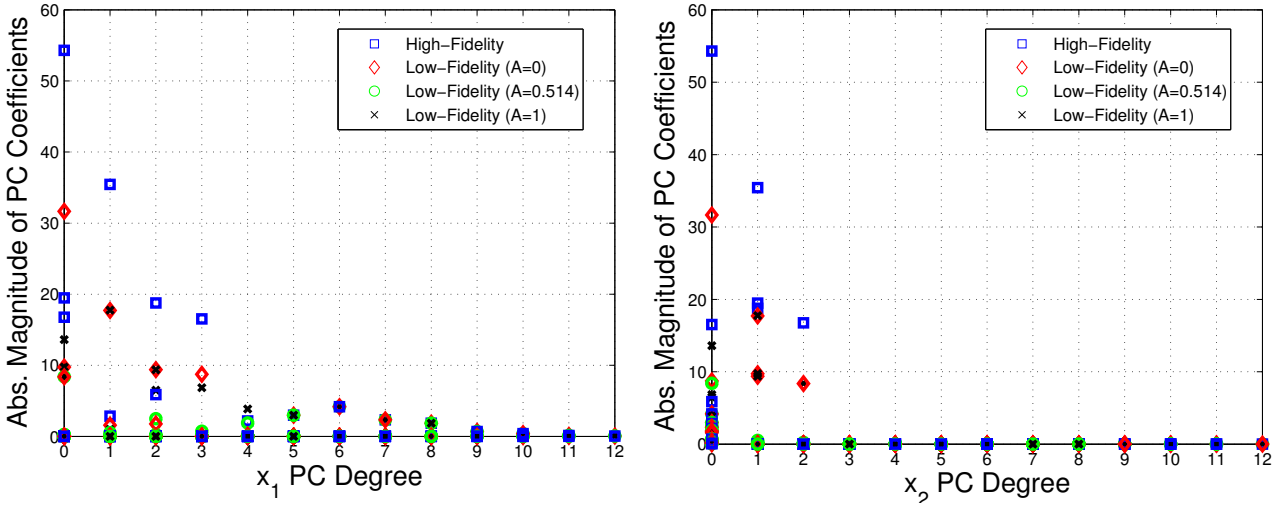


(A) $x_1$-axis (B) $x_2$-axis

FIGURE 4.10: Absolute magnitudes of the PCE coefficients of the HF and LF Branin functions up to PC degree of 12 seen from (a) the $x_1$-axis and (b) the $x_2$-axis.

### 4.3.4 Ten dimensional Trid function

The Trid function is a ten-dimensional one characterized by unimodality and serves as a good benchmark UQ test problem (even though the term "unimodal" is more properly associated with optimization problems). The MF version was developed [157] with a single parameter $A$ that can be tuned to control the correlation and RMSE between the LF and HF functions.

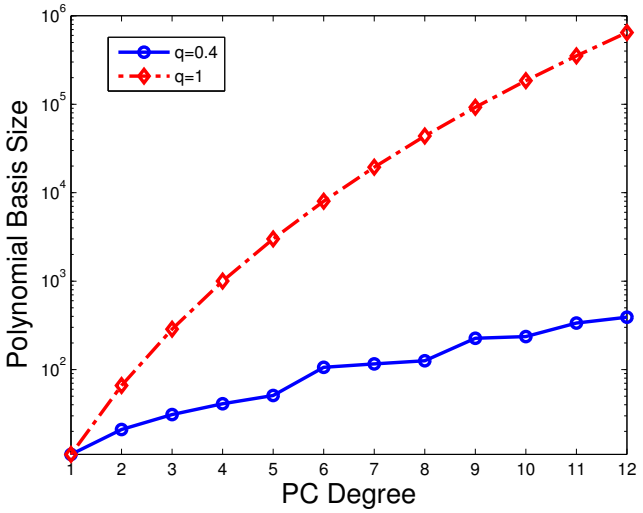


FIGURE 4.11: Polynomial basis size for the Trid function ($n = 10$ with $q = 0.4, 1$).

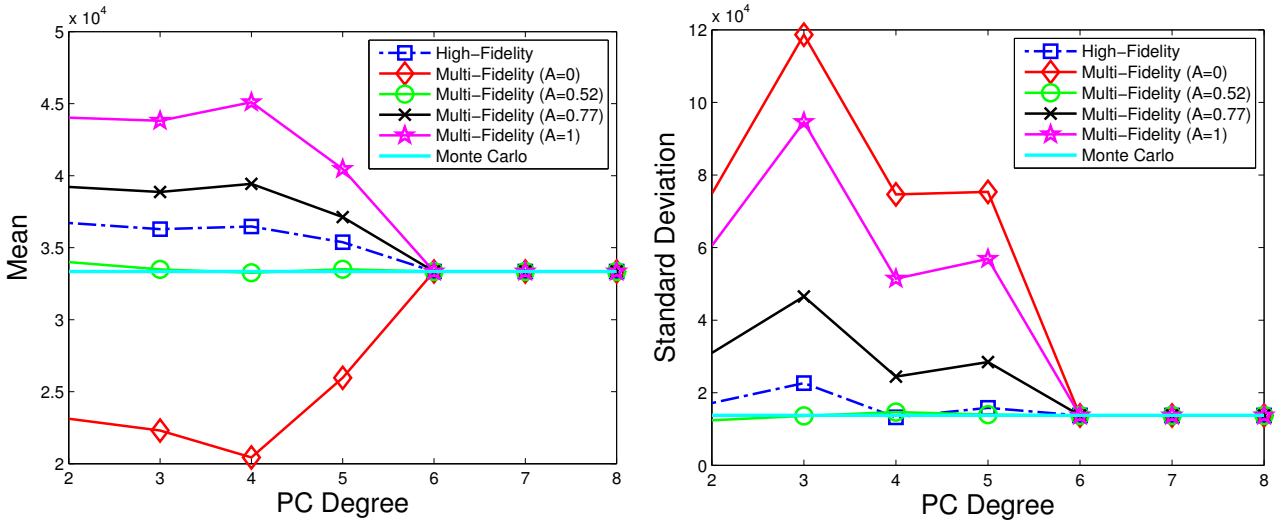


(A) Mean

(B) Standard deviation

FIGURE 4.12: Mean and standard deviation convergence histories for the Trid function obtained with PCNIPC and MF-PCNIPC with a 10th-order LF-PCE.

The HF Trid function is expressed as:

$$f_h = \sum_{i=1}^{10}(x_i - 1)^2 - \sum_{i=2}^{10} x_i x_{i-1} \tag{4.14}$$

where $x_i \in [-100, 100]$ and the LF function is as follows, where $A$ is tunable in the range $[0, 1]$:

$$f_l = \sum_{i=1}^{10}(x_i - A)^2 - (A - 0.65)\sum_{i=2}^{10} i x_i x_{i-1} \tag{4.15}$$

We used four settings of parameter $A$ to explore how it affects the approximation quality of the MF

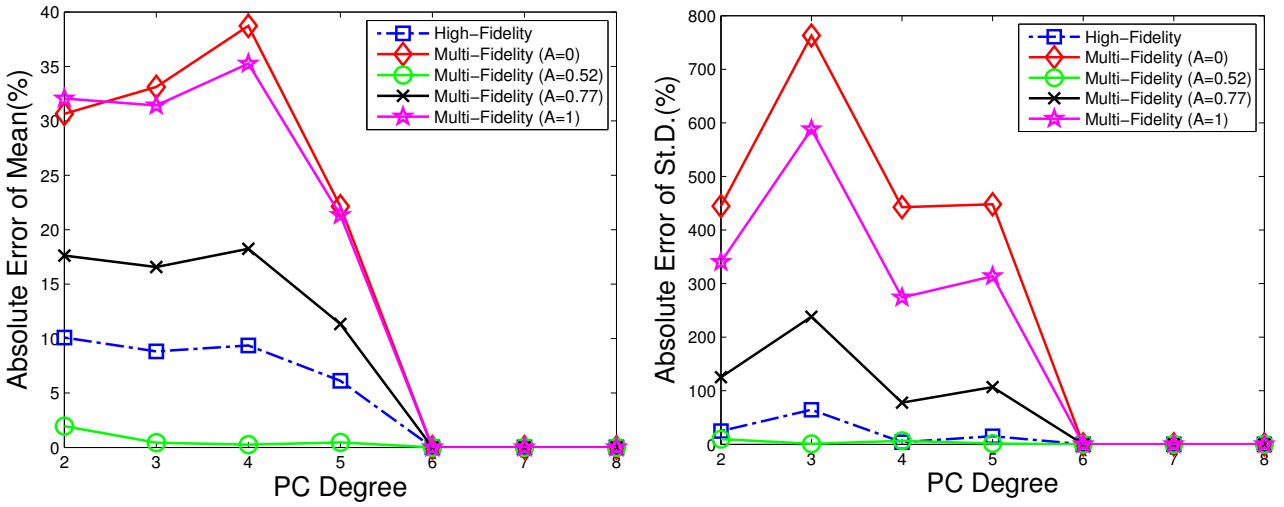


(A) Mean

(B) Standard deviation

FIGURE 4.13: Mean and standard deviation error convergence histories for the Trid function obtained with PCNIPC and MF-PCNIPC with a 10th-order LF-PCE.

scheme compared to its HF counterpart. The values of $A$ used in the study are: $A = 0$ ($R^2 = 0.6875$, RMSE $= 3.9042 \times 10^4$); $A = 0.52$ ($R^2 = 0.9102$, RMSE $= 4.05 \times 10^3$); $A = 0.77$ ($R^2 = 0.0391$, RMSE $= 1.74 \times 10^4$); and $A = 1$ ($R^2 = 0.0812$, RMSE $= 3.6312 \times 10^4$). Because of the high dimensionality of the Trid function, the values of $q_l$ and $q_c$ were both set to 0.4 and the polynomial degree of the LF-PCE in the MF-PCNIPC scheme was set to 10. The growth in the size of the polynomial basis with $q = 0.4$ is shown in Fig. 4.11, and the convergence of mean and standard deviation and the errors in these are shown in Fig. 4.12 and Fig. 4.13, respectively.

The results show that on this particular function only one of the LF function cases ($A = 0.52$) improves the efficiency of the PCE approximation. All MF and single-(high)-fidelity PCE cases converge with high accuracy for a PC degree of 6 or more, suggesting that a PCE with a 6th-degree polynomial captures all important polynomial bases of the Trid function. Nonetheless, for PCE degrees from 2 to 6, the MF scheme using a LF function with $A = 0, 0.77$, or 1 fails to improve the accuracy of the approximation.

The failure of the LF case with $A = 0.77$ is likely due to the near zero correlation to the HF Trid function. The unsuccessful MF approximation using $A = 0$ is probably due to the very high RMSE and moderate $R^2$ value meaning that the LF function could not help improved accuracy. The reason for the failure of MC-PCNIPC with a LF function with $A = 1$ is straightforwardly due to the very high RMSE and low correlation value.

Only the LF Trid function with $A = 0.52$ successfully reduces the error of the MF scheme compared to its HF counterpart. The error level is below 3% for a PC degree of 2, while the HF expansion has a mean error of about 10% with the same polynomial degree. This again shows the importance of knowing that the use of a LF function with a moderate $R^2$ but a high RMSE could result in a very

poor MF approximation scheme. Overall, a MF approximation is very likely to be successful if the LF function has a high correlation and low RMSE when compared to the HF one.

## 4.4 Aerodynamic Test Cases

We tested MF-PCNIPC on a couple of selected aerodynamic test problems. The cases tested were a 2D NACA 0012 airfoil and three-dimensional (3D) common research model (CRM) with an Euler solver, both in the transonic flow. The open source SU2 code [149] was employed to find the flow field and obtain the aerodynamic coefficients. The work ratio $W$ [125], which measures the ratio of the computational cost of the LF to the HF simulations, is defined by:

$$W = CC_{\text{low}}/CC_{\text{high}} \tag{4.16}$$

where $CC_{\text{high}}$ and $CC_{\text{low}}$ are the computational times for the HF and LF simulations, respectively.

The total computational cost needed for UQ can be calculated as:

$$CC_t = N_{s_h} + N_{s_l}W \tag{4.17}$$

where $CC_t$ is the total computational cost for UQ and $N_{s_h}$ and $N_{s_l}$ are the numbers of samples for the HF and LF simulations, respectively. If partially-converged simulations are used for the LF simulations (as explained later), the total computational cost is calculated as:

$$CC_t = N_{s_h} + (N_{s_l} - N_{s_h})W \tag{4.18}$$

because some of the LF samples are calculated jointly with the corresponding HF samples.

### 4.4.1 NACA 0012 Airfoil in Euler Flow under Uncertain Flight conditions

The first real-world demonstration is a NACA 0012 airfoil case governed by the Euler equation. For this problem we used and compare two types of the LF simulations:

- Type A: partially-converged simulations
- Type B: simulations with fewer mesh elements

The first type of LF simulation that we tested was partially-converged simulations that stop at a certain iteration before full convergence. Application of partially-converged simulations is well-established in the aerodynamic optimization field to accelerate the optimization process [158, 159] but not for UQ

purposes. Here we used the partially-converged simulations to increase the accuracy of UQ at reduced computational cost in our MF framework. Using partially-converged simulations as the LF simulations has the advantage of reducing computational cost because LF samples that coincide with HF samples are evaluated together. Moreover, the computational cost and the accuracy of the LF samples can be varied by flexibly choosing the cut-off iteration of the partially-converged simulations. The criterion for fully-converged simulations in the NACA 0012 case was the lift-to-drag ratio ($L/D$) residual reaching a value of $10^{-6}$.

The second type of LF simulation has fewer mesh elements compared to the HF one: the number of elements for LF and HF are 3601 and 11825, respectively (see Fig. 4.14). The computational time needed for a LF simulation with fewer mesh elements is roughly 20% of that for a HF simulation. The LF simulation time is not negligible, so it also has to be used wisely in conjunction with HF simulations.

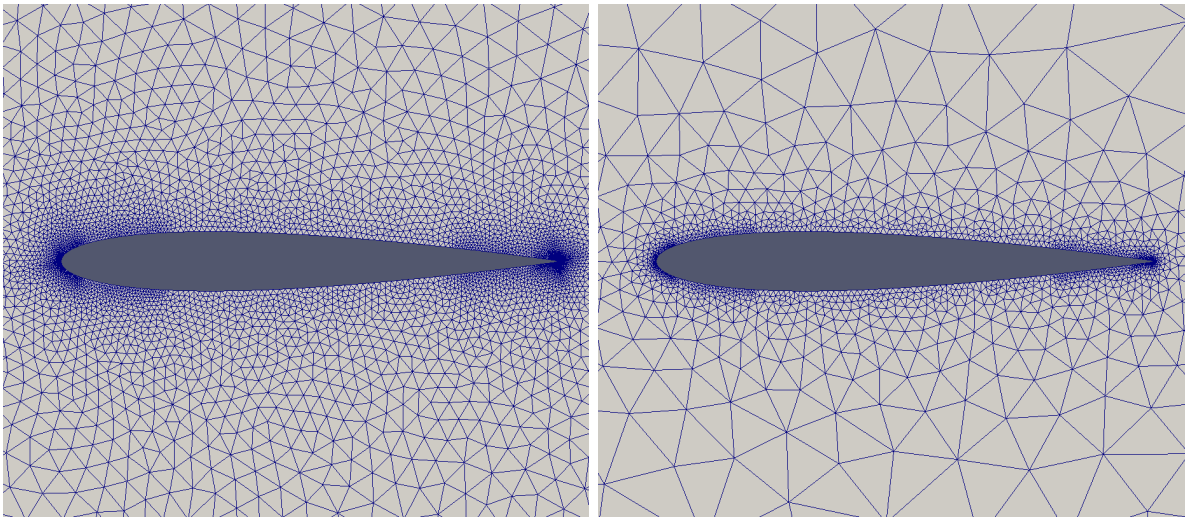

(c) High-fidelity (d) Low-fidelity

FIGURE 4.14: Mesh used in NACA 0012 case.

The second type of low-fidelity function that we tested is the partially converged simulation that stops at a certain iteration before it fully converged. Application of partialy converged simulation is well demonstrated on the aerodynamic optimization field to accelerate the optimization process[158, 159]. In this thesis we use the partially converged simulation to increase the accuracy of UQ with fewer computational time on multi-fidelity framework. Using partially converged simulation as the low-fidelity simulation has the advantage of reduced computational time because the low-fidelity samples that coincide with the high-fidelity samples are evaluated together. Moreover, the computational cost and the accuracy of the low-fidelity samples could be determined by flexibly choosing the cut-off iterations.

The case was evaluated at a nominal Mach number of 0.8 and angle of attack of 2 °. For this problem, the random variables are the Mach number and angle of attack with the probability distributions listed in Table 4.2. The quantities of interest are $C_l, C_d$ and $L/D$.

| Random variable | Probability distribution |
|---|---|
| Mach number (–) | Uniform [0.77.0.83] |
| Angle of attack (°) | Uniform [1.5.2.5] |

TABLE 4.2: Random variable distributions for the transonic NACA 0012 airfoil test case.

On this problem, we used $q_l$ and $q_c$ of 1 due to the low dimensionality of this problem. We varied the degree offset $r$ between the low- and correction-expansion from 1 to 2. We then investigated and studied the effect of different type of the low-fidelity samples to the approximation accuracy.

For the partially converged simulation, the value of cut-off iteration has to be determined and this could be done by analyzing the convergence trend of the CFD iterations and the $R^2$ and RMSE of the low-fidelity samples to the high-fidelity one.

#### 4.4.1.1 Convergence of $R^2$ and RMSE

We first investigated the convergence of the aerodynamic coefficient, for which the results are shown in Fig. 4.15. The convergence trend in the figures were obtained in the nominal flight condition. The result shows that the convergence was relatively fast and the aerodynamic coefficients began to reach the converged value at about 80 iterations. Before the 80th iteration, the flow calculated by CFD was still not yet fully developed; thus, is not reliable for the LF solver. However, as it is indicated in Fig. 4.15d a relatively stable L/D value was achieved starts from about 350th iteration and subsequent iterations refine the aerodynamic coefficients until it fully converged.

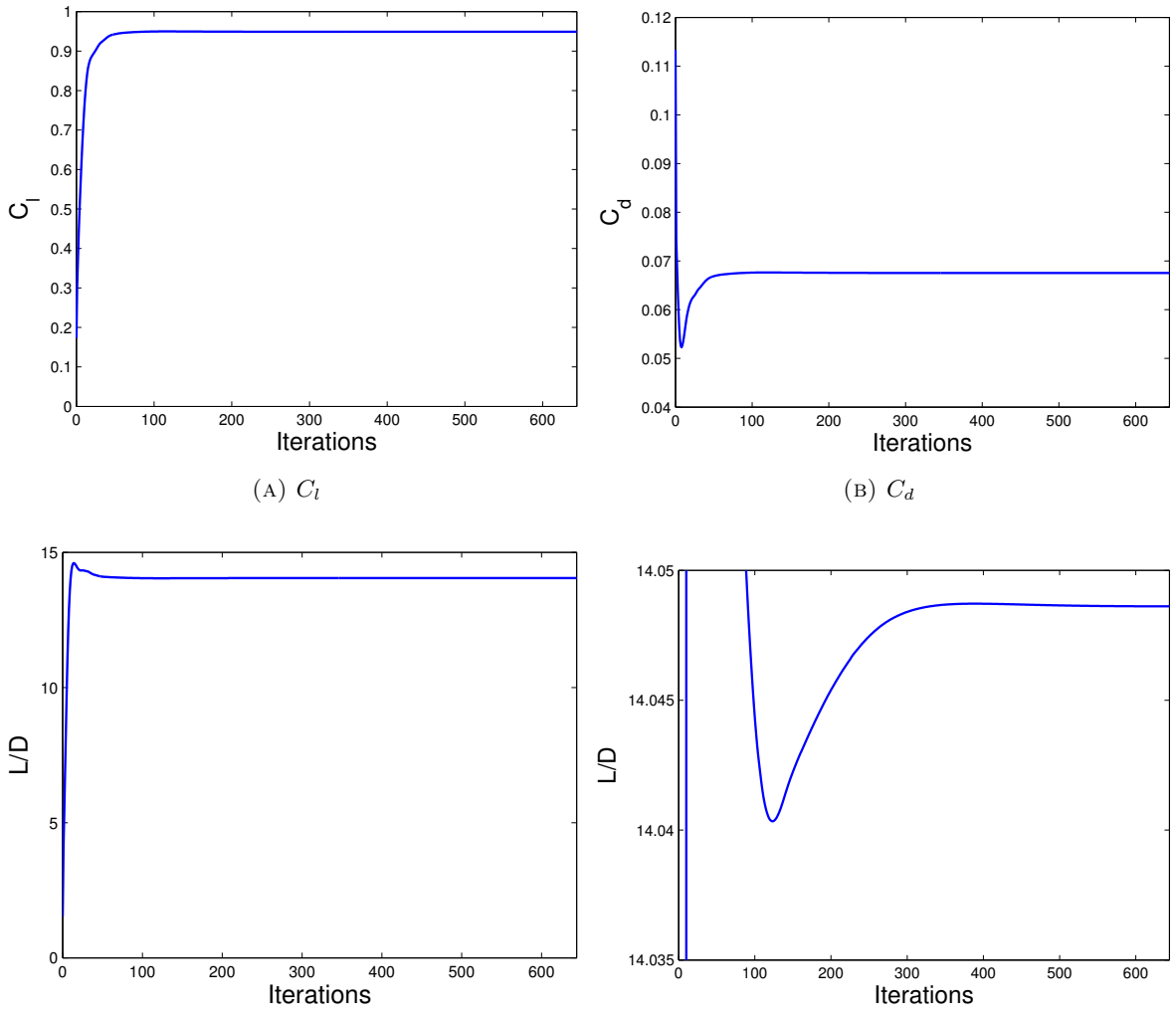


(A) $C_l$ (B) $C_d$

(C) $L/D$ (D) $L/D$(zoom)

FIGURE 4.15: Convergence of the aerodynamic coefficients for NACA 0012 case.

Monitoring CFD convergence with a single condition is not enough to determine an appopriate cut-off iteration because the trend could differ from case to case. Other simulations in different flight conditions might need a lower or higher number of iterations to converge. Thus, an ensemble of measurements of $R^2$ and RMSE needs to be gathered and analyzed to properly define the cut-off iteration. The number of samples used for this calculation was 100, with the samples being generated using a Halton sequence.

The convergence of the $R^2$ and RMSE are shown in Figs. 4.16, 4.17, and 4.18. A high correlation is observed starts from the early iterations for the $C_d$ and $L/D$ while the correlation value of the $C_l$ needs more iterations. The figure shows that a very high correlation value higher than 0.99 is observed at about 100th iterations.

After this investigation, we used the cut-off iteration value of 100. This value ensures that the flow is already developed with high correlation and low RMSE (see Table 4.3) which are the criterion for accurate multi-fidelity uncertainty quantification. Beside of that, this value is a good trade-off between

| Random Variables | $R^2$ | RMSE |
|---|---|---|
| $C_l$ | 0.999 | 0.0027 |
| $C_d$ | 0.999 | 0.0003 |
| $L/D$ | 1 | 0.0071 |

TABLE 4.3: $R^2$ and RMSE of the partially converged simulation(type A) to the fully converged simulation with fine mesh on NACA 0012 case.

| Random Variables | $R^2$ | RMSE |
|---|---|---|
| $C_l$ | 0.772 | 0.047 |
| $C_d$ | 0.923 | 0.0054 |
| $L/D$ | 0.995 | 0.429 |

TABLE 4.4: $R^2$ and RMSE of the simulation with coarse mesh to the fully converged simulation with fine mesh on NACA 0012 case.

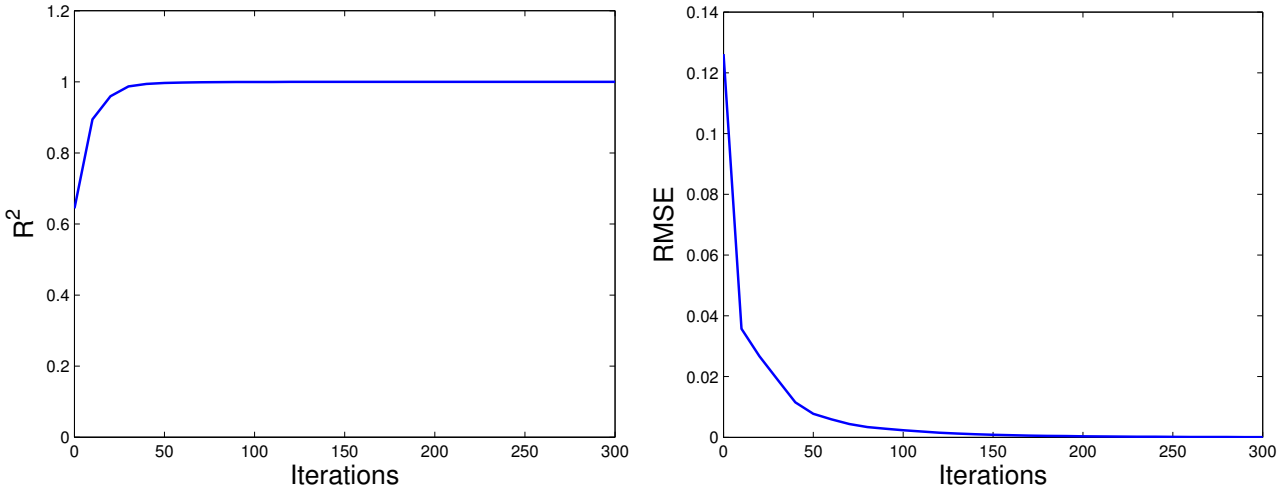


(A) $R^2$ (B) RMSE

FIGURE 4.16: Convergence of $R^2$ and RMSE of $C_l$ for NACA 0012 airfoil case with 100 realizations and Euler solver.

the accuracy and computational cost. For the type B low-fidelity samples, the $R^2$ and RMSE values are shown in Table 4.4.

#### 4.4.1.2 Statistical Moments Result

The convergence histories of the mean and standard deviation for this particular problem (NACA 0012 in Euler flow) are shown in Figs. 4.19, 4.20, and 4.21. We also varied the degree offset $r$ value by 1 and 2. We compared the result with the statistical moments generated by HF-PCNIPC of 7th degree polynomials as a benchmark.

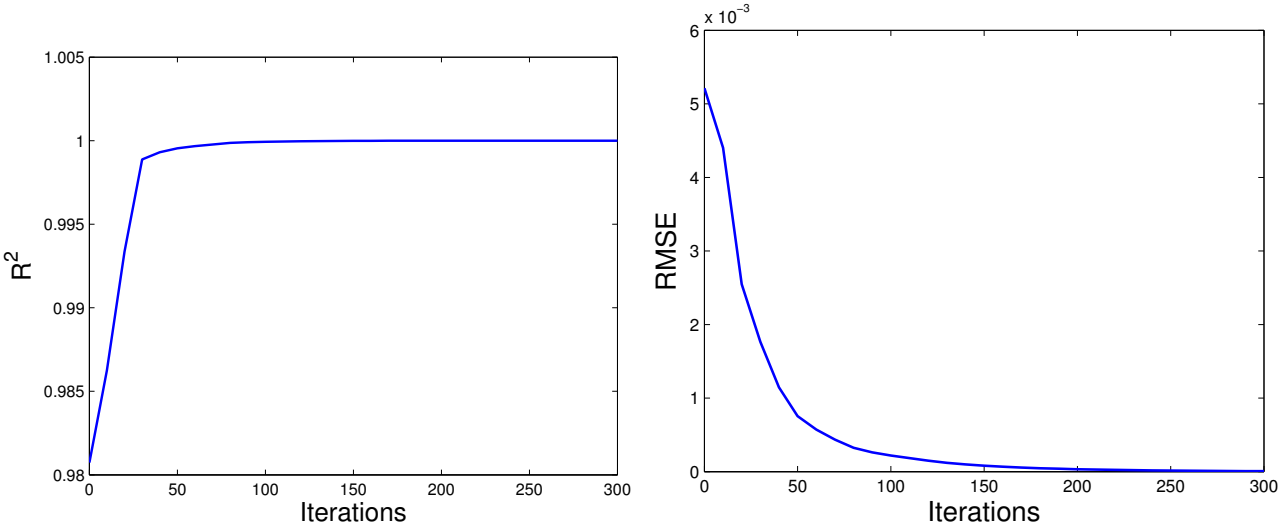


(A) $R^2$ (B) RMSE

FIGURE 4.17: Convergence of $R^2$ and RMSE of $C_d$ for NACA 0012 airfoil case with 100 realizations and Euler solver.

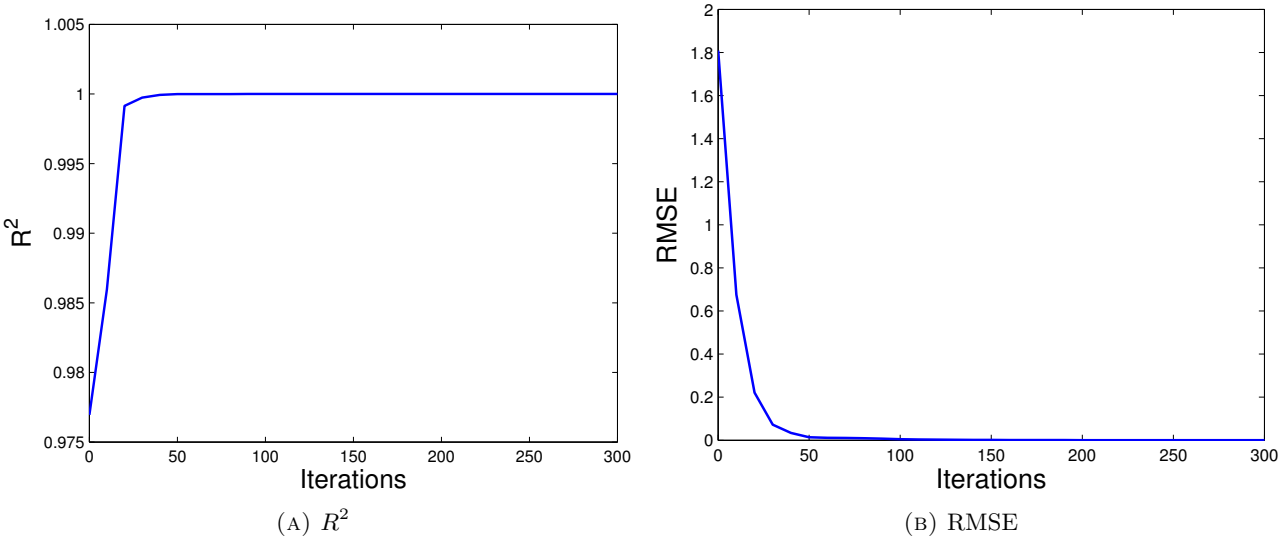


(A) $R^2$ (B) RMSE

FIGURE 4.18: Convergence of $R^2$ and RMSE of $L/D$ for NACA 0012 airfoil case with 100 realizations and Euler solver.

The result generally shows that an improvement in the estimation of the statistical moments can be obtained by employing the multi-fidelity scheme compares to the single high-fidelity expansion. Comparison of type A and type B low-fidelity samples reveals that the partially converged simulation gives more accurate approximation of the stochastic response surface with lower computational cost.

Results from the approximation of the $C_d$ response surface indicates that the multi-fidelity approximation with type A low-fidelity samples and $r = 2$ could obtain the error for mean and standard deviation below 1% with only 8.33 equivalent of the high-fidelity function calls where the single high-fidelity expansion needs 3th order polynomials (20 function evaluations) to reach the same level of error value. A more accurate approximation can be obtained by setting the polynomial order of the low- and correction-expansion to 4 and 2, respectively, where the error now reach the level below 0.2% with 15 high-fidelity function equivalent calls. Significant gain can be obtained by using type A low-fidelity samples because its correlation to the high-fidelity samples is very high. On the other hand, the use of type B low-fidelity samples with either $r = 1$ and $r = 2$ cannot produce a higher accuracy approximation relative to the high-fidelity expansion even though the correlation is relatively high. This lower accuracy is mainly due to the relatively high RMSE.

In approximating the statistical moments of $L/D$, an error level below 0.5% for the mean and standard deviation was obtained with the equivalent of 15 HF function calls and $r = 2$ using Type A LF samples, while the single-fidelity approximation with 20 HF functions (3th order polynomials) gives an error of 2% for the standard deviation. A substantial improvement (the errors in the standard deviation are reduced from 43% to 1.9%) is observed when the 1st-order correction polynomial is assisted by a 3rd order LF expansion. A significant gain can be obtained using Type A LF samples because the correlation with HF samples is very high. Applying Type B LF samples also yields higher accuracy in both mean and standard deviation compared to a HF expansion with a similar order of correction polynomial expansion; high correlation values contribute to this improved accuracy. However, the use of Type B LF samples with either $r = 1$ or $r = 2$ is not as effective as Type A samples, mainly due to the high RMSE and higher computational cost. The HF-PCNIPC process gives error levels in mean and standard deviation below 0.5% with the equivalent of more than 30 HF function calls, whereas when Type A LF samples are used only 15 HF function calls are needed to achieve the same accuracy (a saving of about 50% in computational cost). In contrast to the $C_d$ case, type B low-fidelity samples gives higher accuracy compares to the high-fidelity expansion with the same order of high/correction polynomial expansion for both mean and standard deviation; high correlation value contributes to this improved accuracy.

Things become more difficult when the method was applied to the $C_l$ response surface. However, the MF-PCNIPC was still able to create more accurate modelled response surface compares to the high-fidelity expansion with the expense of additional low-fidelity function calls. The MF-PCNIPC with type A low fidelity samples and $r = 2$ reduced the approximation error of standard deviation to the level below 1% with equivalently 15 high-fidelity evaluations. In contrast, none of the single-fidelity scheme

able to reach this error level even though the order of the polynomials is increased to 5 (56 function evaluations). On the other hand, the use of type B low-fidelity samples for MF-PCNIPC scheme only results in deterioration of the approximation accuracy and it become more evident when the polynomial order is high. This is reasonable because the correlation and RMSE value of type B low-fidelity to the high-fidelity samples are moderate. This means that there is a possibility that the low-fidelity PCE exhibits high order main effect interaction that do not exist on high-fidelity PCE.

To summarize, type A low-fidelity samples (partially converged simulation) gives more advantage than type B low-fidelity samples in viewpoint of accuracy and computational cost. Because the low- and high-fidelity samples are highly correlated, using a degree offset $r = 2$ gives more benefit than using $r = 1$. Moreover, the use of type A low fidelity samples for MF-PCNIPC ensures higher accuracy with relatively low additional computational cost compared to the high-fidelity NIPC.

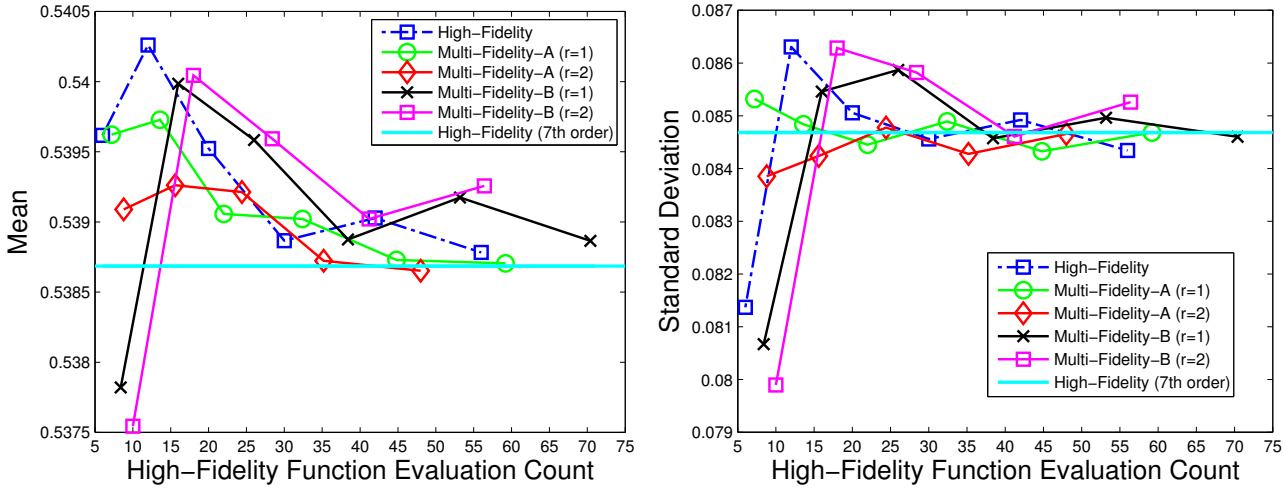


(A) Mean

(B) Standard Deviation

FIGURE 4.19: Convergence of mean and standard deviation of $C_l$ for NACA 0012 case with Euler solver and two-dimensional random variables.

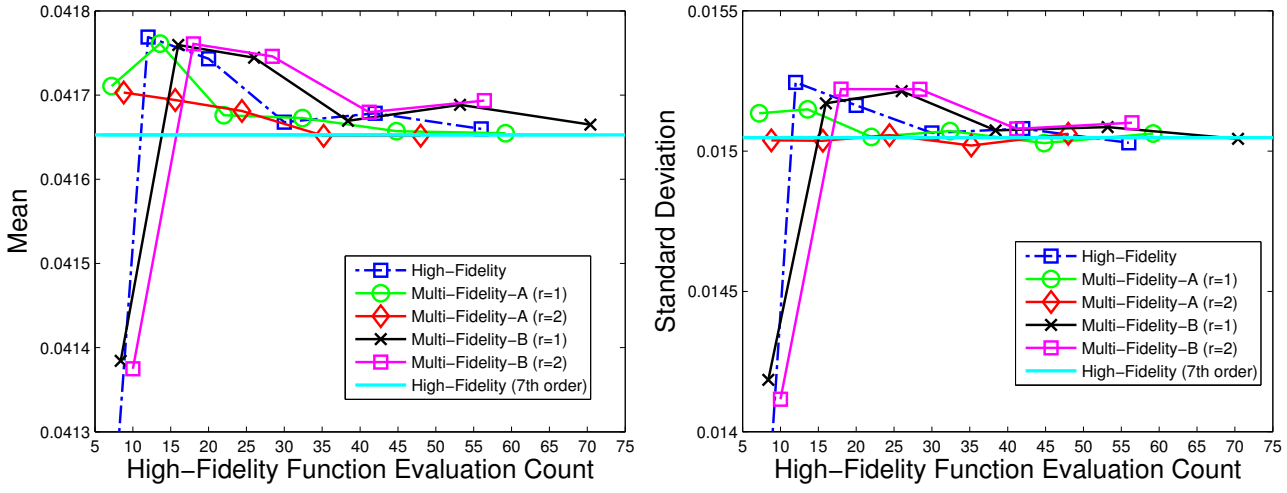


(A) Mean (B) Standard Deviation

FIGURE 4.20: Convergence of mean and standard deviation of $C_d$ for NACA 0012 case with Euler solver and two-dimensional random variables.

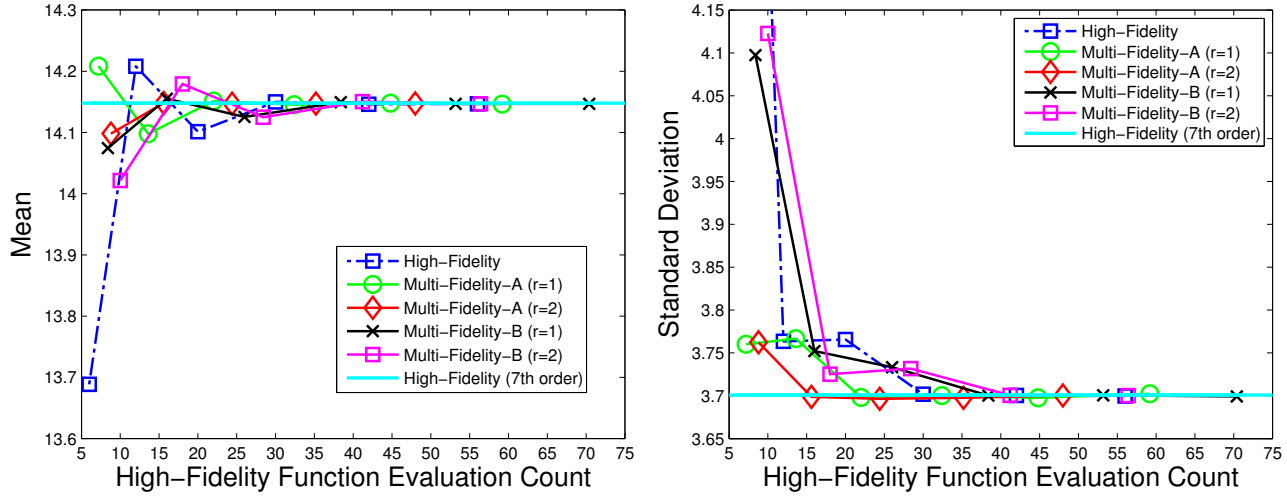


(A) Mean (B) Standard Deviation

FIGURE 4.21: Convergence of mean and standard deviation of $L/D$ for NACA 0012 case with Euler solver and two-dimensional random variables.

### 4.4.2 RAE 2822 Airfoil under Uncertain Flight Condition in Transonic Flow

In this case Reynolds-Averaged Navier-Stokes (RANS) simulation was used to solve the flow field around the airfoil and to obtain the aerodynamic coefficients of the RAE2822 airfoil. RANS solver of an open source code of SU2 were used. The hybrid of structured and unstructured mesh were employed to discretize the flow domain where the number of mesh elements is 22842 shown in Fig. 4.22 (the mesh for RANS simulation is available online at https://github.com/su2code/TestCases). The

random variables in this case were Mach number and angle of attack. The RANS CFD scheme uses multi-grid level 3, weighted least squares for spatial gradients, Sparalt-Almaras (SA) turbulence model, Euler implicit time discretization method, JST convective numerical method with 2nd order spatial numerical order integration and Venkatakrishnan slope limiter. In this case, the high-fidelity RANS simulation was performed with a tight criterion for convergence until it fully converged. To supplement the high-fidelity simulations, we applied two different types of low fidelity simulations:

- Type A: partially converged simulations.
- Type B: simulation with Euler as the governing equation.

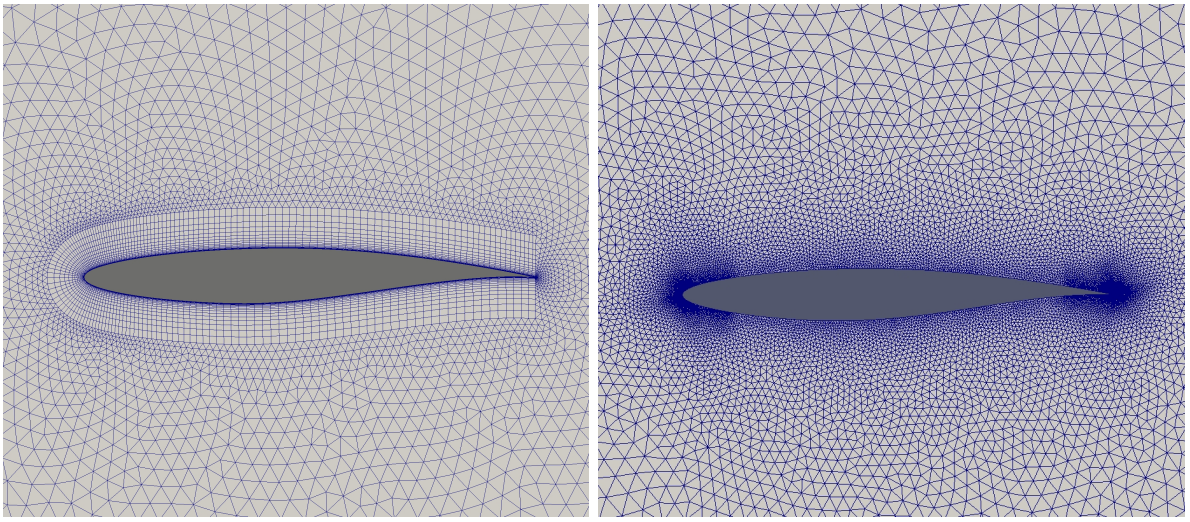

(A) High-fidelity (RANS) (B) Low-fidelity (Euler)

FIGURE 4.22: Mesh used in the present RANS simulation of RAE2822 airfoil.

A partially converged simulation has the same physics with the high-fidelity simulation but miss the accuracy because of the partially converged flow that is not yet perfectly developed. The computational cost of the low-fidelity samples with partially converged simulation depends on the cut-off iteration defined by the user and the correlation might be different for each cases and the fluid equation involved. We investigated the convergence trend and statistical quality of the result from RANS simulation on a set of samples to determine the cut-off iteration. On the other hand, Euler simulation is very fast to evaluate relative to the RANS simulation but it solves different flow physics because it eliminates the viscosity term in the Navier-Stokes equation.

| **Random variable** | **Probability distribution** |
|---|---|
| Mach number (–) | Uniform [0.72 0.74] |
| Angle of attack (°) | Uniform [2.2 2.3] |

TABLE 4.5: Random variable distributions for the RAE2822 airfoil test case.

We use the value of 1 for both $q_l$ and $q_c$ with the degree offset $r$ between the low- and correction-expansion were varied from 1 to 2. As in the Euler NACA 0012 case, for the type A low-fidelity samples the cut-off iteration needed to be determined so we performed analysis on the convergence of CFD iterations, $R^2$ and RMSE.

#### 4.4.2.1 Convergence of $R^2$ and RMSE

Fig. 4.23 depicts the typical convergence trend of $C_l$, $C_d$ and $L/D$ by using RANS solver for the RAE2822 airfoil. The convergence trends shown in the figures were obtained with the flight condition of Mach number and angle of attack of 0.735 and 2.24°, respectively. As it could be seen from the figures, the simulation needed about 800 iterations to reach a relatively stable value. A fully-converged simulation itself needed about 2400 iterations to achieve a drag residual error of $10^{-8}$. Before the 800th iterations, the flow was not yet fully developed and resulted in the fluctuating value of the aerodynamic coefficients. Using the data below 800th iteration as the low-fidelity samples was then not reliable due to this fluctuation. However, beside of the aerodynamic coefficients convergence trend, the $R^2$ and RMSE needed to be checked to assess the quality of partially to the fully converged simulations.

The $R^2$ and RMSE were calculated using 80 samples generated by Halton sequence on the probability space. Based on the investigation and the depiction shown in Fig. 4.24, 4.25, and 4.26, the low-fidelity simulations started to gives good prediction (high correlation, low errors) of the fully-converged simulation at nearly the iteration of 800, which is roughly costs 1/3 computational time of the fully-converged one. Before the 800th iteration, the $R^2$ and RMSE are still fluctuating that might be caused by the flow which was not yet fully developed. Even though the RMSE and $R^2$ at a very low iterations seems very representative of the fully-converged simulation with very high correlation, this value is not reliable due to the previously mentioned condition. The RMSE at very low iterations are very high and is not suggested for the multi-fidelity scheme.

The convergence trend of the $R^2$ and RMSE are similar for the $C_d$ and $L/D$ but not for $C_l$. The plateau value of $R^2$ was already reached at 800th iterations for $C_d$ and $L/D$. However, the convergence trend of $C_l$ still exhibits a fluctuation after 800th iteration even though the RMSE was low. At 800th iteration, the $R^2$ and RMSE of the three aerodynamic coefficients for partially to fully converged simulation are listed in Table 4.6:

| Random Variables | $R^2$ | RMSE |
|---|---|---|
| $C_l$ | 0.956 | 0.017 |
| $C_d$ | 0.999 | 0.000556 |
| $C_m$ | 0.991 | 0.00363 |
| $L/D$ | 0.999 | 0.834 |

TABLE 4.6: $R^2$ and RMSE of the partially to the fully converged simulation for RAE 2822 case.

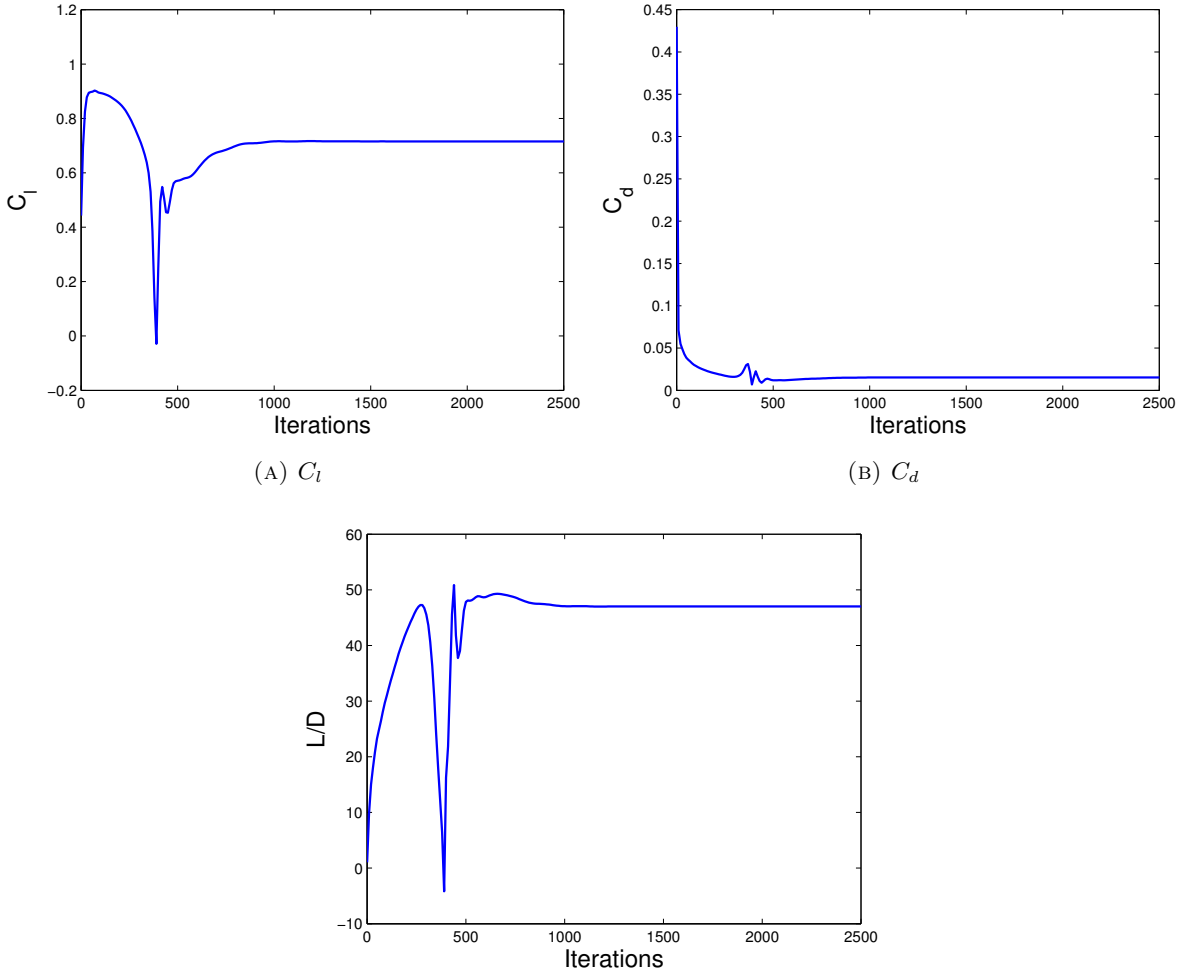


(A) $C_l$

(B) $C_d$

(C) $C_l$

FIGURE 4.23: Convergence of the aerodynamic coefficients for RAE 2822 case using RANS simulation.

Based on this observation, we used the cut-off iteration of 800 as a low-fidelity simulations. As we could see from Table 4.6, the correlation is very high and the RMSE is very low. Using iteration of 800 for the low-fidelity simulation and the mean of converged iterations of 2453, this means that the work ratio using this multi-fidelity scheme is roughly about 3.

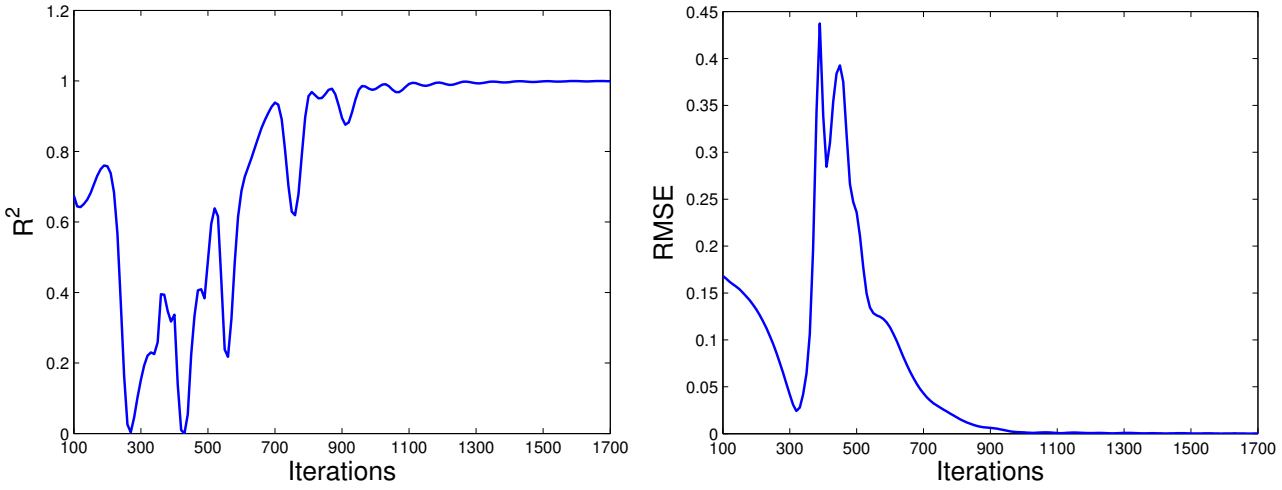


(A) $R^2$ (B) RMSE

FIGURE 4.24: Convergence of $R^2$ and RMSE of $C_l$ for RAE2822 airfoil with RANS solver.

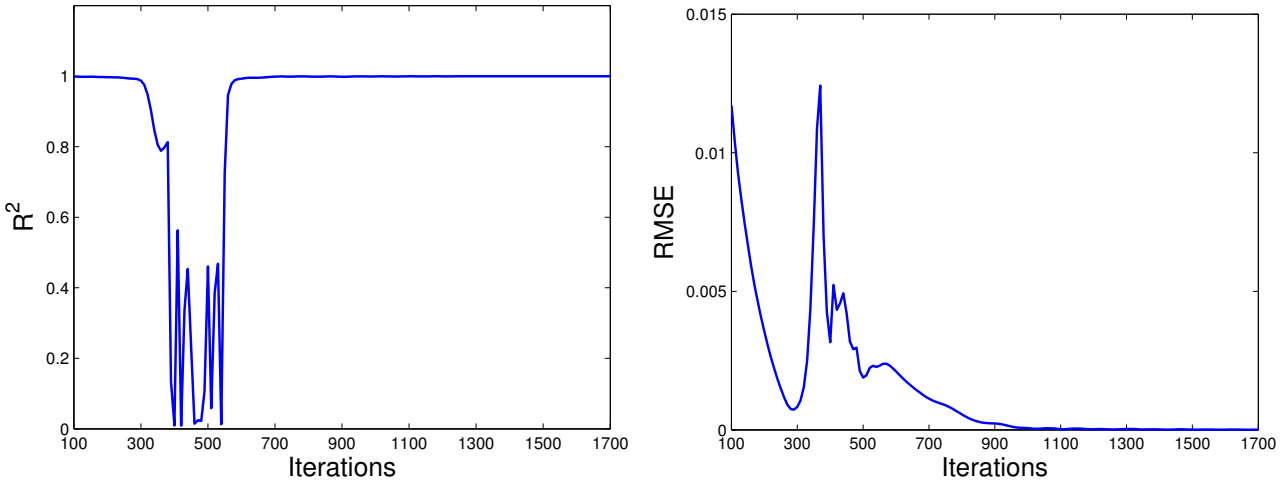


(A) $R^2$ (B) RMSE

FIGURE 4.25: Convergence of $R^2$ and RMSE of $C_d$ for RAE2822 airfoil with RANS solver.

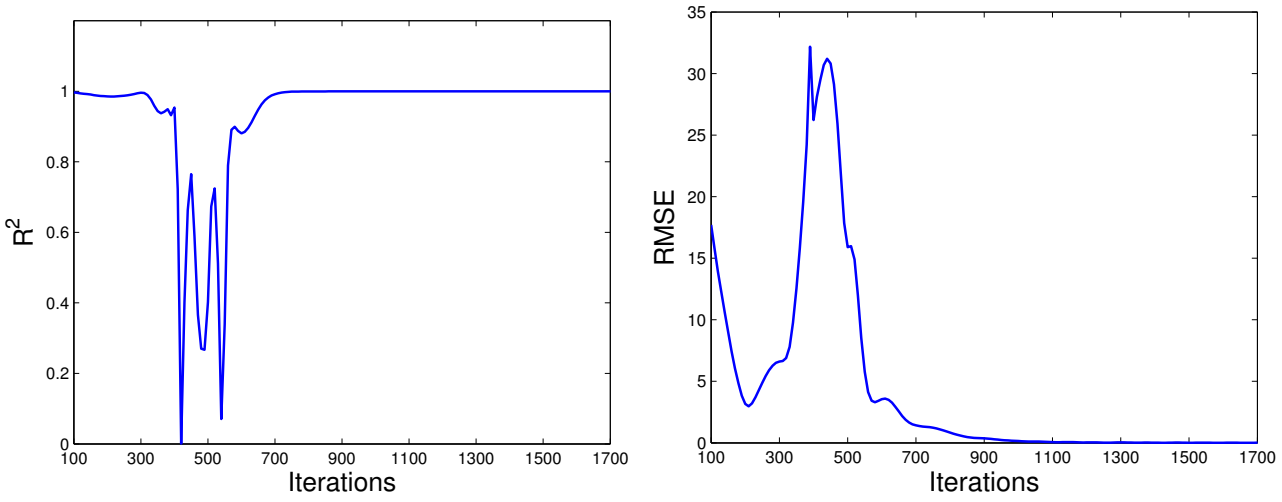


(A) $R^2$ (B) RMSE

FIGURE 4.26: Convergence of $R^2$ and RMSE of $L/D$ for RAE2822 airfoil with RANS solver.

As for the second type of low-fidelity simulations, the $R^2$ and RMSE value are listed in Table 4.7. The result from this investigation shows a high correlation between Euler and RANS simulation but the RMSE is quite high compares to the partially converged simulation for all aerodynamic coefficients which was due to the simplification of the problem into the Euler simulation. Because of the relatively fast evaluation, the work ratio of the type B low-fidelity simulation is 30 compares to the RANS simulation on this particular problem.

TABLE 4.7: $R^2$ and RMSE of the Euler to the RANS solver on RAE 2822 case.

| **Random Variables** | $R^2$ | **RMSE** |
|---|---|---|
| $C_l$ | 0.964 | 0.256 |
| $C_d$ | 0.980 | 0.00423 |
| $C_m$ | 0.989 | 0.0912 |
| $L/D$ | 0.951 | 4.365 |

With these two types of the low-fidelity simulations, MF-PCNIPC and HF-PCNIPC were then used to approximate the mean and standard deviation of the RAE2822 problem.

#### 4.4.2.2 Statistical Moments Result

The result of the mean and standard deviation approximated by PCNIPC and MF-PCNIPC for $C_l$, $C_d$, and $L/D$ are depicted in Figs. 4.27, 4.28, and 4.29. It was difficult to obtain a monotonous convergence

of error due to the numerical error and limited amount of samples so we use 7th order high-fidelity NIPC as a benchmark.

As it could be seen from the results, the use of multi-fidelity scheme with type A low-fidelity samples (partially converged simulation) can successfully reduced the error of mean and standard deviation relative to the 7th order high-fidelity approximation, in general. On the other hand, type B low-fidelity samples (Euler simulations) gives little or no advantages to increase the quality of the approximation as it is indicated in the Figs. 4.27, 4.28, and 4.29.

In approximating the $L/D$ response surface, the MF-PCNIPC with $r = 2$ and type A low fidelity samples is able to reach sufficiently accurate approximation with only equivalent of 18 high-fidelity function evaluations while the HF-PCNIPC needs higher number of function evaluations of 42. As the result shows, using $r = 2$ gives more accurate results than $r = 1$ by only a little additional computational cost. The use of MF-PCNIPC shows a not monotonous convergence for the standard deviation but the approximation is sufficiently accurate. Using $r = 1$ only gives little additional useful information thus its accuracy is lower than the $r = 2$. Type B low-fidelity samples gives no advantage and only made the approximation become worse. There is also no difference observed between applying $r = 1$ and $r = 2$ for the type B low-fidelity samples.

Approximation of $C_d$ response surface also shows similar with $L/D$ as it is indicated by the similar trend of the mean and standard deviation convergence. The improved accuracy by using MF-PCNIPC with type A low-fidelity samples is evident even though a monotonous convergence trend was not observed for the standard deviation. Again, no clear advantage could be obtained by using the type B low fidelity samples. A slight improvement could be observed if the 1st order correction polynomial is used, however this improvement is questionable because further increment of polynomial order shows no refinement.

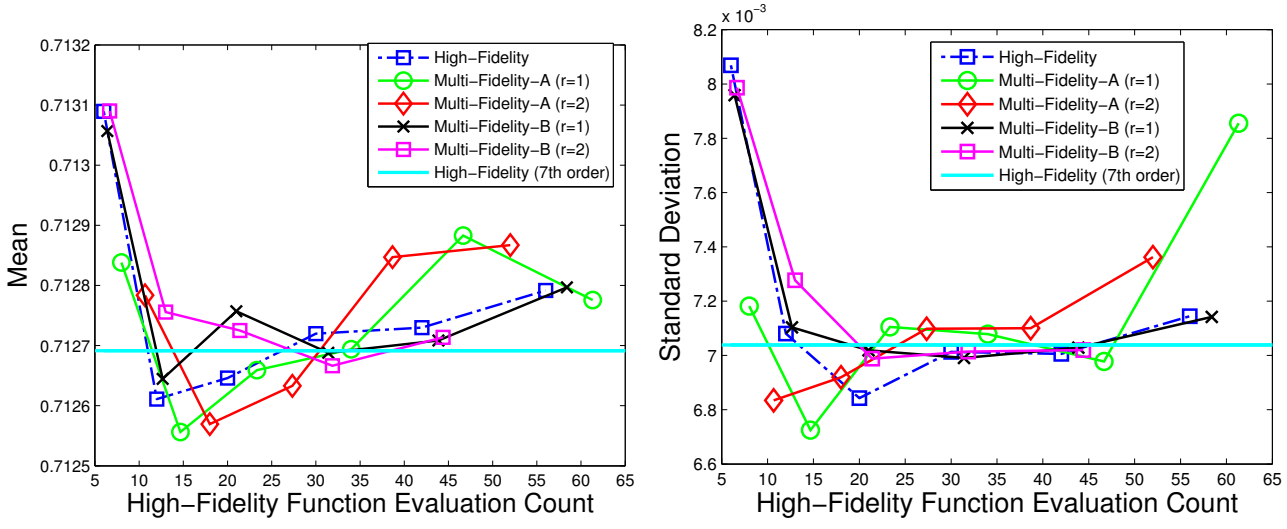


(A) Mean

(B) Standard Deviation

FIGURE 4.27: Convergence of mean and standard deviation of $C_l$ for RAE 2822 case with two-dimensional random variables.

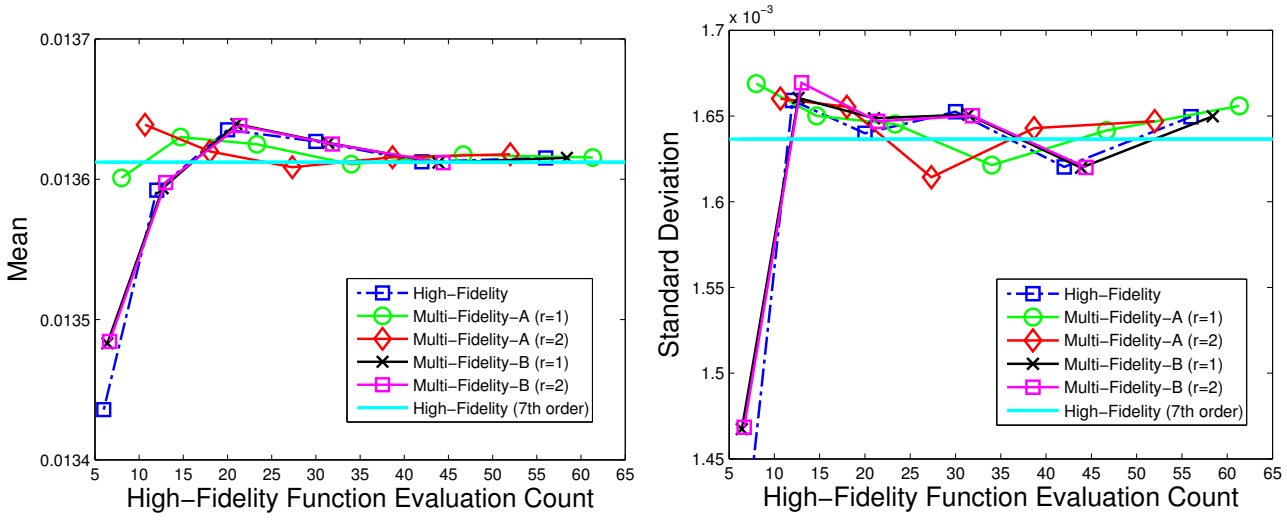


(A) Mean (B) Standard Deviation

FIGURE 4.28: Convergence of mean and standard deviation of $C_d$ for RAE 2822 case with two-dimensional random variables.

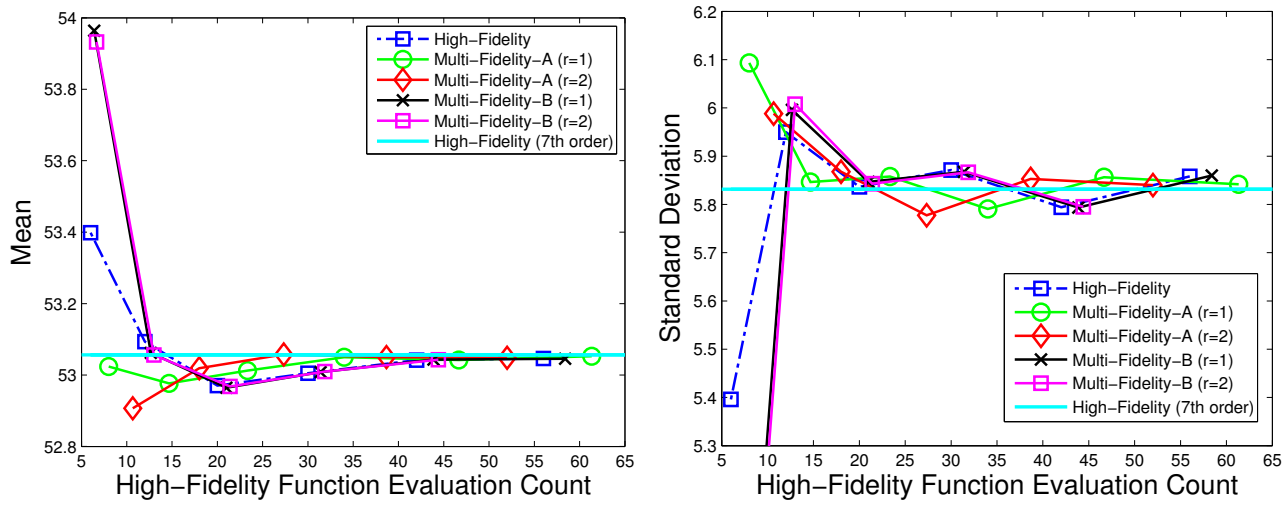


(A) Mean (B) Standard Deviation

FIGURE 4.29: Convergence of mean and standard deviation of $L/D$ for RAE 2822 case with two-dimensional random variables.

A different behaviour is observed on the approximation of $C_l$ response surface. On lower order polynomials, an adequate error level can be reached with the application of multi-fidelity scheme and type A low fidelity samples. However, the application of multi-fidelity approximation with higher order polynomials exhibits an increase of the errors value in both mean and standard deviation. The error starts to increase at the correction PC degree of 4 when the low-fidelity PC degree is either 5 or 6. This suggest that the type A low-fidelity response surface of $C_l$ exhibits a high-order non-linearity compares to the high-fidelity one. Such behaviour of non-linearity is not corrected by the correction expansion

thus caused an increased errors. As it was expected, the use of Euler solvers as the low-fidelity samples could not aid the high-fidelity samples and no advantage could be achieved (in high order polynomial it became worse).

To summarize, the application of MF-PCNIPC to RAE2822 problem could improve the quality of approximation if the partially converged simulation is used as the low-fidelity samples on this particular problem. The use Euler simulations, even though it is very fast relative to the RANS simulation, offers no benefit to the multi-fidelity scheme and could results in worse approximation in some cases. However, careful consideration is needed because too high polynomial order could results in an inaccurate value as it is observed on the $C_l$ approximation. This inaccurate value might be explained by the numerical errors on the CFD simulations or the high non-linear characteristics of the low-fidelity samples that are not exist in the high-fidelity samples. A good practice is to use a moderate polynomial order for both the low- and correction-expansion to filter the noises and errors. On this particular problem, using a 2nd and a 4th order polynomials for low- and correction-expansion, respectively, were enough to ensure an accurate approximation of the low-fidelity scheme with moderate computational cost.

### 4.4.3 Euler Flow around Common Research Model

After the two dimensional (airfoil) numerical experiments, we tested the MF-PCNIPC on the Euler simulation around the three dimensional common research model (CRM). This case is available on the test cases of SU2 and is available freely on the internet (see https://github.com/su2code/TestCases). For this simulation the number of mesh elements is 38402 arranged in a structured way as it is depicted in Fig. 4.30. The high fidelity simulation on this case is the fully-converged simulation while the low-fidelity simulation is the partially converged simulation until a certain number of iteration. The criterion for the full convergence is the residual of the drag value reached the value of $10^{-6}$. To determine the cut-off iteration for the low fidelity simulation, an analysis of the converge trend, $R^2$, and RMSE is performed just like the previous aerodynamic examples.

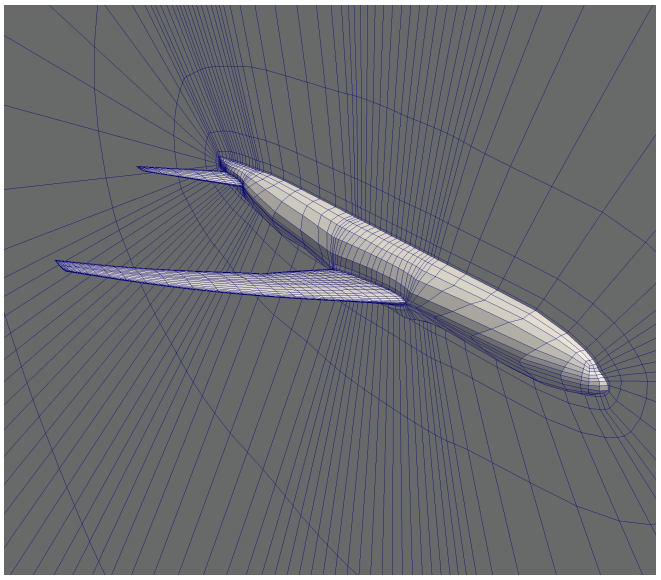

FIGURE 4.30: Mesh used in the present Euler simulation of CRM body.

We set two cases of UQ for the CRM model:

1. Variation in Mach number and angle of attack.
2. Variation in Mach number, angle of attack, sideslip angle, freestream temperature, and freestream pressure.

For both cases, the QoI is the lift-to-drag ratio.

#### 4.4.3.1 Variations in $M, \alpha$

The random variables for the first CRM case are listed in Table 4.8.

| **Random variable** | **Probability distribution** |
|---|---|
| $M$ (–) | Uniform [0.82; 0.84] |
| $\alpha$ (°) | Uniform [2;4] |

TABLE 4.8: Random variable distributions for the first CRM test case.

Before the multi-fidelity UQ was performed, we investigated the convergence trend of the simulation to give an information of at what typical iteration is that the partially converged simulation is predictive enough of the fully-converged one. For the first CRM case, the iteration is quite fast to reach steady level value where the residual reach the value of $10^{-6}$ in about 700 iterations as it is shown in Fig. 4.31. The convergence trend experiences a peak before it started to stabilized. A near steady state level (but not fully converged) is reached at about 175 iterations where further iterations refine the calculation until it is fully converged.

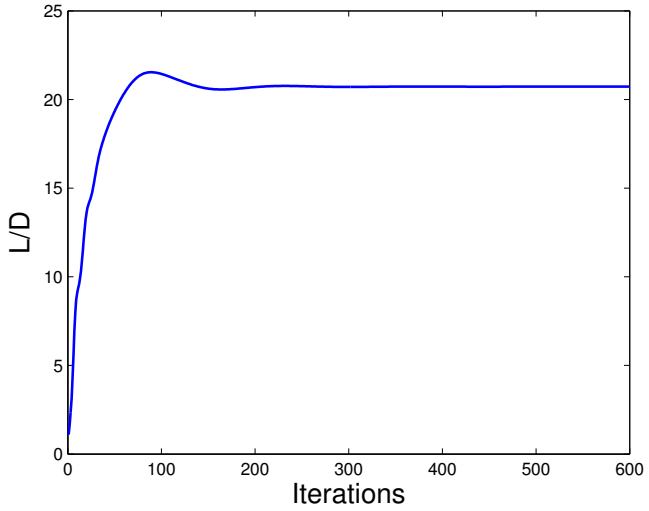


FIGURE 4.31: Convergence of the $L/D$ for CRM case evaluated with Euler solver.

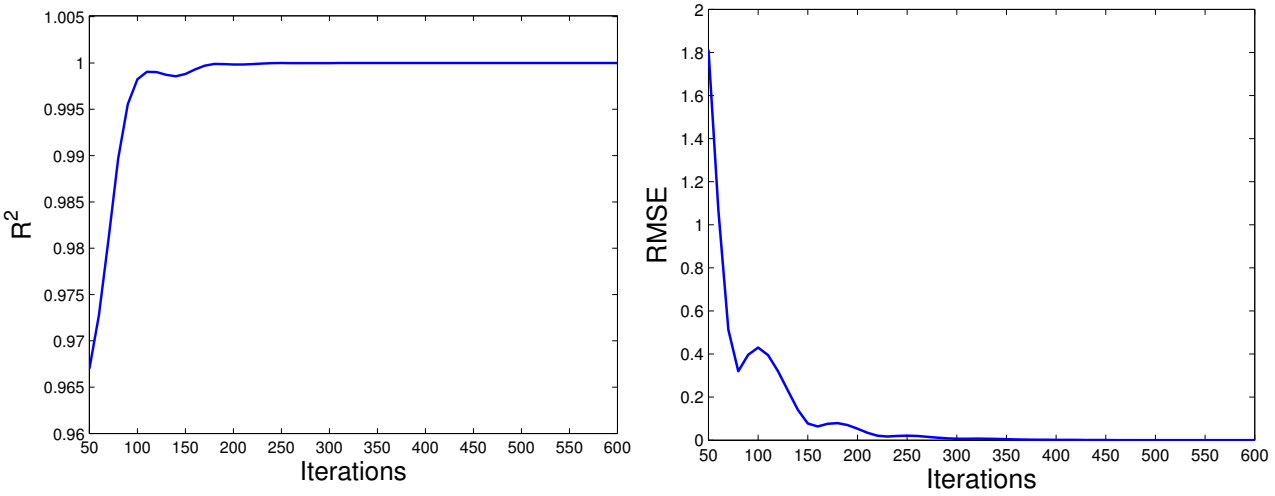


(A) $R^2$

(B) RMSE

FIGURE 4.32: Convergence of $R^2$ and RMSE of L/D for CRM case with Euler solver.

We then analyzed the convergence of RMSE and $R^2$ with respect to the CFD iterations. The result of this investigation is shown in Fig 4.32. Result shows that the low-fidelity simulations have a high correlation with the fully-converged simulations where sufficiently predictive low-fidelity responses could be observed from about 100 iterations where the $R^2$ and RMSE value are 0.998 and 0.418, respectively, at this point. Partially converged simulation with 100 iterations is also a good trade-off between the accuracy and the computational cost for UQ using MF-PCNIPC. Considering the trade-off between accuracy and computational time, we chose the iteration number of 100 for the low-fidelity samples. This means that the work ratio relative to the fully converged simulation is about 6. The computational cost for MF-PCNIPC is then calculated using the equation 4.18.

To investigate the performance of MF-PCNIPC on the first case of CRM problem, we varied the

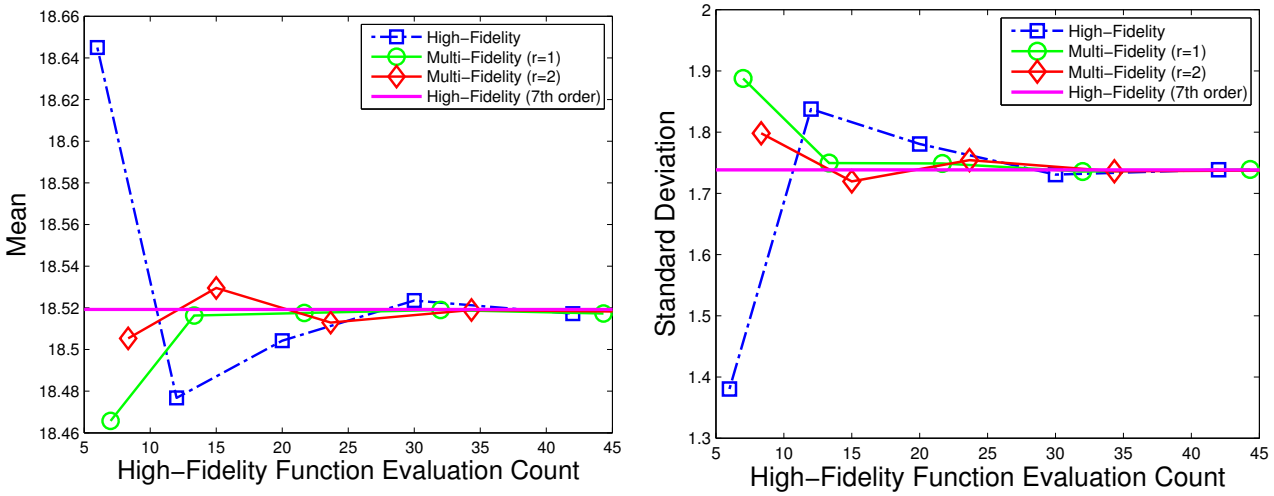


(A) Mean

(B) Standard Deviation

FIGURE 4.33: Convergence of the mean and standard deviation of $L/D$ for the two-dimensional CRM problem obtained with PCNIPC and MF-PCNIPC with various offset value.

correction degree and the degree offset to see how much advantage could be obtained by applying MF-PCNIPC on this particular problems. The hyperbolic exponent is kept to the value of 1 due to the low-dimensionality of the problem. Convergence of mean and standard deviation for both single-fidelity and multi-fidelity approximation are depicted in Fig. 4.33 where the MF-PCNIPC reached an error level of standard deviation below 0.1% by using 15 exact function evaluations compares to the PCNIPC that needs 30 simulations.

As it could be seen from the results, higher accuracy of mean and standard deviation approximation could be obtained by supplying the high-fidelity approximation with low-fidelity expansion of any polynomial degree. The most significant improvement is seen on the approximation with high-fidelity NIPC and polynomial degree of 1 where the aid from low-fidelity samples help to capture the higher degree main effects and interaction reduces the approximation error with MF-PCNIPC. Furthermore, this better accuracy is obtained with low additional computational cost by utilizing the partially converged simulations. The estimated mean and standard deviation values show a converging trend as the polynomial order is increased and more samples added. Considering the computational cost and accuracy, it is seems that the MF-PCNIPC with $r = 2$ and correction degree of 2 (equivalent to 15 high-fidelity function evaluations) is sufficient to accurately predicts the behavior of the response surface and calculate the mean and standard deviation. Due to the presence of numerical error in the CFD simulation, it is quite difficult to reach the machine precision so a sufficiently accurate approximation is enough as long as the important behaviour of the response surface is captured.

The second case is more complex because it involves higher dimensionality of the random variables, which are Mach number, angle of attack, sideslip angle ($\beta$), freestream pressure $P_\infty$ and temperature $T_\infty$ listed in Table 4.9. For this case we use $q = 0.6$ to reduce the number of collocation points but still retain the interaction term between the variables. Analysis of the $R^2$ and RMSE (shown in Fig. 4.34)

| Random variable | Probability distribution |
|---|---|
| $M$ (–) | Uniform [0.82; 0.84] |
| $\alpha$ (°) | Uniform [2; 4] |
| $\beta$ (°) | Uniform [0; 2] |
| $P_\infty$ (Pa) | Uniform [96259; 106390] |
| $T_\infty$ (K) | Uniform [273.74; 302.56] |

TABLE 4.9: Random variable distributions for the second CRM test case.

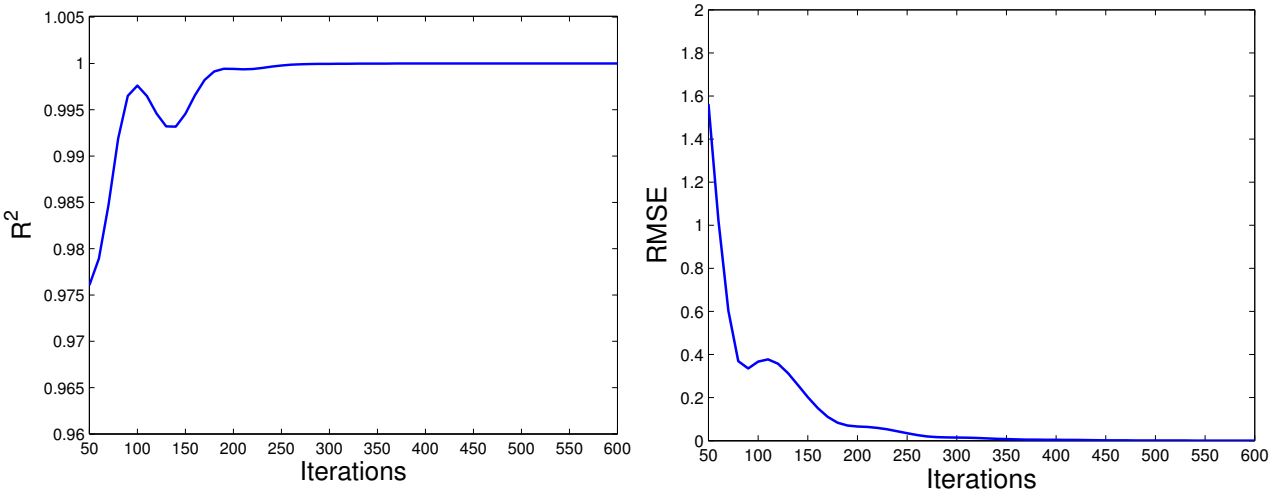


(A) $R^2$.

(B) RMSE.

FIGURE 4.34: Convergence of $R^2$ and RMSE for CRM case with Euler solver and five-dimensional random variables.

obtained from 400 samples show that high correlation ($R^2$=0.997) can be achieved from the iteration of 100 where at this point the RMSE is relatively low enough (RMSE = 0.34). The correlation slightly decreases after the 100th iterations and reach a plateau at the iteration of about 250. The trend is roughly the same with the two-dimensional example thus we also use the simulation with iteration of 100 as the low-fidelity samples.

The sensitivity analysis was performed to investigate and rank the contribution of the variables to the QoI at the 5th dimensional case where the result of this investigation is shown in Table 4.10. Sensitivity analysis result shows that even though on this problem the dimensionality is quite high, there were only three variables that give significant contribution to the variations in aerodynamic coefficients which are $M, \alpha$, and $\beta$. From these three random variables, angle of attack $\alpha$ is the most significant random variable that contributes to about 95% of all variations while the Mach number and sideslip angle take account of about 2.42% and 2.17% variation. The variations that comes from freestream pressure and temperature were very low and could be neglected. Thus for further procedure such as robust optimization, the problem could be simplified by only considering the most significant random variables. This analysis is particularly useful if the user/designer wants to perform robust optimization procedure but needs to reduce the complexities of the problem and eliminates some of least significant random variables beforehand.

TABLE 4.10: Sensitivity indices of the random variables of the 5th dimensional random case.

| **Random Variables** | ***S*** |
|---|---|
| $M$ | 2,42% |
| $\alpha$ | 95.27% |
| $\beta$ | 2.18% |
| $P_\infty$ | $6.3 \times 10^{-6}$% |
| $M_\infty$ | $2.4 \times 10^{-6}$% |

Results of the convergence of the mean and standard deviation approximated by MF-PCNIPC and high-fidelity PCNIPC is shown in Fig. 4.35. Shown in the figure is also the result obtained by 8th order high-fidelity expansion as a benchmark for comparison. The trend shows that the approximated mean and standard deviation moved toward converge value with the higher PC degree. As it could be seen from the figure, the MF-PCNIPC with degree offset of 2 is able to reach sufficient accuracy of mean and standard deviation using 45.3 high-fidelity computational cost while the MF-PCNIPC with the degree offset of 1 and high-fidelity PCNIPC need about 70.33 and 122 high-fidelity cost, respectively. Using the offset of 1 was not sufficient enough because the low-fidelity expansion only captures little additional information to aid the high-fidelity (correction) expansion. By using the offset of 2, the additional useful informations were captured thus greatly reduce the approximation error with extra low computational cost. Therefore, a good practice is to apply the offset parameter as high as possible but not too high due to the possibility of overfitting.

This example shows that the application of MF-PCNIPC using partially-converged Euler simulation as the low-fidelity samples gives great advantage to reduce the computational cost and reach sufficiently accurate approximation of mean and standard deviation. It is important to check the values of $R^2$, RMSE, and CFD convergence trend to determine the cut-off iteration for the low-fidelity samples to gain as much advantage as possible.

## 4.5 Consideration for Real Problem

For very expensive real-world problems it is necessary to be very strict with the computational budget. The number of samples that can be afforded might need to be determined before deciding the polynomial degree and generating the collocation points. An excellent method for single-(high)-fidelity NIPC to deal with this issue is by applying the least-angle-regression (LAR) method on a fixed number of samples. The LAR method retains the polynomial basis that makes the largest contribution and ensures the numerical stability of the approximation. However, this could cause a problem for MF-PCNIPC because there is the possibility of mismatch between the LF and correction expansions where the correction basis is not a subset of the LF-PCE. This could result in a situation where aspects of the LF basis needing correction are not corrected by the correction expansion. Therefore, we still use

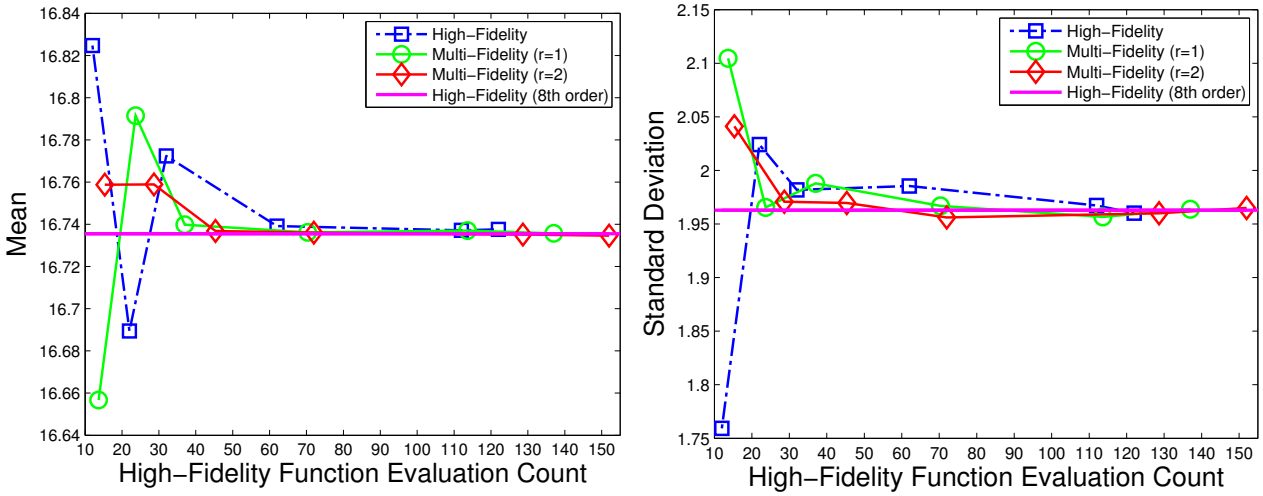


(A) Mean.

(B) Standard Deviation.

FIGURE 4.35: Convergence of the mean and standard deviation of $L/D$ for the five-dimensional CRM problem obtained with PCNIPC and MF-PCNIPC with various offset value.

ordinary PCNIPC as the basis algorithm by using an OSR value of 2 for our application and leave the implementation of more advanced methods such as LAR to future work.

As for the sampling method, an adaptive sampling scheme could be employed but we have not explored this possibility. If the number of samples is already fixed, a good choice is to use an optimized LHS for the LF samples and select the optimum subset for the HF samples. The adaptive step could be performed afterwards to enrich the sampling plan. An advantage of the low-discrepancy sequence that we used in this thesis is that its nested properties allow easy enrichment of the sampling plan. We employ low-discrepancy sequences for all the test problems described in this thesis because our present focus is to develop the framework of MF-PCNIPC rather than adaptive features.

For robust optimization purpose, experiment can be performed to determine the best choice of the polynomial basis for the low- and correction-expansion. The purpose of this is to find the best polynomial basis set that has tolerable accuracy but with low computational cost. Because metaheuristics optimizer will call a numerous number of function evaluations, it is advantageous to first reducing the number of samples for robustness calculation by this preliminary experiment. The best set can then be chosen by comparison with high order polynomial expansion or using statistical criterion such as leave-one-out error. We demonstrated this preliminary experiment further on the next chapter.

## 4.6 Lesson Learned

In this thesis we present a MF extension of NIPC based on regression for UQ purposes; the method itself could be employed for other applications such as building a surrogate model for optimization. In

contrast to the similar framework that uses spectral projection to estimate the coefficients, the MF-PCNIPC method allows flexible sampling and choice of polynomial basis and is especially useful on high-dimensionality problems where the sparse grids/tensor product scheme suffers from the curse of dimensionality or in cases where arbitrary sample locations and numbers are needed. This is particularly advantageous if the LF function is very cheap to evaluate compared to the HF one. We tested the method on a number of artificial and aerodynamic test problems to investigate the performance and practical aspects of MF-PCNIPC on various characteristics of the problems.

The results show that more accurate approximations can be obtained if the LF function can predict the behaviour of the HF function sufficiently well. In cases with high correlation between the LF and HF functions ($R^2 > 0.9$), the MF scheme can be safely assumed to be able to increase the approximation accuracy relative to a single HF expansion. However, it must be noted that, even if the LF and HF functions are well-correlated, the result could be disastrous if the RMSE is high. In some cases, like the Branin function, where the correlation is low but the LF function still can capture some fundamental behaviour of the HF function, the MF scheme is able to increase approximation accuracy. However, it is decidedly risky to use a LF function with low correlation to assist the HF approximation in practical applications. A successful MF approximation can be achieved with a LF function that correlates well with the HF function and has the lowest possible RMSE value. In some cases where the LF function is found to be a poor representation of the HF function (low correlation with high RMSE), it is better to use the single-(high)-fidelity expansion alone and discard the LF samples. To determine whether the LF function is sufficiently representative of the HF function or not, the RMSE and $R^2$ should be checked. This procedure is recommended even if there are only a few samples available. Another factor to be considered here is that it is very difficult to achieve convergence to machine precision in real problems because of the presence of numerical errors in the quantity of interest calculated by the PDE solver. Therefore, it is good practice to retain relatively low-to-moderate degree polynomials for real applications.

The tests on the aerodynamic problems showed that tolerable accuracy compared to ordinary PCNIPC can be obtained by employing MF-PCNIPC. Partially-converged simulations turn out to provide good LF samples in these aerodynamic cases because the same physical problems are solved but without achieving fully-converged results. Nonetheless, more studies are needed in more complex cases, such as full-configuration aircraft design using a Reynolds-averaged Navier-Stokes solver. LF simulations with a coarser mesh can also provide a moderately good prediction of the response surface to aid MF UQ. However, coarser-mesh LF simulation is not as flexible as partially-converged LF simulation because additional mesh generation is needed and the fidelity level cannot be determined flexibly: to change the fidelity level additional simulations have to be performed. Coarser meshes mean faster evaluation but with greater likelihood of lower correlation with the HF simulations. Tuning the fidelity level of partially-converged simulations is easy because the necessary information is already available when the fully-converged simulation is finished. The only parameter to be tuned to control the fidelity level is the iteration number for which the $R^2$ and RMSE values can easily be calculated and plotted.

On the next section, we will present an application of the developed multi-fidelity UQ framework and improved multi-objective optimizer to aerodynamic robust optimization.

# Chapter 5

# Application to Aerodynamic Robust Optimization

This chapter deals with the application of the developed and improved algorithms for optimization (using SS-MOMA with achievement scalarizing function) and uncertainty quantification (using MF-PCNIPC) to the robust optimization problem. The case considered here is the robust optimization of transonic airfoil where the Euler equation was used as the governing equation. A study on the optimized solutions was performed to investigate the shape of the optimum airfoils. This knowledge is important for designing airfoils that have high performance but also robust to the presence of the uncertainties. Beside of that, the purpose of robust optimization in this chapter is also to demonstrate the applicability of the developed framework in the real world robust optimization problem. The problem was first defined followed by the parameters used in the optimization and uncertainty quantification. Results and analysis of the optimum airfoils are given next.

## 5.1 Problem Definition

The main objective of this robust optimization problem was to find the Pareto optimum solutions that were robust to the uncertainty in the flight conditions. For this purpose, the problem was modelled into the multi-objective optimization problem that consisted of the mean and standard deviation of the aerodynamic performance as the objectives. Lift-to-drag ratio was chosen as the objective for robust optimization test problem in this current study. A lift-constraint was not set in this problem but it could be easily implemented by using the fixed-lift mode of SU2. Our goal here was then to study the trade-off between the performance and robustness of $L/D$ ratio in the design of the transonic airfoil where SS-MOMA-ASF and MF-PCNIPC were used as the optimizer and UQ algorithm, respectively. Analysis were performed to some selected solutions from the set of non-dominated solutions later to discover some important knowledge and features for future design studies. A more accurate study could

be performed by implementing RANS solver but Euler solver is found to be adequate for this research because the current goal was for conceptual design and demonstration of the proposed methodologies.

Airfoil robust optimization was already studied in some previous research. Example of these previous works are robust optimization of subsonic airfoil subjected to the geometrical uncertainty[77], airfoil robust design with six-sigma method[76], multi-objective robust design in transonic field[75], robust airfoil optimization using maximum expected and expected maximum value approach[160], and robust design using stochastic collocation[161]. In this thesis we performed transonic airfoil optimization with performance and robustness of $L/D$ ratio as the objectives and then performed thorough analysis of the airfoils found in the final non-dominated solutions.

The baseline airfoil for the current optimization problem was the RAE 2822 airfoil which was reproduced using 9-variables PARSEC parameterization with fixed trailing edge ordinate and thickness of 0 and 0.001, respectively. A least square minimization was performed to find the PARSEC parameters with minimum geometrical errors to the RAE 2822 (the same procedure with the aerodynamic example on chapter 5). These parameters were then varied to the range of $\pm 2\%$ and acted as the decision variables for the optimization problem. The uncertain variables for the current problem were the Mach number and angle of attack as listed in Table 5.1. A maximum thickness constraint was given to ensure that the optimum airfoil do not have a too small thickness. The mathematical models for this optimization problem were:

$$\text{minimize:} \quad -\mu(L/D), \sigma(L/D) \tag{5.1}$$

$$\text{Subject to:} \quad t_{\max} \geq 11\% \tag{5.2}$$

TABLE 5.1: Random variable distributions for the robust transonic airfoil optimization test case

| **Random variable** | **Probability distribution** |
|---|---|
| Mach number (–) | Uniform [0.77.0.83] |
| Angle of attack (°) | Uniform [1.5.2.5] |

## 5.2 Optimizer and UQ Algorithm Parameters

### 5.2.1 Optimizer Parameters

To deal with the multi-objective robust optimization problem, we used the SS-MOMA algorithm equipped with achievement scalarization function to guide the local optimization procedure (similar to the aerodynamic optimization example in Chapter 3). The results on Chapter 3 shows that the use of achievement scalarization function or Chebysev to guide the local search significantly improve the performance of the optimizer over the original SS-MOMA with weighted-sum, random mutation

hill climber, and ordinary NSGA-II without surrogates. The surrogate based algorithm wrapped inside memetic algorithm framework also overcome the difficulties of global surrogate modelling in relatively moderate to high dimension. Such advantages are due to the usefulness of local surrogate to capture locality of the landscape of the true functions which is simpler than the true function global landspace. Therefore, the use of local-surrogate framework is to provide the potential direction for the improvement and not to predicts the local landscape with high accuracy.

On the optimization part, the SS-MOMA-ASF was used to solve the optimization problem with the following parameters:

TABLE 5.2: Parameter of SS-MOMA-ASF for transonic airfoil robust optimization

| | |
|---|---|
| Initial population | 40 |
| Population size | 16 |
| Maximum generation | 8 |
| Crossover | Simulated binary crossover |
| Mutation | Polynomial mutation |
| $P_{cro}$ | 0.9 |
| $P_{mut}$ | $1/n$ |

Kriging was used as the surrogate model due to its robustness for various behaviour of any functions. The training time of the Kriging hyperparameters itself was negligible compares to the time needed for robustness evaluation.

The initial population was generated using Halton sequence with very tight population and generation number because the problem itself is quite expensive. The ASF is used for the local search in conjunction with the Chebyshev based search if the solutions cannot be improved further with the ASF.

A geometric constraint was applied to keep the maximum thickness of the airfoils higher than 11%. Because the constraint was deterministic and independent to the random variables involved, the constraint can be simply applied as in the deterministic framework.

### 5.2.2 Uncertainty Quantification Parameters

Before the robust optimization was performed, we studied the efficacy of the MF-PCNIPC to determine the best combination to speed up the calculation but still retain the accuracy. For this, we perform uncertainty quantification procedure on the nominal airfoil (RAE 2822) subjected to the uncertainties of the Mach number and angle of attack as it was already specified before. We used the partially-converged scheme as the low-fidelity samples and analyze the $R^2$ and RMSE convergence trend using 100 samples generated using Halton sequence. The results of this investigation are shown in Fig. 5.1.

The figures show a rapid convergence of the $R^2$ and RMSE before it fully converged to the residual error of $10^{-6}$. From the average of 100 samples, the mean of the iterations needed for convergence was roughly 501. Based on this investigation and the results, we chose the cut-off iterations of 100 as the

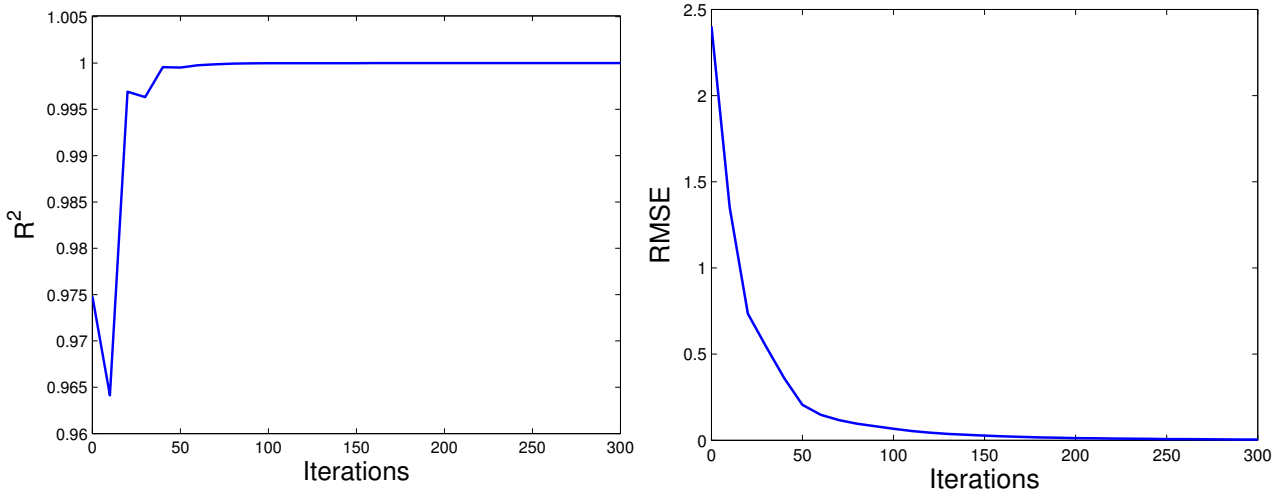


(A) $R^2$ (B) RMSE

FIGURE 5.1: Convergence of mean and standard deviation of RAE 2822 with Euler solver in nominal flight condition.

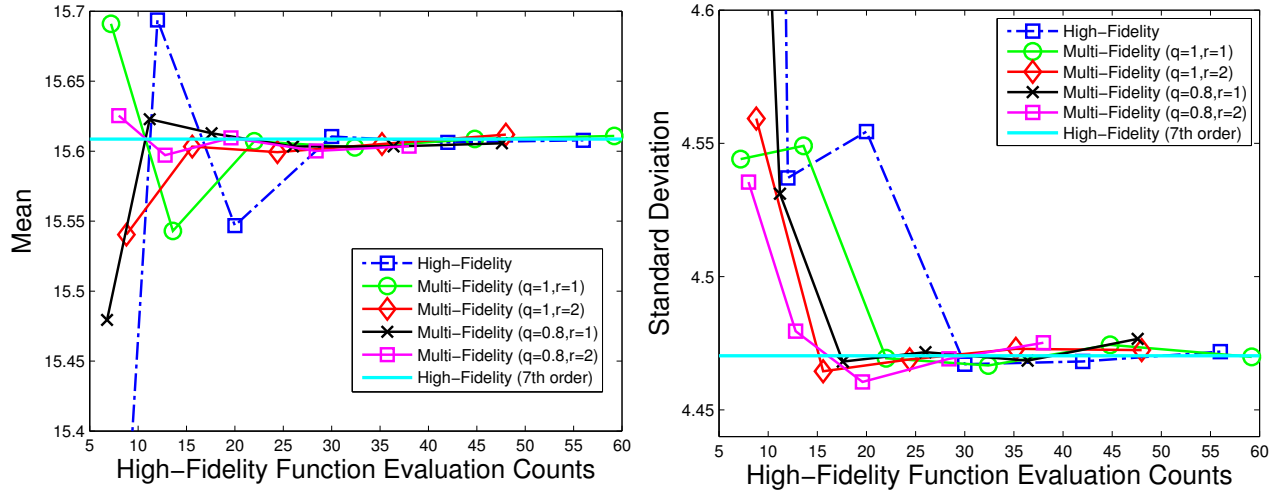


(A) Mean (B) Standard Deviation

FIGURE 5.2: Convergence of $R^2$ and RMSE of RAE 2822 case with Euler solver and two-dimensional random variables

low-fidelity samples which means that the work ratio of the low-fidelity to the high-fidelity samples was about 5.01. At this point the $R^2$ and RMSE values are 1 and 0.0816, respectively, which shows a very high correlation and very low RMSE of the low-fidelity samples with respect to the high-fidelity one. We then performed the UQ procedure by varying the value of $q$ (hyperbolic truncation exponent) and $r$(the degree offset between low- and high-fidelity expansion). The $r$ value was varied to 1 and 2 while it is 0.8 and 1 for the $q$ value so there are four combinations in total. Fig. 5.2 shows the convergence of mean and standard deviation from all of the combination with the 7th order high-fidelity NIPC as the benchmark.

Table 5.3 and 5.4 shows the errors comparison of the results obtained by various multi-fidelity scheme

with the 7th order high-fidelity PCNIPC. As it can be seen from the table, a good tradeoff between the computational cost and the accuracy can be achieved by using MF-PCNIPC scheme with $r = 2$ and $q = 0.8$. Using this set of parameters, the errors relative to the 7th order high-fidelity NIPC are 0.073% and 0.26% for mean and standard deviation, relatively, with computational cost equivalent to about 12.8 high-fidelity function calls. This means that the computational cost saving for statistical moment calculation relative to the 4th and 7th order high-fidelity PCNIPC are 60% and 83.78%, respectively. Therefore, on the robust optimization case in this work we used MF-PCNIPC with $r = 2$ and $q = 0.8$ to calculate the objective functions of the given optimization problem, which were the performance and robustness of L/D.

| **P** | **r=1, q=0.8** | **r=1, q=1** | **r=2, q=0.8** | **r=2, q=1** | **High-fidel** |
|---|---|---|---|---|---|
| 1 | 8.27E-01 (6.8) | 5.28E-01 (7.2) | 1.07E-01 (8) | 4.37E-01 (8.8) | 3.82E+00 (6) |
| 2 | 9.10E-02 (11.2) | 4.20E-01 (13.6) | **7.35E-02 (12.8)** | 3.43E-02 (15.6) | 5.45E-01 (12) |
| 3 | 2.69E-02 (17.6) | 9.97E-03 (22) | 5.73E-03 (19.6) | 5.98E-02 (24.4) | 3.96E-01 (20) |
| 4 | 3.34E-02 (26) | 3.78E-02 (32.4) | 5.41E-02 (28.4) | 2.21E-02 (35.2) | 1.20E-02 (30) |
| 5 | 3.32E-02 (36.4) | 9.03E-04 (44.8) | 3.25E-02 (38) | 2.08E-02 (48) | 1.48E-02 (42) |
| 6 | 1.89E-02 (47.6) | 1.43E-02 (59.2) | - | - | 5.57E-03 (56) |

TABLE 5.3: Error of mean (as percentages)

| ***P*** | **r=1, q=0.8** | **r=1, q=1** | **r=2, q=0.8** | **r=2, q=1** | **High-fidel** |
|---|---|---|---|---|---|
| 1 | 9.92E+00 (6.8) | 1.65E+00 (7.2) | 1.46E+00 (8) | 1.99E+00 (8.8) | 4.47E+01 (6) |
| 2 | 1.36E+00 (11.2) | 1.76E+00 (13.6) | **2.06E-01 (12.8)** | 1.30E-01 (15.6) | 1.49E+00 (12) |
| 3 | 4.87E-02 (17.6) | 2.03E-02 (22) | 2.20E-01 (19.6) | 2.97E-02 (24.4) | 1.88E+00 (20) |
| 4 | 3.00E-02 (26) | 8.10E-02 (32.4) | 2.56E-02 (28.4) | 5.84E-02 (35.2) | 7.11E-02 (30) |
| 5 | 4.10E-02 (36.4) | 9.19E-02 (44.8) | 1.10E-01 (38) | 4.81E-02 (48) | 4.79E-02 (42) |
| 6 | 1.42E-01 (47.6) | 8.98E-03 (59.2) | - | - | 3.46E-02 (56) |

TABLE 5.4: Error of standard deviation (as percentages)

The total computational cost for the transonic airfoil robust optimization case was then $(40 + 8 \times 16 \times 2) \times 12.8 = 3778$ high fidelity function evaluations.

## 5.3 Optimization Results and Analysis

The Pareto front found was shown in the left-hand plot in Figure 5.3. Before moving further into the analysis, the consistency between multi-fidelity and single-fidelity UQ needs to be checked. We did this by performing single high-fidelity UQ on the non-dominated solutions found in the robust optimization. Non-dominated solutions found using multi-fidelity UQ were re-evaluated using a $6^{\text{th}}$-order polynomial with total order rules with high-fidelity simulations. The results of this comparison are shown in the right-hand plot in Figure 5.3. There is evidently some difference between the results of the high-fidelity UQ and multi-fidelity UQ for these designs. Table 5.5 presents the maximum error, minimum error and mean absolute error (MAE) between the single- and multi-fidelity UQ evaluations of the mean and

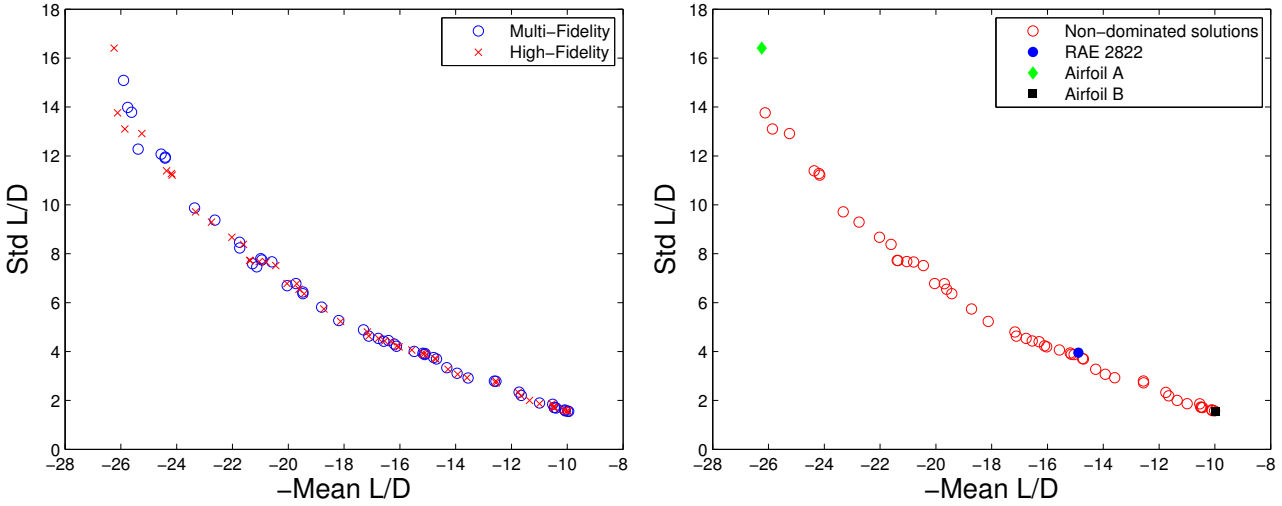


(A) Non-dominated solutions found by the optimizer

(B) Representative airfoils for analysis

FIGURE 5.3: Comparison of the non-dominated solutions found by the optimizer with multi-fidelity UQ with the single high-fidelity evaluations (left) and depiction of the representative airfoils and RAE 2822 in objective space (right).

standard deviation. This comparison shows that the standard deviation is less well approximated by the multi-fidelity method than the mean. The maximum error in the standard deviation is quite large and occurred for a solution for which the stochastic response surface is highly nonlinear. Such non-linearity is typically exists on the solutions with high mean and standard deviation. Such cases are rare, however, and the values of the minimum error and MAE for the standard deviation are acceptably small. The overall difference between high-fidelity and multi-fidelity UQ results is not that large, and the high-fidelity results show that the non-dominated solutions found using multi-fidelity UQ are sufficiently representative that its use could speed up the robust optimization process without significant loss of accuracy.

TABLE 5.5: Error comparisons of mean and standard deviation (as percentages) between multi-fidelity and high-fidelity UQ methods for the transonic airfoil test case.

| | **Min. error** | **Max. error** | **MAE** |
|---|---|---|---|
| **Mean** | 0.0065 | 2.0025 | 0.5257 |
| **Std.** | 0.0101 | 8.2748 | 1.8115 |

Right hand plot in Figure 5.3b shows the location of the extremum and RAE 2822 airfoil in the objective space. For easier explanation we refer to the airfoil with maximum and minimum mean of $L/D$ as the airfoil A and B, respectively (be aware that Figure 5.3 depicts the minus mean of $L/D$). The geometry of these representative airfoils and RAE 2822 are depicted in Figure 5.4; analysis of these geometries will be explained later. The non-dominating results show that the extremum airfoils and RAE 2822 are non-dominating to each other, which means that the extremum airfoils do not dominate the RAE 2822 in both objectives. Analyzing the shape of the Pareto front and the location of the RAE 2822 in objective space relative to the Pareto front, it seems that the objective space of this particular problem

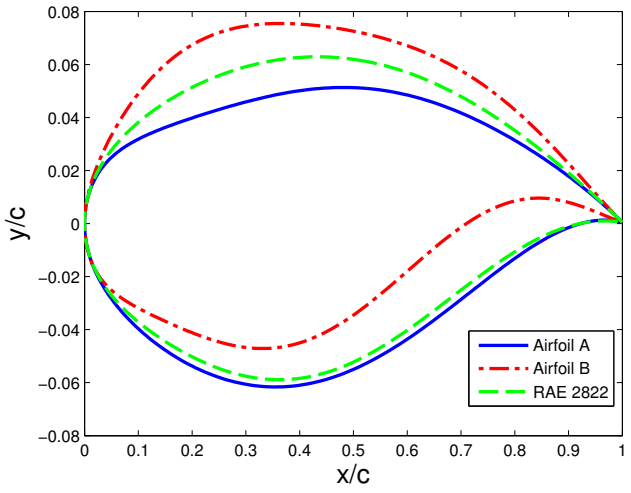


FIGURE 5.4: Geometry of the three representative airfoil from the non-dominated solutions

is characterized by a narrow area that spans from the solutions with minimum to the maximum mean of $L/D$. Nonetheless, the optimization procedure successfully found the evident trade-off between the mean and standard deviation of $L/D$. We explain the geometry analysis next.

To analyze the correlation between optimum airfoils geometry and the objectives (mean and standard deviation), we used a self-organizing map (SOM) [162], or Kohonen map, to map the 52 Pareto solutions into two-dimensional representation that preserved their topological properties. An open-source MATLAB SOM toolbox [163] was used in this paper where the input space to be mapped are the PARSEC decision variables and the two objectives. The Kohonen map obtained from this procedure is shown in Figure 5.5.

The U-matrix indicates how the solutions are clustered where the blue and red color indicates the cluster and the border, respectively. From the SOM analysis, we can again that high L/D designs are accompanied by high standard deviation of L/D. Solutions with high L/D mean and low standard deviation are concentrated in the bottom left and top left region, respectively. The additional advantage of using SOM is that now we are able to analyze the relation between the decision variables and the objectives. Based on the analysis of the figure, designs with high L/D mean and standard deviation typically have upper surface's crest abscissca ($X_{up}$) nearer to the half-chord position with smaller value of the ordinates ($Y_{up}$) compares to the low L/D mean designs. This characteristics corresponds to the decreasing drag and this is why the mean of the L/D is increasing. Another characteristics of high L/D design is that they have lower surface's abscissa ($X_{lo}$) closer to the half-chord and relatively large ordinates ($Y_{lo}$). Moreover, trailing edge angle ($\alpha_{TE}$) should also be controlled to lower value to increase the mean of L/D. However, these characteristics produce high mean of L/D but with high standard deviation. The airfoils with low mean and standard deviation of L/D have the opposite characteristics. This means that to increase the stability of L/D, one should do the opposite of altering the airfoil geometry to have high mean of L/D. The geometry changes to increase the stability of L/D is also

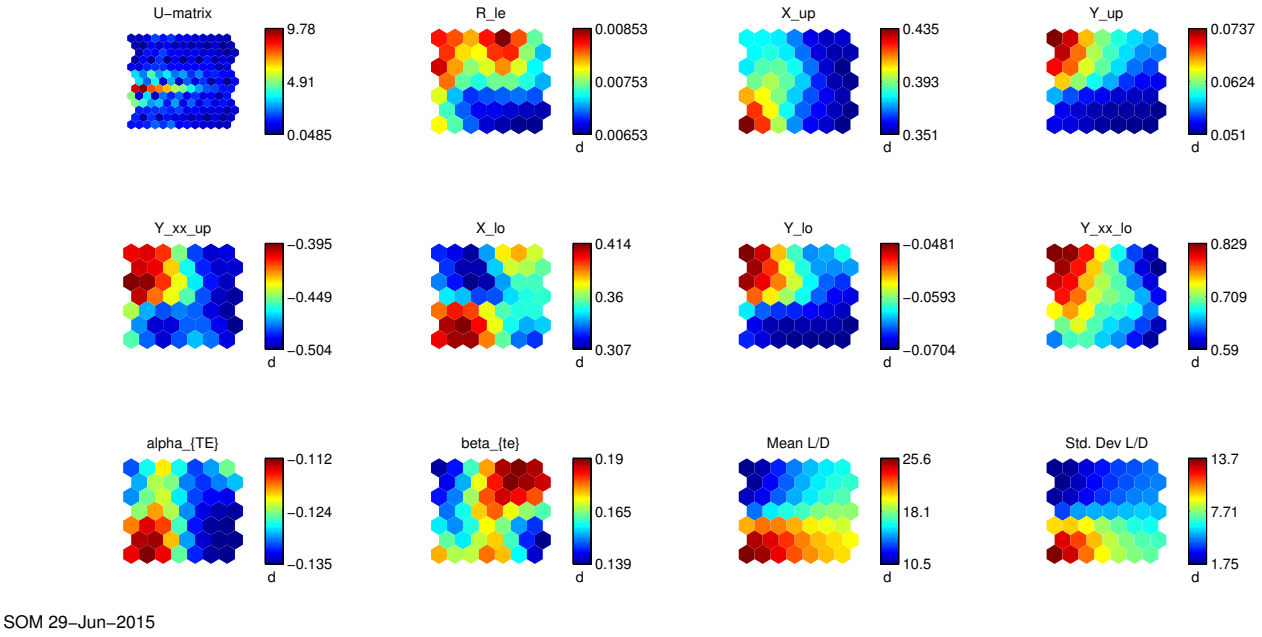


FIGURE 5.5: SOM visualization of the decision and objective spaces of the transonic airfoil robust optimization problem.

equivalent to the increase of the camber. Therefore, based on this analysis, an airfoil that balances the mean and standard deviation of L/D could be obtained by controlling these important features.

From the all non-dominated solutions, airfoil A has the highest mean but is accompanied by very high standard deviation. On the other side, the airfoil B has the lowest mean and very low standard deviation while RAE 2822 is on the midway between the two extremum airfoils. However, investigation of the response surface trend tells a different story as we will explained in the next subsection.

### 5.3.1 Response Surface Analysis

Analyzing the stochastic response surface of $L/D$ for the three representative airfoils (see Figure 5.6), although the extremum airfoils exhibit a trade-off between the two objectives, Airfoil A can nevertheless be considered to be the best airfoil overall. Airfoil A, from viewpoint of $L/D$, is better than the datum airfoil (RAE 2822) in spite of its high standard deviation value. Airfoil A has very low $C_d$ at low Mach number and angle of attack condition with slightly lower $C_l$ than the datum which contributes to the very high $L/D$ ratio on this conditions (see Figure 5.6a and Figure 5.6c). On the other side, at high angle of attack and Mach number conditions, airfoil A has similar values of $C_l$ to the datum airfoil but it has lower $C_d$ which means that airfoil A has better performance in this condition than the datum. Moreover, as it could be observed in Figure 5.6c, airfoil A has the lowest moment coefficient over the stochastic response surface compares to the airfoil B and RAE 2822.

The dramatic drop in $L/D$ of the airfoil A (see Fig. 5.6d), if the angle of attack and Mach number are increased, caused a high standard deviation in $L/D$. However, airfoil A's lowest value of $L/D$ is still higher than the largest value exhibited by Airfoil B over the stochastic response surface, which gives minimum standard deviation of $L/D$ for airfoil B. In this case, the low standard deviation of L/D behavior of Airfoil B does not mean that it exhibits the characteristics needed of a practical airfoil. Airfoil B has a high value of $C_l$ but is accompanied by a very high value of $C_d$ over the stochastic response surface, rendering the airfoil impractical.

Response surface analysis shows that it is important to perform further post-processing to find a practical set of solutions. In this the case, solution A is better in the aspect of $L/D$ than the airfoil B. It is important to notice that high standard deviation does not mean that its objective value is worse over the response surface. In fact, there is a possibility that the high standard deviation is caused by dramatic drop of the objective value but its lowest value still can be considered as a good value (in this case, the lowest $L/D$ of solution A is higher than the highest $L/D$ of solution B). This indicates that other attributes (such as skew) of the stochastic responses surfaces of performance measures should also be considered to choose the airfoils on the non-dominated sets. Moreover, airfoil A can be considered as a robust airfoil from the viewpoint of expected value[72] and consistent improvement over the probabilistic space[73]. Simply said, while the multi-objective approach able to find multiple-solutions in the Pareto front, the approach is quite inefficient because there is only one optimum solution in the true sense that could be found using a single-objective optimization procedure (maximizing the expected value). Nonetheless, since there is no guarantee that all robust optimization problem will behave like this, multi-objective approach is a safe methodology to solve such problems.

To understand the relation between the aerodynamic coefficients and the uncertainty input, further post-analysis was performed by analyzing the result of deterministic simulation and calculating the uncertainty in the pressure field and wall-pressure.

### 5.3.2 Probability Density Function Analysis

As an alternative to the response surface analysis, we build the probability density function (PDF) for the aerodynamic coefficients of all airfoils. This PDF information was easily built by performing sampling using the combined PCE that was used before to approximate the response surface. Moreover, analysis of the stochastic response surface becomes more difficult on higher dimensional random variables so PDF analysis is a convenient method for higher dimension. From the depiction of the PDF of the four aerodynamic coefficients in Fig. 5.7, basically, it gives roughly the same knowledge with the response surface analysis. However, it is now becomes clearer to investigate the random behaviour of the aerodynamic coeficients subjected to the uncertainty. For statistical moments, beside of the mean and standard deviation we also analyze the skewness of the PDF for each aerodynamic coefficients which are depicted in Tables 5.6, 5.7, 5.8, and 5.9.

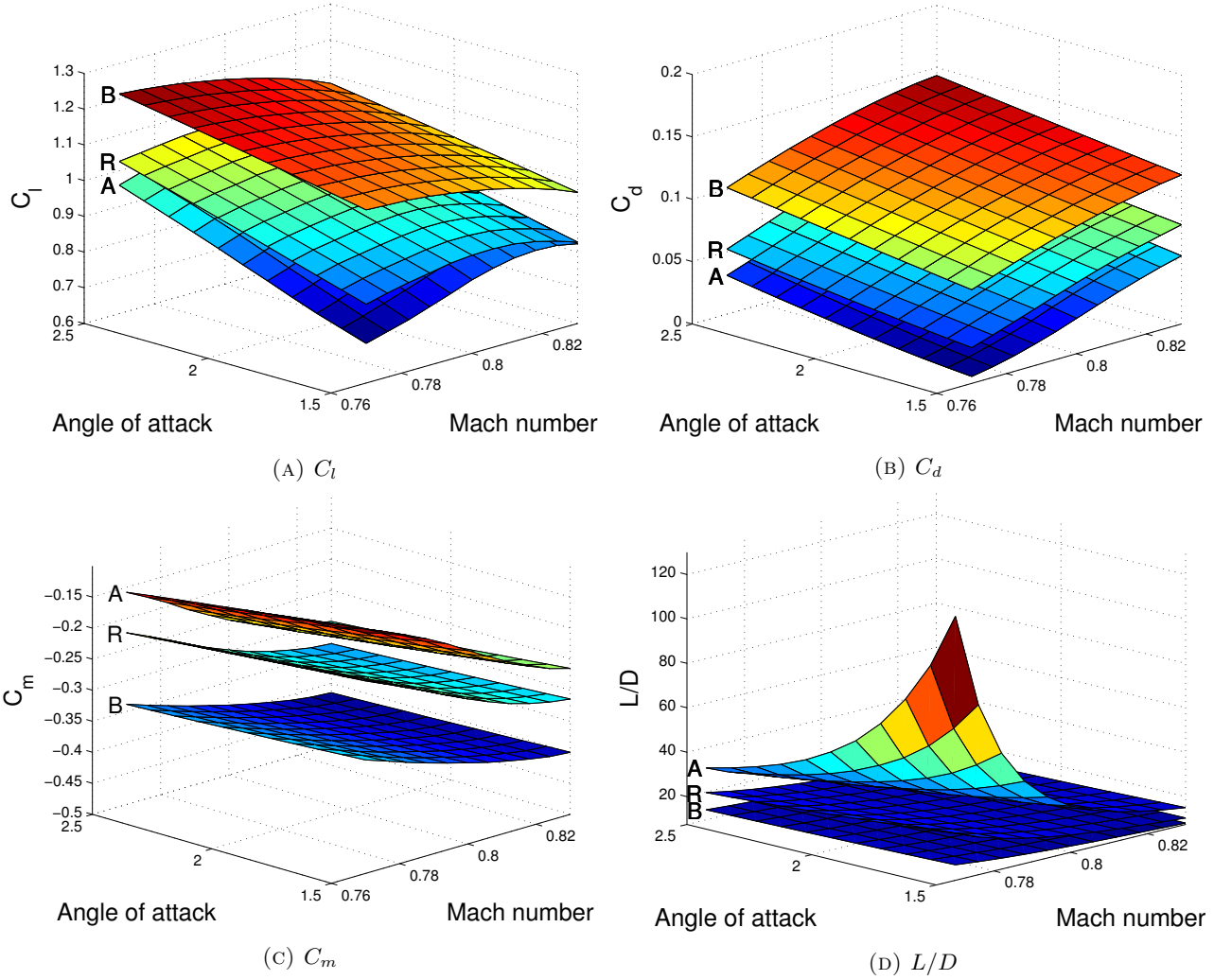


FIGURE 5.6: Aerodynamic coefficients response surface of the three representative airfoils due to the uncertainty in the flow condition

On analyzing the PDF of $C_l$ shown in Fig. 5.7a, airfoil A's PDF of $C_l$ tends to has negative skewness compares to the others. Airfoil A's $C_l$ mean value is also lower than the others with the lowest $C_l$ value over the PDF. By investigating the airfoil B's PDF and the statistical moments of $C_l$, airfoil B has the highest mean with relatively low standard deviation and skewness. This makes the airfoil B is particularly attractive from $C_l$ viewpoint that surpasses airfoil A and RAE 2822. However, as it was already known from the response surface analysis before, airfoil B has the highest $C_d$ mean that hinders its practicality. Airfoil A, that has the lowest $C_d$ mean of all, is the best airfoil from $C_d$ point of view. This is also evident from the depiction of the PDF of $C_d$ shown in Fig. 5.7b.

The representative airfoils and RAE 2822 have an evident characteristic of positive skew for the $C_m$ PDF as it depicted in Fig. 5.7c. Airfoil B has more stable behaviour of the $C_m$ due to its low standard deviation. However, airfoil B produces very high mean value of $C_m$ which, again, hinders its practicality. Airfoil A has higher standard deviation but it has a lower $C_m$ mean value than the airfoil B. RAE 2822 airfoil has the medium characteristics of the other extremums.

It can be observed on the airfoil A's PDF of $L/D$ depicted in Fig. 5.7d that although its $L/D$ standard deviation is high, the PDF is heavily positively skewed with the highest mean value over the other two airfoils. This explains why the $L/D$ performance of airfoil A is better than the other airfoils which is also evident from the qualitative information of the $L/D$ PDF. Airfoil B has a very robust $L/D$ but its low mean $L/D$ value shows that this airfoil is much less efficient from aerodynamic viewpoint than airfoil A and RAE 2822.

TABLE 5.6: Statistical moment of $C_l$ of the representative airfoils and RAE 2822

| | **Mean** | **St.d.** | **Skew** |
|---|---|---|---|
| **Airfoil A** | 0.9049 | 0.0716 | -1.322e-3 |
| **Airfoil B** | 1.1052 | 0.0510 | -2.000 e-5 |
| **RAE 2822** | 0.9450 | 0.0538 | -3.3816 e-6 |

TABLE 5.7: Statistical moment of $C_d$ of the representative airfoils and RAE 2822

| | **Mean** | **St.d.** | **Skew** |
|---|---|---|---|
| **Airfoil A** | 0.0441 | 0.0184 | -3.544e-7 |
| **Airfoil B** | 0.1132 | 0.0150 | -7.920e-7 |
| **RAE 2822** | 0.0678 | 0.0169 | -8.714e-7 |

TABLE 5.8: Statistical moment of $C_m$ of the representative airfoils and RAE 2822

| | **Mean** | **St.d.** | **Skew** |
|---|---|---|---|
| **Airfoil A** | -0.2161 | 0.0506 | 2.8182e-5 |
| **Airfoil B** | -0.3753 | 0.0248 | 5.2547e-6 |
| **RAE 2822** | -0.2768 | 0.0383 | 2.0218e-5 |

TABLE 5.9: Statistical moment of $L/D$ of the representative airfoils and RAE 2822

| | **Mean** | **St.d.** | **Skew** |
|---|---|---|---|
| **Airfoil A** | 25.9757 | 15.3013 | 8412 |
| **Airfoil B** | 9.9614 | 1.5794 | 2.0711 |
| **RAE 2822** | 14.9125 | 4.0212 | 55.3905 |

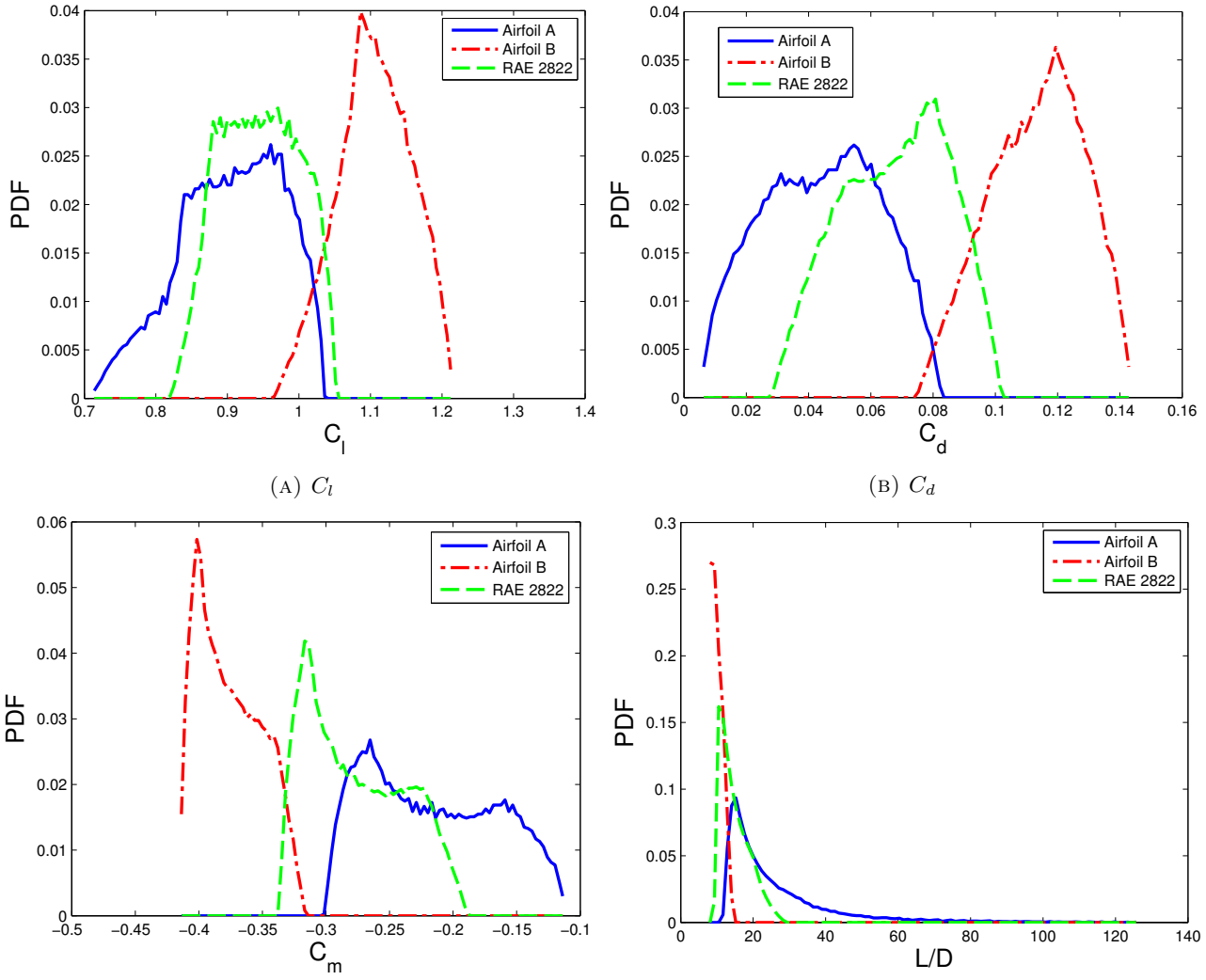


(A) $C_l$ (B) $C_d$

(C) $C_m$ (D) $L/D$

FIGURE 5.7: Probability density function (PDF) of the aerodynamic coefficients for the representative airfoils and RAE 2822

### 5.3.3 Nominal Flow Pressure Field

The robustness property of a solution to the uncertainty can be properly understood by investigating the nominal condition first. Furthermore, analysis of the flow in nominal condition is important to understand the uncertainty amplification mechanism from the nominal condition. Table 5.10 shows the aerodynamic coefficient of the representative and nominal airfoil on the nominal flight condition ($M = 0.8$, $\alpha = 2$). The corresponding pressure field and wall pressure distribution of these airfoils are depicted in Fig. 5.8 and Fig. 5.9, respectively.

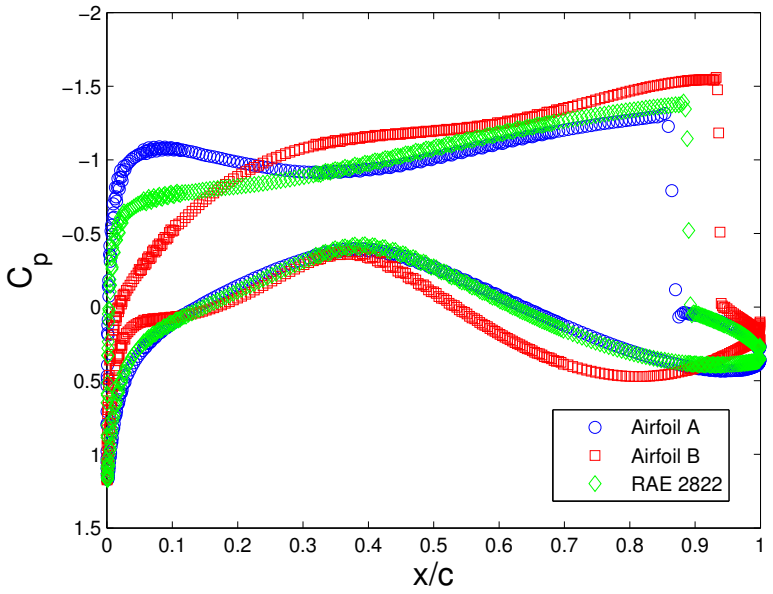


FIGURE 5.8: Surface pressure coefficient of the three representative airfoils on the nominal flow condition

On the nominal condition, the shock wave location on the upper surface is slightly shifted to the leading edge direction from about 0.88 $x/c$ to 0.86 $x/c$ of the datum to airfoil A, respectively. The lower surface shape for airfoil A and RAE 2822 are nearly identical which caused a nearly identical lower pressure distribution for both airfoils. Both airfoils have an almost similar magnitude of radius leading edge but the shape difference for both airfoil can be mainly seen on the upper surface where the upper surface crest's abscisca of the airfoil A moves closer to the trailing edge and its upper surface crest's ordinate is smaller with respect to the RAE 2822 shape. This geometrical change corresponds to the less stronger shock wave that reduces the magnitude of the wave drag as it can be observed from Fig. 5.9a and Fig. 5.9c which are the pressure field of the airfoil A and RAE 2822, respectively. The combination of this slightly lower value of $C_l$ and reduced $C_d$ results in the increased airfoil A's aerodynamic efficiency.

The shape of the airfoil B, in constrast to the airfoil A, is quite a radical departure from the RAE 2822 (See Fig. 5.4). Airfoil B produces stronger magnitude of shock wave compares to the airfoil and RAE 2822 which results in a very high $C_d$. The location of this shock wave shifted closer to the trailing edge compares to the shock location of RAE 2822 which results in a higher moment coefficient. Higher $C_l$ produced by airfoil B is the by product of its large camber. Airfoil B also has larger value of maximum thickness compares to the other two airfoils. However, the $L/D$ of the airfoil B is lower than the other two airfoils which is mainly caused by a high value of $C_d$.

From the practical sense, only the airfoil A can be considered as better or as least non-dominating to the datum RAE 2822 airfoil on the deterministic nominal flight condition. Airfoil B is impractical due to the very high $C_d$ although though it produces higher lift on the nominal flight condition. One could

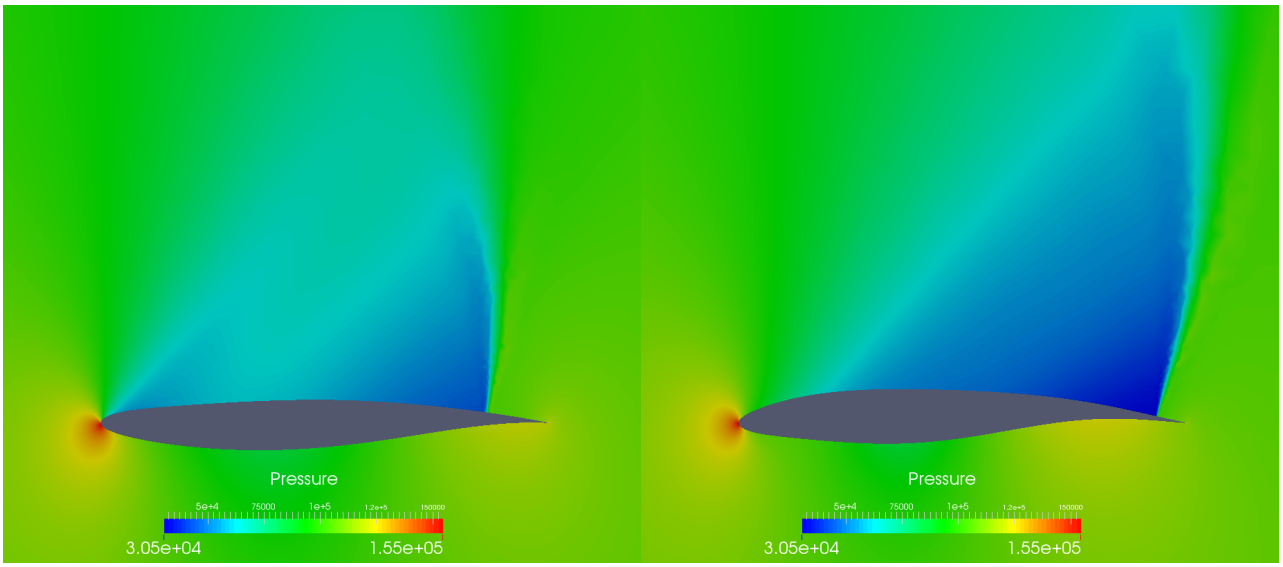


(A) Airfoil A (B) Airfoil B

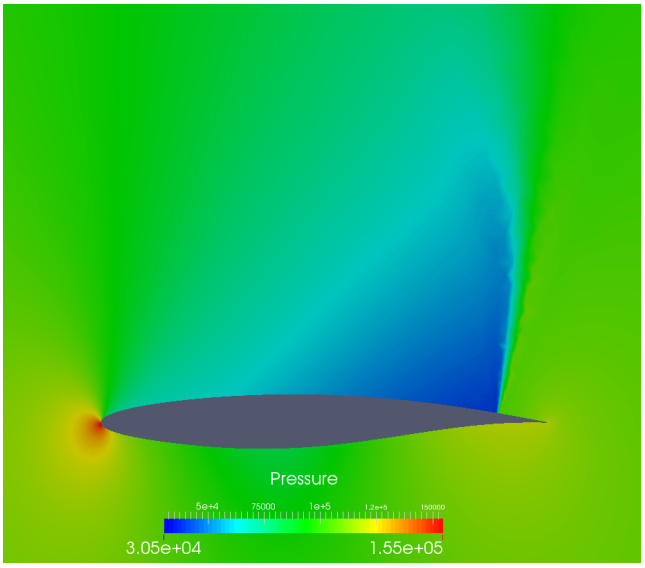


(C) RAE 2822

FIGURE 5.9: Pressure field of the three representative airfoils on the nominal flow condition

also observe that the shape of the airfoil B is a non-supercritical one, that explained its inefficiencies in the transonic flow field.

After analysis of the nominal flight condition, understanding of the uncertainty mechanism can be properly done by considering the uncertainties in the surface pressure distribution and the flow field, which is explained in the next subsection.

TABLE 5.10: Aerodynamic coefficients of the three representative airfoils at nominal condition

| | $C_l$ | $C_d$ | $C_m$ | $L/D$ |
|---|---|---|---|---|
| **Airfoil A** | 0.9211 | 0.0439 | -0.2179 | 20.9659 |
| **Airfoil B** | 1.1160 | 0.1151 | -0.3794 | 9.6924 |
| **RAE 2822** | 0.9228 | 0.0637 | -0.2594 | 14.1815 |

### 5.3.4 Uncertainty in the Flow Field and Surface Pressure Coefficients

Uncertainty quantification of the pressure field typically deal with discontinuous function and might greatly affects the accuracy of PC-NIPC which is based on the global polynomial[164]. Therefore, we used simplex element stochastic collocation (SESC)[108, 164] (see appendix C) that uses piecewise polynomial for uncertainty quantification of the pressure field. It has been demonstrated in several previous papers that SESC was able to adequately solved UQ problem with discontinuity. A 1st order polynomial was employed for each elements where the grids are generated using newton-cotes quadrature. The grid points for SESC are generated using Newton-Cotes quadrature where Delaunay triangulation[165] is used to build the simplex elements.

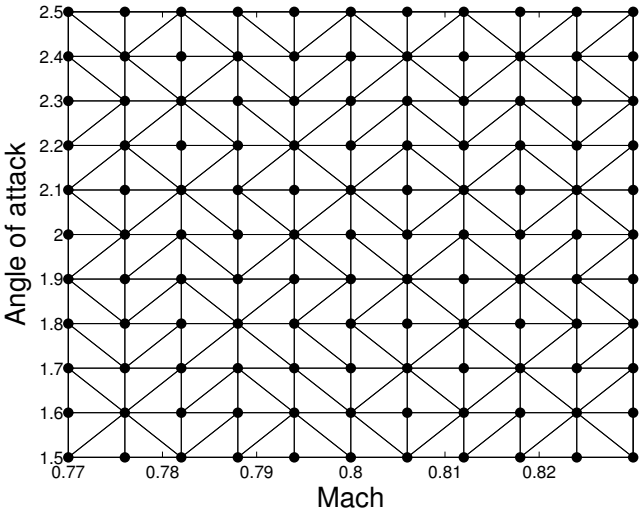


FIGURE 5.10: Grids for SESC

Figs. 5.12, 5.13, and 5.14 depict the mean and standard deviation of the pressure field of the three airfoils where Fig. 5.11 show the corresponding wall pressure distribution's uncertainty bar.

It is clear by seeing the figures that on all airfoils the wall pressure variation is stronger on the upper surface than the lower surface with exception in the part of the lower surface where the curvature changes. As it was already expected, the area with stronger variation is located on the part where the shock occurs; the uncertainty in the flight condition alter the location of this shock wave[164]. As it can be seen from the figures, airfoil A exhibits a stronger variation of the shock wave location, as it is indicated by wider area of pressure jump compares to the airfoil B. Airfoil A also has higher standard deviation of the pressure in the shock and near-shock location than the airfoil B. The high variation in the aerodynamic coefficient of airfoil A is then the result of this stronger movement of the shock wave. On the other side, the standard deviation of the airfoil B's wall pressure is lower than the airfoil A's which results in lower variation of the aerodynamic coefficients. However, the magnitude of the pressure jump of airfoil B is larger than airfoil A which results in very large $C_d$ over the stochastic response surface. The flow characteristics of the RAE 2822 airfoil is on the between of these two extremum

airfoils. It has a medium variation of the shock wave movement located on the midway between the extremums.

The mean pressure field of the representative airfoils and RAE 2822 are almost similar to their deterministic counterpart (Fig. 5.9) so there are not too much new knowledge and information can be gained from the mean pressure field depiction. On the other hand, the pressure field standard deviation shows us clearer information of the shock wave movement and the magnitude of this variation. A small pressure variation can be observed in the upper surface's trailing edge and the location where the curvature changes on the lower surface, thus produces wall pressure variation as in the Fig. 5.11. Fig. 5.12b that depicts the pressure field variation of airfoil A confirm the result of this wall pressure variation where the shock wave movement is large but the overall magnitude is smaller than the shock in airfoil B. As it can be observed from Fig.5.13b the range of shock wave movement of the airfoil B is smaller but the magnitude variation is very high due to the strong power of the shock wave itself. Again, pressure variation characteristics of RAE 2822 airfoil (Fig. 5.14b) is on the midway between the two extremum.

## 5.4 Lesson learned

This chapter demonstrated the capability of SS-MOMA-ASF and MF-PCNIPC to solve aerodynamic robust optimization problem and make the best use of available computational budget. By performing preliminary experiment, we properly determined the multi-fidelity scheme with the best trade-off between the computational budget and the accuracy. The results shows a strong trade-off between the mean and standard deviation of the $L/D$. However, post-processing shows that probably there is only one optimum solution in the true sense which is the solution with maximum mean and standard deviation of the L/D. This is because the solution with maximum $\sigma$ and $\mu$ has lower $L/D$ over the response surface than the other extremum. Moreover, the airfoil with minimum $\sigma$ and $\mu$ has very high $C_d$ that hinders its applicability. Therefore, post processing is highly important to further investigate the solutions in the final non-dominated solutions. Because a specific value of mean and standard deviation do not uniquely define a solution or airfoil[166], other alternative approach for robust optimization such as PDF matching[166] could be considered.

The robust optimization in this chapter uses Euler equation as the governing equation to find the robust airfoils. However, it is very likely that there are some missing informations of the robust optimum airfoils due to the simplication of the governing equation. It is important to further performing airfoil robust optimization procedure that uses Navier-Stokes as its governing equation to obtain more knowledge and information.

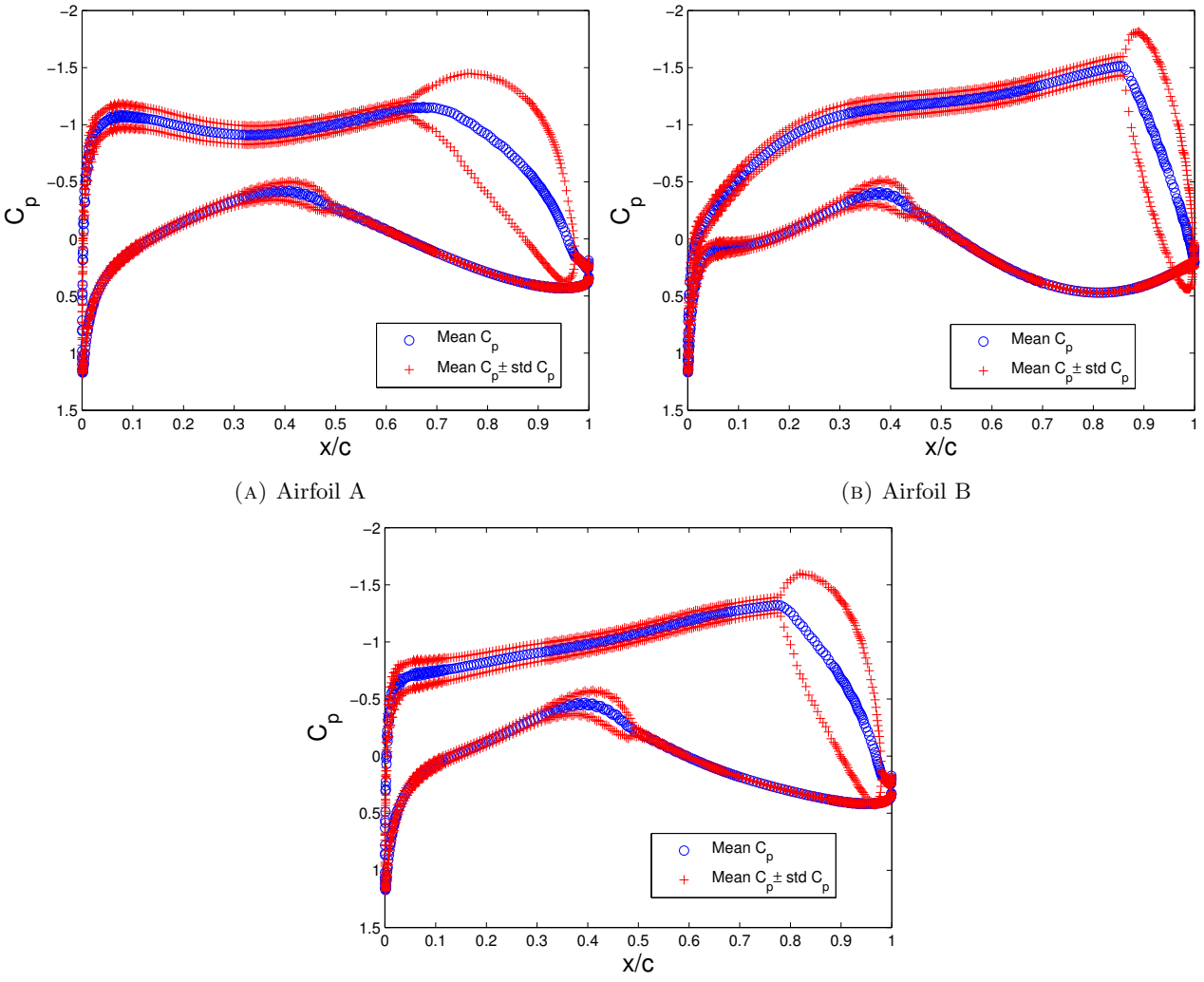


(A) Airfoil A

(B) Airfoil B

(C) RAE 2822

FIGURE 5.11: Mean and standard deviation of the surface pressure coefficient of the three representative airfoils

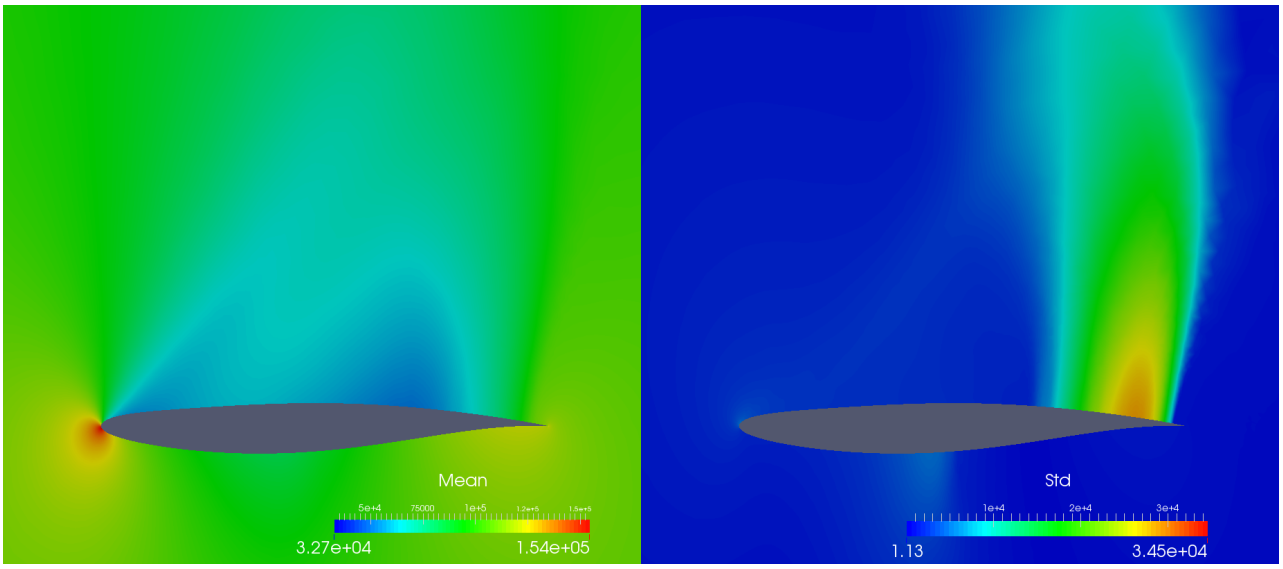


(A) Mean (B) Standard deviation

FIGURE 5.12: Pressure field statistics of the airfoil A

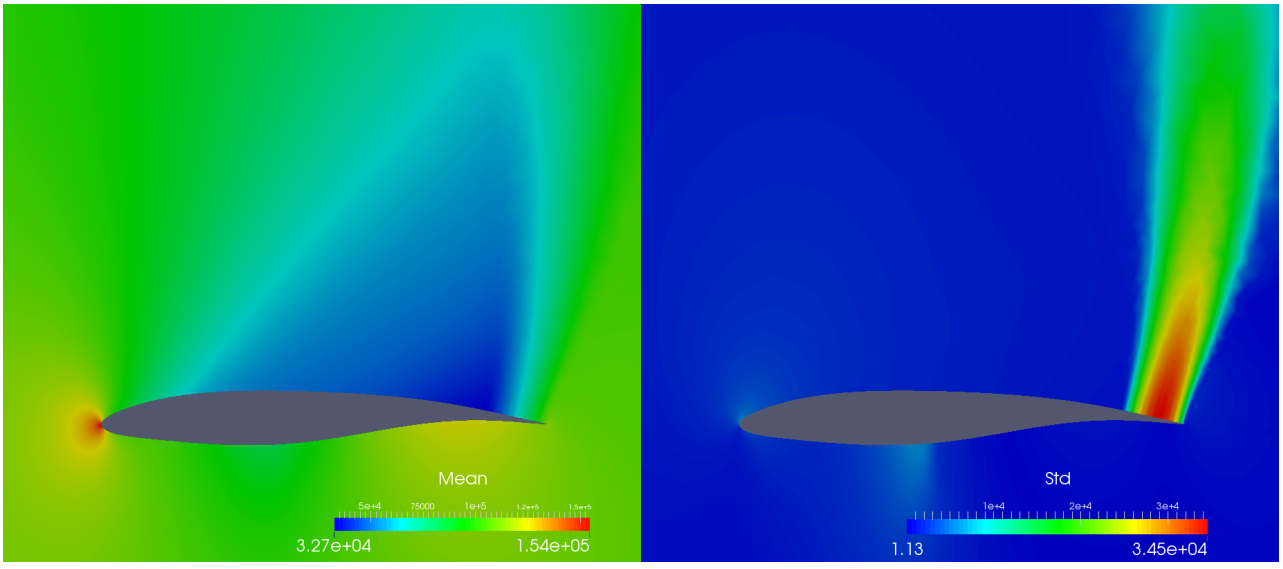


(A) Mean (B) Standard deviation

FIGURE 5.13: Pressure field statistics of the airfoil B

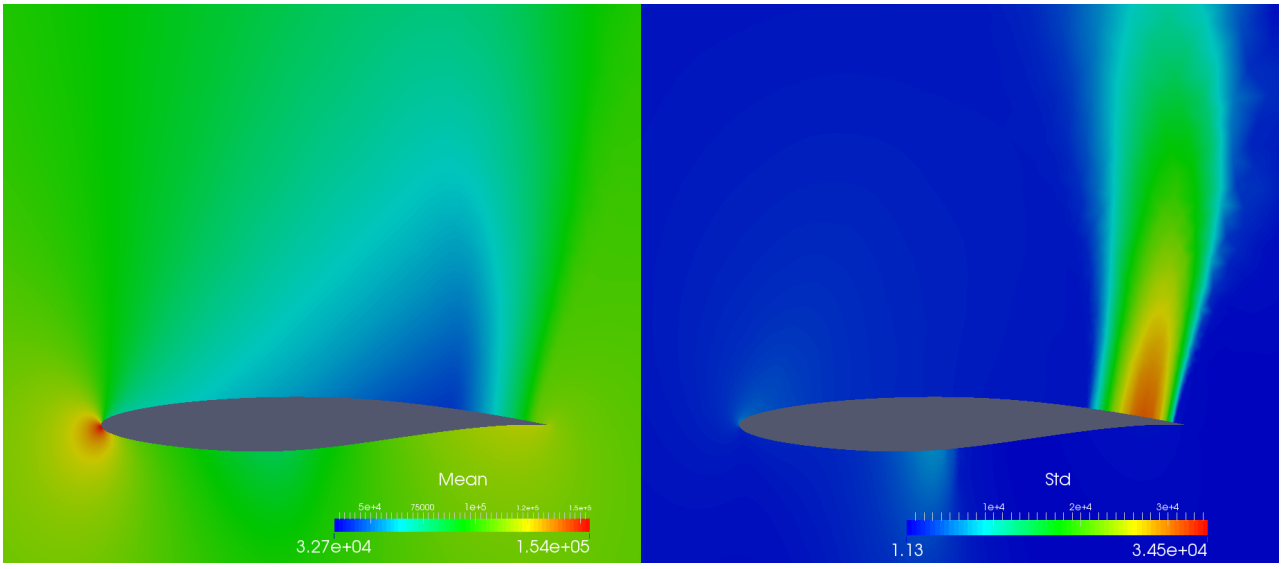


(A) Mean (B) Standard deviation

FIGURE 5.14: Pressure field statistics of the RAE 2822 airfoil

# Chapter 6

# Conclusion and Future Works

## 6.1 Conclusion

The main objectives of this research were mainly to improve the efficiency of engineering robust optimization that uses metaheuristics such as genetic algorithm as the optimizer for expensive problems. Two main modules of the robust optimization using metaheuristics are the optimizer itself and the uncertainty quantification module where improvement of the robust optimization methodology in this thesis were studied on these two parts that could be improved separately. The contribution of this thesis can be seen separately as the contribution to the optimization and the UQ field.

Improvements are mainly done on the optimizer part by increasing the capability of previously existing surrogate-based memetic algorithm framework. A surrogate based memetic algorithm framework, which is the combination of metaheuristics and local search, was chosen as the optimizer due to its higher capability than the non-local search metaheuristics to locate the global optimum solutions with limited budget. In this thesis the single-surrogate multi-objective memetic algorithm (SS-MOMA) algorithm was used as the building block of the optimizer. The SS-MOMA algorithm and its family were previously used the weighted sum to guide the local search procedure.

A local search based on achievement scalarizing function (ASF) and Chebyshev function were introduced to the SS-MOMA algorithm where the result shows that significant improvements could be obtained by employing ASF and Chebyshev type local search with random weights. The main difference between ASF and Chebyshev type local search is that the former uses the individual to be improved as the reference point while the latter uses the upper bound of the offspring solutions. Preliminary study revealed that the use of randomized weights is more beneficial than the fixed weights during the local search using ASF where these weights define the direction of where the local search should move. Study was also performed on how different normalization type affects the search capability of the optimizer. Normalization is important because local searches that are based on the scalarizing function is sensitive

to the scaling of the objectives. We introduce dynamic normalization based on the maximum and minimum value of the offspring instead of normalization based on the estimated bounds of the objectives space where the former clearly dominates the latter on all test functions mainly on the diversity of the solutions.

The weakness of SS-MOMA with weighted sum is evident on the function with non-convex Pareto front. Nonetheless, SS-MOMA with weighted sum was clearly inferior to SS-MOMA with ASF and Chebyshev based method on the biobjective problems. However, SS-MOMA-ASF faces difficulty in the three objectives problems while the SS-MOMA-CHEB encounters no difficulty. Random mutation hill climber (RMHC) based local search which uses the principle of non-domination operator was also introduced but its performance is generally inferior to the ASF-based local search. This suggest that the application of scalarizing function type local search is more advantageous than applying the local search operators that are based on dominance relation.

Constraints were simply applied to the SS-MOMA algorithm by using the adaptive constraint handling and constrained SQP to search the local surrogate. If RMHC is used as the local search, the random mutation will only accept a feasible mutant that dominates the present solution. Result shows that the constraint handling method is working and is capable to solve artificial and real world constrained problems.

The SS-MOMA-ASF in conjunction with the Chebyshev based local search was then applied to multi-objective airfoil optimization with Euler as the governing equation where the objectives were to minimize $C_d/C_l^2$ and $C_m^2$. The result shows that the SS-MOMA-ASF was able to obtain higher quality non-dominated solutions than the NSGA-II and SS-MOMA-ASF on the aerodynamic problem. Satisfying results obtained by SS-MOMA-ASF also shows that the constraint handling and normalization methods works well and are capable to assist the real world optimization problem.

An extension of point collocation polynomial chaos to incorporate multiple levels of simulation fidelity (MF-PCNIPC) was developed and presented in this thesis for uncertainty quantification purpose. The MF-PCNIPC algorithm, as an alternative to the multi-fidelity NIPC based on spectral-projection, offers flexibility on the sampling methods and choice of polynomial basis. Our method is based on the total-order or hyperbolic expansion as the method to generate polynomial basis together with the use of low-discrepancy sequence for sampling. Other sampling and truncation method are also possible but we stressed on the previously mentioned methodology because it offers very high flexibility.

The MF-PCNIPC was tested on several artificial test problems and aerodynamic problems. Typically, the main effect and lower order interaction is corrected by the correction expansion while the higher order main effect/interaction is captured by the low-fidelity expansion that could be evaluated in larger number of samples than the high-fidelity expansion. Results on artificial problem clearly shows an evident improvement of the approximation quality and reduced error if the MF-PCNIPC is applied compares to the high-fidelity PCNIPC. Such improvements could be achieved if the low-fidelity function

is predictive enough of the high-fidelity function. However, if the low-fidelity functions do not correlate well and has large error relative to the true function, the resulting multi-fidelity approximation only become worse than the high-fidelity expansion so careful check is needed. The check is done by analyzing the value of RMSE and $R^2$ where the sufficiently predictive low-fidelity functions have a tolerable RMSE and $R^2$ value of at least larger than 0.9. If such conditions were not fulfilled, it was suggested to use only the high-fidelity expansion and excludes the low-fidelity samples. Test on aerodynamic problems prove the capability of MF-PCNIPC to efficiently and flexibly reduces the approximation error for the same number of high-fidelity samples. This is also due to the chosen low-fidelity function which is predictive enough. For the aerodynamic problems, we investigated two type of low-fidelity samples: 1.) simulation with lower number of mesh and 2.) partially converged simulation. Result shows that the MF-NIPC that used partially converged simulation as the low-fidelity samples produced higher accuracy than the simulation with lower number of mesh elements. Morever, partially converged simulation gives additional benefit from computational cost point of view because some of the low-fidelity samples are evaluated together with the high-fidelity one (fully converged simulations).

The MF-PCNIPC and SS-MOMA-ASF as the algorithm for UQ and optimizer, respectively, were then applied to airfoil robust optimization problem. The case is the robust optimization of transonic airfoil in Euler flow with the mean and standard deviation of lift-to-drag ratio as the objectives. After the Pareto front had been obtained, some selected solutions were calculated again using single-fidelity PCNIPC with high number of samples, to see if the results from MF-PCNIPC were representative enough of the true optimized solutions. The low and acceptable error between the robustness calculated by MF-PCNIPC and more expensive calculation shows that the optimized solutions were representative enough of the exact values. This means that acceleration of the optimization could be performed by implementing multi-fidelity UQ for robust optimization that uses metaheuristics optimizer.

The robust optimization result shows that the airfoil that has high $L/D$ mean and standard deviation exhibits stronger movement of the shock wave when the random variables are perturbed. This caused stronger effects of perturbation (thus higher standard deviation) in contrast to the other extremum airfoil. However, more detail investigation by analyzing the trend of stochastic response surface shows that the airfoil with high mean and high standard deviation of $L/D$ is better in the true sense compares to the other extremum airfoil. This is because this airfoil has the value of $L/D$ over the stochastic response surface which is higher than the airfoil with minimum mean of $L/D$. Post-processing of the results is then important to reveal the detail characteristics of the optimized solutions. Uncertainty quantification in the pressure fields reveals that the stronger movement of the shock wave due to the perturbation of the flight condition caused higher variation of the aerodynamic coefficients.

## 6.2 Future Works

Future works of this thesis can be seen from three separate constituents: global optimization using metaheuristics, uncertainty quantification, and robust optimization part.

On the optimization part, it would be interesting to consider alternative algorithm to be wrapped inside the surrogate-based memetic algorithm framework. For example, instead of using NSGA-II that serves as a building block for SS-MOMA, other algorithms such as MOEA/D, SPEA-2, SMS-EMOA, HypE, or even NSGA-III can be equipped with the surrogate-based local search and compared with the existing SS-MOMA framework. Such potential development has a potential improvement for the search capability of the surrogate-based memetic algorithm. Moreover, the adaptivity of the weights instead of random weights is also a potential avenue for further improvement. Combination with other type of more advanced scalarizing function or other type of local search also needs to be investigated.

UQ is a vast and rapidly advancing methodology thus the future works here mainly focus on the multi-fidelity part. One potential study is by developing and improving the MF-PCNIPC to deal with UQ problem with epistemic type or mixed uncertainty. Special treatment is needed because the nature of the epistemic uncertainty is not probabilistic. Several researches are currently tackling such problems and progressing in this direction, but the use of multiple level of fidelity is quite rare. Moreover, advanced algorithm such as least-angle-regression could be employed and studied to improve the capability of MF-PCNIPC. Adaptive sampling is also a potential avenue. However, such developments would be more complicated than the single-fidelity NIPC because now there are two level of fidelity to be considered.

Finally, future robust optimization could include the improvements in the optimization/UQ methodology or the framework of the robust optimization itself. It is also potential research avenue to improve the existing optimizer for user-preference optimization where the goal is to find specific solutions with the supplied reference points of targeted robustness properties. Multi-objectives optimization in the presence of mixed uncertainty also needs to be considered.

# Appendix A

# Mechanisms of Genetic Algorithm

This appendix explain the mechanism of canonical genetic algorithm. Some type of genetic algorithms could differs slightly or greatly in the mechanism (such as micro-genetic algorithm[167] that has restart operator) but their building block are relatively similar to the canonical genetic algorithm. General explanation is given first followed by the detail of the operators commonly used in genetic algorithm. Materials on this section mainly refers to the various genetic algorithms textbooks[168, 16]

## A.1 General Explanation

Genetic algorithm is widely used in the field of optimization to find the optimum point of the given problem (maximum or minimum) and where mostly the desired one is the location of the global optimum. Genetic algorithm starts with the initial population consist of a set of possible solutions called individuals encoded into binary string or other encoding scheme and a set of genetic algorithm parameters like crossover probability, mutation probability, number of strings, number of variables, and so on.

Fitness values of the initial populations are determined by evaluation of the objective function where these values are used in the selection mechanism. Evaluation could be done by first decoding the code representation of solution. In binary encoding, number of genes is important to generate good solution(s) in optimization process. Higher number of string leads to more accurate solution with the drawback of longer computing time (even though it is negligible in expensive problems) while less number of genes could not represent the solutions good enough with the advantage of faster computing time. Fine tuning of string number is significant to make a balance between computing time and good result. An important alternative is to use real-coded genetic algorithm where instead of using strings the solutions are now represented using the real values of the parameters themselves. The objective function can then be evaluated by using analytical equation, numerical approximation, or even experiment.

The use of numerical approximation such as computational partial differential equation solver is very common in aerospace design and optimization.

Next, the genetic algorithm employs three main types of mechanism to create the next generation from the current population which are selection, crossover/recombination, and mutation. Selection mechanism (such as tournament selection or roulette wheel, to be explained in its own subsection) will choose the individuals to become the parents for crossover mechanism. Usually in almost all selection mechanism, the individuals with relatively higher fitness value than the other would have higher probability to be selected for crossover. After selection has been done, the next stage that will be employed is the reproduction.

Term of reproduction applies to both of crossover / recombination and mutation. Crossover involves two or more parents and is analogue to the 'sexual reproduction' mechanism in biology, while mutation is related to the 'asexual reproduction' or just simply the natural mutation that could occurred in the genetic constitution of living things. Crossover is the main reproduction mechanism that has more significant contribution where interactions between selected parents from selection mechanism are substantial to generate brand new offspring that would drive genetic algorithm towards the optimum solution. This phase is controlled by the probability of crossover determined in the beginning of genetic algorithm; if the random number is less than the probability of crossover then crossover would surely occurred. Various crossover methods are also existed, where the differences are ranging from the used encoding scheme, number of parents, possible offspring solution, and so on. However, only crossover applied leads to a higher probability of being trapped into the local optimum and this is where mutation plays a role to keep the diversity for genetic algorithm to find the true optimum solution.

Mutation is the secondary reproduction mechanism after crossover where new individuals are created by making changes to a single individual. The changes could be made by altering the genes in binary encoding or randomly alter the real number representation in real coded genetic algorithm. Probability of mutation is usually set to a very low number; a high number of mutations could leads to failure of genetic algorithm to find the global optimum.

The new population would then replace the old population and new generation begins from decoding the code scheme. Genetic algorithm stops when a termination criterion is already fulfilled and takes the best solution in the last generation as the optimum solution. In the next sub-chapters, three main mechanism of genetic algorithm will be explained briefly.

## A.2 Operators

### Encoding procedure and initialization

Genetic algorithm requires genetic representation of the solution domain where encoding process plays an important part for this purpose. The first proposed encoding scheme is the binary encoding which encodes the solution into an array of binary bits. Another representation of solution other than binary encoding is in the form of discrete-decimal or the real number (Fig. A.1 shows these three kinds of genetic representation). An initial population is generated in the first step of genetic algorithm where each member of this population takes the form of genetic representation being used; the initial population can be generated randomly or in a schematic order. After creating the initial population, each individual is then evaluated and assigned a fitness value.

The illustration in Fig. A.1 shows three variables which are encoded into three genes for real-number encoding and nine genes for discrete-decimal and binary encoding. Bounded by the upper bound ($X^U$) and lower bound ($X^L$), where $n$ is the length of chromosome or a number of genes within chromosome.

Real-number encoding follows the formulation below:

$$x = X^L + (X^U - X^L)g \tag{A.1}$$

for discrete-decimal encoding:

$$x = X^L + (X^U - X^L)(g_1 10^{-1} + g_2 10^{-2} + ... + g_n 10^{-n})) \tag{A.2}$$

and finally, the formulation for binary encoding is:

$$x = X^L + (X^U - X^L)(g_1 2^{-1} + g_2 2^{-2} + ... + g_n 2^{-n}) \tag{A.3}$$

For discrete-decimal and binary encoding, the real number has to be represented in genes specified by the number of bit string within a length of chromosome whereas real-number encoding does not need any genetic representation and makes no distinction between the genotype and phenotype. Longer length of genes means more accurate solution but with longer computing time while lower amount of genes steers to less computing time but sacrificing the accuracy of solution.

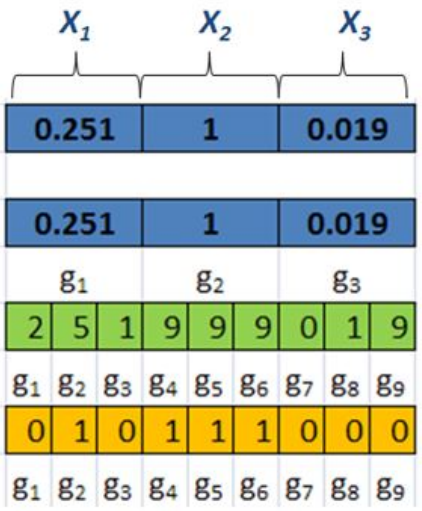


FIGURE A.1: Encoding procedure in genetic algorithm.

### Selection

Selection is the mechanism to choose the fitter individuals from the population to produce successive generation with hopes that the offspring solutions will have better fitness than their parents. Selection is a probabilistic mechanism based on individual's fitness so that individuals with high fitness have more chance to be selected. An individual can also be selected more than once during the selection process. There existed several methods for selection: roulette wheel, tournament selection, scaling techniques, and so on. Two popular methods among them are roulette wheel and tournament selection. Roulette wheel was the first selection method proposed in the canonical genetic algorithm and can be visualized as a circle diagram constructed by segments where larger segments are occupied by chromosomes with higher fitness value. Within the interval given, a random value is assigned to determine which chromosome that will be taken as the parents.

The procedure of roulette-wheel selection as it is shown in Fig. A.2 may be explained as follows:

1. Fitness value from each individual is normalized by dividing the fitness value by the sum of all fitness values means that the total resulting normalized fitness values equal to 1.
2. Sort the population by descending fitness value.
3. Compute the accumulated normalized fitness values, where accumulated fitness value is the sum of each individual fitness value added by the fitness values of all previous individual.
4. Generate a random number between 0 and 1.
5. The selected individual is the first one whose accumulated normalized value is greater than the generated random number.

The other popular method is tournament selection where a tournament is held among randomly individual chosen from the population and the fitter one would be considered as the winner and selected as a parent for crossover. Tournament selection is easy to implement and its procedures are as follows:

1. Choose $k$ random individual from population to fill the mating pool with size of $k$.
2. Choose the most fitter individual from the mating pool and consider it as a parent for next generation.

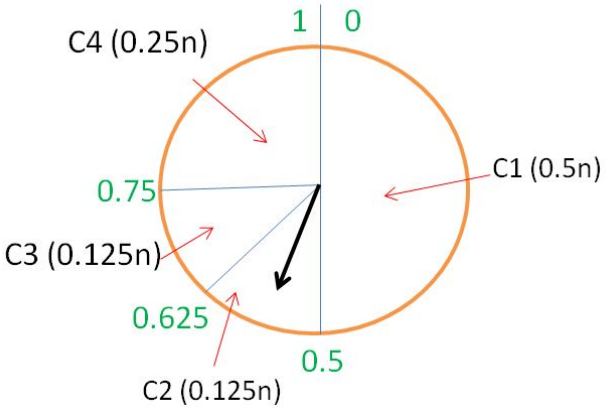


FIGURE A.2: Roulette wheel selection in Genetic Algorithm.

**Evaluation**

Evaluation in genetic algorithm is simply the evaluation of the objective functions using experiment, analytical, or numerical equation. One important thing to be noted is the difference between objective and fitness function in genetic algorithm. Objective function is a function to estimate thevalue or goodness with respect to a particular set of parameters where fitness function is used to determine the performance of solutions to be selected as a parent to generate offspring for the next generation. However, in many optimization of single objective function cases the objective is simply equal to the fitness function. This difference of objective function and fitness can be seen clearly in many multi-objective optimization problems where the fitness function is determined by the domination of each solution to other solution, for example.

**Crossover/Recombination**

One important mechanism in genetic algorithm is crossover where the selected parents from the selection mechanism are recombined and exchanging features to generate new individuals which hopefully has better characteristics compared to the parents. Crossover is necessary because it serves as the main mechanism to drive genetic algorithm into optimality. However, crossover method alone is not sufficient

enough for genetic algorithm to find the global optima. Mutation mechanism which is explained in the next subsection is important to keep the diversity so the genetic algorithm is not easily trapped into the local optimum.

To give a clear and simple explanation about how crossover works, a simple one-point crossover (simplest form of $n$-point crossover) in binary encoding genetic algorithm will be explained and illustrated in Fig. A.3. Consider a chromosome with genes amount of 12 and one-point crossover with cut off point in the fifth genes. Cut off point in fifth genes will divide Parent 1 into section $X_1$ (1st – 4th genes) and $X_2$ (5th – 12th genes), and the similar goes to Parent 2 into the section $X_3$ and $X_4$. The new offsprings from this parents will be the combination of genes $X_1$ - $X_4$ (Offspring 1) and $X_3$ – $X_2$ (Offspring 2). This is the means of exchanging traits and information between parents in binary encoding one-point crossover where the new offsprings are expected to have fitter characteristics and could drive the optimization problem into the optimum solution.

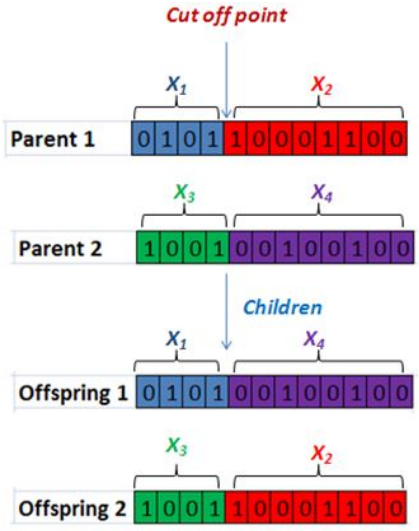


FIGURE A.3: One point crossover for binary genetic algorithm.

Real coded genetic algorithm (RCGA) offers the advantage in the choice of crossover method compares to the binary coded genetic algorithm. While binary coded genetic algorithm provides only a few crossover method ($n$-point crossover, uniform crossover), real coded genetic algorithm has more variation of crossover method and also clearer interpretation and location of the new offsprings. Example of such methods are arithmetical crossover, uniform arithmetical crossover, simulated binary crossover, sphere crossover, and so on. Instead of dealing with the genes in crossover, RCGA works directly with real number representation of the solution.

Because of the genetic algorithm in this work is a real-coded type, crossover method used in current work is simulated binary crossover (SBX) that takes two parents to generate new offsprings. SBX crossover starts by choosing two parents written as $p_1$ and $p_2$. After that, $\beta^L$ and $\beta^U$ which are the spread factors for the lower and upper bounds of the problem variable, respectively, are defined as the

following:

$$\beta^L = \frac{p_1 + p_2 - 2X_i^L}{|p_2 - p_1|} \tag{A.4}$$

$$\beta^U = \frac{2X_i^U - p_1 - p_2}{|p_2 - p_1|} \tag{A.5}$$

and $P(\beta)$ is the probability distribution approximated by a polynomial probability distribution as folows:

$$P(\beta) = \begin{cases} 0.5(\eta_c + 1)\beta^{n_c} & \text{if } \beta \leq 1 \\ 0.5(\eta_c + 1)\frac{1}{\beta^{n_c+2}} & \text{otherwise} \end{cases} \tag{A.6}$$

Where the distribution index $\eta_c$ is a non-negative real number. A large value of $\eta_c$ gives a higher probability for creating solutions near to the parent and vice versa. The procedure to generate the offspring $c_1$ and $c_2$ are then as follows:

$$c_1 = 0.5[(p_1 + p_2) - \beta_1'(p_2 - p_1)] \tag{A.7}$$

$$c_2 = 0.5[(p_1 + p_2) + \beta_1'(p_2 - p_1)] \tag{A.8}$$

**Mutation**

Although crossover is the main mechanism in the reproduction phase of the genetic algorithm, crossover alone is not sufficient to mobilize the search process into global optimum in many cases. Crossover without mutation has a great probability to get trapped into the local optima; hence the global optimum somehow is very difficult to be found only by the application of crossover mechanism. The role of mutation operator is then to keep the diversity of population so the genetic algorithm would not be easily trapped in the local optimum. In binary encoding, mutation is done by flipping the bit of 0 values into 1 and vice versa. Mutation in binary encoding is usually settled up in low probability (typically between 0.001 and 0.1) to guarantee that mutation would not mess up the search process into global optimum. The mutation in binary encoding is depicted in Fig. A.4.

Technique of mutation is quite different in RCGA. If mutation in binary encoding is done by flipping the bit, mutation in RCGA is performed by changing the value of the individual's vector randomly or by using special techniques such as polynomial mutation[12].

In this work, polynomial mutation is used to perturb the solutions and produce a mutated solutions. The mutated offpsring is generated as follow:

$$x' = \begin{cases} x + \bar{\delta_L}(x - X_i^L) & \text{for } u \leq 0.5, \\ x - \bar{\delta_R}(X_i^U - x) & \text{for } u > 0.5, \end{cases} \tag{A.9}$$

$$\bar{\delta_L} = (2u)^{1/(1+\eta_m)} - 1 \text{ for } u \leq 0.5, \tag{A.10}$$

$$\bar{\delta_R} = 1 - (2(1-u))^{1/(1+\eta_m)} \text{ for } u \leq 0.5. \tag{A.11}$$

We use mutation probabilty of $1/n$ where $n$ is the number of decision variables as it suggested in the original paper of NSGA-II[12].

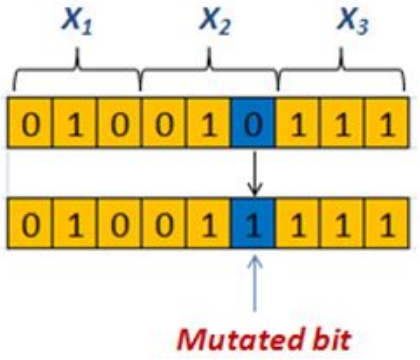


FIGURE A.4: Mutation for binary genetic algorithm.

**Elitism**

Because of genetic algorithm works stochastically, there is no guarantee that monotic improvement of fitness value would occur. A mechanism called elitism is then applied to ensure the monotonic improvement of genetic algorithm. Elitism works by maintaining the best individuals during the successive generation and only can be replaced if genetic algorithm found any individual better in term of fitness than the previous best individual. Number of elite individuals usually set to one or two, but one elite only is enough to maintain monotonic improvement. Elite individuals could also participate as a parent chosen by selection method to generate their offsprings for next generation.

# Appendix B

# Airfoil Parameterization

We use two types of airfoil parameterization in this study which are PARSEC[169] and CST[154] which are explained in this appendix section.

## B.1 PARSEC Parameterization

PARSEC method uses the polynomial function to generate the airfoil coordinate $y_u$ and $y_l$ for upper and lower surface, respectively, as:

$$y_u = \sum_{i=1}^{6} a_i x^{i-\frac{1}{2}} \tag{B.1}$$

$$y_l = \sum_{i=1}^{6} b_i x^{i-\frac{1}{2}} \tag{B.2}$$

where $a_i$ and $b_i$ are real coefficients. PARSEC parameterization uses eleven geometry-related design parameters to generate the real coefficients: leading edge radius($R_{le}$), curvature of the upper crest($Y_{xx_{up}}$) and lower crest ($Y_{xx_{lo}}$), ordinate and abscissa of the upper surface ($Y_{up}, X_{up}$) and lower surface ($Y_{lo}, X_{lo}$), trailing edge thickness and location ($T_{TE}, T_{off}$), and trailing edge direction and wedge angle($\alpha_{TE}, \beta_{TE}$). The boundary conditions for Equations B.1 and B.2 are:

$$y(1) = T_{off} \tag{B.3}$$

$$\tan\left(\alpha_{TE} - \frac{1}{2}\beta_{TE}\right) = \left(\frac{dy}{dx}\right)_{x=1} = \sum_{i=1}^{6}\left(i - \frac{1}{2}\right) a_i x_{TE}^{i-\frac{1}{2}} \tag{B.4}$$

$$Y_{up} = \sum_{i=1}^{6} a_i X_{up}^{i-\frac{1}{2}} \tag{B.5}$$

$$0 = \left(\frac{dy}{dx}\right)_{x=X_{up}} = \sum_{i=1}^{6} \left(i - \frac{1}{2}\right) a_i X_{up}^{i-\frac{3}{2}} \tag{B.6}$$

$$\left(\frac{d^2y}{dx^2}\right)_{x=X_{up}} = Y_{XX_{up}} = \sum_{i=1}^{6} \left(i - \frac{3}{2}\right)\left(i - \frac{1}{2}\right) a_i X_{up}^{i-\frac{3}{2}} \tag{B.7}$$

$$R_{le} = \left[\frac{\left[1 + \left(\frac{dy}{dx}\right)^2\right]^{\frac{3}{2}}}{\frac{d^2y}{dx^2}}\right] = \frac{a_1^2}{2} \Leftrightarrow a_1 = \sqrt{2R_{le}} \tag{B.8}$$

These boundary conditions applied to both upper and lower surface, the coefficients $a_i$ and $b_i$ can then be computed by solving the following linear equation:

$$\begin{bmatrix} 1 & 1 & 1 & 1 & 1 \\ X_{up}^{\frac{3}{2}} & X_{up}^{\frac{5}{2}} & X_{up}^{\frac{7}{2}} & X_{up}^{\frac{9}{2}} & X_{up}^{\frac{11}{2}} \\ \frac{3}{2} & \frac{5}{2} & \frac{7}{2} & \frac{8}{2} & \frac{11}{2} \\ \frac{3}{2}X_{up}^{\frac{1}{2}} & \frac{5}{2}X_{up}^{\frac{3}{2}} & \frac{7}{2}X_{up}^{\frac{5}{2}} & \frac{9}{2}X_{up}^{\frac{7}{2}} & \frac{11}{2}X_{up}^{\frac{9}{2}} \\ \frac{3}{4}X_{up}^{\frac{-1}{2}} & \frac{15}{4}X_{up}^{\frac{1}{2}} & \frac{45}{4}X_{up}^{\frac{3}{2}} & \frac{63}{4}X_{up}^{\frac{5}{2}} & \frac{99}{4}X_{up}^{\frac{7}{2}} \end{bmatrix} = \begin{bmatrix} a_2 \\ a_3 \\ a_4 \\ a_5 \\ a_6 \end{bmatrix} = \begin{bmatrix} \left[T_{off} + \frac{1}{2}T_{TE} - a_1\right] \\ Y_{up} - a_1 X_{up}^{\frac{1}{2}} \\ \tan\left(\alpha_{TE} - \frac{1}{2}\beta_{TE}\right) - \frac{1}{2}a_1 \\ -\frac{1}{2}a_1 X_{up}^{-\frac{1}{2}} \\ Y_{XX_{up}} + \frac{1}{4}a_1 X_{up}^{-\frac{3}{2}} \end{bmatrix} \tag{B.9}$$

$$\begin{bmatrix} 1 & 1 & 1 & 1 & 1 \\ X_{lo}^{\frac{3}{2}} & X_{lo}^{\frac{5}{2}} & X_{lo}^{\frac{7}{2}} & X_{lo}^{\frac{9}{2}} & X_{lo}^{\frac{11}{2}} \\ \frac{3}{2} & \frac{5}{2} & \frac{7}{2} & \frac{8}{2} & \frac{11}{2} \\ \frac{3}{2}X_{lo}^{\frac{1}{2}} & \frac{5}{2}X_{lo}^{\frac{3}{2}} & \frac{7}{2}X_{lo}^{\frac{5}{2}} & \frac{9}{2}X_{lo}^{\frac{7}{2}} & \frac{11}{2}X_{lo}^{\frac{9}{2}} \\ \frac{3}{4}X_{lo}^{\frac{-1}{2}} & \frac{15}{4}X_{lo}^{\frac{1}{2}} & \frac{45}{4}X_{lo}^{\frac{3}{2}} & \frac{63}{4}X_{lo}^{\frac{5}{2}} & \frac{99}{4}X_{lo}^{\frac{7}{2}} \end{bmatrix} = \begin{bmatrix} b_2 \\ b_3 \\ b4 \\ b_5 \\ b_6 \end{bmatrix} = \begin{bmatrix} \left[T_{off} - \frac{1}{2}T_{TE} + a_1\right] \\ Y_{lo} + a_1 X_{lo}^{\frac{1}{2}} \\ \tan\left(\alpha_{TE} + \frac{1}{2}\beta_{TE}\right) + \frac{1}{2}a_1 \\ \frac{1}{2}a_1 X_{lo}^{-\frac{1}{2}} \\ Y_{XX_{lo}} - \frac{1}{4}a_1 X_{lo}^{-\frac{3}{2}} \end{bmatrix} \tag{B.10}$$

## B.2 Class Shape Transformation

The upper surface and lower surface of Class Shape Transformation (CST) where $C$ and $S$ are class and shape function, respectively, are expressed as[154, 170]:

$$\left(\frac{z}{c}\right)_{lower} = C_{N_1}^{N_2}\left(\frac{x}{c}\right) S_U\left(\frac{x}{c}\right) + \frac{x}{c}\frac{z_{te}}{c} + \frac{x}{c}\frac{dz_{te}}{2c} \tag{B.11}$$

$$\left(\frac{z}{c}\right)_{lower} = C_{N_1}^{N_2}\left(\frac{x}{c}\right) S_U\left(\frac{x}{c}\right) + \frac{x}{c}\frac{z_{te}}{c} - \frac{x}{c}\frac{dz_{te}}{2c} \tag{B.12}$$

The class function $C$ is defined as:

$$C_{N_1}^{N_2}\left(\frac{x}{c}\right) = \left(\frac{x}{c}\right)^{N_1}\left(-\frac{x}{c}\right)^{N_2} \tag{B.13}$$

The general shape function $S_U$ and $S_L$ are defined as:

$$S_U\left(\frac{x}{c}\right) = \sum_{i=0}^{N_U} A_U(i) S\left(\frac{x}{c}, i\right) \tag{B.14}$$

$$S_L\left(\frac{x}{c}\right) = \sum_{i=0}^{N_L} A_L(i) S\left(\frac{x}{c}, i\right) \tag{B.15}$$

Where $A_U$ and $A_L$ are upper and lower surface weights, respectively. $N_U$ and $N_L$ are the CST order of upper and lower surface, respectively. The component shape function, which could be different for upper and lower surface depending on CST order $N$, is expressed as:

$$S\left(\frac{x}{c}, i\right) = K_i^N\left(\frac{x}{c}\right)^i\left(-\frac{x}{c}\right)^{N-i} \tag{B.16}$$

Where $K$ is binomial coefficient and defined as follows:

$$K_i^N = \frac{N!}{i!(N-i)!)} \tag{B.17}$$

# Appendix C

# Simplex Element Stochastic Collocation

The stochastic response surface of the flow field and pressure distribution could exhibits discontinuity that makes standard polynomial chaos expansion fails. This failure is mainly caused by the inadequacy of the global polynomials to precisely capture the presence of discontinuity. Several ways to deal with this problem is to use the methods based on rational function or piecewise basis. In this thesis, we used simplex element stochastic collocation (SESC) which is based on the piecewise basis polynomial to calculate the uncertainty in the flow field and surface pressure. We refer to the original paper for the explanation of the SESC method[164].

## C.1 General Formulation

SESC method divides the probability space into a number simplex elements where a polynomial interpolation is used to approximate the response surface for each element.

The main interest is to find the probability distribution of $R(x,\xi)$ and its statistical moments $\mu_{R_i}(x,\xi)$ given by:

$$\mu_{R_i} = \int_{\Omega} R(x,\xi)^i f_\xi(\xi) d\xi \tag{C.1}$$

$$\mu_{R_i} = \sum_{j=1}^{n_e} \int_{\Omega_j} R(x,\xi)^i f_\xi(\xi) d\xi \tag{C.2}$$

$$\sum_{j=1}^{n_e} \int_{\Omega_j} f_\xi(\xi) d\xi = 1 \tag{C.3}$$

Where $f_\xi$ is the probability distribution of the random variables and $n_e$ is the number of discretization elements. The integral in each element is estimated by approximating the local response surface by an interpolation $w(\xi)$ of the samples $\mathbf{v} = \{v_1, ...v_{n_s}\}$ with $n_s$ is the number of samples.

The interpolant $w(\xi)$ in SESC method is a piecewise polynomial functions defined by:

$$w(\xi) = w_j(\xi), \text{ for } \xi \in \Omega_j$$

Where $w_j(\xi)$ is the polynomial interpolation of order $p$ of the samples in the element $\Omega_j$ using $\mathbf{v}_j = \{v_{k_{j,0}}, ...v_{k_{j,N}}\}$ at the sampling point $\{\xi_{k_{j,0}}, ...\xi_{k_{j,N}}\}$ in element $\Omega_j$, where $k_{j,l} \in \{1, ..., n_e\}, l = 0, ..., N$, and

$$N + 1 = \frac{(n_\xi + p)!}{n_\xi! p!} \tag{C.4}$$

The expression of the truncated polynomial chaos expansion (PCE) for element $\Omega_j$ is exactly the same as in the ordinary PCE where the coefficients for each element's PCE can be found by using least squares.

The statistical moments of the problem of interest can then be estimated by the following expression:

$$\mu_{R_i} \approx \mu_{R_i} = \sum_{j=1}^{n_v} \int_{\Omega_j} w_j(x, \xi)^i f_\xi(\xi) d\xi \tag{C.5}$$

Calculation of the statistical moments can then be readily performed using a Monte Carlo simulation and equation C.5, which is now very cheap to evaluate. New prediction could be made by using the piecewise polynomial of the corresponding element where the new prediction site lies. For practical application, the corresponding element can be determined by searching the nearest element center to the prediction site.

In the application in this thesis, we used a first-order polynomial interpolation to build the local interpolant in each element $\Omega_j$. The simplex elements $\Omega_j$ for 1st order polynomial interpolation could be built by using Delaunay triangulation given a definite number of samples. The grid points can be generated using Newton-Cotes points or any other methods followed by the adaptive scheme[108]. An example of the mesh with 1st order polynomial and random sampling is depicted in Fig. C.1.

Our application in this thesis used the simplest form of the SESC due to the low-dimensionality of the problem. For treatment of more complex problems (high dimensionality, non-hypercube probability spaces), reader could refer to the more advanced development of the SESC method[108, 111].

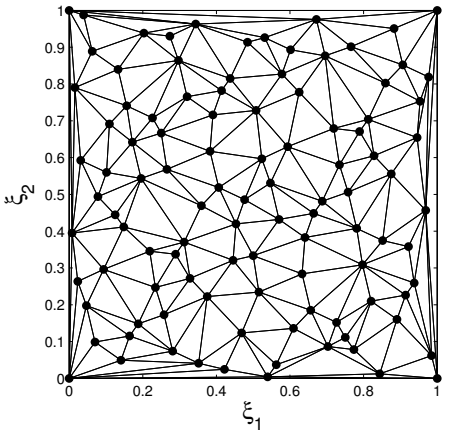


FIGURE C.1: SESC mesh with 104 random samples (four in the corners) and 1st order polynomial.

# Bibliography


[1] Martins, J. R. and Lambe, A. B., "Multidisciplinary design optimization: a survey of architectures," *AIAA journal*, Vol. 51, No. 9, 2013, pp. 2049–2075.

[2] Hicks, R. M. and Henne, P. A., "Wing design by numerical optimization," *Journal of Aircraft*, Vol. 15, No. 7, 1978, pp. 407–412.

[3] Jameson, A., "Aerodynamic design via control theory," *Journal of scientific computing*, Vol. 3, No. 3, 1988, pp. 233–260.

[4] Chernukhin, O. and Zingg, D. W., "Multimodality and global optimization in aerodynamic design," *AIAA journal*, Vol. 51, No. 6, 2013, pp. 1342–1354.

[5] Holland, J. H., *Adaptation in natural and artificial systems: an introductory analysis with applications to biology, control, and artificial intelligence.*, U Michigan Press, 1975.

[6] Beyer, H.-G. and Schwefel, H.-P., "Evolution strategies–A comprehensive introduction," *Natural computing*, Vol. 1, No. 1, 2002, pp. 3–52.

[7] Kennedy, J., "Particle swarm optimization," in "Encyclopedia of Machine Learning," Springer, pp. 760–766, 2010.

[8] Zhang, Q. and Li, H., "MOEA/D: A multiobjective evolutionary algorithm based on decomposition," *IEEE Transactions on Evolutionary Computation*, Vol. 11, No. 6, 2007, pp. 712–731.

[9] Beume, N., Naujoks, B., and Emmerich, M., "SMS-EMOA: Multiobjective selection based on dominated hypervolume," *European Journal of Operational Research*, Vol. 181, No. 3, 2007, pp. 1653–1669.

[10] Colorni, A., Dorigo, M., Maniezzo, V., et al., "Distributed optimization by ant colonies," in "Proceedings of the first European conference on artificial life," Paris, France, Vol. 142, 1991, pp. 134–142.

[11] Weyland, D., "A Rigorous Analysis of the Harmony Search Algorithm: How the Research Community can be," *Modeling, Analysis, and Applications in Metaheuristic Computing: Advancements and Trends: Advancements and Trends*, p. 72.

[12] Deb, K., Pratap, A., Agarwal, S., and Meyarivan, T., "A fast and elitist multiobjective genetic algorithm: NSGA-II," *Evolutionary Computation, IEEE Transactions on*, Vol. 6, No. 2, 2002, pp. 182–197.

[13] Deb, K. and Jain, H., "An evolutionary many-objective optimization algorithm using reference-point-based nondominated sorting approach, part i: Solving problems with box constraints," *Evolutionary Computation, IEEE Transactions on*, Vol. 18, No. 4, 2014, pp. 577–601.

[14] Bader, J. and Zitzler, E., "HypE: An algorithm for fast hypervolume-based many-objective optimization," *Evolutionary computation*, Vol. 19, No. 1, 2011, pp. 45–76.

[15] Voutchkov, I. and Keane, A., "Multi-objective optimization using surrogates," in "Computational Intelligence in Optimization," Springer, pp. 155–175, 2010.

[16] Deb, K., *Multi-objective optimization using evolutionary algorithms*, Vol. 16, John Wiley & Sons, 2001.

[17] Kim, D. H., Abraham, A., and Cho, J. H., "A hybrid genetic algorithm and bacterial foraging approach for global optimization," *Information Sciences*, Vol. 177, No. 18, 2007, pp. 3918–3937.

[18] Robinson, J., Sinton, S., and Rahmat-Samii, Y., "Particle swarm, genetic algorithm, and their hybrids: optimization of a profiled corrugated horn antenna," in "Antennas and Propagation Society International Symposium, 2002. IEEE," IEEE, Vol. 1, 2002, pp. 314–317.

[19] Kao, Y.-T. and Zahara, E., "A hybrid genetic algorithm and particle swarm optimization for multimodal functions," *Applied Soft Computing*, Vol. 8, No. 2, 2008, pp. 849–857.

[20] Jat, S. N. and Yang, S., "A hybrid genetic algorithm and tabu search approach for post enrolment course timetabling," *Journal of Scheduling*, Vol. 14, No. 6, 2011, pp. 617–637.

[21] Caponio, A. and Neri, F., *Integrating cross-dominance adaptation in multi-objective memetic algorithms*, Springer, 2009.

[22] Knowles, J. D. and Corne, D. W., "M-PAES: A memetic algorithm for multiobjective optimization," in "Evolutionary Computation, 2000. Proceedings of the 2000 Congress on," IEEE, Vol. 1, 2000, pp. 325–332.

[23] Knowles, J. and Corne, D., "Memetic algorithms for multiobjective optimization: issues, methods and prospects," in "Recent advances in memetic algorithms," Springer, pp. 313–352, 2005.

[24] Ray, T., Isaacs, A., and Smith, W., "A memetic algorithm for dynamic multiobjective optimization," in "Multi-Objective Memetic Algorithms," Springer, pp. 353–367, 2009.

[25] Lim, D., Jin, Y., Ong, Y.-S., and Sendhoff, B., "Generalizing surrogate-assisted evolutionary computation," *Evolutionary Computation, IEEE Transactions on*, Vol. 14, No. 3, 2010, pp. 329–355.

[26] Moscato, P. et al., "On evolution, search, optimization, genetic algorithms and martial arts: Towards memetic algorithms," *Caltech concurrent computation program, C3P Report*, Vol. 826, 1989, p. 1989.

[27] Chen, X., Ong, Y.-S., Lim, M.-H., and Tan, K. C., "A multi-facet survey on memetic computation," *IEEE Transactions on Evolutionary Computation*, Vol. 15, No. 5, 2011, pp. 591–607.

[28] Dawkins, R., *The selfish gene*, Oxford university press, 2006.

[29] Lara, A., Sanchez, G., Coello Coello, C. A., and Schütze, O., "HCS: A new local search strategy for memetic multi-objective evolutionary algorithms," *IEEE Transactions on Evolutionary Computation*, Vol. 14, No. 1, 2010, pp. 112–132.

[30] Jeong, S., Murayama, M., and Yamamoto, K., "Efficient optimization design method using kriging model," *Journal of aircraft*, Vol. 42, No. 2, 2005, pp. 413–420.

[31] Yamazaki, W., Rumpfkeil, M. P., and Mavriplis, D. J., "Design optimization utilizing gradient/hessian enhanced surrogate model," *AIAA Paper*, Vol. 4363, 2010, p. 2010.

[32] Jouhaud, J.-C., Sagaut, P., Montagnac, M., and Laurenceau, J., "A surrogate-model based multidisciplinary shape optimization method with application to a 2D subsonic airfoil," *Computers & Fluids*, Vol. 36, No. 3, 2007, pp. 520–529.

[33] Samad, A., Kim, K.-Y., Goel, T., Haftka, R. T., and Shyy, W., "Multiple surrogate modeling for axial compressor blade shape optimization," *Journal of Propulsion and Power*, Vol. 24, No. 2, 2008, pp. 301–310.

[34] Keane, A. J., "Comparison of several optimization strategies for robust turbine blade design," *Journal of Propulsion and Power*, Vol. 25, No. 5, 2009, pp. 1092–1099.

[35] Sato, K., Kumano, T., Yonezawa, M., Yamashita, H., Jeong, S., and Obayashi, S., "Low-Boom and Low-Drag Optimization of the Twin Engine Version of Silent Supersonic Business Jet," *Journal of Fluid Science and Technology*, Vol. 3, 2008, pp. 576–585.

[36] Keane, A., "Wing optimization using design of experiment, response surface, and data fusion methods," *Journal of Aircraft*, Vol. 40, No. 4, 2003, pp. 741–750.

[37] Kumano, T., Jeong, S., Obayashi, S., Ito, Y., Hatanaka, K., and Morino, H., "Multidisciplinary design optimization of wing shape for a small jet aircraft using kriging model," *AIAA paper*, Vol. 932, 2006, p. 2006.

[38] Hosder, S., Watson, L. T., Grossman, B., Mason, W. H., Kim, H., Haftka, R. T., and Cox, S. E., "Polynomial response surface approximations for the multidisciplinary design optimization of a high speed civil transport," *Optimization and Engineering*, Vol. 2, No. 4, 2001, pp. 431–452.

[39] Cressie, N., "The origins of kriging," *Mathematical geology*, Vol. 22, No. 3, 1990, pp. 239–252.

[40] Forrester, A. I., Sóbester, A., and Keane, A. J., "Multi-fidelity optimization via surrogate modelling," in "Proceedings of the Royal Society of London A: Mathematical, Physical and Engineering Sciences," The Royal Society, Vol. 463, 2007, pp. 3251–3269.

[41] J. Toal, D. J. and Keane, A. J., "Efficient multipoint aerodynamic design optimization via cokriging," *Journal of Aircraft*, Vol. 48, No. 5, 2011, pp. 1685–1695.

[42] Keane, A. J., "Cokriging for robust design optimization," *AIAA journal*, Vol. 50, No. 11, 2012, pp. 2351–2364.

[43] Keane, A. J., "Statistical improvement criteria for use in multiobjective design optimization," *AIAA journal*, Vol. 44, No. 4, 2006, pp. 879–891.

[44] Ong, Y. S., Nair, P. B., and Keane, A. J., "Evolutionary optimization of computationally expensive problems via surrogate modeling," *AIAA journal*, Vol. 41, No. 4, 2003, pp. 687–696.

[45] Simpson, T. W., Mauery, T. M., Korte, J. J., and Mistree, F., "Kriging models for global approximation in simulation-based multidisciplinary design optimization," *AIAA journal*, Vol. 39, No. 12, 2001, pp. 2233–2241.

[46] Jain, A. K., Mao, J., and Mohiuddin, K., "Artificial neural networks: A tutorial," *Computer*, Vol. 29, No. 3, 1996, pp. 31–44.

[47] Smola, A. J. and Schölkopf, B., "A tutorial on support vector regression," *Statistics and computing*, Vol. 14, No. 3, 2004, pp. 199–222.

[48] Choudhury, A., Nair, P. B., Keane, A. J., et al., "A Data Parallel Approach for Large-Scale Gaussian Process Modeling." in "SDM," SIAM, 2002, pp. 95–111.

[49] Zhou, Z., Ong, Y. S., Lim, M. H., and Lee, B. S., "Memetic algorithm using multi-surrogates for computationally expensive optimization problems," *Soft Computing*, Vol. 11, No. 10, 2007, pp. 957–971.

[50] Pilát, M. and Neruda, R., "ASM-MOMA: Multiobjective memetic algorithm with aggregate surrogate model," in "IEEE Congress on Evolutionary Computation (CEC), 2011," IEEE, 2011, pp. 1202–1208.

[51] Massaro, A. and Benini, E., "Multi-Objective Optimization of Helicopter Airfoils Using Surrogate-Assisted Memetic Algorithms," *Journal of Aircraft*, Vol. 49, No. 2, 2012, pp. 375–383.

[52] Pilat, M. and Neruda, R., "The effect of different local search algorithms on the performance of multi-objective optimizers," in "IEEE Congress on Evolutionary Computation (CEC), 2014," IEEE, 2014, pp. 2172–2179.

[53] Derbel, B., Brockhoff, D., Liefooghe, A., and Verel, S., "On the Impact of Scalarizing Functions on Evolutionary Multiobjective Optimization," in "Parallel Problem Solving from Nature (PPSN XIII)," Springer, pp. 548–558, 2014.

[54] Anderson, W. K. and Venkatakrishnan, V., "Aerodynamic design optimization on unstructured grids with a continuous adjoint formulation," *Computers & Fluids*, Vol. 28, No. 4, 1999, pp. 443–480.

[55] Leung, T. M. and Zingg, D. W., "Aerodynamic shape optimization of wings using a parallel newton-krylov approach," *AIAA journal*, Vol. 50, No. 3, 2012, pp. 540–550.

[56] Straathof, M. H. and L. Van Tooren, M. J., "Adjoint Optimization of a Wing Using the Class-Shape-Refinement-Transformation Method," *Journal of Aircraft*, Vol. 49, No. 4, 2012, pp. 1091–1100.

[57] Kirn, S., Alonso, J. J., and Jameson, A., "Design optimization of high-lift configurations using a viscous continuous adjoint method," , 2002.

[58] Reuther, J., Jameson, A., Farmer, J., Martinelli, L., and Saunders, D., *Aerodynamic shape optimization of complex aircraft configurations via an adjoint formulation*, Research Institute for Advanced Computer Science, NASA Ames Research Center, 1996.

[59] Hu, R., Jameson, A., and Wang, Q., "Adjoint-based aerodynamic optimization of supersonic biplane airfoils," *Journal of Aircraft*, Vol. 49, No. 3, 2012, pp. 802–814.

[60] Choi, S., Lee, K., Potsdam, M. M., and Alonso, J. J., "Helicopter rotor design using a time-spectral and adjoint-based method," *Journal of Aircraft*, Vol. 51, No. 2, 2014, pp. 412–423.

[61] Jones, M. and Yamaleev, N. K., "Adjoint-Based Optimization of Three-Dimensional Flapping-Wing Flows," *AIAA Journal*, pp. 1–14.

[62] Yamamoto, K. and Inoue, O., "Applications of genetic algorithm to aerodynamic shape optimization," in "Proceedings of the 12th AIAA Computational Fluid Dynamics Conference, volume," , 1995, pp. 43–51.

[63] Obayashi, S. and Oyama, A., "Three-dimensional aerodynamic optimization with genetic algorithm," in "ECCOMAS computational fluid dynamics conference," , 1996, pp. 420–424.

[64] Oyama, A., Obayashi, S., Nakahashi, K., and Nakamura, T., "Transonic wing optimization using genetic algorithm," .

[65] Quagliarella, D. and Della Cioppa, A., "Genetic algorithms applied to the aerodynamic design of transonic airfoils," *Journal of aircraft*, Vol. 32, No. 4, 1995, pp. 889–891.

[66] Bedon, G., Castelli, M. R., and Benini, E., "Optimization of a Darrieus vertical-axis wind turbine using blade element–momentum theory and evolutionary algorithm," *Renewable Energy*, Vol. 59, 2013, pp. 184–192.

[67] Vasile, M., Minisci, E., Quagliarella, D., Moens, F., and Wervaecke, C., "Multi-point optimization of shapes and settings of high-lift system by means of evolutionary algorithm and Navier-Stokes equations," *Engineering Computations*, Vol. 30, No. 4, 2013, pp. 601–622.

[68] Sasaki, G., Tatsukawa, T., Nonomura, T., Yonemoto, K., Oyama, A., Matsumoto, T., and Narumi, T., "Multi-objective Optimization of Airfoil of Mars Exploration Aircraft using Evolutionary Algorithm," .

[69] Sasaki, D. and Nakahashi, K., "Aerodynamic optimization of an over-the-wing-nacelle-mount configuration," *Modelling and Simulation in Engineering*, Vol. 2011, 2011, p. 11.

[70] Arias-Montano, A., Coello Coello, C. A., and Mezura Montes, E., "Multiobjective evolutionary algorithms in aeronautical and aerospace engineering," *Evolutionary Computation, IEEE Transactions on*, Vol. 16, No. 5, 2012, pp. 662–694.

[71] Forrester, A. I. and Keane, A. J., "Recent advances in surrogate-based optimization," *Progress in Aerospace Sciences*, Vol. 45, No. 1, 2009, pp. 50–79.

[72] Lewis, R. M. and Huyse, L., "Aerodynamic shape optimization of two-dimensional airfoils under uncertain conditions," Tech. rep., DTIC Document, 2001.

[73] Li, W., Huyse, L., and Padula, S., "Robust airfoil optimization to achieve drag reduction over a range of mach numbers," *Structural and Multidisciplinary Optimization*, Vol. 24, No. 1, 2002, pp. 38–50.

[74] Peigin, S. and Epstein, B., "Robust optimization of 2D airfoils driven by full Navier–Stokes computations," *Computers & fluids*, Vol. 33, No. 9, 2004, pp. 1175–1200.

[75] Padovan, L., Pediroda, V., and Poloni, C., "Multi Objective Robust Design Optimization of Airfoils in Transonic Field," in "Multidisciplinary Methods for Analysis Optimization and Control of Complex Systems," Springer, pp. 283–295, 2005.

[76] Shimoyama, K., Oyama, A., and Fujii, K., "Multi-objective six sigma approach applied to robust airfoil design for Mars airplane," *AIAA paper*, Vol. 1966.

[77] Dodson, M. and Parks, G. T., "Robust aerodynamic design optimization using polynomial chaos," *Journal of Aircraft*, Vol. 46, No. 2, 2009, pp. 635–646.

[78] Ghisu, T., Jarrett, J. P., and Parks, G. T., "Robust design optimization of airfoils with respect to ice accretion," *Journal of Aircraft*, Vol. 48, No. 1, 2011, pp. 287–304.

[79] Kato, H., Mashiko, H., Tokuyama, Y., Funazaki, K., and Takida, J., "Robust Aerodynamic Shape Optimization of Supersonic Turbine Using Non-Intrusive Polynomial Chaos Expansion," in "9th World Congress on Structural and Multidisciplinary Optimization," Shizuoka, Japan, 2011.

[80] Cinnella, P. and Hercus, S. J., "Robust optimization of dense gas flows under uncertain operating conditions," *Computers & Fluids*, Vol. 39, No. 10, 2010, pp. 1893–1908.

[81] Shimoyama, K., *Robust aerodynamic design of mars exploratory airplane wing with a new optimization method*, Ph.D. thesis, The University of Tokyo Japan, 2006.

[82] Song, W., "Multiobjective memetic algorithm and its application in robust airfoil shape optimization," in "Multi-Objective Memetic Algorithms," Springer, pp. 389–402, 2009.

[83] Walter, M., *A stochastic expansion-based approach for design under uncertainty*, Ph.D. thesis, Georgia Institute of Technology, 2013.

[84] Beyer, H.-G. and Sendhoff, B., "Robust optimization–a comprehensive survey," *Computer methods in applied mechanics and engineering*, Vol. 196, No. 33, 2007, pp. 3190–3218.

[85] Ghahramani, Z. and Rasmussen, C. E., "Bayesian monte carlo," in "Advances in neural information processing systems," , 2002, pp. 489–496.

[86] Padulo, M., Campobasso, M. S., and Guenov, M. D., "Novel uncertainty propagation method for robust aerodynamic design," *AIAA journal*, Vol. 49, No. 3, 2011, pp. 530–543.

[87] Eldred, M. S. and Burkardt, J., "Comparison of non-intrusive polynomial chaos and stochastic collocation methods for uncertainty quantification," in "Proceedings of the 47th AIAA Aerospace Sciences Meeting," AIAA, Orlando, FL, 2009-0976, 2009.

[88] Xiu, D. and Karniadakis, G. E., "Modeling uncertainty in flow simulations via generalized polynomial chaos," *Journal of computational physics*, Vol. 187, No. 1, 2003, pp. 137–167.

[89] Knio, O. and Le Maitre, O., "Uncertainty propagation in CFD using polynomial chaos decomposition," *Fluid Dynamics Research*, Vol. 38, No. 9, 2006, pp. 616–640.

[90] Hosder, S., Walters, R. W., and Perez, R., "A non-intrusive polynomial chaos method for uncertainty propagation in CFD simulations," *AIAA paper*, Vol. 891, 2006, p. 2006.

[91] Eldred, M. S., Webster, C. G., and Constantine, P., "Evaluation of non-intrusive approaches for Wiener-Askey generalized polynomial chaos," in "Proceedings of the 10th AIAA Non-Deterministic Approaches Conference, number AIAA-2008-1892, Schaumburg, IL," Vol. 117, 2008, p. 189.

[92] Smolyak, S. A., "Quadrature and interpolation formulas for tensor products of certain classes of functions," in "Dokl. Akad. Nauk SSSR," Vol. 4, 1963, p. 123.

[93] Ma, X. and Zabaras, N., "An adaptive hierarchical sparse grid collocation algorithm for the solution of stochastic differential equations," *Journal of Computational Physics*, Vol. 228, No. 8, 2009, pp. 3084–3113.

[94] Nobile, F., Tempone, R., and Webster, C. G., "A sparse grid stochastic collocation method for partial differential equations with random input data," *SIAM Journal on Numerical Analysis*, Vol. 46, No. 5, 2008, pp. 2309–2345.

[95] Babuška, I., Nobile, F., and Tempone, R., "A stochastic collocation method for elliptic partial differential equations with random input data," *SIAM review*, Vol. 52, No. 2, 2010, pp. 317–355.

[96] Constantine, P. G., Eldred, M. S., and Phipps, E. T., "Sparse pseudospectral approximation method," *Computer Methods in Applied Mechanics and Engineering*, Vol. 229, 2012, pp. 1–12.

[97] Conrad, P. R. and Marzouk, Y. M., "Adaptive Smolyak pseudospectral approximations," *SIAM Journal on Scientific Computing*, Vol. 35, No. 6, 2013, pp. A2643–A2670.

[98] Wang, Q., Moin, P., and Iaccarino, G., "A high order multivariate approximation scheme for scattered data sets," *Journal of Computational Physics*, Vol. 229, No. 18, 2010, pp. 6343–6361.

[99] Boopathy, K. and Rumpfkeil, M. P., "Unified Framework for Training Point Selection and Error Estimation for Surrogate Models," *AIAA Journal*, Vol. 53, No. 1, 2014, pp. 215–234.

[100] Zhang, Y., Hosder, S., Leifsson, L., and Koziel, S., "Robust airfoil optimization under inherent and model-form uncertainties using stochastic expansions," in "50 th AIAA Aerospace Sciences Meeting Including the New Horizons Forum and Aerospace Exposition, Nashville, TN," , 2012, pp. 2012–0056.

[101] Zhang, Y. and Hosder, S., "Robust Design Optimization Under Mixed Uncertainties With Stochastic Expansions," *Journal of Mechanical Design*, Vol. 135, No. 8, 2013, p. 081005.

[102] Zhang, Y. and Hosder, S., "Efficient Robust Design with Stochastic Expansions," in "Surrogate-Based Modeling and Optimization," Springer, pp. 247–284, 2013.

[103] West IV, T. K., Hosder, S., and Johnston, C. O., "Multistep uncertainty quantification approach applied to hypersonic reentry flows," *Journal of Spacecraft and Rockets*, Vol. 51, No. 1, 2013, pp. 296–310.

[104] Adya, S., Han, D., and Hosder, S., "Uncertainty quantification integrated to CFD modeling of synthetic jet actuators," *International Journal of Flow Control*, Vol. 2, No. 3, 2010, pp. 169–181.

[105] Shah, H., Hosder, S., and Winter, T., "A Mixed Uncertainty Quantification Approach Using Evidence Theory and Stochastic Expansions," *International Journal for Uncertainty Quantification*, Vol. 5, No. 1.

[106] Blatman, G. and Sudret, B., "Adaptive sparse polynomial chaos expansion based on¡ i¿ least angle regression¡/i¿," *Journal of Computational Physics*, Vol. 230, No. 6, 2011, pp. 2345–2367.

[107] Blatman, G. and Sudret, B., "Principal component analysis and Least Angle Regression in spectral stochastic finite element analysis," in "ICASP11 Conference, Zurich (Switzerland)," Vol. 60, 2011.

[108] Witteveen, J. A. and Iaccarino, G., "Simplex stochastic collocation with random sampling and extrapolation for nonhypercube probability spaces," *SIAM Journal on Scientific Computing*, Vol. 34, No. 2, 2012, pp. A814–A838.

[109] Shimoyama, K., Kawai, S., and Alonso, J. J., "Dynamic adaptive sampling based on Kriging surrogate models for efficient uncertainty quantification," *Structures, structural dynamics, and materials and co-located conferencesAmerican Institute of Aeronautics and Astronautics*.

[110] Witteveen, J. A. and Iaccarino, G., "Simplex stochastic collocation with ENO-type stencil selection for robust uncertainty quantification," *Journal of Computational Physics*, Vol. 239, 2013, pp. 1–21.

[111] Witteveen, J. A. and Iaccarino, G., "Subcell resolution in simplex stochastic collocation for spatial discontinuities," *Journal of Computational Physics*, Vol. 251, 2013, pp. 17–52.

[112] Chantrasmi, T., Doostan, A., and Iaccarino, G., "Padé–Legendre approximants for uncertainty analysis with discontinuous response surfaces," *Journal of Computational Physics*, Vol. 228, No. 19, 2009, pp. 7159–7180.

[113] Chantrasmi, T. and Iaccarino, G., "Forward and Backward Uncertainty Propagation for Discontinuous System Response Using the Padé-Legendre Method," *International Journal for Uncertainty Quantification*, Vol. 2, No. 2.

[114] Foo, J., Wan, X., and Karniadakis, G. E., "The multi-element probabilistic collocation method (ME-PCM): Error analysis and applications," *Journal of Computational Physics*, Vol. 227, No. 22, 2008, pp. 9572–9595.

[115] Foo, J. and Karniadakis, G. E., "Multi-element probabilistic collocation method in high dimensions," *Journal of Computational Physics*, Vol. 229, No. 5, 2010, pp. 1536–1557.

[116] Kersaudy, P., Sudret, B., Varsier, N., Picon, O., and Wiart, J., "A new surrogate modeling technique combining Kriging and polynomial chaos expansions–Application to uncertainty analysis in computational dosimetry," *Journal of Computational Physics*, Vol. 286, 2015, pp. 103–117.

[117] Sudret, B., "Global sensitivity analysis using polynomial chaos expansions," *Reliability Engineering & System Safety*, Vol. 93, No. 7, 2008, pp. 964–979.

[118] Crestaux, T., Le Maıtre, O., and Martinez, J.-M., "Polynomial chaos expansion for sensitivity analysis," *Reliability Engineering & System Safety*, Vol. 94, No. 7, 2009, pp. 1161–1172.

[119] Blatman, G. and Sudret, B., "Efficient computation of global sensitivity indices using sparse polynomial chaos expansions," *Reliability Engineering & System Safety*, Vol. 95, No. 11, 2010, pp. 1216–1229.

[120] Choi, S., Alonso, J. J., Kroo, I. M., and Wintzer, M., "Multi-fidelity design optimization of low-boom supersonic business multi-fidelity design optimization of low-boom supersonic business jets," in "Proceedings of the 10th AIAA/ISSMO Multidisciplinary Analysis and Optimization Conference, No. AIAA 2004-4371 in AIAA Paper, 2004. 14 of 15 American Institute of Aeronautics and Astronautics 8 Alexandrov," Citeseer, 1997.

[121] Leifsson, L. and Koziel, S., "Multi-fidelity design optimization of transonic airfoils using physics-based surrogate modeling and shape-preserving response prediction," *Journal of Computational Science*, Vol. 1, No. 2, 2010, pp. 98–106.

[122] Barrett, T. R., Bressloff, N. W., and Keane, A. J., "Airfoil shape design and optimization using multifidelity analysis and embedded inverse design," *AIAA journal*, Vol. 44, No. 9, 2006, pp. 2051–2060.

[123] Collins, K. B., *A multi-fidelity framework for physics based rotor blade simulation and optimization*, ProQuest, 2008.

[124] Zheng, L., Hedrick, T. L., and Mittal, R., "A multi-fidelity modelling approach for evaluation and optimization of wing stroke aerodynamics in flapping flight," *Journal of Fluid Mechanics*, Vol. 721, 2013, pp. 118–154.

[125] Ng, L. W.-T. and Eldred, M. S., "Multifidelity uncertainty quantification using nonintrusive polynomial chaos and stochastic collocation," in "Proceedings of the 14th AIAA Non-Deterministic Approaches Conference," AIAA, Honolulu, HI, 2012-1852, 2012.

[126] Padrón, A. S., Alonso, J. J., Palacios, F., Barone, M., and Eldred, M. S., "Multi-Fidelity Uncertainty Quantification: Application to a Vertical Axis Wind Turbine Under an Extreme Gust," .

[127] Shah, H., Hosder, S., Koziel, S., Tesfahunegn, Y. A., and Leifsson, L., "Multi-fidelity Robust Aerodynamic Design Optimization Under Mixed Uncertainty," .

[128] Miettinen, K., *Nonlinear multiobjective optimization*, Vol. 12, Springer Science & Business Media, 1999.

[129] Srinivas, N. and Deb, K., "Muiltiobjective optimization using nondominated sorting in genetic algorithms," *Evolutionary computation*, Vol. 2, No. 3, 1994, pp. 221–248.

[130] Coello Coello, C. A. and Lechuga, M. S., "MOPSO: A proposal for multiple objective particle swarm optimization," in "Evolutionary Computation, 2002. CEC'02. Proceedings of the 2002 Congress on," IEEE, Vol. 2, 2002, pp. 1051–1056.

[131] Deb, K., Pratap, A., and Meyarivan, T., "Constrained test problems for multi-objective evolutionary optimization," in "Evolutionary Multi-Criterion Optimization," Springer, 2001, pp. 284–298.

[132] Forrester, A., Sobester, A., and Keane, A., *Engineering design via surrogate modelling: a practical guide*, John Wiley & Sons, 2008.

[133] Toal, D. J., Bressloff, N., Keane, A., and Holden, C., "The development of a hybridized particle swarm for kriging hyperparameter tuning," *Engineering optimization*, Vol. 43, No. 6, 2011, pp. 675–699.

[134] Shafer, G. et al., *A mathematical theory of evidence*, Vol. 1, Princeton university press Princeton, 1976.

[135] Xiu, D., *Numerical methods for stochastic computations: a spectral method approach*, Princeton University Press, 2010.

[136] Gander, M. J. and Karp, A. H., "Stable computation of high order Gauss quadrature rules using discretization for measures in radiation transfer," *Journal of Quantitative Spectroscopy and Radiative Transfer*, Vol. 68, No. 2, 2001, pp. 213–223.

[137] Gautschi, W., *Orthogonal polynomials: computation and approximation*, Oxford university press, 2004.

[138] Hosder, S., Walters, R. W., and Balch, M., "Efficient sampling for non-intrusive polynomial chaos applications with multiple uncertain input variables," in "Proceedings of the 48th AIAA/ASME/ASCE/AHS/ASC Structures, Structural Dynamics and Materials Conference," AIAA, Honolulu, HI, 2007-1939, 2007.

[139] Axerio-Cilies, J. A., *Predicting Formula 1 tire aerodynamics: sensitivities, uncertainties and optimization*, Ph.D. thesis, Stanford University, 2012.

[140] McKay, M. D., Beckman, R. J., and Conover, W. J., "Comparison of three methods for selecting values of input variables in the analysis of output from a computer code," *Technometrics*, Vol. 21, No. 2, 1979, pp. 239–245.

[141] Lim, D., Ong, Y.-S., Jin, Y., and Sendhoff, B., "A study on metamodeling techniques, ensembles, and multi-surrogates in evolutionary computation," in "Proceedings of the 9th annual conference on Genetic and evolutionary computation," ACM, 2007, pp. 1288–1295.

[142] Sindhya, K., Miettinen, K., and Deb, K., "A hybrid framework for evolutionary multi-objective optimization," *IEEE Transactions on Evolutionary Computation*, Vol. 17, No. 4, 2013, pp. 495–511.

[143] Wierzbicki, A. P., "On the completeness and constructiveness of parametric characterizations to vector optimization problems," *Operations-Research-Spektrum*, Vol. 8, No. 2, 1986, pp. 73–87.

[144] Aarts, E. H. and Lenstra, J. K., *Local search in combinatorial optimization*, Princeton University Press, 2003.

[145] Knowles, J. D., *Local-search and hybrid evolutionary algorithms for Pareto optimization*, Ph.D. thesis, Department of Computer Science Local-Search and Hybrid Evolutionary Algorithms for Pareto OptimiZation Joshua D. Knowles Submitted in partial fulfilment of the requirements for the degree of Doctor of Philosophy in Computer Science. Department of Computer Science, University of Reading, 2002.

[146] Messac, A., Ismail-Yahaya, A., and Mattson, C. A., "The normalized normal constraint method for generating the Pareto frontier," *Structural and Multidisciplinary Optimization*, Vol. 25, No. 2, 2003, pp. 86–98.

[147] Deb, K., "Multi-objective genetic algorithms: Problem difficulties and construction of test problems," *Evolutionary computation*, Vol. 7, No. 3, 1999, pp. 205–230.

[148] Dellnitz, M., Schütze, O., and Hestermeyer, T., "Covering Pareto sets by multilevel subdivision techniques," *Journal of optimization theory and applications*, Vol. 124, No. 1, 2005, pp. 113–136.

[149] Aerospace Design Lab, "SU2 The Open-Source CFD Code http://su2.stanford.edu/," , 2014.

[150] Persson, P.-O. and Strang, G., "A simple mesh generator in MATLAB," *SIAM review*, Vol. 46, No. 2, 2004, pp. 329–345.

[151] Ray, T. and Tsai, H., "Swarm algorithm for single-and multiobjective airfoil design optimization," *AIAA journal*, Vol. 42, No. 2, 2004, pp. 366–373.

[152] Vicini, A. and Quagliarella, D., "Inverse and direct airfoil design using a multiobjective genetic algorithm," *AIAA journal*, Vol. 35, No. 9, 1997, pp. 1499–1505.

[153] Halton, J. H., "Algorithm 247: Radical-inverse quasi-random point sequence," *Communications of the ACM*, Vol. 7, No. 12, 1964, pp. 701–702.

[154] Kulfan, B. M., "Universal parametric geometry representation method," *Journal of Aircraft*, Vol. 45, No. 1, 2008, pp. 142–158.

[155] Shah, H., Hosder, S., Koziel, S., Tesfahunegn, Y. A., and Leifsson, L., "Multi-fidelity robust aerodynamic design optimization under mixed uncertainty," *Aerospace Science and Technology*, Vol. 45, 2015, pp. 17–29.

[156] Xiong, S., Qian, P. Z., and Wu, C. J., "Sequential design and analysis of high-accuracy and low-accuracy computer codes," *Technometrics*, Vol. 55, No. 1, 2013, pp. 37–46.

[157] Toal, D. J., "Some considerations regarding the use of multi-fidelity Kriging in the construction of surrogate models," *Structural and Multidisciplinary Optimization*, pp. 1–23.

[158] Forrester, A. I., Bressloff, N. W., and Keane, A. J., "Optimization using surrogate models and partially converged computational fluid dynamics simulations," *Proceedings of the Royal Society A: Mathematical, Physical and Engineering Science*, Vol. 462, No. 2071, 2006, pp. 2177–2204.

[159] Clyde R, G., Gene J-W, H., and Perry A, N., "Simultaneous Aerodynamic Analysis and Design Optimization (SAADO) for a 3-D Rigid Wing," .

[160] Croicu, A.-M., Hussaini, M. Y., Jameson, A., and Klopfer, G., "Robust Airfoil Optimization Using Maximum Expected Value and Expected Maximum Value Approaches," *AIAA journal*, Vol. 50, No. 9, 2012, pp. 1905–1919.

[161] Lurati, L., "Robust airfoil design under uncertain operation conditions using stochastic collocation," , 2008.

[162] Kohonen, T., "The self-organizing map," *Neurocomputing*, Vol. 21, No. 1, 1998, pp. 1–6.

[163] Vesanto, J., Himberg, J., Alhoniemi, E., and Parhankangas, J., *SOM toolbox for Matlab 5*, Citeseer, 2000.

[164] Witteveen, J. A. S., Doostan, A., Pecnik, R., and Iaccarino, G., "Uncertainty quantification of the transonic flow around the RAE 2822 airfoil," *Center for Turbulence Research, Annual Briefs, Stanford University*.

[165] Okabe, A., Boots, B., Sugihara, K., and Chiu, S. N., *Spatial tessellations: concepts and applications of Voronoi diagrams*, Vol. 501, John Wiley & Sons, 2009.

[166] Seshadri, P., Constantine, P., Iaccarino, G., and Parks, G., "Aggressive design: A density-matching approach for optimization under uncertainty," *arXiv preprint arXiv:1409.7089*.

[167] Coello, C. A. C. C. and Pulido, G. T., "A micro-genetic algorithm for multiobjective optimization," in "Evolutionary multi-criterion optimization," Springer, 2001, pp. 126–140.

[168] Haupt, R. L. and Haupt, S. E., *Practical genetic algorithms*, John Wiley & Sons, 2004.

[169] Sobieczky, H., "Parametric airfoils and wings," in "Recent Development of Aerodynamic Design Methodologies," Springer, pp. 71–87, 1999.

[170] Palar, P. S. and Tsuchiya, T., "Study on modified CST Parameterization Method for Subsonic and Transonic Airfoil Multi objective Optimization," in "Proceedings of the Asia-Pacific International Symposium on Aerospace Technology," Takamatsu, Japan, 2013.

[171] Lara, A., Sanchez, G., Coello Coello, C. A., and Schutze, O., "HCS: a new local search strategy for memetic multiobjective evolutionary algorithms," *Evolutionary Computation, IEEE Transactions on*, Vol. 14, No. 1, 2010, pp. 112–132.

[172] Li, H. and Zhang, Q., "Multiobjective optimization problems with complicated Pareto sets, MOEA/D and NSGA-II," *IEEE Transactions on Evolutionary Computation*, Vol. 13, No. 2, 2009, pp. 284–302.

[173] Hosder, S., Walters, R. W., and Balch, M., "Point-collocation nonintrusive polynomial chaos method for stochastic computational fluid dynamics," *AIAA Journal*, Vol. 48, No. 12, 2010, pp. 2721–2730.

[174] Deb, K. and Gupta, H., "Introducing robustness in multi-objective optimization," *Evolutionary Computation*, Vol. 14, No. 4, 2006, pp. 463–494.

[175] Wickramasinghe, U. K., Carrese, R., and Li, X., "Designing airfoils using a reference point based evolutionary many-objective particle swarm optimization algorithm," in "2010 IEEE Congress on Evolutionary Computation (CEC)," IEEE, Barcelona, Spain, 2010, pp. 1–8.

[176] Powell, S. and Sóbester, A., "Application-Specific Class Functions for the Kulfan Transformation of Airfoils," in "Proceedings of the 13th AIAA/ISSMO Multidisciplinary Analysis Optimization Conference," AIAA, Fort Worth, TX, 2010-9269, 2010.

[177] Xiu, D. and Karniadakis, G. E., "The Wiener–Askey polynomial chaos for stochastic differential equations," *SIAM Journal on Scientific Computing*, Vol. 24, No. 2, 2002, pp. 619–644.

[178] Srinivas, N. and Deb, K., "Multi-objective function optimization using non-dominated sorting genetic algorithms," *Evolutionary Computation*, Vol. 2, No. 3, 1995, pp. 221–248.

[179] Robinson, G. and Keane, A., "Concise orthogonal representation of supercritical airfoils," *Journal of Aircraft*, Vol. 38, No. 3, 2001, pp. 580–583.

[180] Ray, T. and Smith, W., "A surrogate assisted parallel multiobjective evolutionary algorithm for robust engineering design," *Engineering Optimization*, Vol. 38, No. 8, 2006, pp. 997–1011.

[181] Paenke, I., Branke, J., and Jin, Y., "Efficient search for robust solutions by means of evolutionary algorithms and fitness approximation," *Evolutionary Computation, IEEE Transactions on*, Vol. 10, No. 4, 2006, pp. 405–420.

[182] Laboratory of Computer and Information Science, "SOM toolbox https://github.com/ilarinieminen/SOM-Toolbox," .

[183] Stein, M., "Large sample properties of simulations using Latin hypercube sampling," *Technometrics*, Vol. 29, No. 2, 1987, pp. 143–151.

[184] Hooke, R. and Jeeves, T. A., ""Direct Search"Solution of Numerical and Statistical Problems," *Journal of the ACM (JACM)*, Vol. 8, No. 2, 1961, pp. 212–229.

[185] Jin, Y. and Branke, J., "Evolutionary optimization in uncertain environments-a survey," *Evolutionary Computation, IEEE Transactions on*, Vol. 9, No. 3, 2005, pp. 303–317.

[186] Ong, Y.-S., Nair, P. B., and Lum, K. Y., "Max-min surrogate-assisted evolutionary algorithm for robust design," *Evolutionary Computation, IEEE Transactions on*, Vol. 10, No. 4, 2006, pp. 392–404.

[187] Zingg, D. W. and Elias, S., "Aerodynamic optimization under a range of operating conditions," *AIAA journal*, Vol. 44, No. 11, 2006, pp. 2787–2792.

[188] Nobile, F., Tempone, R., and Webster, C. G., "An anisotropic sparse grid stochastic collocation method for partial differential equations with random input data," *SIAM Journal on Numerical Analysis*, Vol. 46, No. 5, 2008, pp. 2411–2442.

[189] Gerstner, T. and Griebel, M., "Numerical integration using sparse grids," *Numerical algorithms*, Vol. 18, No. 3-4, 1998, pp. 209–232.

[190] Xiu, D. and Hesthaven, J. S., "High-order collocation methods for differential equations with random inputs," *SIAM Journal on Scientific Computing*, Vol. 27, No. 3, 2005, pp. 1118–1139.

[191] Barthelmann, V., Novak, E., and Ritter, K., "High dimensional polynomial interpolation on sparse grids," *Advances in Computational Mathematics*, Vol. 12, No. 4, 2000, pp. 273–288.